

AMPHIPHILIC INVERTIBLE POLYMERS: SELF-ASSEMBLY INTO FUNCTIONAL
MATERIALS DRIVEN BY ENVIRONMENT POLARITY

A Dissertation
Submitted to the Graduate Faculty
of the
North Dakota State University
of Agriculture and Applied Science

By

Ivan Hevus

In Partial Fulfillment
for the Degree of
DOCTOR OF PHILOSOPHY

Major Department: Coatings and Polymeric Materials

July 2012

Fargo, North Dakota

North Dakota State University

Graduate School

Title:

AMPHIPHILIC INVERTIBLE POLYMERS: SELF-ASSEMBLY INTO FUNCTIONAL
MATERIALS DRIVEN BY ENVIRONMENT POLARITY

By

Ivan Hevus

The Supervisory Committee certifies that this disquisition complies with North Dakota State University's regulations and meets the accepted standards for the degree of

DOCTOR OF PHILOSOPHY

SUPERVISORY COMMITTEE:

Dr. Andriy Voronov

Chair

Dr. Dean C. Webster

Dr. Bret J. Chisholm

Dr. Iskander Akhatov

Approved:

07-16-2012

Date

Dr. Dean C. Webster

Department Chair

ABSTRACT

Stimuli-responsive polymers adapt to environmental changes by adjusting their chain conformation in a fast and reversible way. Responsive polymeric materials have already found use in electronics, coatings industry, personal care, and bio-related areas.

The current work aims at the development of novel responsive functional polymeric materials by manipulating environment-dependent self-assembly of a new class of responsive macromolecules strategically designed in this study, – amphiphilic invertible polymers (AIPs).

Environment-dependent micellization and self-assembly of three different synthesized AIP types based on poly(ethylene glycol) as a hydrophilic fragment and varying hydrophobic constituents was demonstrated in polar and nonpolar solvents, as well as on the surfaces and interfaces. With increasing concentration, AIP micelles self-assemble into invertible micellar assemblies composed of hydrophilic and hydrophobic domains.

Polarity-responsive properties of AIPs make invertible micellar assemblies functional in polar and nonpolar media including at interfaces. Thus, invertible micellar assemblies solubilize poorly soluble substances in their interior in polar and nonpolar solvents. In a polar aqueous medium, a novel stimuli-responsive mechanism of drug release based on response of AIP-based drug delivery system to polarity change upon contact with the target cell has been established using invertible micellar assemblies loaded with curcumin, a phytochemical drug. In a nonpolar medium, invertible micellar assemblies were applied simultaneously as nanoreactors and stabilizers for size-controlled synthesis of silver nanoparticles stable in both polar and nonpolar media. The developed amphiphilic nanosilver was subsequently used as seeds to promote anisotropic growth of CdSe semiconductor nanoparticles that have potential in different applications ranging from physics to medicine.

Amphiphilic invertible polymers were shown to adsorb on the surface of silica nanoparticles strongly differing in polarity. AIP modified silica nanoparticles are able to adsolubilize molecules of poorly water-soluble 2-naphthol into the adsorbed polymer layer. The adsolubilization ability of adsorbed invertible macromolecules makes AIP-modified silica nanoparticles potentially useful in wastewater treatment or biomedical applications.

Finally, the invertible micellar assemblies were used as functional additives to improve the appearance of electrospun silicon wires based on cyclohexasilane, a liquid silicon precursor. AIP-assisted fabrication of silicon wires from the liquid cyclohexasilane precursor has potential as a scalable method for developing electronic functional materials.

ACKNOWLEDGMENTS

First and foremost, I express my most sincere gratitude and appreciation to my advisor, Dr. Andriy Voronov, for his guidance, support and help in conducting research throughout all my years at the NDSU. He is the person I learned a lot from, both in terms of research and personal life. His invaluable advice I will always remember.

I would also like to thank the members of my Advisory and Examination Committee, Dr. Dean C. Webster, Dr. Bret J. Chisholm, and Dr. Iskander Akhatov, for their time, assistance, and input in the successful completion of my research.

My sincere appreciation goes to all past and present members of Dr. Voronov research group for their help and support. My special thanks go to Dr. Ananiy Kohut for his sense of humor and companionship, as well as for his invaluable support and encouragement during my first years at the NDSU. I appreciate Andriy Popadyuk and Olena Kudina for assistance with countless matters. I thank Ruvimbo Chitemere and Donna Kautzman, the students I had an honor to supervise, for being always cheerful and positive. I also greatly appreciate the help and friendship of Dr. Ihor Tarnavchyk and his wonderful wife Maryna.

I thank Dr. Doug Schulz, Justin Hoey, and Jeremiah Smith at Center for Nanoscale Science and Engineering, for providing me with an exciting ability to work with cyclohexasilane, unique experience of working in a glovebox, fruitful discussions, and valuable advice.

I thank Shane Stafslie and Justin Daniels at CNSE, and Dr. Chengwen Sun and Amit Modgil at the Department of Pharmaceutical Sciences for their assistance with cell viability measurements.

I would like to thank Dr. Angel Ugrinov, Dr. John Bagu, and Daniel Wanner at the Department of Chemistry and Biochemistry for their help with the instruments. I also thank Scott Payne at NDSU Center for Electron Microscopy for SEM and TEM images.

I am very thankful to Dr. Yuri Melnichenko, Dr. Lilin He, Dr. William Heller, Dr. Carrie Gao, Dr. Jinkui Zhao, and Dr. Changwoo Do at the Oak Ridge National Laboratory for their generous on-site assistance with SANS measurements and numerous helpful discussions and advice.

To all CPM faculty, staff, and students, I owe a debt of gratitude for creating such a wonderful spirit of friendship and collaboration at the department.

My deepest appreciation goes to my parents, Orest and Anna Hevus. I felt their support even though they were thousands of miles away from me.

Finally, I would like to express my immense gratitude to my wife, Lydia. I am absolutely sure I could not complete the process without her love, understanding, and moral support.

DEDICATION

To my wife, Lydia.

TABLE OF CONTENTS

ABSTRACT	iii
ACKNOWLEDGMENTS	v
DEDICATION	vii
LIST OF TABLES	xiv
LIST OF FIGURES	xvi
LIST OF ABBREVIATIONS.....	xxii
CHAPTER 1. INTRODUCTION: STIMULI-RESPONSIVE POLYMERS.....	1
1.1. Introduction to Stimuli-Responsive Polymers	1
1.2. Types of Stimuli-Responsive Polymeric Materials.....	2
1.3. Temperature-Responsive Polymers.....	6
1.3.1. Thermoresponsive Polymers Exhibiting LCST	7
1.3.2. Thermoresponsive Amphiphilic Block Copolymers	10
1.3.3. Thermoresponsive Biopolymers	11
1.4. pH-Responsive Polymers	12
1.4.1. pH-Responsive Polyacids	13
1.4.2. pH-Responsive Polybases	15
1.5. Other Types of Stimuli-Responsive Polymers	15
1.5.1. Moisture- and Solvent-Responsive Polymers.....	15
1.5.2. Photoresponsive Polymers	16
1.5.3. Field-Responsive Polymers	17
1.5.4. Antigen-Responsive Polymers.....	17
1.6. Application of Stimuli-Responsive Polymers	18

1.6.1. Smart and Self-Healing Coatings.....	18
1.6.2. Biomimetic Micro- and Nanoactuation	18
1.6.3. Biointerfaces and Bioseparation	18
1.6.4. Catalysis.....	19
1.6.5. Drug Delivery Systems.....	19
1.7. Research Scope.....	20
1.8. References	20
CHAPTER 2. APPLICATION-BASED DESIGN OF AMPHIPHILIC INVERTIBLE POLYMERS.....	31
2.1. Abstract	31
2.2. Introduction	31
2.3. Experimental	35
2.3.1. Materials	35
2.3.2. Characterization	35
2.3.3. Synthesis of the AIPs.....	36
2.4. Results and Discussion.....	38
2.4.1. Amphiphilic Invertible Polyesters Based on Poly(ethylene Glycol) and Aliphatic Dicarboxylic Acids (AIPes-1)	38
2.4.2. Amphiphilic Invertible Polyurethanes Based on Poly(ethylene Glycol) and Polytetrahydrofuran (AIPUs)	42
2.4.3. Amphiphilic Invertible Polyesters Based on Poly(ethylene Glycol) and Polytetrahydrofuran (AIPes-2)	51
2.5. Conclusions	56
2.6. References	57

CHAPTER 3. MICELLIZATION, SELF-ASSEMBLY, AND RESPONSIVE PROPERTIES OF AMPHIPHILIC INVERTIBLE POLYMERS IN POLAR AND NONPOLAR MEDIA	60
3.1. Abstract	60
3.2. Introduction	61
3.3. Experimental	63
3.3.1. Materials	63
3.3.2. Characterization	63
3.4. Results and Discussion	66
3.4.1. Determination of the Critical Micelle Concentration of AIP Aqueous Solutions	66
3.4.2. Environment-Dependent Micellization and Responsive Properties of the AIPs in Polar and Nonpolar Media	71
3.4.3. Self-Assembly of Amphiphilic Invertible Polymers in Polar and Nonpolar Media	83
3.4.4. Morphological Study of AIP Micelles and Micellar Assemblies	96
3.5. Conclusions	101
3.6. References	102
CHAPTER 4. FUNCTIONAL SELF-ASSEMBLY OF AMPHIPHILIC INVERTIBLE POLYMERS IN POLAR MEDIUM: NANOCONTAINERS AND STIMULI-RESPONSIVE DRUG DELIVERY SYSTEM	108
4.1. Abstract	108
4.2. Introduction	109
4.3. Experimental	111
4.3.1. Materials	111
4.3.2. Characterization	112
4.3.3. Loading and Release Study	112

4.3.4. Phase Transfer Study	113
4.3.5. Cytotoxicity Study	114
4.4. Results and Discussion	116
4.4.1. AIPE Micellar Assemblies as Nanocontainers for Insoluble Molecules	116
4.4.2. Amphiphilic Invertible Polymers as Potential Responsive Drug Delivery Systems: Model Dye Experiments	119
4.4.3. Amphiphilic Invertible Polymers as Potential Responsive Drug Delivery Systems: Curcumin Transfer	123
4.5. Conclusions	133
4.6. References	134
CHAPTER 5. FUNCTIONAL SELF-ASSEMBLY OF AMPHIPHILIC INVERTIBLE POLYMERS IN NONPOLAR MEDIUM: NANOREACTORS FOR NANOPARTICLE DEVELOPMENT	137
5.1. Abstract	137
5.2. Introduction	138
5.3. Experimental	141
5.3.1. Materials	141
5.3.2. Characterization	142
5.3.3. Solubilization Study	142
5.3.4. Synthesis of Silver Nanoparticles	143
5.3.5. Synthesis of Cadmium Selenide Nanoparticles	143
5.4. Results and Discussion	144
5.4.1. Solubilization of Malachite Green by AIPU Micelles	144
5.4.2. Development of Silver Nanoparticles in AIPU Nanoreactors	146

5.4.3. Development of Semiconductor Nanoparticles Using AIPU-Stabilized Nanosilver Seeds	155
5.5. Conclusions	160
5.6. References	161
CHAPTER 6. FUNCTIONAL SELF-ASSEMBLY OF AMPHIPHILIC INVERTIBLE POLYMERS ON THE SURFACES AND AT THE INTERFACES: ADSOLUBILIZATION AND DEVELOPMENT OF SILICON NANOWIRES	165
6.1. Abstract	165
6.2. Introduction	166
6.3. Experimental	168
6.3.1. Materials	168
6.3.2. Characterization	168
6.3.3. Adsorption Study	169
6.3.4. Adsolubilization Study.....	169
6.3.5. Desorption Study	170
6.3.6. AIPe-Assisted Electrospinning of Silicon Wires	170
6.4. Results and Discussion	171
6.4.1. The Use of AIPes for Modification of Silica Nanoparticles Differing by Polarity	171
6.4.2. Adsolubilization of 2-Naphthol Molecules into Adsorbed AIPes	174
6.4.3. AIPes as Functional Additives in Precursors for Electrospinning Silicon-Containing Materials	180
6.5. Conclusions	189
6.6. References	190
CHAPTER 7. CONCLUSIONS	194
7.1. Future Work	197

7.1.1. Evaluation of AIP Micellar Morphologies in the Nonpolar Media	197
7.1.2. Improvement of AIP Based Drug Delivery Vehicle Formulations	197

LIST OF TABLES

<u>Table</u>	<u>Page</u>
2.1. Characteristics of the AIPE-1 Polyesters.....	39
2.2. Calculated Hydrodynamic Radii (in nm) of AIPES-1 in Different Solvents	41
2.3. Characteristics of the AIPUs.....	47
2.4. Calculated Hydrodynamic Radii (in nm) of AIPUs in Different Solvents	49
2.5. Characteristics of the AIPE-2 Polyesters.....	52
2.6. Calculated Hydrodynamic Radii (in nm) of AIPES-2 in Different Solvents	56
3.1. Critical Micelle Concentration of Amphiphilic Invertible Polymers.	68
3.2. PTHF/PEG Proton Ratio of Amphiphilic Invertible Polyurethanes in Different Solvents .	76
3.3. Advancing Water and Diiodomethane Contact Angles and Surface Energies of Thin Polyurethane Films on Different Substrates	81
3.4. The Ratio of Hydrophilic to Hydrophobic Protons Calculated from Integral Intensities of AIPE Proton Signals in ¹ H NMR Spectra.	86
3.5. Geometric Parameters of Micelles of PEG ₆₀₀ PTHF ₂₅₀ at Different Concentrations	98
3.6. Geometric Parameters of Micelles of PEG ₆₀₀ PTHF ₆₅₀ at Different Concentrations	99
3.7. Geometric Parameters of Micelles of S6 at Different Concentrations	99
3.8. Geometric Parameters of Micelles of D3 at Different Concentrations.....	100
4.1. Transfer of Nile Red and AIPES-2 from the Aqueous to the Nonpolar Media.....	122
4.2. Physical Properties of Blank and Curcumin-Loaded AIPE Micellar Assemblies at 1% Concentration.....	123
4.3. Phase Transfer Characteristics of Curcumin-Loaded AIPE Micellar Assemblies at 1% Concentration.....	128
5.1. Particle Size and Polydispersity Indices of Silver Nanoparticles Developed in 20% and 30% AIPU Solutions.	153

6.1. Correlation Coefficients, Equilibrium Constants, and A_m Values for AIPE Adsorption on Hydrophilic and Hydrophobized Silica	180
6.2. Post-Treatment of Silicon Containing Wires Electrospun from the AIPE/CHS/PMMA Composition.....	184

LIST OF FIGURES

<u>Figure</u>	<u>Page</u>
1.1. Principal types of responsive polymer systems, their dimensional changes, and types of stimuli they respond to.	3
1.2. LCST-associated response of PNIPAAm.	7
1.3. Structures and lower critical solution temperatures of several LCST-based thermoresponsive polymers.	8
1.4. Chemical structures of PEO–PPO amphiphilic block copolymers: (A) Pluronics® and (B) Tetronics®.	10
1.5. Chemical structures of pH-responsive polyacids (A) and polybases (B).	14
1.6. Structures of typical photochromic compounds used in responsive polymers.	16
2.1. A principal scheme of AIP structure and environment-dependent formation of AIP micelles.	33
2.2. Synthesis of amphiphilic invertible polyesters based on poly(ethylene glycol) and aliphatic dicarboxylic acids.	38
2.3. FTIR (A) and ¹ H NMR (B) spectra of the amphiphilic invertible polyester D10.	40
2.4. Specific viscosities of the AIPE-1 solutions in solvents differing by polarity (C = 0.01 g/mL).	41
2.5. Synthesis of amphiphilic invertible polyurethanes with an alternating (A) and a random (B) distribution of the hydrophilic and hydrophobic fragments along the polymer backbone.	43
2.6. FTIR spectra of (1) PTHF-650, (2) isocyanate terminated PTHF-650, (3) amphiphilic polyurethane PEG ₁₀₀₀ - <i>alt</i> -PTHF ₆₅₀	45
2.7. ¹ H NMR spectrum of the AIPU PEG ₁₀₀₀ - <i>alt</i> -PTHF ₆₅₀	48
2.8. Specific viscosities of the AIPU solutions in solvents differing by polarity (C = 0.01 g/mL).	49
2.9. Synthesis of the PEG-PTHF based amphiphilic invertible polyesters (AIPEs-2).	51
2.10. FTIR spectra of (1) PTHF-250, (2) carboxyl terminated prepolymer based on PTHF-250, (3) amphiphilic invertible polyester PEG ₁₀₀₀ PTHF ₂₅₀	53

2.11. ^1H NMR spectrum of the polyester PEG ₃₀₀ PTHF ₂₅₀	54
2.12. Specific viscosities of the AIPE-2 solutions in solvents differing by polarity ($C = 0.01$ g/mL).....	55
3.1. Surface tension isotherms of the aqueous solutions of AIPEs-1 (A) and AIPEs-2 (B).....	67
3.2. (A) Excitation spectra of pyrene in the aqueous solutions of polyester S6 at different concentrations. (B) The intensity ratio $I_{336.5}/I_{333}$ of the excitation spectra of pyrene in aqueous solutions of AIPEs-1 versus AIPE-1 concentration.....	69
3.3. (A) Excitation spectra of pyrene in the aqueous solutions of polyester PEG ₆₀₀ PTHF ₆₅₀ at different concentrations. (B) The intensity ratio $I_{336.5}/I_{333}$ of the excitation spectra of pyrene in four aqueous solutions of AIPEs-2 versus AIPE-2 concentration.....	70
3.4. Expanded regions of ^1H NMR spectra of the polyester S6 in different solvents.....	72
3.5. Three AIP architectures in solvents differing by polarity: (A) expanded macromolecule, (B) inverse micelle with a hydrophilic interior and a hydrophobic exterior, and (C) micelle with a hydrophobic interior and a hydrophilic exterior.....	72
3.6. Expanded regions of ^1H NMR spectra of the AIPU PEG _{1000-<i>alt</i>} -PTHF ₁₀₀₀ in different solvents.....	75
3.7. Expanded regions of ^1H NMR spectra of PEG ₆₀₀ PTHF ₆₅₀ in different solvents.....	79
3.8. Response of the AIP thin film to changing polarity of the medium.....	82
3.9. Expanded regions of ^1H NMR spectra of S6 recorded in D ₂ O at different concentrations.....	84
3.10. Expanded regions of ^1H NMR spectra of PEG ₆₀₀ PTHF ₆₅₀ recorded in D ₂ O at different concentrations.....	85
3.11. Formation of micellar assemblies due to self-assembly of AIP micelles in polar and nonpolar media.....	85
3.12. Width at half-height of hydrophilic and hydrophobic proton peaks of S6 and PEG ₆₀₀ PTHF ₆₅₀ in D ₂ O.....	87
3.13. Expanded proton regions of ^1H NMR spectra of amphiphilic invertible polyester S6 recorded in toluene- d_8 at different concentrations.....	89
3.14. Expanded PEG and PTHF proton regions of ^1H NMR spectra of PEG _{1000-<i>co</i>} -PTHF ₁₀₀₀ recorded in benzene- d_6 at different concentrations.....	90

3.15. Width at half-height of PEG and PTHF proton peaks of the AIPU PEG _{1000-co} -PTHF ₁₀₀₀ in benzene- <i>d</i> ₆	91
3.16. Representative MDSC thermograms of the amphiphilic invertible polyurethanes with (A) long hydrophilic and hydrophobic fragments: (1) PEG _{600-alt} -PTHF ₁₀₀₀ , (2) PEG _{1000-co} -PTHF ₁₀₀₀ and (B) short hydrophilic and hydrophobic fragments: (3) PEG _{600-alt} -PTHF ₆₅₀ , (4) PEG _{600-co} -PTHF ₆₅₀	92
3.17. A schematic representation of the microphase separation in the AIPUs with (A) alternating and (B) random distribution of hydrophilic PEG and hydrophobic PTHF fragments.....	94
3.18. A schematic representation of the microphase separation in the AIPUs based on short-chain polyols: (A) PEG _{600-alt} -PTHF ₆₅₀ with an alternating and (B) PEG _{600-co} -PTHF ₆₅₀ with a random distribution of hydrophilic PEG and hydrophobic PTHF fragments.....	95
3.19. SANS patterns recorded on aqueous solutions of amphiphilic invertible polyesters S6 (A), D3 (B), PEG ₆₀₀ PTHF ₂₅₀ (C), and PEG ₆₀₀ PTHF ₆₅₀ (D) at different concentrations.....	97
3.20. TEM images of the micelles of S6 (A), D3 (B), PEG ₆₀₀ PTHF ₂₅₀ (C), and PEG ₆₀₀ PTHF ₆₅₀ (D).....	100
3.21. Particle size distribution of spherical micelles made from D3 and PEG ₆₀₀ PTHF ₆₅₀ as determined by DLS at 1% w/w.....	101
4.1. Diffusion mechanism (A) and stimuli-responsive (inversion) mechanism (B) for delivery of poorly water-soluble drugs using polymeric micellar platforms.....	110
4.2. Solubilization of Sudan Red B by AIPE aqueous solutions.....	117
4.3. UV-Vis spectra of Sudan Red B solubilized by aqueous solution of polyester S6 at different polyester concentrations.....	117
4.4. UV-Vis spectra of 1% aqueous solutions of AIPE-2 micelles loaded with Nile red.....	118
4.5. Appearance of the two-phase system consisting of 1% aqueous solution of AIPE-2 micellar assemblies loaded with Nile red and toluene before (left) and after the polymer-mediated transfer (right).....	120
4.6. UV-Vis spectra of Nile red solutions transferred by AIPES-2 to toluene (A) and 1-octanol (B). Appearance of dye solutions in toluene (C) and 1-octanol (D) after the transfer.....	121

4.7. The size of blank and curcumin-loaded AIPE micellar assemblies as determined by dynamic light scattering: (1) D10, (2) curcumin–D10, (3) PEG ₆₀₀ PTHF ₆₅₀ , and (4) curcumin–PEG ₆₀₀ PTHF ₆₅₀	124
4.8. Chemical stability of curcumin in AIPE micellar assemblies in the aqueous medium with time.	126
4.9. Representative UV-vis spectra of curcumin in (1) aqueous phase before the transfer, as well as in (2) 1-octanol and (3) aqueous phase after the transfer from water to 1-octanol.	127
4.10. Possible mechanisms of AIPE-mediated curcumin delivery from water to 1-octanol.	129
4.11. Cell viability of HEK 293 cells treated with various concentrations of blank AIPE micellar assemblies.	131
4.12. Cytotoxicity of curcumin-loaded AIPE micellar assemblies on T47D breast carcinoma cells after 18, 42, and 66 h incubation.	132
5.1. (A) Photographs of Malachite green in toluene (left) and solubilized in the AIPU micellar solution (right). (B) UV-vis spectra of Malachite green solubilized in benzene by different concentrations of PEG _{1000-<i>alt</i>} -PTHF ₆₅₀	144
5.2. UV-Vis spectra of Malachite green solubilized in benzene by (A) alternating AIPUs and (B) random AIPUs (0.5 g/100 mL).	145
5.3. Development of silver nanoparticles in the AIPU nanoreactors.	147
5.4. UV-Vis spectra of silver nanoparticles synthesized in 20% w/w benzene solutions of (A) alternating and (B) random AIPUs and 30% w/w benzene solutions of (C) alternating and (D) random AIPUs. All samples were dispersed in acetone after the synthesis (reactive mixture : acetone ratio as 1 : 100).	148
5.5. X-ray diffraction pattern of silver nanoparticles synthesized in 30% w/w benzene solution of PEG _{1000-<i>alt</i>} -PTHF ₆₅₀	149
5.6. Dependence of precursor solubilization on the AIPU hydrophilic fragment length.	150
5.7. X-ray diffraction pattern of silver nanoparticles synthesized in 30% benzene solution of PEG _{1000-<i>co</i>} -PTHF ₆₅₀ revealing the presence of the silver oxide.	151
5.8. Photograph of silver nanoparticles developed in nanoreactors made from PEG _{1000-<i>co</i>} -PTHF ₁₀₀₀ dispersed in (1) acetone (a polar solvent) and (2) benzene (a nonpolar solvent).	151

5.9. Size distribution of silver nanoparticles prepared in (A) 20% and (B) 30% AIPU solutions: (1) PEG ₁₀₀₀ - <i>alt</i> -PTHF ₆₅₀ , (2) PEG ₁₀₀₀ - <i>alt</i> -PTHF ₁₀₀₀ , (3) PEG ₁₀₀₀ - <i>co</i> -PTHF ₆₅₀ , (4) PEG ₁₀₀₀ - <i>co</i> -PTHF ₁₀₀₀ , (5) PEG ₆₀₀ - <i>co</i> -PTHF ₆₅₀	152
5.10. TEM micrograph of silver nanoparticles developed in nanoreactors prepared from 30% solution of PEG ₁₀₀₀ - <i>co</i> -PTHF ₆₅₀	153
5.11. Development of cadmium selenide nanoparticles using silver nanoparticle seeds stabilized by AIPUs.	156
5.12. UV-Vis spectra of CdSe nanoparticles recovered at different reaction times.	157
5.13. A representative X-ray diffraction pattern of cadmium selenide nanoparticles synthesized using nanosilver seeds.....	158
5.14. Size distribution of cadmium selenide nanoparticles developed using nanosilver seeds. .	159
5.15. TEM micrograph of cadmium selenide nanoparticles.	159
6.1. Adsorption isotherm of S10 and D10 on hydrophilic (A) and hydrophobized (B) silica nanoparticles.	172
6.2. Adsolubilization of 2-naphthol by AIPE adsorbed on the surface of hydrophilic and hydrophobized silica nanoparticles.....	174
6.3. Amount of 2-naphthol adsolubilized into the adsorbed S10 and D10 layer on hydrophilic (A) and hydrophobized (B) silica.	175
6.4. Desorption of S10 and D10 from hydrophilic (A) and hydrophobized (B) silica nanoparticles versus feed polymer concentration.	176
6.5. Adsolubilized amount of 2-naphthol versus AIPE adsorption.	177
6.6. Polymer adsorption versus equilibrium polymer concentration at the first stage (adsorption of AIPES on hydrophilic (A) and hydrophobic (B) silica substrate).	178
6.7. Polymer adsorption versus equilibrium polymer concentration at the second stage (adsolubilization of 2-naphthol on hydrophilic (A) and hydrophobic (B) silica substrate).....	179
6.8. Development of silicon through the use of cyclohexasilane.	181
6.9. Interaction between CHS and S6 macromolecules in acetonitrile (A) and in benzene (B).	182
6.10. A representative Raman spectrum of electrospun CHS/S6/PMMA wires.	185

6.11. SEM micrograph of electrospun wires developed from the CHS/PMMA composition. ..	186
6.12. SEM micrographs of wires electrospun from ink 1 (S6:CHS:PMMA as 0.5:5:10) and subjected to different post-treatment types: Sample I (A, B), Sample II (C, D), Sample III (E), and Sample IV (F).....	187
6.13. SEM micrographs of wires electrospun from ink 2 (S6:CHS:PMMA as 1:5:10) and subjected to different post-treatment types: Sample I (A), Sample II (B), and Sample IV (C, D).	188

LIST OF ABBREVIATIONS

2,4-TDI.....	2,4-Tolylene Diisocyanate
AIP	Amphiphilic Invertible Polymer
AIPE.....	Amphiphilic Invertible Polyester
AIPE-1	Amphiphilic Invertible Polyester synthesized on the basis of poly(ethylene glycol) and aliphatic dicarboxylic acid
AIPE-2	Amphiphilic Invertible Polyester synthesized on the basis of poly(ethylene glycol) and polytetrahydrofuran
AIPU	Amphiphilic Invertible Polyurethane
BET.....	Brunauer-Emmett-Teller Theory
CHS.....	Cyclohexasilane
Cmc.....	Critical Micelle Concentration
DLS	Dynamic Light Scattering
DMEM	Dulbecco's Modified Eagle Medium
DMSO.....	Dimethyl Sulfoxide
FBS	Fetal Bovine Serum
FTIR.....	Fourier Transform Infrared Spectroscopy
GPC.....	Gel Permeation Chromatography
HBSS.....	Hank's Buffered Salt Solution
HLB.....	Hydrophilic-Lipophilic Balance
LCST.....	Lower Critical Solution Temperature
MDSC	Modulated Differential Scanning Calorimetry
M_n	Number Average Molecular Weight
MTT	3-[4,5-dimethylthiazol-2-yl]-2,5-diphenyltetrazolium bromide

M_w	Weight Average Molecular Weight
NIPAAm	<i>N</i> -Isopropylacrylamide
NMR	Nuclear Magnetic Resonance
PDI	Polydispersity Index
PEO	Poly(Ethylene Oxide)
PEG	Poly(Ethylene Glycol)
Pluronic®	Poly(ethylene oxide)-poly(propylene oxide)-poly(ethylene oxide) triblock copolymer
PMMA	Poly(Methyl Methacrylate)
PNIPAAm	Poly(<i>N</i> -Isopropylacrylamide)
PPO	Poly(Propylene Oxide)
PS	Polystyrene
PTHF	Polytetrahydrofuran
PVP	Poly(2-Vinyl Pyridine)
SANS	Small Angle Neutron Scattering
SEM	Scanning Electron Microscopy
TEM	Transmission Electron Microscopy
THF	Tetrahydrofuran
TOPSe	Trioctylphosphine Selenide
UCST	Upper Critical Solution Temperature
UV-vis	Ultraviolet-Visible Spectroscopy
XRD	X-Ray Diffraction

CHAPTER 1. INTRODUCTION: STIMULI-RESPONSIVE POLYMERS

1.1. Introduction to Stimuli-Responsive Polymers

Life is often considered as being polymeric *per se*: polymers such as polysaccharides, proteins, and nucleic acids are present as basic components in living cells.¹ One of the most prominent features of such biopolymers is their abrupt response to the slightest changes in external stimuli. Thus, very minor changes in one or several polymer properties occur in response to a varying parameter up to a certain critical point, at which a small change in a varying parameter triggers a drastic change in the dependent property. After the transition is completed, no significant further response is observed.² Hence, it is not surprising that unique responsive properties of biopolymers served as an inspiration for the scientists who strived to develop artificial materials with similar characteristics. Since then, synthetic polymers designed to mimic stimuli-responsive behavior have been developed into numerous categories to meet the requirements for different industrial and scientific uses. Based on their properties, these polymers have been called “stimuli-sensitive”,³ “stimuli-responsive”,⁴ “intelligent”,⁵ “smart”,⁶ or “environmentally sensitive” polymers.⁷ Stimuli-responsive polymer systems are able to recognize environmental stimulus as a signal, evaluate the signal magnitude, and then change their chain conformation in a fast response.⁸ The transformations on the molecular level, however, often lead to the visible transitions at the macroscopic level, revealing themselves as a change in solution color or turbidity, increase in the hydrogel degree of swelling, etc. The responses are revealed as changes in one or more of the following – solubility, shape, self-assembly, surface characteristics, sol-to-gel transition, etc.⁹ The transitions are also reversible, as the system returns to its original condition when the trigger is removed.²

Triggers that cause response of polymer systems are traditionally categorized as either physical or chemical stimuli.¹⁰ Physical stimuli such as temperature,¹¹ electric¹² or magnetic fields,¹³ light or radiation forces¹⁴ and mechanical stress affect polymer energy levels and change molecular interactions at critical onset points. Chemical stimuli (pH,^{15,16} moisture,¹⁷ solvents,¹⁸ change in ionic strength,¹⁵ addition of an oppositely charged polymer,¹⁹ polycation-polyanion complex formation,²⁰ and presence of metabolic chemicals²¹) alter the interactions between polymer chains or between polymer chains and solvents.¹⁰ A new type of stimuli, namely biochemical triggers, have been suggested as a separate category in recent publications;^{22,23} this type of stimuli involves responses to antigens, enzymes, ligands, and biochemical agents.⁶ Several polymer-based platforms are capable of responding to two or more trigger types. Thus, a range of temperature-responsive polymers have been also reported to be sensitive to pH shifts.²⁴⁻²⁷ Finally, so-called dual-responsive polymer systems are able to induce response upon exposure to two or more signal types.²⁸ The use of responsive polymer systems is especially promising in biomedical applications such as in biotechnology,^{2,4,29} drug delivery,³⁰⁻³² and chromatography of biological compounds.^{5,33}

1.2. Types of Stimuli-Responsive Polymeric Materials

Several “smart” system types have been developed and used in various forms (Figure 1.1), among the major ones being (1) stimuli-responsive (hydro)gels, (2) stimuli-responsive micelles, (3) stimuli-responsive surfaces and interfaces, (4) stimuli-responsive solutions, and (5) stimuli-responsive solids.

The mobility of responsive polymer chains varies greatly depending on the physical form of a “smart” material, thus affecting the extent of response achievable in them. Thus, spatial responsiveness is easily achievable with minimal energy inputs in the systems with high solvent

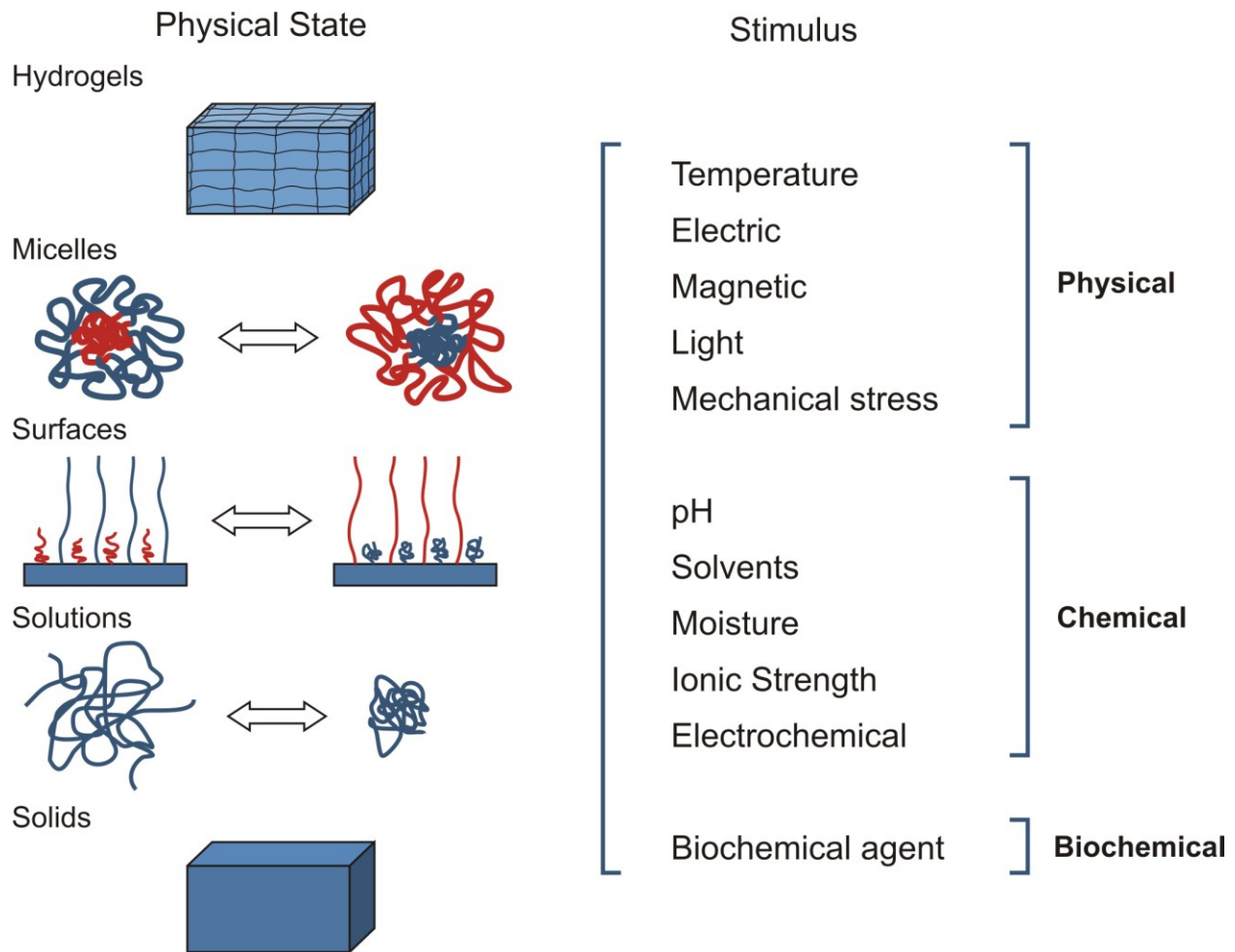


Figure 1.1. Principal types of responsive polymer systems, their dimensional changes, and types of stimuli they respond to.

(diluent) concentration. At the same time, dimensional response to external stimuli is limited in highly crosslinked or solid systems, therefore, a strategic principle in designing such systems is that very small dimensional changes on a molecular level should lead to extensive alteration of their physico-chemical properties.³⁴

Polymer hydrogels are three-dimensional crosslinked polymer networks, in which some chains are solvated by water that fills the interstitial sites, but the other fragments are linked with each other by means of chemical bonds or physical interactions. Hydrogels exhibit extraordinary

capacity (>20%) for absorbing water into a 3D polymeric network.³⁵ Hydrogels swell upon contact with aqueous medium, but they do not dissolve in water and maintain the three-dimensional structure after swelling. One of the easiest ways to adjust the dimensions of stimuli-responsive hydrogels is to monitor their swelling/deswelling behavior.³⁶ Control over swelling degree in a hydrogel can be achieved by stimuli-responsive adjustment of the balance between hydrophilicity and hydrophobicity of swollen polymer chains.^{37,38} Hence, stimuli-responsive behavior of this hydrogel type, namely dramatic changes in the swelling degree according to the change in external stimulus, is realized through incorporation of responsive fragments into the 3D polymer system.

Responsive behavior of the other hydrogel types is achieved due to a phase change rather than a dimension change. Thus, altering hydrophobic interactions of crosslinked hydrogel areas in an aqueous environment due to changes in external stimuli could lead to a reversible sol-gel transition.^{39,40} Side chains of hydrogels could be modified to undergo temperature-dependent order-disorder transitions associated with the formation of crystalline aggregates. Such behavior is often triggered in shape memory gels that can be deformed and then restored to the original shape upon exposure to external stimuli.⁴¹

Polymeric micelles comprise another significant type of stimuli-responsive polymer systems. Micelles are formed as a result of self-assembly of amphiphilic polymers due to incompatibility of macromolecular fragments or better solvation of one of the fragments by a solvent.⁴² Up to now, stimuli-responsive micelles have been designed using the two major approaches. According to the first one, stimuli-responsive components are incorporated in the hydrophilic or hydrophobic fragments of an amphiphilic polymer resulting in stimuli-responsive inner or outer parts of the micellar structures.^{43,44} The other approach uses stimuli-responsive

change of the micellar hydrophilic-lipophilic balance to trigger reversible micellization/demicellization.^{45,46} Noteworthy, micelles can form hydrogels above a certain high concentration known as micelle gelation concentration, therefore, the task of distinguishing reversible micelles from reversible hydrogels is sometimes problematic.⁴⁷

Highly responsive surfaces and interfaces are often fabricated by functionalizing substrates such as metals,⁴⁸ polymers,^{26,49} or inorganic materials^{50,51} with stimuli-responsive polymers. Such substrate functionalization is achieved by (1) spontaneous formation of a responsive surface (often observed in polymer blends, where one of the components has responsive behavior), (2) grafting thin films (also called brushes) of responsive polymer onto the surface; (3) depositing thin responsive polymer films using a variety of methods.⁵² Responsive polymer surfaces could change their wettability and permeability, as well as their adhesive, adsorptive, mechanical and optical properties upon exposure to external stimuli. Such polymer films could be designed to rapidly switch wetting (from wettable to non-wettable), adhesion to certain materials (from sticky to non-sticky surfaces), transparency, appearance, etc.⁵²

The solubility of responsive polymers can also be adjusted by external stimuli. Combination of stimuli-responsive polymers with different conjugate molecules can lead to materials with stimuli-sensitive solubility. Polymer conjugates can be developed through the use of covalent bonding^{48,50,53} or secondary bonding such as electrostatic forces⁵⁴ or hydrophobic interactions.⁵⁵ After the conjugation of a responsive polymer with conjugate molecules such as proteins or drugs, the activity of the conjugate molecules is greatly dependent on changes in polymer hydrophilicity or hydrophobicity that could be induced by external stimuli.¹⁰

Designing stimuli-responsive solid polymers represents a challenge due to the limited amount of free volume in such materials.³⁴ In order to improve elasticity of stimuli-sensitive

solids, responsive constituents are often combined with other fragments which provide higher free volume content.^{56,57} Thus, copolymerization of lower T_g components with stimuli-responsive segments is frequently used during fabrication of stable thermoplastic solid networks with responsive properties.^{58,59} In this case, it is the presence of localized “voids” in the polymer network that provides space for rearrangements of polymeric chains upon exposure to certain stimuli.

Another method of developing stimuli-responsive solid polymer materials is the use of multicomponent systems with different surface energy components. In such systems, a low surface energy constituent is located at the surface of the material, while the component with the high surface energy is buried underneath.⁶⁰⁻⁶³ A certain stimulus triggers rearrangements in polymer chains that lead to migration of the high surface energy components to the surface of the material.⁶⁴ A similar approach uses stratification across the film thickness as a method to develop phase-separated materials capable of responding to temperature, pH, and ionic strength.^{65,66}

1.3. Temperature-Responsive Polymers

Temperature is arguably the most widely used type of stimulus used to trigger changes in environmentally responsive polymer systems. Changes in temperature are easy to control and apply both *in vivo* and *in vitro*, therefore temperature-responsive polymers have found a variety of applications in the biomedical field.^{10,67,68} In the aqueous solution, temperature-responsive polymers often exhibit a critical solution temperature at which the system experiences phase separation. If a polymer solution is monophasic above a specific temperature and undergoes phase separation below it, the temperature at which a phase transition occurs is known as an upper critical solution temperature (UCST) or a higher critical solution temperature (HCST). In contrast, if a system forms one phase below a certain temperature and is biphasic above it, it

possesses a so called lower critical solution temperature (LCST) also known as a cloud point. The LCST or UCST-associated phase transition is completely reversible, and the critical solution temperature is known to be dependent on polymer composition, concentration, and molecular weight.⁶⁹

Poly(*N*-isopropylacrylamide) (PNIPAAm) is a typical example of a polymer that exhibits LCST behavior in the aqueous solution (Figure 1.2).⁷⁰ The polymer is soluble in the aqueous solution below 32 °C due to the hydrophilic interactions caused by hydrogen bonding. Above this temperature, hydrophobic interactions become dominant and phase separation occurs.⁷¹

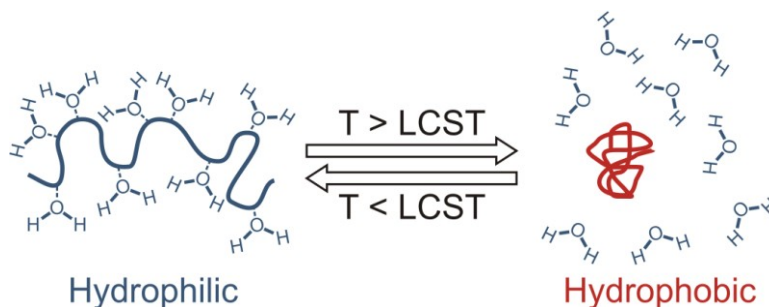


Figure 1.2. LCST-associated response of PNIPAAm.

The other type of temperature-responsive behavior in the aqueous medium is based on the intermolecular interactions that could cause polymer self-assembly, hydrogel shrinkage, or physical crosslinking. Thus, temperature-dependent micellization of poly(ethylene oxide)-poly(propylene oxide)-poly(ethylene oxide) (PEO–PPO–PEO) triblock copolymers commonly known as Pluronics® or Poloxamers is caused by hydrophobic interactions leading to aggregation of poly(propylene oxide) fragments above a critical micelle temperature (CMT).⁷²

1.3.1. Thermoresponsive Polymers Exhibiting LCST

The LCST can be defined as the temperature at which a polymer solution undergoes phase separation from one phase to two phases. The transition is related to change from the

enthalpy-controlled behavior (below the LCST) to the entropy-controlled one (above the LCST) that causes polymer precipitation. The polymer LCST can be tailored by incorporating different hydrophilic or hydrophobic fragments in polymer structure. Thus, copolymerization of NIPAAm with the hydrophilic acrylamide causes an increase in LCST from ca. 32 °C up to ca. 45 °C for a copolymer containing 18% acrylamide. In contrast, copolymerization of NIPAAm with a hydrophobic *N-tert*-butyl acrylamide (*N-t*BAAm) resulted in decrease of LCST up to ca. 10 °C when the monomer ratio in a synthesized copolymer was as 3 : 2, respectively.⁶

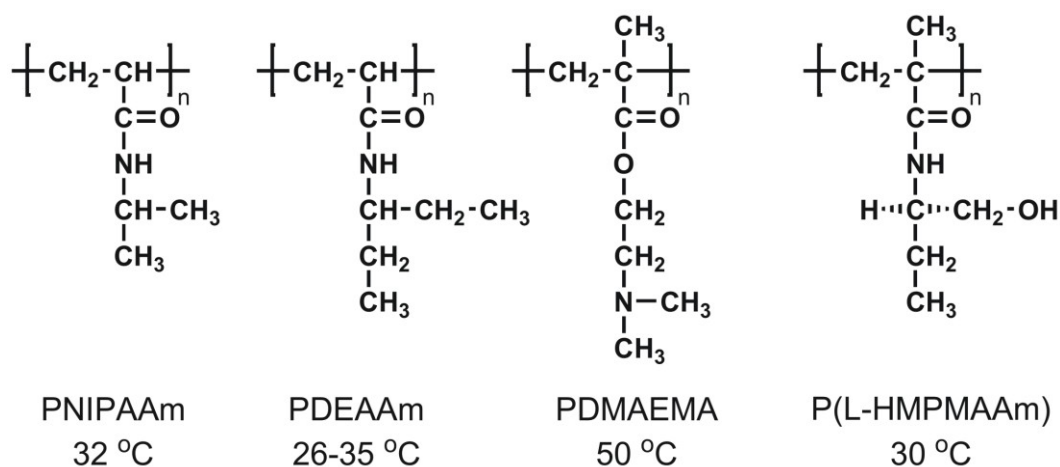


Figure 1.3. Structures and lower critical solution temperatures of several LCST-based thermoresponsive polymers.

Poly(*N*-substituted acrylamides) are the most widely used type of the LCST-based thermoresponsive polymers (Figure 1.3). Changing the chemical structure of the side chains has allowed varying polymer lower critical solution temperature in the range of several dozens of degrees. Among the poly(*N*-substituted acrylamides), PNIPAAm is the most widely studied, since it exhibits a phase transition in water at ca. 32 °C, i.e. close to human body temperature.⁷³ The temperature-responsive behavior of PNIPAAm and PNIPAAm-based copolymers has been targeted in numerous publications in order to understand the mechanism of thermal sensitivity

and to use PNIPAAm-based materials in specific applications.^{70,74-77} The other types of temperature-sensitive polymers include poly(*N*-vinyl alkylamides) such as poly(*N*-vinyl caprolactam) with the LCST of ca. 34–36 °C and poly(*N*-vinyl isobutyramide) with the transition temperature of 39 °C, poly(*N*-vinyl piperidine) (LCST ca. 4–5 °C), poly(ethylene glycol) (LCST ca. 100 °C), etc. Increasing hydrophilicity of the thermoresponsive polymer commonly tends to increase LCST, while the use of hydrophobic comonomers or incorporation of hydrophobic fragments into the polymer structure has the opposite effect.

Deswelling behavior of PNIPAAm-based polymers could be controlled by manipulating polymer architectures. Grafted hydrogels developed from the graft copolymers such as poly(NIPAAm-*graft*-PEG)⁷⁸ or crosslinked PNIPAAm grafted with oligoNIPAAm⁷⁹ demonstrated a rapid response to a change of temperature. Acceleration of thermoresponsive deswelling has been also successfully achieved in hydrogels prepared via copolymerization of NIPAAm with acrylic acid (AA),⁷⁸ or by grafting hydrophilic chains onto PNIPAAm hydrogel networks.⁸⁰ By incorporating oligomer fragments with different LCSTs, polymer systems with more than one swelling transition could be fabricated.⁸¹

The recent studies of NIPAAm copolymers have been predominantly focused on biological applications of these thermoresponsive materials. Among the other uses, they have been probed in development of bioconjugates, gene delivery, tissue engineering, enzyme immobilization, bioseparation, and cell culture.^{6,82-85} Despite PNIPAAm itself suffers from poor biodegradability, this drawback has been overcome by combining this polymer with biodegradable systems, such as gelatin, ethylcellulose, poly(amino acids), etc.^{76,86,87} Thermally-sensitive behavior of PNIPAAm-based hydrogels has been also used to control drug release using a temperature on-off profile in controlled drug delivery systems.⁸⁸

1.3.2. Thermoresponsive Amphiphilic Block Copolymers

Several types of amphiphilic block copolymers are known to exhibit temperature-responsive micellization behavior and sol-gel transitions. The most well-studied thermoresponsive polymers of this type are PEO–PPO block copolymers commercially known as Pluronics® (Poloxamers) and Tetronics® (Figure 1.4). At high concentration in the aqueous solution PEO–PPO block copolymers exhibit a sol-gel phase transition slightly below the body temperature, a gel-sol transition at ca. 50°C, and an LCST.⁸⁹ Their gelation temperature depends on polymer composition and concentration. For example, a 20% aqueous solution of a Pluronic F127 forms a gel at 37 °C.⁹⁰

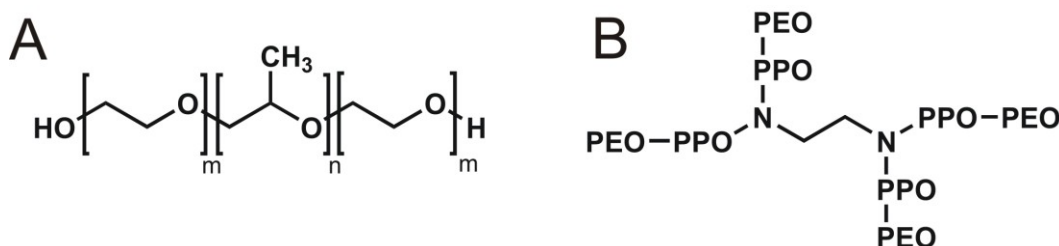


Figure 1.4. Chemical structures of PEO–PPO amphiphilic block copolymers: (A) Pluronics® and (B) Tetronics®.

One of the ways to obtain the desired performance from thermoresponsive block copolymers is by substituting PPO block with the other hydrophobic fragments. Thus, the replacement of the PPO segment with a poly(1,2-butylene oxide) (PBO) block resulted in a dramatic decrease of the polymer critical micelle concentration (cmc), i.e. a concentration at which polymer molecules start self-assembling into micelles.⁹¹ The non-biodegradability of the PEO–PPO block copolymers has been addressed by substituting PPO block with biodegradable poly(*L*-lactic acid) (PLLA) and (*DL*-lactic acid-*co*-glycolic acid) (PLGA).^{92,93} The other types of

biodegradable thermoresponsive amphiphilic block copolymers include cyclotriphosphazenes and poly(organophosphazenes) modified with poly(ethylene glycol) and amino acid esters.^{94,95}

Thermoresponsive amphiphilic copolymers have found industrial applications as detergents, foaming agents and emulsifiers.^{96,97} The biocompatibility of Pluronics has led to many applications of these polymers in the medical and pharmaceutical fields.⁹⁸ Thus, they have been used for wound healing,⁹⁹ cartilage restoration,¹⁰⁰ and as *in situ* drug depots for controlled delivery systems.¹⁰¹⁻¹⁰³ The potential use of Pluronics as an artificial skin has also been reported.¹⁰⁴ Extended drug release profiles have been detected for PEG-PLGA-PEG triblock copolymers with release of hydrophobic drugs lasting up to two months.¹⁰⁵

Synthetic block copolypeptides composed of both hydrophilic and hydrophobic fragments share the similar design philosophy with synthetic block copolymers and also demonstrate temperature sensitivity. In the aqueous solution synthetic polypeptides form hydrogels even at low concentration due to the formation of α -helix conformations.¹⁰⁶ Variation of the hydrophobic building blocks has been used as a tool to control random coil secondary structure of polypeptides.¹⁰⁷ Other synthetic strategies leading to synthetic polypeptides explore the benefits of using recombinant DNA methods. Designed polypeptides have been claimed to undergo conformational changes in response to both temperature and pH.¹⁰⁸

1.3.3. Thermoresponsive Biopolymers

Thermoresponsive behavior has been detected for several types of biopolymers as well. Among the others, agarose, gelatin, and gellan develop helix conformations leading to temperature controlled physical crosslinking and gelation.^{109,110} However, hydrogels formed from these biopolymers often suffer from poor mechanical properties and the use of chemical crosslinkers is required to improve the physical stability of the gel. The formed crosslinks,

however, frequently affect the responsive properties of the hydrogels in an adverse way. Thus, irreversible thermal transition of crosslinked gelatin has been reported: after heating had destroyed gelatin helix structures, no gelation was observed upon cooling the sample back.¹¹⁰

Temperature-controlled complex formation from biopolymer and another biopolymer(s),¹¹¹ surface active compound,¹¹² or salts¹¹⁰ in the aqueous solution has been described. Thermoresponsive complexation has been reported to cause a volume change or a sol-gel transition. Thus, aqueous solutions of chitosan/polyol salt system underwent gelation upon heating to the body temperature, a feature that was used to deliver biologically active growth factors and to form an encapsulating matrix for tissue engineering applications.¹¹¹ In contrast, reversible formation of thermoresponsive gels from the mixtures of pectin and chitosan upon lowering the temperature has been reported.¹¹³ Gelation temperature has been shown to increase with increasing pectin concentration. The authors claimed that the development of crosslinking junctions between pectin and chitosan molecules under gelation temperature was the driving force for a reversible gelation process.

1.4. pH-Responsive Polymers

The group of pH-responsive polymers consists of the polymers for which response is triggered by increasing or decreasing the net charge of the molecule. pH-Responsive macromolecules contain ionizable functional groups that are capable of donating or accepting protons upon changes in pH.¹¹⁴ Due to the presence of multiple ionizable groups, such polymers are considered polyelectrolytes. When pH of the medium reaches a certain value equal to the inverse logarithm of the dissociation constant of an ionizable group (pK_a for the acidic groups or pK_b for the basic fragments), a sudden change of the degree of ionization occurs. The rapid change in overall charge of the pH-responsive polyelectrolyte causes a drastic change in the

hydrodynamic volume which, in turn, leads to conformational changes in the polymer macrochain.³⁴ It is believed that polymer conformation is changed due to the osmotic pressure applied on the pH-responsive macromolecule by mobile counterions that neutralize the polymer charge.^{10,115}

Two principal types of the pH-responsive polymers exist: weak polyacids and weak polybases. Weak polyacids, for example poly(acrylic acid) (PAAc), are protonated at low pH and become negatively ionized at neutral and high pH.¹¹⁶ In contrast, polybases such as poly(4-vinylpyridine) accept protons at high pH and release them at neutral and low pH.²⁷ Two key approaches towards tuning the pH range that triggers the polymer phase transition exist: (1) incorporating ionizable fragments with the dissociation constant (pK_a or pK_b) that matches the targeted pH range, and (2) modification of polyelectrolyte with hydrophobic fragments with careful control over their chemical properties, concentration, and distribution along the macrochain.⁹⁰ The first approach is usually carried out by combining several different ionizable fragments to gain control over pH-responsive properties. The second strategy includes designing polyelectrolyte chains consisting of several types of ionizable and hydrophobic monomers. When the charge of ionizable fragments is neutralized, electrostatic repulsion forces disappear and the properties of pH-sensitive polymers are governed by hydrophobic interactions. Hence, adjusting the nature of the hydrophobic fragments is a useful way to tune polymer conformation in the uncharged state.

1.4.1. pH-Responsive Polyacids

Poly(carboxylic acids) with pK_a values ranging from 4 to 8 are the most typical examples of pH-sensitive polymers bearing anionic groups (Figure 1.5A). Frequently used polyacids such as poly(acrylic acid) and poly(methacrylic acid) (PMAAc) dissociate into protons and

carboxylate anions at high (basic) pH and accept protons at low (acidic) pH.¹¹⁷ Weak polyacids become polyelectrolytes at high pH and interactions between the macromolecules become governed by electrostatic repulsion forces between the negative charges of the COO^- groups. The rapid change of the nature of intermolecular interactions from primarily hydrophobic to primarily electrostatic and vice versa provides the necessary driving force for dissolution/precipitation of macromolecular chains, hydrophilicity/hydrophobicity of the surface, or swelling/deswelling behavior in hydrogels.¹⁰ Increasing hydrophobicity of polyacids causes them to adopt a more compact macromolecular conformation in the uncharged state and undergo a more abrupt phase transition upon changing pH.¹¹⁸

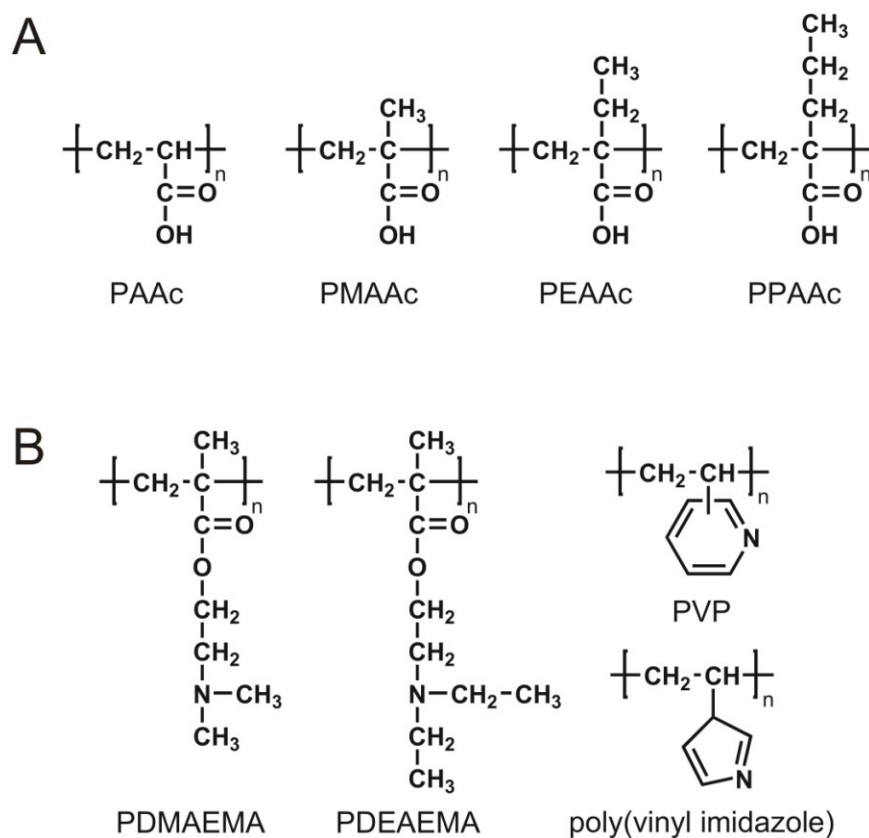


Figure 1.5. Chemical structures of pH-responsive polyacids (A) and polybases (B).

Other examples of pH-sensitive polymers are the derivatives of *p*-aminobenzene sulfonamide, polysaccharides containing carboxylic groups, synthetic polypeptides, etc.¹⁰

1.4.2. pH-Responsive Polybases

The examples of weak pH-responsive polybases include polymers such as poly(*N,N'*-dimethyl aminoethyl methacrylate) (PDMAEMA) and poly(*N,N'*-diethyl aminoethyl methacrylate) (PDEAEMA) (Figure 1.5B). Due to the presence of amino groups in the macromolecules, such polymers form positively charged ammonium salts during interaction with protons at acidic pH and release protons under basic conditions to form the free amine. As in the case of polyacids, longer hydrophobic fragments in polyamine molecules cause stronger hydrophobic interactions in the neutral state and lead to more compact macromolecular conformations.¹¹⁹ Amine-containing polymers such as poly(vinylimidazole) (PVI),¹²⁰ poly(vinylpyridine) (PVP),¹²¹ and poly(*N*-acryloyl-*N'*-alkylpiperazine)¹²² have been also reported to have pH-responsive properties. Quaternized poly(propylene imine) dendrimers have been probed as pH-sensitive controlled release systems.¹²³

1.5. Other Types of Stimuli-Responsive Polymers

1.5.1. Moisture- and Solvent-Responsive Polymers

Water molecules are known to increase the flexibility of certain polymer chains due to the plasticizing effect.¹²⁴ If such polymer had previously been deformed, exposure to water could cause the recovery of its shape, a feature used in moisture-responsive shape memory polymers. Shape recovery rate can be greatly improved if the polymer contains hydrophilic or water-soluble units in the macromolecule.¹²⁵ Thus, incorporation of pyridine fragments (that are responsive to water) has been used to significantly accelerate and improve strain recovery in

shape memory polyurethanes.¹²⁶ Using the proposed approach, shape memory polymers sensitive to suitable organic solvents can be developed.¹²⁷

1.5.2. Photoresponsive Polymers

Polymeric materials with incorporated photochromic fragments or chromophores exhibit conformational changes in response to light. In turn, photochromism is defined as a reversible change of chemical species between two states having distinguishable light absorptions in different regions induced in one or both directions by electromagnetic radiation.¹²⁸ The introduction of photochromic moieties triggers changes in physical and/or chemical properties of photoresponsive polymers upon irradiation.³⁴

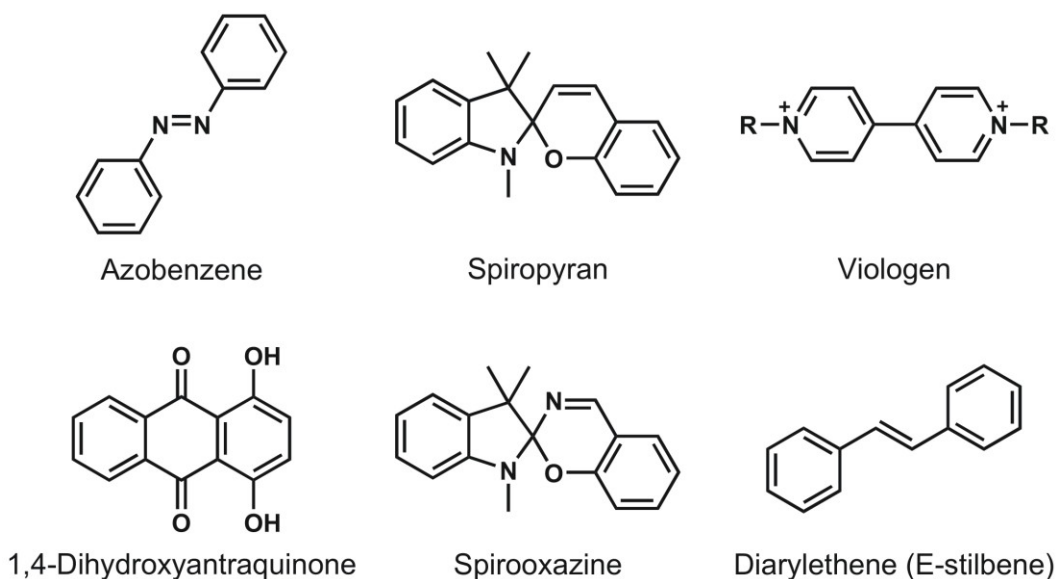


Figure 1.6. Structures of typical photochromic compounds used in responsive polymers.

Typical organic photochromic compounds include azobenzenes, spirooxazines, spiropyrans, viologens, fulgides, 1,4-dihydroxyanthraquinone, and diarylethenes (Figure 1.6). They fall into three general categories based on different photochromism types: (1) isomerization of molecules, (2) ionization of molecules, and (3) redox reaction of molecules.¹²⁹

Photoresponsive polymeric materials have found a variety of applications in photo-optical media,

photomechanical systems, photoswitches, micropatterning, nonlinear optical media, and clothing.¹²⁹⁻¹³¹

1.5.3. Field-Responsive Polymers

Field-responsive polymers are capable of executing mechanical work (expansion, contraction, elongation, and bending) upon exposure to an electric or magnetic field. The use of an electric or magnetic field as an external stimulus is advantageous, since a precise control over the field magnitude and a rapid and controllable shape change could be achieved.¹³²

The characteristics of field-responsive polymer materials include easy actuation, quick and simple miniaturization, low noise, and mechanical properties similar to those of biological systems.¹³³ Polymers with field-responsive fragments have been applied in mechanical engineering and the biomedical area as contact lenses, sensors, drug delivery systems, artificial muscles, and biomimetic actuators.¹³⁴⁻¹³⁶

1.5.4. Antigen-Responsive Polymers

Recently, a reversible antigen-responsive polymer network has been fabricated via immobilization of antigen (rabbit immunoglobulin G, IgG) and the corresponding antibody (goat anti-rabbit IgG) onto the semi-interpenetrating polymer network.¹³⁷ The attached antibody exhibited a higher binding ability to the free antigen compared to the attached antigen. Therefore, exposure of antigen-responsive polymer network to the free antigen caused hydrogel swelling by breaking non-covalent crosslinks between the attached antigen and antibody. It was claimed that the antigen-responsive property of the developed polymer network could be useful in applying the material as a component of a drug delivery system.¹³⁷

1.6. Application of Stimuli-Responsive Polymers

Nowadays, stimuli-responsive polymers are used in applications ranging from household goods to nanochemistry and nanotechnology. A number of applications for these functional materials are listed below.

1.6.1. Smart and Self-Healing Coatings

Responsive polymer materials are a tool of choice for tailoring structures and properties of smart coatings.⁶⁵ After applying a composition to the substrate, external stimuli could be used to affect the phase separation and self-assembly of the components in the composition to attain a coating with programmed properties. For example, this method has been already used to develop superhydrophobic surfaces by film stratification.¹³⁸ Furthermore, anti-corrosive coatings with self-healing capabilities fabricated using the layer-by-layer deposition could be developed using polymers that respond to changes in a corrosive environment (i.e. high ionic strength).¹³⁹

1.6.2. Biomimetic Micro- and Nanoactuation

Thin films developed from light-, pH-, and temperature-responsive polymers have been used for micro- and nanoactuation, i.e. transforming chemical energy directly into mechanical work. The reported actuation mechanisms for flexible responsive structures are based on wetting/dewetting, swelling/deswelling, or adsorption/desorption of polymer surface layers.¹⁴⁰ In the future, biomimetic actuators could be used as the basis for “soft” machines designed using biological rather than mechanical principles.²

1.6.3. Biointerfaces and Bioseparation

Stimuli-responsive polymer biointerfaces are useful from several points of view.⁵² First, the use of stimuli-responsive polymers enables tailoring adhesion between stimuli-responsive materials and proteins and cells.¹⁴¹ Second, exposure and masking of functional groups of

responsive polymers at the biointerface (which is very important for the presentation of regulatory signals and modulation of activity of the biomolecules) is possible to achieve using a stimuli-responsive mechanism.¹⁴² Third, accurate dynamic control over the permeation of chemicals through polymeric nanoporous membranes as well as interaction of biomolecules and ions with responsive surfaces are supposed to improve polymer separation.¹⁴³ The use of stimuli-responsive polymers grafted on the membrane surface provides an exciting opportunity to control drug permeation through nano- and microporous membranes.

1.6.4. Catalysis

Stimuli-responsive polymers have been successfully applied in both conventional catalysis and biocatalysis.^{144,145} Conjugation of stimuli-responsive polymers with catalytic nanoparticles or enzymes could thus create new opportunities for bio- and chemical technologies. Thus, incorporation of catalytically active nanoparticles in a stimuli-responsive polymer matrix allows for careful control over the nanoparticle catalytic activity by exposing or hiding nanoparticle catalyst as a response to changes in external stimuli.¹⁴⁶ When enzymes are linked to responsive polymer chains, changes in the polymer conformation due to effect of the environmental stimuli can significantly affect both enzyme activity and access of the substrate to the enzyme molecule. A wide range of pH- and thermally-sensitive polymers have been used to develop reversibly-soluble biocatalysts. In the soluble state, such catalysts accelerate an enzymatic reaction; after the reaction is complete, an environmental trigger causes the precipitation of the polymer thus enabling separation of the enzyme catalyst.^{147,148}

1.6.5. Drug Delivery Systems

Application of stimuli-responsive polymers in drug carriers has enormous potential due to the possibility to achieve stimuli-responsive drug release and improve the drug release profile

to mimic biological demand.² An ideal “smart” drug delivery polymeric system is assumed to provide prolonged *in vivo* circulation, successfully deliver the cargo drug to the target tissue, completely release the drug into the target cell, and match the desired kinetics of the release.⁵² Enhanced drug release profile is usually achieved in response to changes in pH, glutathione concentration, or the presence of enzymes specific to certain target cells.^{149,150}

1.7. Research Scope

Even though the use of responsive polymers becomes more and more widespread, little attention is paid to studying self-assembly and environment-dependent rearrangement in responsive polymers triggered by the polarity of the medium. The current work aims at improving the existing situation by developing novel responsive functional polymeric materials by manipulating environment-dependent self-assembly of a new class of responsive macromolecules – amphiphilic invertible polymers (AIPs). AIPs described in the study are strategically designed to ensure a broad range of their surface activity, self-assembly behavior, and invertible properties of micellar assemblies developed from these polymers.

Amphiphilic invertible polymers are expected to self-assemble into micellar assemblies in the media differing by polarity. AIP invertible micellar assemblies are expected to be functional in polar and nonpolar media (including interfaces) where they could be used in a broad range of applications.

1.8. References

1. Kirsebom, H.; Galaev, I.Y.; Mattiasson, B. *J. Polym. Sci. Part B Polym. Phys.* **2011**, *49*, 173–178.
2. Galaev, I.Y.; Mattiasson, B. *Trends Biotechnol.* **1999**, *17*, 335–340.
3. Lendlein, A.; Shastri, V.P. *Adv. Mater.* **2010**, *22*, 3344–3347.

4. Jeong, B.; Gutowska, A. *Trends Biotechnol.* **2002**, *20*, 305–311.
5. Kikuchi, A.; Okano, T. *Progr. Polym. Sci.* **2002**, *27*, 1165–1193.
6. Hoffman, A.S.; Stayton, P.S.; Bulmus, V.; Chen, G.; Jinping, C.; Chueng, C.; et al. *J. Biomed. Mater. Res.* **2000**, *52*, 577–586.
7. Qiu, Y.; Park, K. *Adv. Drug Delivery Rev.* **2001**, *53*, 321–339.
8. Okano, T., Ed. *Biorelated polymers and gels*; Academic Press: San Diego, CA, 1998.
9. Kumar, A.; Srivastava, A.; Galaev, I.Y.; Mattiasson, B. *Prog. Polym. Sci.* **2007**, *32*, 1205–1237.
10. Gil, E.S.; Hudson, S.M. *Prog. Polym. Sci.* **2004**, *29*, 1173–1222.
11. Okano, T. In *Responsive Gels: Volume Transitions II*; Dušek, K., Ed.; Advances in Polymer Science, Vol. 110; Springer: Berlin, 1993; pp 180–197.
12. Filipcsei, G.; Feher, J.; Zrinyi, M. *J. Mol. Struct.* **2000**, *554*, 109–117.
13. Zrinyi, M. *Colloid. Polym. Sci.* **2000**, *278*, 98–103.
14. Juodkazis, S.; Mukai, N.; Wakaki, R.; Yamaguchi, A.; Matsuo, S.; Misawa, H. *Nature* **2000**, *408*, 178–181.
15. Twaites, B.R.; de las Heras Alarcón, C.; Cunliffe, D.; Lavigne, M.; Pennadam, S.; Smith, J.R.; Górecki, D.C.; Alexander, C. *J. Controlled Release* **2004**, *97*, 551–566.
16. Feil, H.; Bae, Y.H.; Feijen, T.; Kim, S.W. *Macromolecules* **1992**, *25*, 5228–5230
17. Yang, B.; Huang, W.M.; Li, C.; Li, L. *Polymer* **2006**, *47*, 1348–1356.
18. Siegal, R.A.; Firestone, B.A. *Macromolecules* **1988**, *21*, 3254–3259.
19. Kabanov, V.A. *Polym. Sci.* **1994**, *36*, 143–156.
20. Leclercq, L.; Boustta, M.; Vert, M. *J. Drug Target.* **2003**, *11*, 129–138.
21. Lomadze, N.; Schneider, H.-J. *Tetrahedron Lett.* **2005**, *46*, 751–754.

22. Mano, J.F. *Adv. Eng. Mater.* **2008**, *10*, 515–527.
23. Alexander, C.; Shakesheff, K.M. *Adv. Mater.* **2006**, *18*, 3321–3328.
24. Gan, L.H.; Gan, Y.Y.; Deen, G.R. *Macromolecules* **2000**, *33*, 7893–7897.
25. Bignotti, F.; Penco, M.; Sartore, L.; Peroni, I.; Mendichi, R.; Casolaro, M.; D'Amore, A. *Polymer* **2000**, *41*, 8247–8256.
26. Peng, T.; Cheng, Y.L. *Polymer* **2001**, *41*, 2091–2100.
27. Pinkrah, V.T.; Snowden, M.J.; Mitchell, J.C.; Seidel, J.; Chowdhry, B.Z.; Fern, G.R. *Langmuir* **2003**, *19*, 585–590.
28. Kurisawa, M.; Yui, N. *J. Controlled Release* **1998**, *54*, 191–200.
29. Sharma, S.; Kaur, P.; Jain, A.; Rajeswari, M.R.; Gupta, M.N. *Biomacromolecules* **2003**, *4*, 330–336.
30. Gupta, P.; Vermani, K.; Garg, S. *Drug Discov. Today* **2002**, *7*, 569–579.
31. Sershen, S.; West J. *Adv. Drug Delivery Rev.* **2002**, *54*, 1225–1235.
32. Weidner, J. *Drug Discov. Today* **2001**, *6*, 1239–1248.
33. Anastase-Ravion, S.; Ding, Z.; Pelle, A.; Hoffman, A.S.; Letourneur, D. *J. Chromatogr. B* **2001**, *761*, 247–254.
34. Liu, F.; Urban, M.W. *Prog. Polym. Sci.* **2010**, *35*, 3–23.
35. Bajpai, A.K.; Shukla, S.K.; Bhanu, S.; Kankane, S. *Prog. Polym. Sci.* **2008**, *33*, 1088–1118.
36. Kopeček, J. *Biomaterials* **2007**, *28*, 5185–5192.
37. Annaka, M.; Tanaka, C.; Nakahira, T.; Sugiyama, M.; Aoyagi, T.; Okano, T. *Macromolecules* **2002**, *35*, 8173–8179.

38. Varga, I.; Gilanyi, T.; Meszaros, R.; Filipcsei, G.; Zrinyi, M. *J. Phys. Chem. B* **2001**, *105*, 9071–9076.
39. Jeong, B.; Lee, K.M.; Gutowska, A.; An, Y.H. *Biomacromolecules* **2002**, *3*, 865–868.
40. Vercruyse, K.P.; Li, H.; Luo, Y.; Prestwich, G.D. *Biomacromolecules* **2002**, *3*, 639–643.
41. Osada, Y.; Matsuda, A. *Nature* **1995**, *376*, 219.
42. Kohut, A.; Kudina, O.; Dai, X.; Schulz, D.L.; Voronov, A. *Langmuir* **2011**, *27*, 10356–10359.
43. Kohori, F.; Yokoyama, M.; Sakai, K.; Okano, T. *J. Controlled Release* **2002**, *78*, 155–163.
44. Neradovic, D.; van Nostrum, C.F.; Hennink, W.E. *Macromolecules* **2001**, *34*, 7589–7591.
45. Zhang, R.; Liu, J.; He, J.; Han, B.; Zhang, X.; Liu, Z.; Jiang, T.; Hu, G. *Macromolecules* **2002**, *35*, 7869–7871.
46. Lin, H.; Cheng, Y. *Macromolecules* **2001**, *34*, 3710–3715.
47. Okabe, S.; Sugihara, S.; Aoshima, S.; Shibayama, M. *Macromolecules* **2002**, *35*, 8139–8146.
48. Nath, N.; Chilkoti, A. *J. Am. Chem. Soc.* **2001**, *123*, 8197–8202.
49. Magoshi, T.; Ziani-Cherif, H.; Ohya, S.; Nakayama, Y.; Matsuda, T. *Langmuir* **2002**, *18*, 4862–4872.
50. Rama, Rao G.V.; Krug, M.E.; Balamurugan, S.; Xu, H.; Xu, Q.; Lopez, G.P. *Chem. Mater.* **2002**, *14*, 5075–5080.
51. Kohut, A.; Ranjan, S.; Voronov, A.; Peukert, W.; Tokarev, V.; Bednarska, O.; Gevus, O.; Voronov, S. *Langmuir* **2006**, *22*, 6498–6506.

52. Stuart, M.A.; Huck, W.T.; Genzer, J.; Müller, M.; Ober, C.; Stamm, M.; Sukhorukov, G.B.; Szleifer, I.; Tsukruk, V.V.; Urban, M.; Winnik, F.; Zauscher, S.; Luzinov, I.; Minko, S. *Nat. Mater.* **2010**, *9*, 101–113.
53. Ohya, S.; Nakayama, Y.; Matsuda, T. *Biomacromolecules* **2001**, *2*, 856–863.
54. Bennis, J.M.; Choi, J.; Mahato, R.I.; Park, J.; Kim, S.W. *Bioconjug. Chem.* **2000**, *11*, 637–645.
55. Leroux, J.; Roux, E.; Garrec, D.L.; Hong, K.; Drummond, D.C. *J. Controlled Release* **2001**, *72*, 71–84.
56. Falsafi, A.; Tirrell, M. *Langmuir* **2000**, *16*, 1816–1824.
57. Ghosh, B.; Urban, M.W. *Science* **2009**, *323*, 1458–1460.
58. Liu, F.; Urban, M.W. *Macromolecules* **2008**, *41*, 6531–6539.
59. Liu, F.; Urban, M.W. *Macromolecules* **2008**, *41*, 352–360.
60. Crevoisier, G.; Fabre, P.; Corpart, J.M.; Leibler, L. *Science* **1999**, *285*, 1246–1249.
61. Lewis, K.B.; Ratner, B.D. *J. Colloid Interface Sci.* **1993**, *159*, 77–85.
62. Senshu, K.; Yamashita, S.; Mori, H.; Ito, M.; Hirao, A.; Nakahama, S. *Langmuir* **1999**, *15*, 1754–1762.
63. Mori, H.; Hirao, A.; Nakahama, S.; Senshu, K. *Macromolecules* **1994**, *27*, 4093–4100.
64. Luzinov, I.; Minko, S.; Tsukruk, V. *Prog. Polym. Sci.* **2004**, *29*, 635–698.
65. Urban, M.W. *Polym. Rev.* **2006**, *46*, 329–339.
66. Urban, M.W.; Lestage, D.J. *Polym. Rev.* **2006**, *46*, 445–466.
67. Meyer, D.E.; Kong, G.A.; Dewhirst, M.W.; Zalutsky, M.R.; Chilkoti, A. *Cancer Res.* **2001**, *61*, 1548–1554.

68. Chilkoti, A.; Dreher, M.R.; Meyer, D.E.; Raucher, D. *Adv. Drug Delivery Rev.* **2002**, *54*, 613–630.
69. de Las Heras Alarcón, C.; Pennadam, S.; Alexander, C. *Chem. Soc. Rev.* **2005**, *34*, 276–285.
70. Zhang, X.; Zhuo, R.; Yang, Y. *Biomaterials* **2002**, *26*, 1313–1318.
71. Fujishige, S.; Ando, K.K.I. *J. Phys. Chem.* **1989**, *93*, 3311–3313.
72. Brown, W.; Schillen, K.; Hvidt, S. *J. Phys. Chem.* **1992**, *96*, 6038–6044.
73. Schild, H.G. *Prog. Polym. Sci.* **1992**, *17*, 163–249.
74. Chen, G.; Hoffman, A.S. *Nature* **1995**, *373*, 49–52.
75. Neradovic, D.; Hinrichs, W.L.J.; Kettenes-Van der Bosch, J.J.; Hennick, W.E. *Macromol. Rapid Comm.* **1999**, *20*, 577–581.
76. Yoshida, T. *J. Polym. Sci., Part A: Polym. Chem.* **2003**, *41*, 779–787.
77. Vernon, B.; Kim, S.W.; Bae, Y.H. *J. Biomed. Mater. Res.* **2000**, *51*, 69–79.
78. Kaneko, Y.; Nakamura, S.; Sakai, K.; Aoyagi, T.; Kikuchi, A.; Sakurai, Y.; Okano, T. *Macromolecules* **1998**, *31*, 6099–6105.
79. Uchida, K.; Kaneko, Y.; Sakai, K.; Kikuchi, A.; Sakurai, Y.; Okano, T. *Nature* **1995**, *374*, 240–242.
80. Annaka, M.; Sugiyama, M.; Kasai, M.; Nakahira, T.; Matsuura, T.; Seki, H.; Aoyagi, T.; Okano, T. *Langmuir* **2002**, *18*, 7377–7383.
81. Inoue, T.; Chen, G.; Nakamae, K.; Hoffman, A.S. *Polym. Gels Networks* **1997**, *5*, 561–575.
82. Bulmus, V.; Ding, Z.; Long, C.J.; Stayton, P.S.; Hoffman, A.S. *Bioconjugate. Chem.* **2000**, *11*, 78–83.

83. Shimizu, T.; Yamato, M.; Kikuchi, A.; Okano, T. *Tissue Eng.* **2001**, *7*, 141–151.
84. Vernon, B.; Kim, S.W.; Bae, Y.H. *J. Biomater. Sci. Polym. Ed.* **1999**, *10*, 183–198.
85. Kim, H.K.; Park, T.G. *Enzyme Microb. Technol.* **1999**, *25*, 31–37.
86. Ichikawa, H.; Fukumori, Y. *J. Controlled Release* **2000**, *63*, 107–119.
87. Chun, S.W.; Kim, J.D. *J. Controlled Release* **1996**, *38*, 39–47.
88. Okano, T.; Bae, Y.H.; Jacobs, H.; Kim, S.W. *J. Controlled Release* **1990**, *11*, 255–265.
89. Bromberg, L.E.; Ron, E.S. *Adv. Drug Delivery Rev.* **1998**, *31*, 197–221.
90. Aguilar, M.R.; Elvira, C.; Gallardo, A.; Vázquez, B.; Román, J.S. In *Topics in Tissue Engineering*, Vol. 3, Ashammakhi, N.; Reis, R.L.; Chiellini, E., Eds.; University of Oulu: Oulu, Finland, 2007; pp 6/1–6/27.
91. Li, H.; Yu, G.; Price, C.; Booth, C.; Hecht, E.; Hoffmann, H. *Macromolecules* **1997**, *30*, 1347–1354.
92. Jeong, B.; Bae, Y.H.; Lee D.S.; Kim, S.W. *Nature* **1997**, *388*, 860–862.
93. Jeong, B.; Bae, Y.H.; Kim, S.W. *Macromolecules* **1999**, *32*, 7064–7069.
94. Lee, S.B.; Song, S.; Jin, J.; Sohn, Y.S. *J. Am. Chem. Soc.* **2000**, *122*, 8315–8316.
95. Song, S.; Lee, S.B.; Jin, J.; Sohn, Y.S. *Macromolecules* **1999**, *32*, 2188–2193.
96. Schmolka, I. R. *J. Am. Oil Chem. Soc.* **1977**, *54*, 110–116.
97. Clover, B.; Hammouda, B. *Langmuir* **2010**, *26*, 6625–6629.
98. Patel, H. R.; Patel, R. P.; Patel, M. M. *Int. J. Pharm. Tech. Res.* **2009**, *1*, 299–303.
99. Schmolka, I. *J. Biomed. Mater. Res.* **1972**, *6*, 571–582.
100. Cao, Y.L.; Ibarra, C.; Vacanti, C. In *Tissue Engineering: Methods and Protocols*, Morgan, J.R.; Yarmush, M.L., Eds.; Humana Press: Totowa, NJ, 2006; pp 75–84.
101. Kabanov, A.V.; Alakhov, V.Y. *Crit. Rev. Ther. Drug Carrier Syst.* **2002**, *19*, 1–72.

102. Liaw, J.; Chang, S.; Hsiao, F. *Gene Ther.* **2001**, *8*, 999–1004.
103. Kabanov, A.V.; Batrakova, E.; Miller, D. *Adv. Drug Delivery Rev.* **2003**, *55*, 151–164.
104. DiBiase, M.; Rhodes, C.F. *Drug Develop. Ind. Pharm.* **1996**, *22*, 823–831.
105. Jeong, B.; Bae, Y.H.; Kim, S.W. *J. Controlled Release* **2000**, *63*, 155–163.
106. Kopeček, J. *Nature* **2002**, *417*, 388–391.
107. Deminng, T.J. *Nature* **1997**, *390*, 386–389.
108. Petka, W.A.; Harden, J.L.; McGrath, K.P.; Wirtz, D.; Tirrell, D.A. *Science* **1998**, *281*, 389–392.
109. Ramzi, M.; Rochas, C.; Guenet, J. *Macromolecules* **1998**, *31*, 6106–6111.
110. Kuijpers, A.J.; Engbers, G.H.M.; Feijen, J.; De Smedt, S.C.; Meyvis, T.K.L.; Demeester, J.; Krijgsveld, J.; Zaat, S.A.J.; Dankert, J. *Macromolecules* **1999**, *32*, 3325–3333.
111. Chenite, A.; Chaput, C.; Wang, D.; Combes, C.; Buschmann, M.D.; Hoemann, C.D.; Leroux, J.C.; Atkinson, B.L.; Binette, F.; Selmani, A. *Biomaterials* **2000**, *21*, 2155–2161.
112. Isogai, N.; Gong, J.P.; Osada, Y. *Macromolecules* **1996**, *29*, 6803–6806.
113. Nordby, M.H.; Kjøniksen, A.; Nystrom, B.; Roots, J. *Biomacromolecules* **2003**, *4*, 337–343.
114. He, E.; Yue, C.Y.; Tam, K.C. *Langmuir* **2009**, *25*, 4892–4899.
115. Tonge, S.R.; Tighe, B.J. *Adv. Drug Delivery Rev.* **2001**, *53*, 109–122.
116. Philippova, O.E.; Hourdet, D.; Audebert, R.; Khokhlov, A.R. *Macromolecules* **1997**, *30*, 8278–8285.
117. Torres-Lugo, M.; Peppas, N.A. *Macromolecules* **1999**, *32*, 6646–6651.
118. Morawetz, H. *Macromolecules* **1996**, *29*, 2689–2690.

119. Lee, A.S.; Butun, V.; Vamvakaki, M.; Armes, S.P.; Pople, J.A.; Gast, A.P. *Macromolecules* **2002**, *35*, 8540–8551.
120. Sutton, R.C.; Thai, L.; Hewitt, J.M.; Voycheckand, C.L.; Tan, J.S. *Macromolecules* **1988**, *21*, 2432–2439.
121. Gohy, J.; Lohmeijer, B.G.G.; Varshney, S.K.; Decamps, B.; Leroy, E.; Boileau, S.; Schubert, U.S. *Macromolecules* **2002**, *35*, 9748–9755.
122. Gan, L.H.; Roshan, D.G.; Loh, X.J.; Gan, Y.Y. *Polymer* **2001**, *42*, 65–69.
123. Sideratou, Z.; Tsiourvas, D.; Paleos, C.M. *Langmuir* **2000**, *16*, 1766–1769.
124. Huang, W.M.; Yang, B. *Appl. Phys. Lett.* **2005**, *86*, 114105/1–114105/3.
125. Jung, Y.C.; So, H.H.; Cho, J.W. *J. Macromol. Sci. B* **2006**, *45*, 453–461.
126. Chen, S.; Hu, J.; Yuen, C.; Chan, L. *Polymer* **2009**, *50*, 4424–4428.
127. Lv, H.; Leng, J.; Liu, Y.; Du, S. *Adv. Eng. Mater.* **2008**, *10*, 592–595.
128. Crano, J.C., Guglielmetti, R.J., Eds. *Organic Photochromic and Thermochromic Compounds. Vol. 1: Main Photochromic Families*; Plenum Press: New York, NY, 1999; p 2.
129. Hu, J.; Meng, H.; Li, G.; Ibekwe, S.I. *Smart Mater. Struct.* **2012**, *21*, 053001/1–053001/23.
130. Wang, S.; Choi, M.-S.; Kim, S.-H. *J. Photochem. Photobiol. A* **2008**, *198*, 150–155.
131. Tian, R.; Bhatambreker, N.; Liao, Y.; Su, M. *J. Appl. Polym. Sci.* **2008**, *109*, 3244–3248.
132. Murdan, S. *J. Controlled Release* **2003**, *92*, 1–17.
133. Jung, K.; Nam, J.; Choi, H. *Sens. Actuators A* **2003**, *107*, 183–192.
134. Ahn, S.-K.; Kasi, R. M.; Kim, S.-C.; Sharma, N.; Zhou, Y. *Soft Matter* **2008**, *4*, 1151.
135. Shiga, T. *Adv. Polym. Sci.* **1997**, *134*, 131–163.

136. Kim, S.J.; Kim, H.I.; Park, S.J.; Kim, I.Y.; Lee, S.H.; Lee, T.S.; Kim, S.I. *Smart. Mater. Struct.* **2005**, *14*, 511–514.
137. Miyata, T.; Asami, N.; Uragami, T. *Nature* **1999**, *399*, 766–769.
138. Motornov, M.; Sheparovych, R.; Lupitskyy, R.; MacWilliams, E.; Minko, S. *Adv. Mater.* **2008**, *20*, 200–205.
139. Andreeva, D.V.; Fix, D.; Mohwald, H.; Shchukin, D.G. *Adv. Mater.* **2008**, *20*, 2789–2794.
140. Singamaneni, S.; LeMieux, M.C.; Lang, H.P.; Gerber, C.; Lam, Y.; Zauscher, S.; Datskos, P.G.; Lavrik, N.V.; Jiang, H.; Naik, R.R.; Bunning, T.J.; Tsukruk, V.V. *Adv. Mater.* **2008**, *20*, 653–680.
141. Lutolf, M.P.; Lauer-Fields, J.L.; Schmoekel, H.G.; Metters, A.T.; Weber, F.E.; Fields, G.B.; Hubbell, J.A. *Proc. Natl. Acad. Sci. USA* **2003**, *100*, 5413–5418.
142. Hayashi, G.; Hagihara, M.; Dohno, C.; Nakatani, K. *J. Am. Chem. Soc.* **2007**, *129*, 8678–8679.
143. Nagase, K.; Kobayashi, J.; Kikuchi, A.; Akiyama, Y.; Kanazawa, H.; Okano, T. *Langmuir* **2008**, *24*, 511–517.
144. Lu, Y.; Proch, S.; Schrunner, M.; Drechsler, M.; Kempe, R.; Ballauf, M. *J. Mater. Chem.* **2009**, *19*, 3955–3961.
145. Chen, J.-P.; Hsu, M.-S. *J. Mol. Catal. B: Enzym.* **1997**, *2*, 235–241.
146. Lu, Y.; Mei, Y.; Drechsler, M.; Ballauff, M. *Angew. Chem. Int. Ed.* **2006**, *45*, 813–816.
147. Chen, G.; Hoffman, A.S. *J. Biomater. Sci. Polym. Ed.* **1994**, *5*, 371–382.
148. Nagayama, H.; Maeda, Y.; Shimasaki, C.; Kitano, H. *Macromol. Chem. Phys.* **1995**, *196*, 611–620.

149. Oishi, M.; Hayashi, H.; Michihiro, I.D.; Nagasaki, Y. *J. Mater. Chem.* **2007**, *17*, 3720–3725.
150. Kakizawa, Y.; Kataoka, K. *Adv. Drug Delivery Rev.* **2002**, *54*, 203–222.

CHAPTER 2. APPLICATION-BASED DESIGN OF AMPHIPHILIC INVERTIBLE POLYMERS

2.1. Abstract

In this chapter, the development of amphiphilic invertible polymers (AIPs) based on poly(ethylene glycol) (PEG) as a hydrophilic constituent and varying hydrophobic fragments is described. The structures of AIPs are strategically designed with the purpose of developing novel responsive functional polymeric materials by manipulating environment-dependent AIP self-assembly. Three AIP classes have been developed: amphiphilic invertible polyesters (AIPEs-1) based on PEG and aliphatic dicarboxylic acids, amphiphilic invertible polyurethanes (AIPUs) based on PEG and polytetrahydrofuran (PTHF), and amphiphilic invertible polyesters (AIPEs-2) based on PEG and PTHF. Changing the AIP class and the nature of the hydrophobic fragments in the invertible macromolecules has been used as a tool to tune the hydrophilic-lipophilic balance (HLB) of the AIPs in order to tailor their surface activity, self-assembly behavior, and invertible properties. The AIP macromolecules have been demonstrated to respond to the polarity of the surrounding environment by changing their hydrodynamic radius, a behavior that could be correlated to their chemical structure.

2.2. Introduction

Amphiphilic molecules, that is, molecules with a polar and a nonpolar moiety, arrange themselves at interfaces and tend to build aggregates in solution.¹ The molecules of amphiphilic polymers contain hydrophobic and hydrophilic constituents distributed along the polymer macrochain. Poly(ethylene) glycol is frequently used as a hydrophilic fragment of the amphiphilic polymer macromolecules since this polymer is known to be well soluble in water, highly hydrated, and able to serve as an efficient steric stabilizer for various nanoscale systems

(micelles, nanoparticles, liposomes, nanocapsules, etc.) in biological media.^{2,3} PEG-based copolymers such as Pluronics® are studied in a broad range of applications in aqueous environments that include crystallization,^{4,5} surface modification for biocompatibility,^{6,7} control of particle aggregation in solution,^{8,9} and drug delivery.^{10,11} At low polymer concentration, Pluronics® exist in solution as isolated polymer coils, or unimers.^{12,13} The increasing length of the hydrophobic fragment in the macromolecule results in an increasing surface activity of polymeric surfactant respective to its increasing ability to adsorption at the interface. The ability to undergo intermolecular interaction is a unique property of polymeric surfactants leading to the formation of monomolecular micelles even in a very dilute solution.¹⁴⁻¹⁷ Further increase of polymer concentration results in the formation of micellar gels or crystals.

The behavior of amphiphilic copolymers in organic solvents is, in many respects, similar to that of surfactants in water.¹⁸⁻²⁰ They form micelles, which are able, for example, to solubilize otherwise insoluble substances, or stabilize colloidal particles. Amphiphilic polymeric surfactants can lower the surface tension at the interface between organic solvents and water, forming direct or inverse disordered or liquid-crystalline microemulsions.^{21,22}

Recently, the focus of research in the field of adaptive/responsive materials has moved to the design of polymers with a “smart” behavior. “Smart” polymer chains adapt to the surrounding environment or applied stimuli by changing the conformation and location of their backbone, side chains, segments, pendant groups, or end groups.^{23,24} Responsive polymers can regulate transport of ions and molecules, change wettability and adhesion of different species on external stimuli, etc.²⁵ A broad range of potential synthetic copolymers provides opportunities for designing a multitude of different smart materials that vary in length, chemical composition, and chain configuration.²⁶ For example, amphiphilic invertible homopolymers in which each

repeating unit contains a hydrophilic and a hydrophobic head group have demonstrated the capability of forming environment-dependent micellar or inverse micellar assemblies.²⁷⁻²⁹ Segmented polyurethanes with alternating hydrophilic and hydrophobic segments have shown low surface energies in both air and water and, thus, are believed to exhibit switchable behavior as well.³⁰⁻³⁵

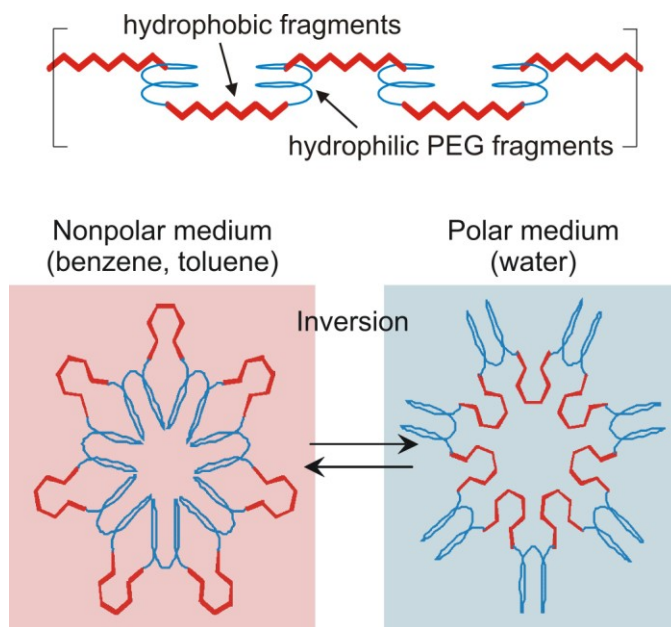


Figure 2.1. A principal scheme of AIP structure and environment-dependent formation of AIP micelles.

Hence, the development of amphiphilic invertible polymers based on poly(ethylene glycol) as a hydrophilic constituent and capable of forming invertible nanoassemblies is proposed as a novel approach allowing to manipulate the polymeric micelle formation and the following self-arrangement of the micelles into the invertible assemblies as a response to changing polymer concentration and polarity of the environment (Figure 2.1). The hydrophilic-lipophilic balance of the amphiphilic macromolecule has been found to be a powerful tool for controlling polymer micellization, dimensions of micellar assemblies, and ability to switch its

macromolecular conformation. Changing the nature or the length of hydrophobic fragments of a macromolecule is one of the possible ways to tune the HLB of amphiphilic invertible polymers. For this purpose, three AIP classes with different hydrophobic fragments have been developed: amphiphilic invertible polyesters based on PEG and aliphatic dicarboxylic acids (AIPes-1), amphiphilic invertible polyurethanes based on PEG and polytetrahydrofuran (AIPUs), and amphiphilic invertible polyesters based on PEG and PTHF (AIPes-2). Three key properties: (1) the ability to self-assemble with increasing polymer concentration, (2) rapid reversible switching of macromolecular conformation in solvents differing by polarity, and (3) encapsulating otherwise non-soluble molecules in both polar and nonpolar media are targeted by designing AIP macromolecules with hydrophilic and hydrophobic constituents alternately distributed along the polymer backbone. The incompatibility of alternating short amphiphilic fragments results in microphase separation at a very small length scale which, in turn, enables a greater degree of control over the AIP self-assembly and responsive properties.^{36,37} The invertible complex nanoassemblies with a controlled size and morphology developed from the AIPs are expected to be functional in both polar and nonpolar environment and are prospective for a broad range of applications.

The ability to encapsulate insoluble molecules in a polar aqueous medium would make AIP nanoassemblies promising for the pharmaceutical industry (controlled release, targeted devices), agriculture (micronutrients delivery, development of fertilizers), and cosmetics (encapsulation of functional ingredients and their delivery). In nonpolar media, AIP nanoassemblies could be potentially used as nanoreactors for the synthesis of “smart” nanoparticles having a protective shell made from both hydrophilic and hydrophobic polymeric fragments, that are, therefore, dispersible and highly stable in both polar and nonpolar solvents.

2.3. Experimental

2.3.1. Materials

Poly(ethylene glycol) (average molecular weight M_n 300, 600, and 1000 g/mol), Terathane PTHF (M_n 650 and 1000 g/mol), tolylene 2,4-diisocyanate (2,4-TDI), and chloroform-*d* were purchased from Aldrich. Solvents (toluene, benzene, acetone, and carbon tetrachloride, ACS grade), succinic anhydride, sebacic and dodecanedioic acids were obtained from VWR International. All reagents and materials were used as received.

2.3.2. Characterization

Average molecular weight and polydispersity index (PDI) of synthesized AIPs were measured by gel permeation chromatography (GPC) using a Waters Corp. modular chromatograph consisting of a Waters 515 HPLC pump, a Waters 2410 refractive index detector, and a set of two 10 μm PL-gel mixed-B columns; the column temperature was set at 40 $^{\circ}\text{C}$. Tetrahydrofuran (THF) was used as the carrier solvent at a flow rate of 1.0 mL/min; 200 μL of a 5 mg/mL THF solution were injected for each sample. All samples were filtered through a 0.45 μm PTFE filter (Nalgene) before running. A molecular weight calibration curve was generated with polystyrene standards of low polydispersity (Polymer Laboratories, USA).

The Fourier transform infrared spectra were recorded with a Nicolet 8700 FTIR spectrometer (Thermo Scientific) using KBr optical discs (Alfa Aesar).

^1H NMR spectra were recorded on a JEOL ECA 400 MHz NMR spectrometer equipped with a 24-place autosampler carousel using chloroform-*d* as a solvent.

Specific viscosity η_{sp} of polymer solutions in a number of solvents, including acetone, a 1:1 mixture of acetone and water, toluene (or benzene), a 1:1 mixture of acetone and toluene (or benzene), and carbon tetrachloride, was measured with an Ubbelohde viscometer.

The hydrodynamic radii (R_m) of AIP macromolecules in solvents differing by polarity were calculated from the specific viscosity data according to the following equation

$$R_m = \left(\frac{3V_m}{4\pi} \right)^{1/3},$$

where V_m is the volume of macromolecular architectures. The expression for V_m is:

$$V_m = \frac{\omega M}{cN_A},$$

where ω is volume fraction of macromolecules in solution, M is polymer molecular weight, c is polymer concentration, and N_A is Avogadro's number.

Polymer volume fraction is calculated using the viscosity data according to Newton's equation for spherical particles:

$$\omega = \frac{\eta/\eta_0 - 1}{\alpha},$$

where η and η_0 are the viscosity of the polymer solution and pure solvent respectively, and α is the coefficient equal to 2.5 for spherical particles.

2.3.3. Synthesis of the AIPs

2.3.3.1. Polyesters Based on PEG and Aliphatic Dicarboxylic Acids (AIPes-1)

A three-necked flask fitted with a nitrogen inlet, a thermometer, and a Dean-Stark trap with a reflux condenser was charged with poly(ethylene glycol) (0.1 mol), dicarboxylic (sebacic or dodecanedioic) acid (0.1 mol), and toluene. A 1:3 (w/v) monomer mixture/toluene solution was used. The Dean-Stark trap was filled with toluene. The reactive mixture was agitated and heated to dissolve the dicarboxylic acid completely, then 75% sulfuric acid (0.1 mL) was added to catalyze the polyesterification reaction. The mixture was refluxed under nitrogen for about 20 h. To neutralize sulfuric acid, a 40% NaOH solution (0.175 mL) was added, and the mixture was

stirred at room temperature for 12 h. Sodium sulfate that formed was separated by centrifugation. Toluene was removed under reduced pressure. Polymers were dried under vacuum at 60 °C for at least 24 h.

2.3.3.2. PEG-PTHF Based Polyurethanes (AIPUs)

2.3.3.2.1. Synthesis of Random Polyurethanes. A solution of PEG (0.01 mol) and PTHF (0.01 mol) in an aromatic solvent (toluene or benzene) (60 mL) was refluxed for 3 h with a Dean-Stark trap in order to remove residual moisture. Subsequently, 2,4-TDI (0.02 mol) was added while stirring. The mixture was stirred at 40 °C for 12 h and then toluene was removed under reduced pressure. Residual polymers were dried under vacuum at 60 °C for at least 24 h.

2.3.3.2.2. Synthesis of Alternating Polyurethanes. A solution of PTHF (0.01 mol) in benzene (60 mL) was refluxed for 3 h with a Dean-Stark trap, and 2,4-TDI (0.02 mol) was then added while stirring. After stirring the mixture at 40 °C for 12 h, a solution of PEG (0.01 mol) in benzene (60 mL) was added while stirring. The resulting mixture was stirred for another 12 h at 40 °C. Subsequently, benzene was removed under reduced pressure and residual polymers were dried under vacuum at 60 °C for at least 24 h.

2.3.3.3. PEG-PTHF Based Polyesters (AIPes-2)

2.3.3.3.1. Formation of Acid-Terminated Prepolymers. Polytetrahydrofuran (0.1 mol) and succinic anhydride (0.2 mol) were melted together and the melt was maintained at 95 °C for 3 h. The course of the reaction was controlled by determining acid value of the reactive mixture and via FTIR spectroscopy (from the disappearance of the C=O anhydride adsorption bands at 1786 and 1862 cm⁻¹).

2.3.3.3.2. Synthesis of AIPes-2. A mixture of the corresponding acid-terminated prepolymer from Stage 1 (0.1 mol) and poly(ethylene glycol) (0.1 mol) was dissolved in toluene.

A 1 : 3 (w/v) monomer mixture : toluene ratio was used. Subsequently, 75% sulfuric acid (0.1 mL) was added to catalyze the reaction. The mixture was refluxed with a Dean-Stark trap for about 20 h. When the acid value reached 3.6–4.1 mg KOH/g, the reactive mixture was cooled down to room temperature. To neutralize the sulfuric acid, a 10% sodium hydroxide solution (0.33 mL) was added, and the mixture was stirred at room temperature for 12 h. Sodium sulfate that formed was separated by centrifugation. Toluene was removed under reduced pressure. The resulting polymer was dried under vacuum at 60 °C for at least 24 h.

2.4. Results and Discussion

2.4.1. Amphiphilic Invertible Polyesters Based on Poly(ethylene Glycol) and Aliphatic Dicarboxylic Acids (AIPES-1)

To synthesize AIPES-1, poly(ethylene glycols) of different molecular weight (PEG-300, PEG-600, and PEG-1000) have been reacted with sebacic and dodecanedioic acids (Figure 2.2).^{37,38} The polyesterification reaction has resulted in multiblock AIPES structures with varying length of hydrophilic and hydrophobic constituents alternately distributed along the polymer backbone.

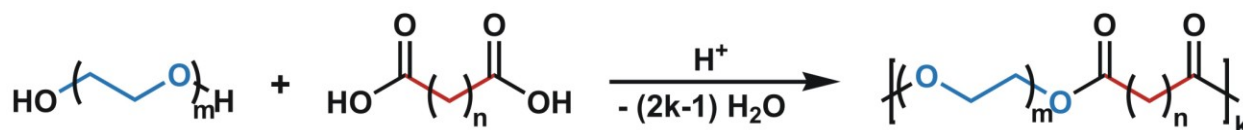


Figure 2.2. Synthesis of amphiphilic invertible polyesters based on poly(ethylene glycol) and aliphatic dicarboxylic acids.

Since the interaction between dicarboxylic acids and polyols is an equilibrium process, the water formed in the reaction must be continuously removed from the reactive mixture in order to shift the equilibrium towards polyester formation.³⁶ To facilitate water removal, the

reaction was carried out in toluene, an azeotrope-forming solvent, and toluene-water azeotrope was collected in a Dean-Stark trap. The polyesterification reaction has been catalyzed by sulfuric acid (1–4 mol. %). The course of the polyesterification has been monitored by measuring the amount of water evolved during the process and by analyzing the acid value of the reactive mixture.

The characteristics of the developed AIPES-1 are given in Table 2.1. The Davies hydrophilic-lipophilic balance of the amphiphilic invertible polyesters has been varied between 9.2 and 15.4 by changing length of hydrophilic and hydrophobic fragments that could potentially lead to different surface activity and ability to self-assemble in polar and nonpolar solvents.

Table 2.1. Characteristics of the AIPES-1 Polyesters

Polymer	m	n	HLB*	M_n , g/mol	PDI
S10	22.3	8	15.4	6,000	1.95
D10	22.3	10	14.4	5,000	1.53
S6	13.2	8	11.4	6,500	1.42
D3	6.4	10	9.2	5,500	1.44

* Hydrophilic-lipophilic balance values have been calculated according to Reference 39

The structure of the AIPES-1 has been confirmed by FTIR and ^1H NMR spectroscopy, the characteristic spectra of an amphiphilic invertible polyester are presented in Figure 2.3. In the FTIR spectrum (Figure 2.3A), the presence of poly(ethylene glycol) fragments is revealed by the

intensive doublet of absorption bands at 1145–1110 cm^{-1} caused by the valence (stretching) vibration of the ester and ether C–O bonds. A narrow intense absorption band at 1730 cm^{-1} is attributed to the stretching vibration of the carbonyl group. Finally, the presence of $-(\text{CH}_2)_n-$ groups is demonstrated by a broad absorption band at ca. 2900 cm^{-1} (valence vibration), as well as absorption bands at 1450 cm^{-1} (deformation vibration) and 730 cm^{-1} (pendulum vibration).

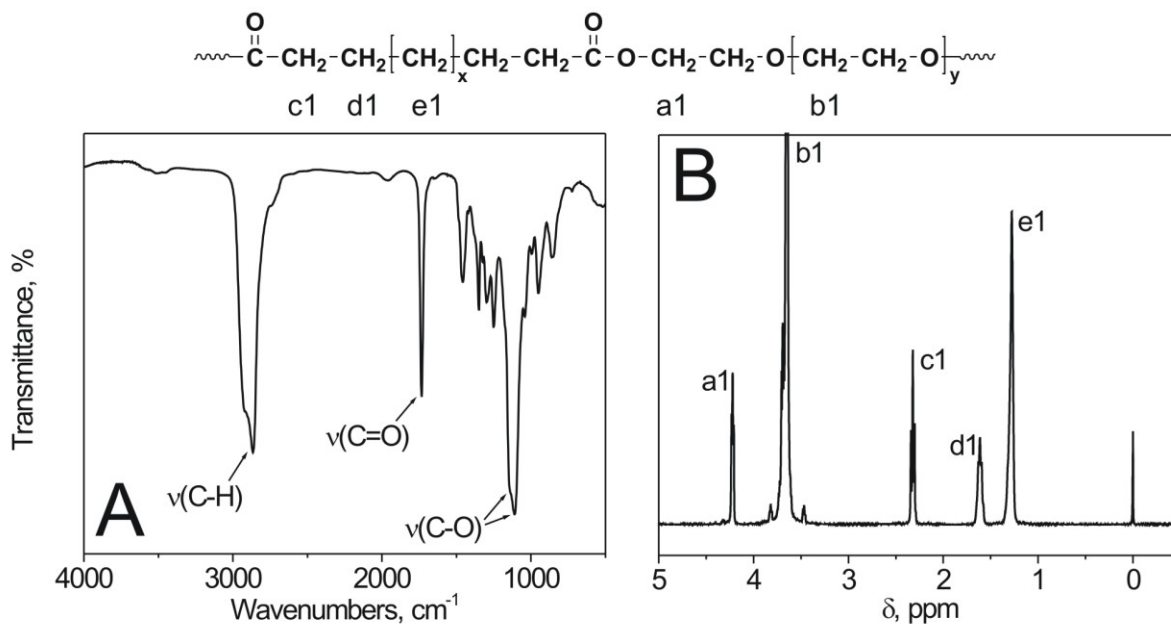


Figure 2.3. FTIR (A) and ^1H NMR (B) spectra of the amphiphilic invertible polyester D10.

In the ^1H NMR spectrum of a polyester D10 (Figure 2.3B) in CDCl_3 , protons of the hydrophilic poly(ethylene glycol) fragments reveal themselves as signals at 3.64 ppm (m, 80H, CH_2OCH_2) and 4.22 ppm (t, 4H, C(O)OCH_2). Conversely, the peaks at 1.28 ppm (m, 12H, $\text{CH}_2\text{CH}_2(\text{CH}_2)_6\text{CH}_2\text{CH}_2$), 1.61 ppm (p, 4H, $\text{OC(O)CH}_2\text{CH}_2$), and 2.32 ppm (t, 4H, OC(O)CH_2) belong to the protons of the hydrophobic dodecanedioate moieties. The NMR spectrum of D10 is typical for all synthesized AIPES-1 in terms of chemical shifts and multiplicities of the proton peaks.

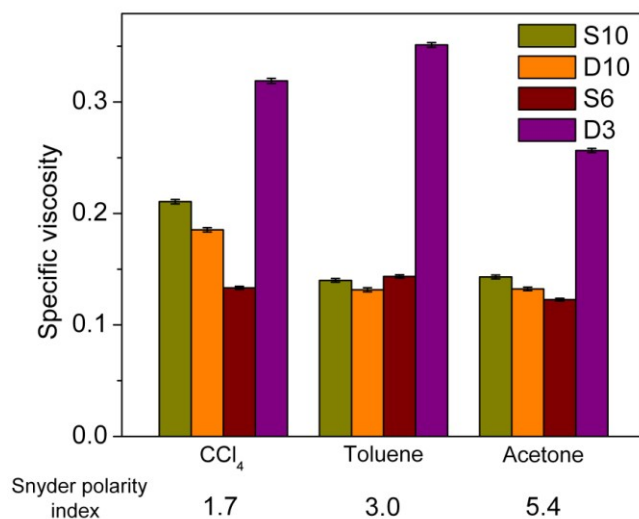


Figure 2.4. Specific viscosities of the AIPE-1 solutions in solvents differing by polarity ($C = 0.01$ g/mL).

Table 2.2. Calculated Hydrodynamic Radii (in nm) of AIPES-1 in Different Solvents

Polymer	CCl ₄	Toluene	Acetone
S10	3.4	3.0	3.0
D10	2.8	2.5	2.5
S6	3.3	3.3	3.2
D3	3.7	3.8	3.5

To confirm the ability of the amphiphilic invertible polyesters to respond to changing polarity of the environment, the specific viscosity of AIPES-1 has been measured in three different media (carbon tetrachloride, toluene, and acetone) at the same polymer concentration (1 g/100 mL, Figure 2.4), and the hydrodynamic radii of the polyester macromolecules have been determined (Table 2.2). The data provided for all amphiphilic invertible polyesters imply

that the nature of the surrounding environment has a significant impact on the size of AIPE-1 macromolecular architectures. In addition to the molecular weight, the viscosity of polymer solutions is known to be influenced by the nature of the solvent and the hydrodynamic interactions in the polymer globule that determine its shape and density. In a good solvent, the macromolecules are expanded and occupy a bigger volume, thus increasing the solution viscosity, while in a bad solvent they become shrunken into the dense globules and the viscosity decreases. As shown in Figure 2.4, the viscosity of polyester solutions in nonpolar carbon tetrachloride and toluene is systematically higher than in polar acetone. Toluene and CCl₄ are assumed to be good solvents for both hydrophilic and hydrophobic fragments of the AIPE-1 macromolecules causing the extension of polar PEG and nonpolar alkyl chains and, therefore, leading to an increase of the hydrodynamic radius of the polymer molecule (Table 2.2). In contrast, according to the solubility parameters, more polar acetone is a poor solvent for the hydrophobic constituents of the AIPes-1, thus decreasing the radius of the polymer globules. Therefore, AIPE-1 macromolecules have been proven to be capable of adjusting their macromolecular conformation to the polarity of the medium.

2.4.2. Amphiphilic Invertible Polyurethanes Based on Poly(ethylene Glycol) and Polytetrahydrofuran (AIPUs)

Tuning hydrophilic-lipophilic balance of amphiphilic polymers is known to be a powerful tool for controlling their micellization and development of micellar assemblies.^{40,41} Due to the limited choice of commercially available long-chain aliphatic dicarboxylic acids, the HLB of the AIPes-1 has been mainly adjusted by varying length of the hydrophilic PEG fragment. Hence, to facilitate HLB tuning, a new class of amphiphilic invertible polymers – amphiphilic invertible polyurethanes (AIPUs) containing hydrophilic PEG and hydrophobic polytetrahydrofuran

constituents, has been developed. The use of PTHF, commercially available in a variety of molecular weights, enables enhanced tuning of the length of the polymer hydrophobic fragment, while the presence of PEG chains allows direct comparison between amphiphilic invertible polyesters and polyurethanes in terms of the effect of composition on polymer properties.

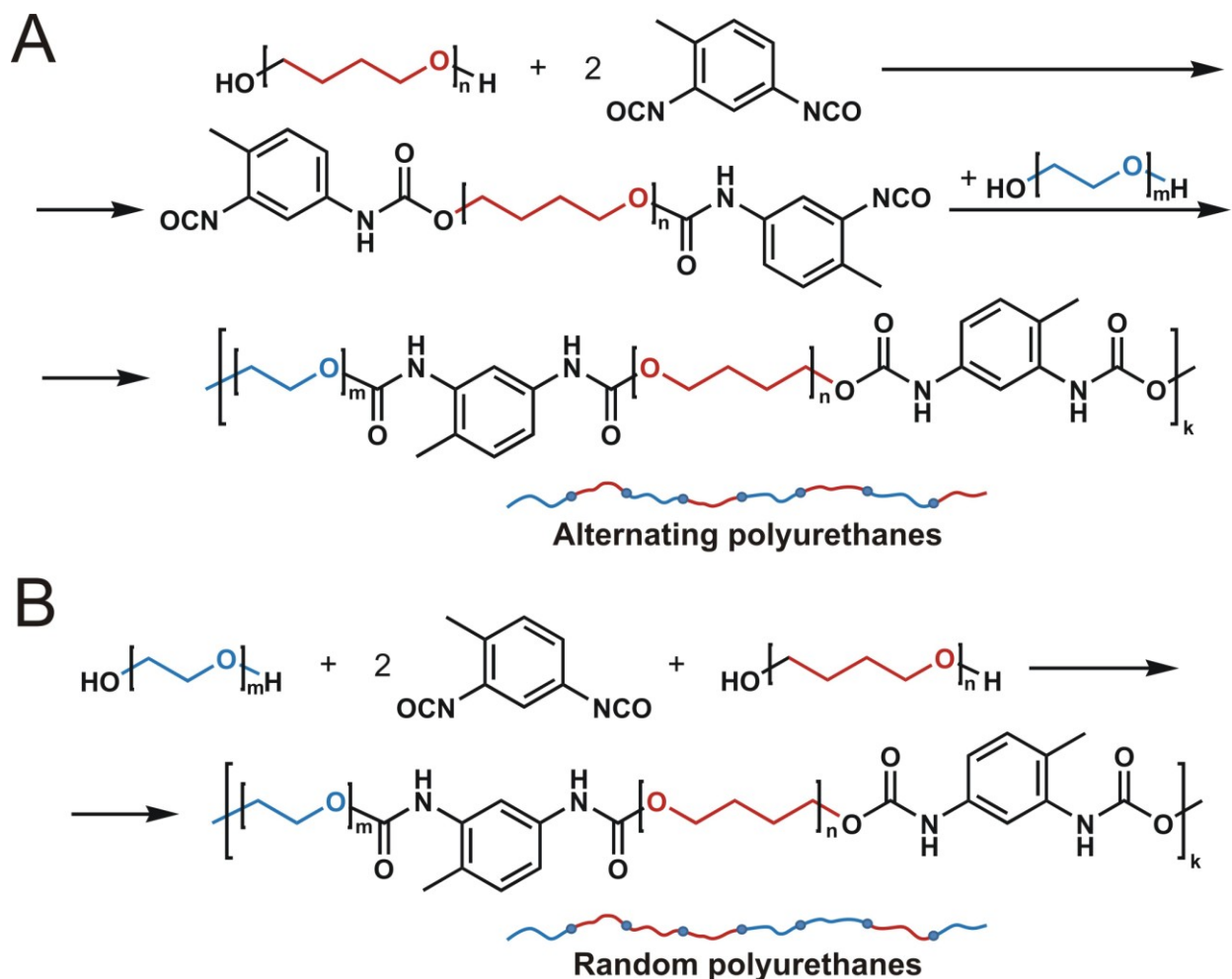


Figure 2.5. Synthesis of amphiphilic invertible polyurethanes with an alternating (A) and a random (B) distribution of the hydrophilic and hydrophobic fragments along the polymer backbone.

Using different synthetic approaches, AIPUs with (1) an alternate and (2) a random distribution of the hydrophilic and hydrophobic constituents in the polymer backbone have been

developed (Figure 2.5). The alternating distribution of the hydrophobic and hydrophilic constituents within the main polymeric backbone is assumed to be beneficial in terms of rapid switching of the macromolecular architecture in response to changing polarity of the environment.³⁷ The random distribution of the fragments provides polymers with varying lengths of hydrophobic and hydrophilic fragments and, thus, with varying ability to form micelles, to invert macromolecular conformation, etc.

For the synthesis of AIPUs, poly(ethylene glycols) with a molecular weight of 600 g/mol (PEG-600) and 1000 g/mol (PEG-1000) have been used as hydrophilic fragments of the macromolecules, whereas polytetrahydrofurans with a molecular weight of 650 g/mol (PTHF-650) and 1000 g/mol (PTHF-1000) have served as hydrophobic fragments.

The alternating polyurethanes have been synthesized in a two-step procedure (Figure 2.5A). In the first step, polytetrahydrofuran has been reacted with a two-fold molar excess of tolylene 2,4-diisocyanate to afford isocyanate terminated PTHF – a prepolymer for the synthesis of amphiphilic polyurethanes. The hydroxy end-groups of PTHF have reacted with one of the isocyanate groups present in tolylene 2,4-diisocyanate. Preferably, the isocyanate group in position 4 has reacted with the OH functionality of PTHF due to its higher reactivity in comparison with that of the isocyanate group in position 2 (the ratio of the corresponding rate constants k_{4-NCO}/k_{2-NCO} in the reaction of 2,4-TDI with polyols at 39–50 °C is as ca. 7:1).⁴² The reaction course has been monitored by FTIR spectroscopy. In the FTIR spectrum of PTHF (Figure 2.6, curve 1), an absorption band at 3455 cm⁻¹ corresponds to the OH stretching vibration. This band is absent in the spectrum of the prepolymer (Figure 2.6, curve 2), whereas new absorption bands at 2273 cm⁻¹ (isocyanate), 1733 cm⁻¹ (C=O in urethane), and 3293 cm⁻¹, 1596 cm⁻¹, 1536 cm⁻¹ (NH in urethane) have appeared. Given the molar ratio of

PTHF : diisocyanate, the above-mentioned difference in the reactivity of isocyanate groups in a 2,4-TDI molecule, and the FTIR spectroscopy data, a prepolymer with the structure depicted in Figure 2.5 is believed to have been formed.

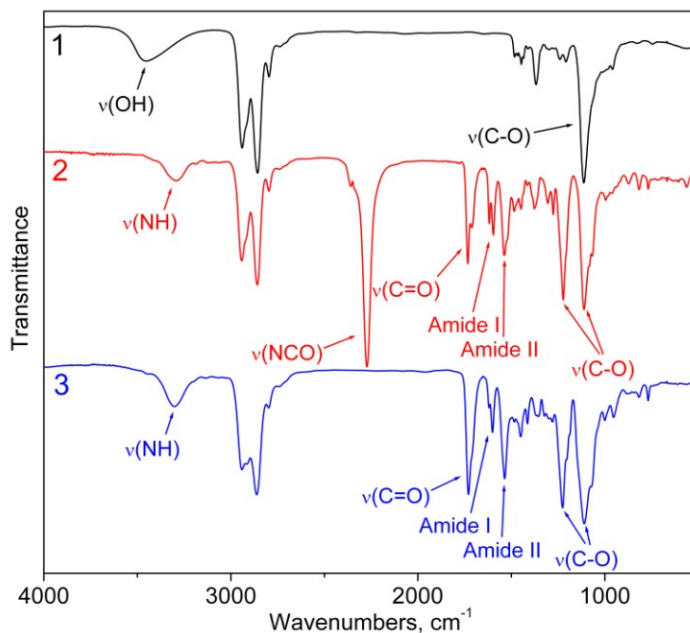


Figure 2.6. FTIR spectra of (1) PTHF-650, (2) isocyanate terminated PTHF-650, (3) amphiphilic polyurethane PEG₁₀₀₀-*alt*-PTHF₆₅₀.

In the second stage, the prepolymer has been reacted with an equimolar amount of hydroxy-terminated poly(ethylene glycol). The isocyanate groups of the prepolymer have reacted with the OH end groups of PEG to give a high-molecular-weight polymer with hydrophilic and lipophilic moieties alternately distributed along a macrochain. The FTIR spectrum of the final AIPU (Figure 2.6, curve 3) shows no absorption bands at 3455 cm⁻¹ (OH group) or at 2273 cm⁻¹ (isocyanate). A clear increase in intensity of the absorption bands corresponding to urethane linkages (as compared to the spectrum of the prepolymer from the first step) implies the formation of new urethane groups due to the reaction between hydroxy and isocyanate

functionalities (Figure 2.5). Hence, the reaction pathway and the structure of both isocyanate terminated PTHF and amphiphilic polyurethane have been confirmed by FTIR spectroscopy.

Random amphiphilic invertible polyurethanes have been synthesized by the reaction of 2,4-TDI with a mixture of PEG and PTHF (Figure 2.5B). The molar ratio of the reactants was as 2 : 1 : 1, respectively. It is known that the OH group in PTHF displays somewhat higher nucleophilicity and, therefore, slightly higher reactivity toward isocyanates than the OH group in PEG.⁴² Thus, PTHF molecules are assumed to be consumed more rapidly during the simultaneous interaction of 2,4-TDI with PEG and PTHF. Although the resultant AIPUs in general have a random distribution of hydrophilic and hydrophobic constituents along the macromolecular backbone (Figure 2.5), some segments are enriched with PTHF fragments while others are enriched with PEG fragments.

Eight amphiphilic invertible polyurethanes differing in the length of hydrophilic and hydrophobic fragments and in the type of fragment distribution (alternating or random) have been developed. AIPU characteristics along with their Griffin HLB values are presented in Table 2.3. Noteworthy, the Griffin method of HLB calculation used for the AIPUs and the Davies method used for amphiphilic invertible polyesters are based on different principles, therefore, the Davies and Griffin HLB data cannot be compared. The Griffin method of calculating hydrophilic-lipophilic balance of an amphiphile is based on the content of hydrophilic poly(ethylene glycol) fragment in the amphiphilic molecules and does not take into account the molecular structure of the amphiphilic compound.⁴³ Hence, HLB data estimated according to this method are not as accurate as the HLB calculated via the Davies method that is based on incremental contributions of each of the functional groups of the amphiphile.³⁹ Still, HLB values calculated according to the Davies method give a reasonably good representation of the relative

hydrophilicity of the amphiphilic macromolecules, especially when the increments required for the calculation of the Davies HLB are not available, as in the case of the AIPUs.

Table 2.3. Characteristics of the AIPUs

Polymer	m	n	HLB*	M_n , g/mol	PDI
PEG ₁₀₀₀ - <i>alt</i> -PTHF ₆₅₀	22.3	8.8	10.9	13,200	1.37
PEG ₁₀₀₀ - <i>alt</i> -PTHF ₁₀₀₀	22.3	13.6	9.2	13,000	1.35
PEG ₆₀₀ - <i>alt</i> -PTHF ₆₅₀	13.2	8.8	8.6	11,400	1.42
PEG ₆₀₀ - <i>alt</i> -PTHF ₁₀₀₀	13.2	13.6	7.0	10,300	1.46
PEG ₁₀₀₀ - <i>co</i> -PTHF ₆₅₀	22.3	8.8	10.9	11,900	1.26
PEG ₁₀₀₀ - <i>co</i> -PTHF ₁₀₀₀	22.3	13.6	9.2	11,200	1.35
PEG ₆₀₀ - <i>co</i> -PTHF ₆₅₀	13.2	8.8	8.6	11,700	1.30
PEG ₆₀₀ - <i>co</i> -PTHF ₁₀₀₀	13.2	13.6	7.0	10,000	1.58

* Hydrophilic-lipophilic balance values have been calculated according to Reference 43

A characteristic ¹H NMR spectrum of an AIPU is shown in Figure 2.7. In the ¹H NMR spectrum of amphiphilic invertible polyurethane PEG₁₀₀₀-*alt*-PTHF₆₅₀ in CDCl₃, protons of the hydrophilic PEG fragment reveal themselves as peaks at 3.63 ppm (m, 80H, CH₂OCH₂CH₂OCH₂), 3.72 ppm (t, 4H, C(O)OCH₂CH₂O), as well as the signal at 4.29 ppm (t, 4H, C(O)OCH₂CH₂O). The signals of polytetrahydrofuran chains are found at 1.62 ppm (m, 32H, CH₂OCH₂CH₂CH₂), 1.75 ppm (m, 4H, C(O)OCH₂CH₂CH₂), 3.41 ppm (m, 32H,

CH₂OCH₂CH₂CH₂), and 4.17 ppm (t, 4H, C(O)OCH₂CH₂CH₂). A peak at 2.18 ppm corresponds to protons of the methyl group in the tolylene fragment (s, 6H, CH₃), while a peak at 6.56 ppm is attributed to the nitrogen-bound hydrogen atom of the urethane group (s, 4H, NH). Finally, hydrogen atoms of the aromatic ring appear as a series of signals at 6.64–7.69 ppm (m, 6H, C₆H₃). The NMR spectrum of PEG₁₀₀₀-*alt*-PTHF₆₅₀ is typical for all synthesized polyurethanes in terms of chemical shifts and multiplicities of proton signals.

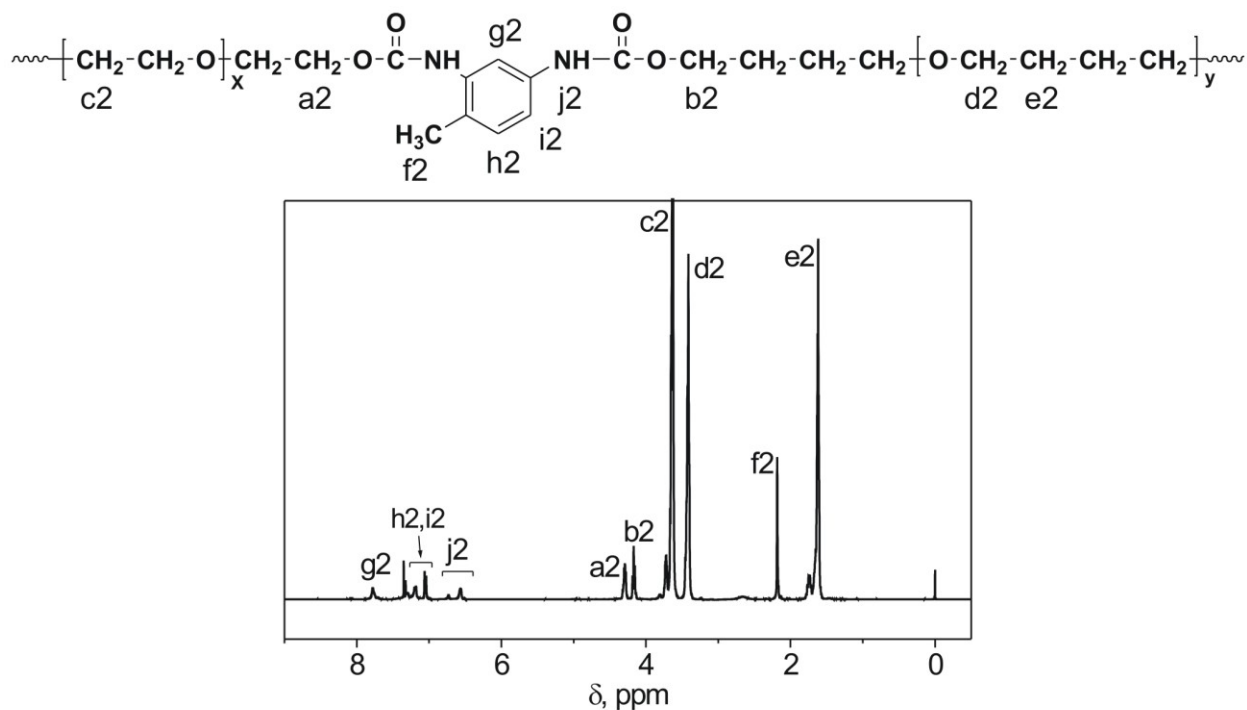


Figure 2.7. ¹H NMR spectrum of the AIPU PEG₁₀₀₀-*alt*-PTHF₆₅₀.

Four solvents of varying polarity were selected to measure the specific viscosity of AIPU solutions: tetrachloromethane, an aromatic solvent (toluene for the alternating polyurethanes and benzene for the random ones), acetone, and a mixture of acetone with a corresponding aromatic solvent (1 : 1 v/v) (Figure 2.8). Using specific viscosity data, hydrodynamic radii of polyurethane macromolecules in solvents differing by polarity have been calculated (Table 2.4).

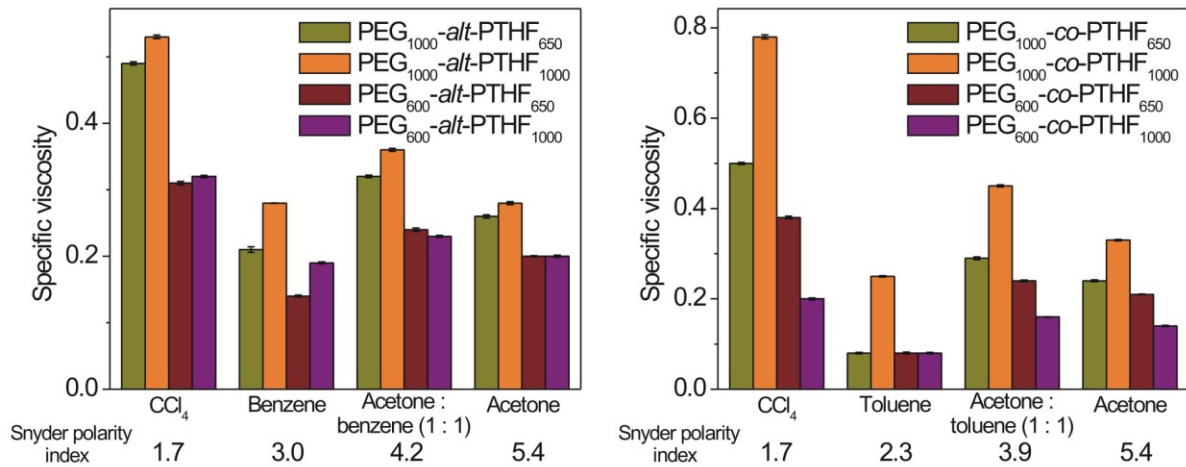


Figure 2.8. Specific viscosities of the AIPU solutions in solvents differing by polarity ($C = 0.01$ g/mL).

Table 2.4. Calculated Hydrodynamic Radii (in nm) of AIPUs in Different Solvents

Polymer	CCl ₄	Aromatic solvent	Acetone : aromatic solvent	Acetone
PEG ₁₀₀₀ -alt-PTHF ₆₅₀	5.2	3.9	4.5	4.2
PEG ₁₀₀₀ -alt-PTHF ₁₀₀₀	5.3	4.3	4.6	4.3
PEG ₆₀₀ -alt-PTHF ₆₅₀	4.3	3.3	4.0	3.7
PEG ₆₀₀ -alt-PTHF ₁₀₀₀	4.2	3.6	3.8	3.6
PEG ₁₀₀₀ -co-PTHF ₆₅₀	4.9	2.7	4.1	3.8
PEG ₁₀₀₀ -co-PTHF ₁₀₀₀	5.7	3.9	4.7	4.3
PEG ₆₀₀ -co-PTHF ₆₅₀	4.5	2.7	3.9	3.7
PEG ₆₀₀ -co-PTHF ₁₀₀₀	3.7	2.7	3.4	3.3

The data in Figure 2.8 and Table 2.4 demonstrate that a change in solvent polarity leads to the changes in viscosity and, thus, in the hydrodynamic radius of the AIPU macromolecular architectures in solution. The AIPU solutions in tetrachloromethane show the highest specific viscosity, indicating that CCl_4 is a good solvent for extending the conformation of amphiphilic polyurethanes in this medium. This implies that both the hydrophilic (PEG) and hydrophobic (PTHF) fragments of the macromolecules are extended in this solvent. Evidently, both the hydrodynamic radius of the AIPU macromolecules and solution viscosity increase. In contrast, the lowest viscosity values were determined for the polyurethane solutions in the aromatic solvents. Benzene and toluene are good solvents for the hydrophobic PTHF fragments of the polyurethane macromolecules. In this medium, the polyurethane macromolecules are assumed to build up micelles with a dense polar core consisting of PEG fragments and urethane linkages. As a result, the AIPU hydrodynamic radius in aromatic solvents becomes smaller, thus decreasing the viscosity. Acetone is a good solvent for both hydrophilic PEG fragments and urethane linkages, hence, the AIPU macromolecules possess a more extended conformation in the acetone solution and in the acetone : aromatic solvent mixtures than in the pure aromatic solvents. For this reason, the hydrodynamic radius of the AIPU macromolecules in acetone or in the presence of acetone becomes larger, increasing the viscosity.

The specific viscosity in a particular solvent depends on AIPU configuration and length of the fragments (Figure 2.8). Solutions based on polymers with longer PEG/PTHF fragments ($\text{PEG}_{1000}\text{-alt-PTHF}_{1000}$ and $\text{PEG}_{1000}\text{-co-PTHF}_{1000}$) show higher viscosity in a particular solvent, obviously due to flexibility and length of the soft segments (i.e., PEG and PTHF) and a lower content of hard segments (i.e., 2,4-TDI, see Chapter 3 for more information). In contrast, the AIPUs based on PEG-600 possess the most compact conformation (and, thus, the lowest

viscosity) because of a higher content of hard segments and a smaller length of the PEG fragment. Finally, the hydrodynamic radii of the PEG₁₀₀₀-*alt*-PTHF₆₅₀ and PEG₁₀₀₀-*co*-PTHF₆₅₀ are closer to those of PEG₁₀₀₀-*alt*-PTHF₁₀₀₀ and PEG₁₀₀₀-*co*-PTHF₁₀₀₀. This implies that the length of the PEG fragment has a more substantial impact on macromolecular flexibility than does the PTHF length. Thus, the characteristics of the AIPUs indicate that their invertibility could be correlated with their chemical structure.

2.4.3. Amphiphilic Invertible Polyesters Based on Poly(ethylene Glycol) and Polytetrahydrofuran (AIPes-2)

Another type of amphiphilic invertible polyesters has been developed on the basis of poly(ethylene glycol) with a molecular weight of 300, 600, and 1000 g/mol as the hydrophilic fragment and polytetrahydrofuran with a molecular weight of 250, 650, and 1000 g/mol as the hydrophobic constituent via a two-step procedure (Figure 2.9). A broad surface activity and self-assembly behavior for AIPes-2 have been targeted by varying their Davies HLB values between 8.6 and 20.1 (Table 2.5).

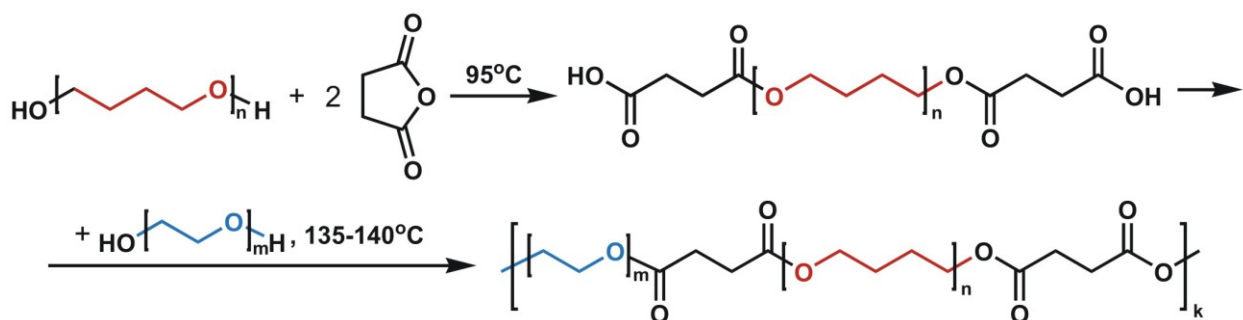


Figure 2.9. Synthesis of the PEG-PTHF based amphiphilic invertible polyesters (AIPes-2).

In the first step, polytetrahydrofuran was melted together with of succinic anhydride (the molar ration PTHF : anhydride was as 1:2) and kept at 95 °C for 3 h giving rise to a prepolymer with terminal carboxylic groups. The reaction progress has been monitored by FTIR

Table 2.5. Characteristics of the AIPE-2 Polyesters

Polymer	m	n	HLB*	M_n	PDI
PEG ₁₀₀₀ PTHF ₂₅₀	22.3	3.2	20.1	4,700	1.51
PEG ₆₀₀ PTHF ₂₅₀	13.2	3.2	17.1	6,400	1.39
PEG ₃₀₀ PTHF ₂₅₀	6.4	3.2	14.9	8,300	1.45
PEG ₁₀₀₀ PTHF ₁₀₀₀	22.3	13.6	13.9	4,200	1.50
PEG ₆₀₀ PTHF ₆₅₀	13.2	8.8	13.8	9,700	1.52
PEG ₃₀₀ PTHF ₁₀₀₀	6.4	13.6	8.6	7,100	1.57

* Hydrophilic-lipophilic balance values have been calculated according to Reference 39

spectroscopy. The interaction between two PTHF terminal hydroxy groups and anhydride fragment has caused the disappearance of the absorption band at 3376 cm^{-1} corresponding to the OH stretching vibration present in the original PTHF (Figure 2.10, curve 1), as well as two characteristic anhydride C=O adsorption bands at 1786 and 1862 cm^{-1} . In turn, several new adsorption bands have appeared in the FTIR spectrum of the prepolymer (Figure 2.10, curve 2): an intensive adsorption band at 1166 cm^{-1} caused by stretching vibration of the ester C–O bonds, a doublet of the narrow intensive adsorption bands at 1714 and 1736 cm^{-1} due to the valence vibration of the carboxylic and ester C=O bonds, respectively, and a broad adsorption band at ca. 3200 cm^{-1} caused by the stretching vibration of the carboxylic O–H bonds. The changes in the

FTIR spectrum reflect the chemical transformations that occurred during formation of the carboxyl terminated prepolymer as illustrated in Figure 2.9.

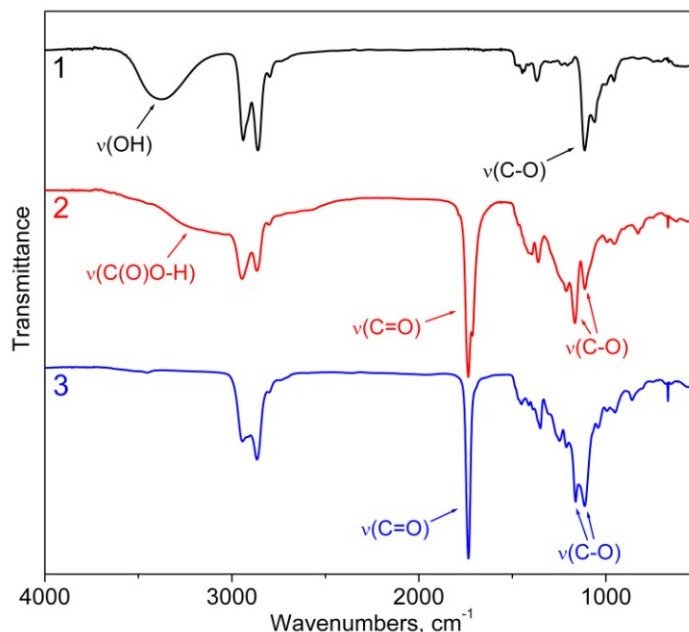


Figure 2.10. FTIR spectra of (1) PTHF-250, (2) carboxyl terminated prepolymer based on PTHF-250, (3) amphiphilic invertible polyester PEG₁₀₀₀PTHF₂₅₀.

In the second stage, polyesterification reaction between the carboxyl terminated prepolymer and an equimolar amount of hydroxy terminated PEG has been carried out in boiling toluene in the presence of a catalytic amount of sulfuric acid. During interaction between the carboxylic groups of the prepolymer and the OH end-groups of poly(ethylene glycol), the final amphiphilic invertible polyester with hydrophilic PEG and hydrophobic PTHF fragments alternately distributed along the macromolecular chain has been developed. To shift the reaction equilibrium towards polyester formation, the water formed during the process has been removed from the reactive mixture in the form of a toluene-water azeotrope and collected in a Dean-Stark trap. As a result of the reaction, adsorption bands belonging to the unreacted carboxylic groups

(C=O vibration at 1714 cm^{-1} and O–H vibration at ca. 3200 cm^{-1}) have disappeared in the FTIR spectrum of the final polyester (Figure 2.10, curve 3). In turn, the presence of the carbonyl group in the AIPE-2 macromolecules is indicated by an intensive adsorption band at 1735 cm^{-1} corresponding to C=O stretching vibration. A doublet of intensive adsorption bands at $1163\text{--}1114\text{ cm}^{-1}$ is caused by stretching vibration of ether and ester C–O bonds. Finally, a broad adsorption band at $2945\text{--}2865\text{ cm}^{-1}$ is due to the stretching vibration of $-(\text{CH}_2)_n-$ groups. To this end, six amphiphilic invertible polyesters differing in the length of hydrophilic PEG and hydrophobic PTHF fragments have been synthesized.

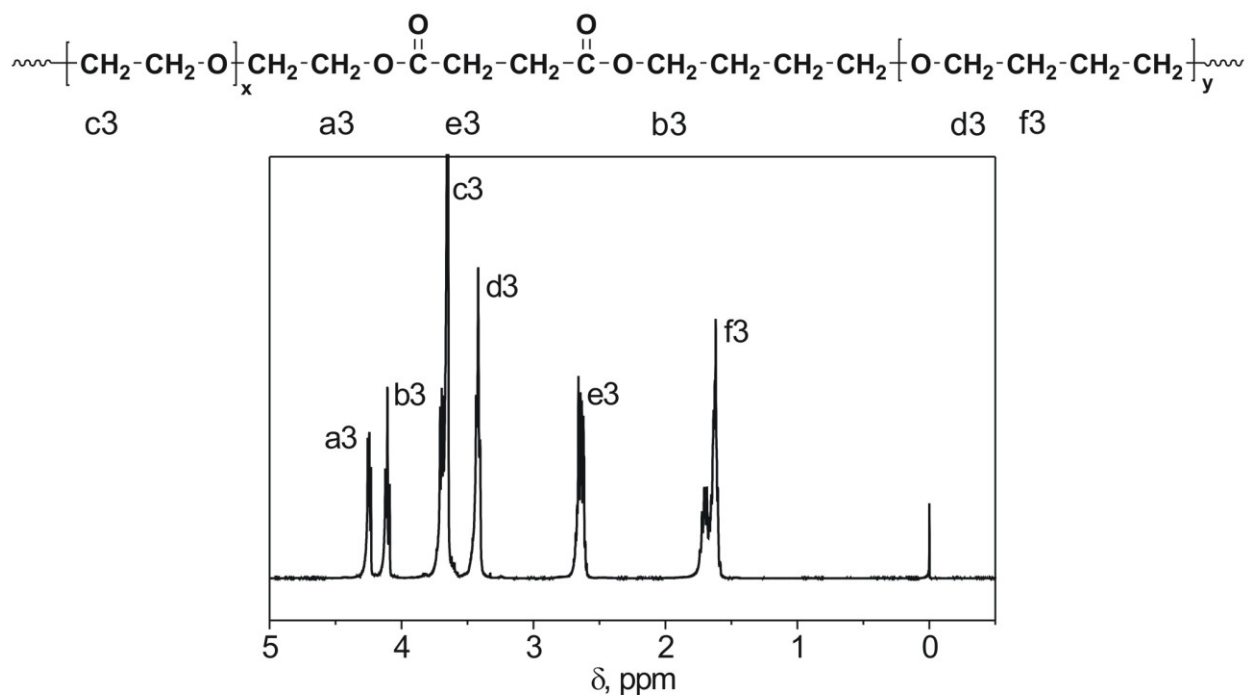


Figure 2.11. ^1H NMR spectrum of the polyester $\text{PEG}_{300}\text{PTHF}_{250}$.

The ^1H NMR spectrum of the polyester $\text{PEG}_{300}\text{PTHF}_{250}$ in chloroform-*d* is presented in Figure 2.11. In the ^1H NMR spectrum of the polyester, peaks corresponding to protons of the PEG chains appear at 3.65 ppm (m, 18H, $\text{CH}_2\text{OCH}_2\text{CH}_2\text{OCH}_2$), 3.69 ppm (t, 4H,

C(O)OCH₂CH₂O), and 4.24 ppm (t, 4H, C(O)OCH₂CH₂O). Polytetrahydrofuran protons show themselves as peaks at 1.62 ppm (m, 8H, CH₂OCH₂CH₂CH₂), 1.70 ppm (m, 4H, C(O)OCH₂CH₂CH₂), 3.42 ppm (m, 8H, CH₂OCH₂CH₂CH₂), and 4.11 ppm (t, 4H, C(O)OCH₂CH₂CH₂). A peak at 2.64 ppm is attributed to an ethylene group of the succinate fragment (tt, 4H, OC(O)CH₂CH₂C(O)O). The NMR spectrum of PEG₃₀₀PTHF₂₅₀ is typical for all synthesized PEG-PTHF based polyesters in terms of chemical shifts and multiplicities of proton peaks.

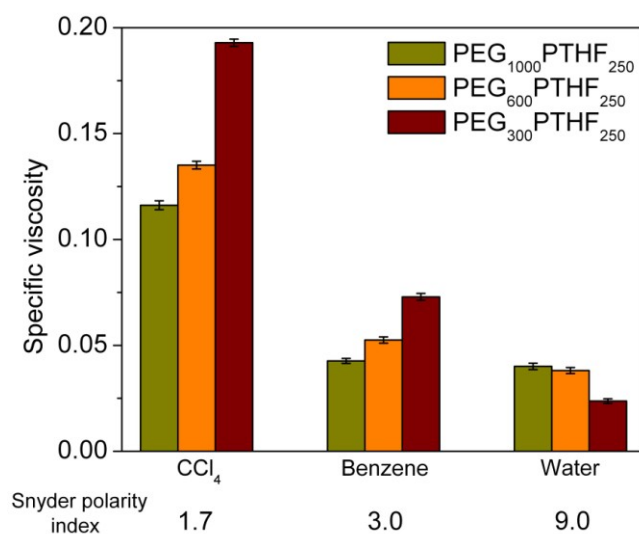


Figure 2.12. Specific viscosities of the AIPE-2 solutions in solvents differing by polarity ($C = 0.01$ g/mL).

Specific viscosity of three AIPEs-2, PEG₁₀₀₀PTHF₂₅₀, PEG₆₀₀PTHF₂₅₀, and PEG₃₀₀PTHF₂₅₀ has been measured in three different solvents (carbon tetrachloride, benzene, and water), and hydrodynamic radii of the AIPE-2 macromolecules have been calculated (Figure 2.12 and Table 2.6). Similar to AIPEs-1 and AIPUs, solutions of AIPEs-2 have the highest specific viscosity in carbon tetrachloride, indicating that AIPE-s macromolecules are extended in this solvent. Aqueous solutions of AIPE-2 polyesters demonstrate the lowest specific viscosity.

Table 2.6. Calculated Hydrodynamic Radii (in nm) of AIPEs-2 in Different Solvents

Polymer	CCl ₄	Benzene	Water
PEG ₁₀₀₀ PTHF ₂₅₀	2.4	1.7	1.7
PEG ₆₀₀ PTHF ₂₅₀	2.7	2.0	1.8
PEG ₃₀₀ PTHF ₂₅₀	3.3	2.4	1.7

Due to insolubility of the hydrophobic PTHF fragments in water, AIPE-2 build micelles with the tight hydrophobic interior and the hydrophilic exterior in the aqueous solution, thus causing a decrease in the hydrodynamic radius and, therefore, lowering solution viscosity. Noteworthy, viscosity of AIPE-2 solutions in a nonpolar benzene increases with decreasing polymer HLB (Table 2.5). AIPEs-2 are assumed to form micelles with a hydrophilic PEG interior and a hydrophobic PTHF exterior in benzene. Since benzene is a good solvent for the hydrophobic PTHF fragments of the polyester macromolecules, hydrophobic polyesters with higher content of nonpolar PTHF units are expected to have increased hydrodynamic radius values leading to an increase in solution viscosity. Thus, it can be concluded from the viscosity data that AIPE-2 macromolecules adjust their conformation to the polarity of the environment.

2.5. Conclusions

Three classes of novel amphiphilic invertible polymers (AIPs), namely polyesters based on PEG and aliphatic dicarboxylic acids (AIPEs-1), polyurethanes on the basis of PEG and PTHF (AIPUs), and polyesters based on PEG and polytetrahydrofuran (AIPEs-2), have been synthesized. The structures of all three AIP classes are strategically designed with the purpose of developing novel responsive polymeric materials by manipulating environment-dependent AIP self-assembly. The use of different polymer types (polyesters and polyurethanes) and

hydrophobic fragments (aliphatic dicarboxylic acids and PTHF) has been considered an instrument to tune AIP hydrophilic-lipophilic balance and vary AIP surface activity, self-assembly behavior, and invertible properties. The AIP macromolecules adjust their hydrodynamic radius in response to changing polarity of the medium, and the changes could be correlated to their chemical structure.

2.6. References

1. Hamley, I.W. *Introduction to Soft Matter: Polymers, Colloids, Amphiphilics and Liquid Crystals*; Wiley: Chichester, UK, 2000.
2. Kwon, G.S.; Kataoka, K. *Adv. Drug Delivery Rev.* **1995**, *16*, 295–309.
3. Torchilin, V.P. *Adv. Drug Delivery Rev.* **2002**, *54*, 235–252.
4. McPherson, A. *Methods Enzymol.* **1985**, *114*, 112–120.
5. Cudney, R.; Patel, S.; Weisgraber, K.; Newhouse, Y.; McPherson, A. *Acta Crystallogr. D Biol. Crystallogr.* **1994**, *50*, 414–423.
6. Harris, J.M. In *Poly(Ethylene Glycol) Chemistry: Biotechnical and Biomedical Applications*; Harris, J. M., Ed.; Plenum Press: New York, NY, 1992.
7. Andrade, J.D.; Hlady, V.; Jeon, S.-I. In *Hydrophilic Polymers: Performance with Environmental Acceptance*; Glass, J.E., Ed.; Advances in Chemistry Series 248; American Chemical Society: Washington, DC, 1996, pp 51–59.
8. Sakai, T.; Alexandridis, P. *Nanotechnology* **2005**, *16*, S344–S353.
9. Alexandridis, P. *Curr. Opin. Colloid Interface Sci.* **1997**, *2*, 478–489.
10. Adams, M.L.; Lavasanifar, A.; Kwon, G. S. *J. Pharm. Sci.* **2003**, *92*, 1343–1355.
11. Lee, M.; Kim, S.W. *Pharm. Res.* **2005**, *22*, 1–10.
12. Mortensen K.; Pedersen, J.S. *Macromolecules* **1993**, *26*, 805–812.

13. Mortensen, K. In *Amphiphilic Block Copolymers*; Alexandridis P.; Lindman, B., Eds.; Elsevier: New York, NY, 2000.
14. Rosch, H. In *Nonionic surfactants*; Schick, M.J., Ed.; Dekker: New York, NY, 1967.
15. Zhou, Z.; Chu, B. *J. Colloid Interface Sci.* **1988**, *126*, 171–180.
16. Aharoni, M.S. *Macromolecules* **1983**, *16*, 1722–1728.
17. Mortensen, K.; Brown, W.; Jorgensen, E. *Macromolecules* **1994**, *27*, 5654–5666.
18. Liu, S.Y.; Armes, S.P. *Angew. Chem. Int. Ed.* **2002**, *41*, 1413–1416.
19. Cogan, K.A.; Gast, A.P. *Macromolecules* **1990**, *23*, 745–753.
20. Halperin, A.; Tirrell, M.; Lodge, T.P. *Adv. Polym. Sci.* **1991**, *100*, 31–71.
21. Winsor, P.A. In *Liquid Crystals and Plastic Crystals*, Vol. 1, Gray, G.W.; Winsor, P.A., Eds.; Ellis Harwood Ltd.: Chichester, U.K., 1974; Chapter 5.
22. Huh, C. *J. Colloid Interface Sci.* **1979**, *71*, 408–426.
23. Luzinov, I.; Minko, S.; Tsukruk, V. *Prog. Polym. Sci.* **2004**, *29*, 635–698.
24. Jeong, B.; Gutowska, A. *Trends Biotechnol.* **2002**, *20*, 305–311.
25. Cohen Stuart, M.A.; Huck, W.T.S.; Genzer, J.; Müller, M.; Ober, C.; Stamm, M.; Sukhorukov, G.B.; Szleifer, I.; Tsukruk, V.V.; Urban, M.; Winnik, F.; Zauscher, S.; Luzinov, I.; Minko, S. *Nature Mater.* **2010**, *9*, 101–113.
26. Russel, T.P. *Science* **2002**, *297*, 964–967.
27. Lukas, J.; Sodhi, R.N.S.; Sefton, M.V. *J. Colloid Interface Sci.* **1995**, *174*, 421–427.
28. Basu, S.; Vutukuri, D.R.; Shyamroy, S.; Sandanaraj, B. S.; Thayumanavan, S. *J. Am. Chem. Soc.* **2004**, *126*, 9890–9891.
29. Arumugam, S.; Vutukuri, D.R.; Thayumanavan, S.; Ramamurthy, V. *J. Am. Chem. Soc.* **2005**, *127*, 13200–13206.

30. Savariar, E.N.; Aathimanikandan, S.V.; Thayumanavan, S. *J. Am. Chem. Soc.* **2006**, *128*, 16224–16230.
31. Takahara, A.; Okkema, A.Z.; Cooper, S.L.; Coury, A.J. *Biomaterials* **1991**, *12*, 324–334.
32. Okkema, A.Z.; Fabrizio, D.J.; Grasel, T.G.; Cooper, S.L.; Zdrahala, R.J. *Biomaterials* **1989**, *10*, 23–32.
33. Deng, Z.; Schreiber, H.P. *J. Adhesion* **1991**, *36*, 71–82.
34. Pike, J.K.; Ho, T. *Chem. Mater.* **1996**, *8*, 856–860.
35. Takahara, A.; Jo, N. J.; Kajiyama, T. *J. Biomater. Sci. Polym. Ed.* **1989**, *1*, 17–29.
36. Takahara, A.; Takahashi, K.; Kajiyama, T. *J. Biomater. Sci. Polym. Ed.* **1993**, *5*, 183–196.
37. Voronov, A.; Kohut, A.; Peukert, W.; Voronov, S.; Gevus, O.; Tokarev, V. *Langmuir* **2006**, *22*, 1946–1948.
38. Sieburg, L.; Kohut, A.; Kislenko, V.; Voronov, A. *J. Colloid Interface Sci.* **2010**, *351*, 116–121.
39. Davies, J.T.; Rideal, E.K. *Interfacial Phenomena*; Academic Press: New York, NY, 1961; 201 p.
40. Azagarsamy, M. A.; Yesilyurt, V.; Thayumanavan, S. *J. Am. Chem. Soc.* **2010**, *132*, 4550–4551.
41. Yesilyurt, V.; Ramireddy, R.; Thayumanavan, S. *Angew. Chem. Int. Ed.* **2011**, *50*, 3038–3042.
42. Wright, P.; Cumming, A.P.C. *Solid Polyurethane Elastomers*; MacLaren and Sons: London, UK, 1969.
43. Griffin, W.C. *J. Soc. Cosmet. Chem.* **1954**, *5*, 249–256.

CHAPTER 3. MICELLIZATION, SELF-ASSEMBLY, AND RESPONSIVE PROPERTIES OF AMPHIPHILIC INVERTIBLE POLYMERS IN POLAR AND NONPOLAR MEDIA

3.1. Abstract

Environment-dependent formation of micelles from a range of amphiphilic invertible polymers (AIPs) has been established. AIP macromolecules have been demonstrated to respond to changing polarity of the medium. In a polar aqueous medium, AIPs build micelles with a hydrophilic corona consisting of PEG fragments and a hydrophobic interior. AIP macromolecules invert their conformation in nonpolar aromatic solvents and form micelles with a hydrophobic exterior and a hydrophilic inner part. Amphiphilic invertible polymers undergo self-assembly upon increasing polymer concentration in solution and form micellar assemblies with hydrophilic and hydrophobic domains in both polar and nonpolar media. Depending on the AIP chemical composition and concentration, a variety of micellar morphologies including spheres, cylinders, and ellipsoids are formed.

Thin AIP films are able to change the surface energy of the substrate regardless of its polarity: nonpolar substrates become more hydrophilic while polar ones become more hydrophobic. The film itself changes its surface energy upon exposure to liquids differing by polarity. If AIP film is in contact with water, the contact interface is enriched with hydrophilic PEG chains. Upon exposure to the nonpolar diiodomethane, amphiphilic macromolecules invert their structure and hydrophobic fragments come to the surface.

Responsive properties of the AIPs could clearly form the basis for the new polymer architectures, both in solution and on the surface, which could be useful in a broad range of applications.

3.2. Introduction

Composed from hydrophilic and hydrophobic constituents, amphiphilic polymer molecules are able to self-organize and build micellar assemblies due to the incompatibility of macromolecular fragments and/or differential solvation of the hydrophilic and hydrophobic fragments by a solvent.¹⁻⁵ Self-assembly of amphiphilic polymers has been established as a useful tool for developing a massive collection of nanosized objects providing control over their dimensions and morphologies.⁶ Aggregation of polymer molecules gives rise to a variety of nanoassemblies including spherical, rod-like, tubular, and lamellar structures, discs, vesicles, cylindrical networks, etc.⁷⁻¹⁸ The formed discrete nanoscale structures have attracted considerable interest because of their great potential in numerous advanced technological applications such as in the electronics industry,¹⁹⁻²³ biomedicine,²⁴⁻³⁴ and pharmaceuticals.³⁵

The use of amphiphilic polymers in an aqueous medium is often based on their ability to form micellar structures with a hydrophobic interior compartment being isolated from the polar aqueous environment by a hydrophilic exterior.^{8,36-37} In nonpolar media, inverse micelles with a hydrophilic inner part and a hydrophobic outer part are formed.³⁸ Such a difference between the internal and external parts of the micelle in terms of chemical composition and properties makes them promising materials for use in targeted cellular delivery of diagnostic or therapeutic agents.^{39,40} In turn, the shape of such persistent structures can also be critical in determining their possible application. For example, particles with higher aspect ratios have been recently demonstrated to be internalized by HeLa cells faster than spherical ones.⁴¹ Conversely, spherical nanostructures modified with the cell transduction domain of HIV-1 Tat protein demonstrated a higher extent of cell uptake as compared to cylinders.⁴² Worm-like micelles and their branched counterparts are probed as templates for asymmetric and aligned nanostructures,⁴³⁻⁴⁵ as well as

drag-reducing additives.^{46,47} Their ability to entangle in aqueous solutions has resulted in them being tested as viscosity enhancers in personal care products and in enhanced oil recovery.^{48,49} Therefore, the enormous effect that the shape of micellar assemblies has on their application makes the issue of manipulating micellar assembly morphologies a critical problem in self-assembly.⁵⁰

The application of external stimuli is known to significantly affect the morphologies of the self-assembled structures developed from amphiphilic polymers.^{51,52} For example, the use of pH as a stimulus is known to lead to changes in the shape of the amphiphilic block copolymer micelles developed from poly(acrylic acid)-*block*-polystyrene.⁵³ Changing morphologies of amphiphilic polymer micelles has also been demonstrated as a response to applying heat, changing the ratio of components in a block copolymer structure, addition of another chemical substance, or varying solvent ratio in a solvent mixture.⁵⁴⁻⁵⁸

The research described in this chapter is aimed at studying the self-assembly and responsive properties of micelles, micellar assemblies, and films developed from amphiphilic invertible polymers. The possibility of conformational switching for AIP architectures can be reached with a controllable presence of oxygen atoms in the main backbone of the polymer. Our structural hypothesis suggests that the presence of hydrophilic and hydrophobic fragments in AIP molecules can lead to changes in morphologies of AIP macromolecular assemblies upon exposure to solvents of different polarities. The following main questions are targeted in this study: (1) How do the AIPs behave upon exposure to the media differing in polarity? (2) Are the AIP micelles capable of self-assembly and formation of micellar assemblies both in a polar and a nonpolar medium with increasing polymer concentration? (3) What morphologies are formed from the AIPs in the micellar state and in thin films?

To this end, a broad study on the behavior of AIPs upon exposure to media of varying polarity has been carried out. ^1H NMR and contact angle measurements have been used to determine whether AIPs are able to form invertible micelles and self-assemble into micellar nanostructures with increasing polymer concentration in different media. Subsequently, a morphological study on AIP micellar assemblies and thin films using small angle neutron scattering, differential scanning calorimetry, and transmission electron microscopy has been carried out.

3.3. Experimental

3.3.1. Materials

Acetone- d_6 , benzene- d_6 , and toluene- d_8 were purchased from Cambridge Isotope Laboratories, Inc. Deuterium oxide, chloroform- d , polystyrene (molecular weight M_w 280,000 g/mol) and poly(2-vinylpyridine) (molecular weight M_w 159,000 g/mol) were all purchased from Aldrich. Solvents (acetone and benzene, ACS grade), pyrene, and phosphotungstic acid hydrate were obtained from VWR International. All reagents and materials were used as received.

Amphiphilic invertible polymers were synthesized from PEG and aliphatic dicarboxylic acids (AIPES-1), PEG, PTHF and 2,4-TDI (AIPUs), and PEG, PTHF and succinic anhydride (AIPES-2) as described in Chapter 2.

3.3.2. Characterization

^1H NMR spectra were recorded on a JEOL ECA 400 MHz NMR spectrometer equipped with a 24-place autosampler carousel using chloroform- d , acetone- d_6 , benzene- d_6 , toluene- d_8 , deuterium oxide, as well as mixtures of benzene- d_6 -acetone- d_6 (9:1 w/w) and acetone- d_6 - D_2O (9:1 w/w) as solvents.

Surface tension measurements were performed by drop shape analysis on a pendant drop produced with an FTÅ125 Contact Angle/Surface Tension Analyzer (First Ten Angstroms). Measurements were carried out at room temperature on polymer solutions of varying concentration (10^{-6} –10% w/w). All glassware was washed in a 1 N NaOH bath and thoroughly rinsed with Millipore water before use. The critical micelle concentrations of the AIPs were determined from the second point of inflection on the surface tension isotherms.

Determination of critical micelle concentration of AIPs via pyrene solubilization method was carried out as follows. First, a solution of pyrene in acetone with a concentration of 5×10^{-4} mol/L was prepared. Each sample was prepared by adding the pyrene solution (20 μ L) into an empty vial, evaporating the acetone for 2 h at room temperature, adding the AIP solution (20 mL), and stirring the solution for at least 24 h before measurements. The final pyrene concentration in water reached 5×10^{-7} mol/L, which is slightly below the pyrene saturation concentration in water at room temperature. For the fluorescence measurements, the solution (ca. 3 mL) was placed in a 1.0×1.0 cm² cell. All spectra were taken using a Fluoromax-3 Fluorescence Spectrometer (Jobin Yvon Horiba) with 90° geometry and a slit opening of 0.5 nm. For fluorescence excitation spectra, $\lambda_{em} = 390$ nm was chosen. Spectra were accumulated with an integration time of 0.5 nm/s. Critical micelle concentration values were determined after fitting the semi-logarithmic plots of intensity ratio $I_{336.5}/I_{333}$ versus log concentration to the sigmoidal curve.

Size distribution of AIP micelles was measured using Malvern Zetasizer Nano-ZS90 at 25 °C. The final numbers represent an average of a minimum of five individual measurements.

Contact angle measurements were carried out using FTÅ 125 Contact Angle/Surface Tension Analyzer. Thin films of polystyrene (PS) and poly(2-vinylpyridine) (PVP) were spin

coated onto polished silicon wafers from benzene solution (5 mg/mL) and dried. Synthesized amphiphilic invertible polymers were deposited onto the surface of unmodified silicon wafers, PS, and PVP by spin-coating from benzene (10 mg/mL). A drop of bidistilled water or diiodomethane (CH_2I_2) was placed on the surface of the substrate afterwards. Advancing contact angles (θ) were measured in 30 s after the drop had been settled. An average value of the contact angles of at least five drops was accepted.

Glass transition and melting temperatures of amphiphilic invertible polyurethanes were determined via modulated differential scanning calorimetry (MDSC) using a TA Instruments Q1000 calorimeter. Dry nitrogen with a flow rate of 50 mL/min was purged through the sample. Samples were subjected to an underlying heating rate of 3 °C/min. The temperature was modulated with the amplitude of ± 0.64 °C every 40 s.

The small angle neutron scattering (SANS) experiments were performed at the Oak Ridge National Laboratory (Tennessee, USA) with a General Purpose Small-Angle Neutron Scattering Diffractometer (CG-2) of the High Flux Isotope Reactor (HFIR) and with an Extended Q-Range Small-Angle Neutron Scattering Diffractometer (EQ-SANS) of the Spallation Neutron Source (SNS). Incident neutron beam with a wavelength of $\lambda = 6.0$ Å and a wavelength distribution $\Delta\lambda/\lambda = 0.14$ was used. The samples were loaded in the standard quartz sample cells (Hellma) with the thickness of 2 mm. At CG-2, two detector positions (0.3 and 12 m) were used in each experiment to cover an overall accessible range of the scattering vector (Q) of 0.0048–0.75 Å⁻¹. At EQ-SANS, using detector distance of 4 m allowed coverage of a Q -range of 0.0048–0.4 Å⁻¹. Neutron scattering patterns were collected in deuterium oxide at a constant temperature of 15, 25, and 35 °C. The data from the two-dimensional area detector were converted into one-dimensional intensity profiles by radial averaging. The SANS data were then corrected to allow

for sample transmission, detector response, empty cell, and background scattering using a sample of pure solvent as reference. Absolute intensity curves $I(Q)$ were subsequently obtained by the direct beam method.

Transmission electron microscopy (TEM) images of AIP micelles were taken using a JEOL JEM-2100 analytical transmission electron microscope. The negative staining technique was used for the TEM studies. A drop of sample solution was allowed to settle on copper grid for 1 min. Excess sample was blotted away with a strip of filter paper and a drop of 1% phosphotungstic acid was allowed to contact with the sample for 1 min. Subsequently, excess solution was removed using filter paper, and the sample was dried in air.

3.4. Results and Discussion

3.4.1. Determination of the Critical Micelle Concentration of AIP Aqueous Solutions

The ability of AIPs to build micelles was demonstrated by determining the critical micelle concentration (cmc) of the polymer aqueous solutions. Since different methods of cmc determination are known to result in conflicting cmc values, two techniques, namely surface tension measurements and pyrene solubilization, have been used to evaluate the AIP critical micelle concentration. Subsequently, the data obtained using the two methods have been compared and analyzed.

Semi-logarithmic plots of the surface tension isotherms for the solutions of AIPs-1 and AIPs-2 are given in Figure 3.1. The surface tension of the surfactant aqueous solution is known to decrease with increasing concentration up to a certain point which corresponds to the critical micelle concentration of the surfactant, and remain reasonably stable above the cmc. Hence, the data in Figure 3.1 indicate that all AIPs are surface-active substances, since they decrease the

surface tension of water up to ca. 45 mN/m. Due to the interaction of hydrophobic fragments and flexibility of the macromolecule, AIPES are assumed to build molecular assemblies with hydrophobic pockets and external hydrophilic corona. Thermodynamically stable copolymer assemblies are known to be formed at low concentration in both polar and nonpolar solvents.^{59,60} The slope observed at low concentrations on the surface tension isotherms of most AIPES may indicate that after the formation of molecular assemblies, they migrate to the interface and form a monomolecular adsorption layer there. The accompanying rapid decrease of the surface tension continues until the cmc point where polymolecular micelles start to form. After the cmc is reached, the surface activity of AIP macromolecules does not change anymore.

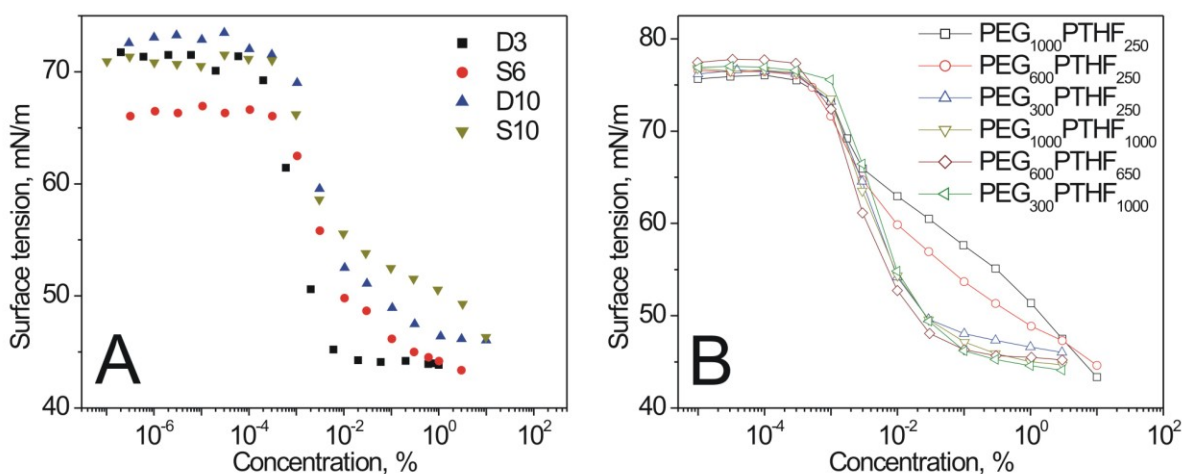
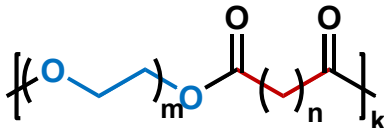
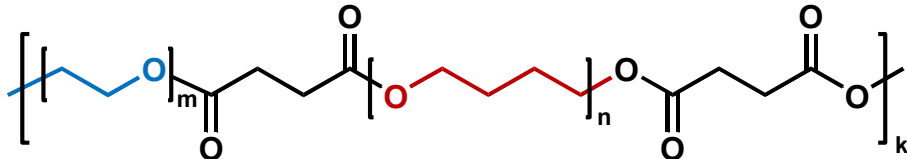


Figure 3.1. Surface tension isotherms of the aqueous solutions of AIPES-1 (A) and AIPES-2 (B).

The critical micelle concentration values for all AIPES-1 and AIPES-2 are presented in Table 3.1. The appearance of the isotherms and cmc values are greatly influenced by both chemical composition and hydrophilic-lipophilic balance of the polymer. As evidenced by their cmc values, surface activity of amphiphilic invertible polyesters based on PEG and dicarboxylic acids increases with decreasing HLB. These polymers tend to build micelles more readily when

the length of the hydrophilic PEG residues in the macromolecule is smaller. A completely different behavior is observed for PEG-PTHF based polyesters. The cmc values of the four polyesters (PEG₃₀₀PTHF₂₅₀, PEG₁₀₀₀PTHF₁₀₀₀, PEG₆₀₀PTHF₆₅₀, and PEG₃₀₀PTHF₁₀₀₀) are reasonably close, while the surface tension isotherms of the two most hydrophilic polyesters (PEG₁₀₀₀PTHF₂₅₀ and PEG₆₀₀PTHF₂₅₀) do not exhibit a well-expressed inflection point. The reason for this behavior is their very good aqueous solubility due to the high content of long hydrophilic PEG fragments in the molecule.

Table 3.1. Critical Micelle Concentration of Amphiphilic Invertible Polymers

AIP	Davies HLB	Critical micelle concentration, mg/L	
		By surface tension measurements	By pyrene solubilization
			
S10	15.4	N/A	568
D10	14.4	190	36.8
S6	12.4	140	32.2
D3	9.2	56	10.4
			
PEG ₁₀₀₀ PTHF ₂₅₀	20.1	N/A	670
PEG ₆₀₀ PTHF ₂₅₀	17.1	N/A	680
PEG ₃₀₀ PTHF ₂₅₀	14.9	200	9.4
PEG ₁₀₀₀ PTHF ₁₀₀₀	13.9	250	N/A
PEG ₆₀₀ PTHF ₆₅₀	13.8	160	3.5
PEG ₃₀₀ PTHF ₁₀₀₀	8.6	260	N/A

To better understand the AIP micellization behavior in aqueous medium, pyrene solubilization experiments have been carried out. In the aqueous micellar solution hydrophobic pyrene molecules become solubilized in the nonpolar micellar interior causing a red shift of the major pyrene fluorescence emission band. Such environment-dependent behavior enables the use of pyrene as a probe to study macromolecular association and determine the cmc of amphiphilic polymers. Unlike surface tension measurements that only show the relative occupancy of the air/water interface by the surfactant molecules, pyrene solubilization experiment provides information about the formation of the hydrophobic micellar interior and, therefore, is a more direct method of evaluating cmc.^{61,62}

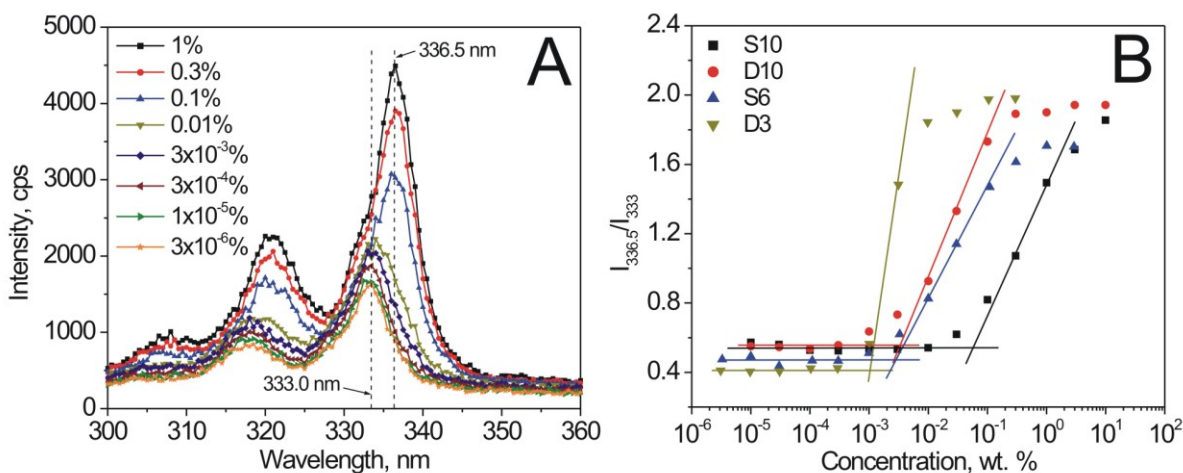


Figure 3.2. (A) Excitation spectra of pyrene in the aqueous solutions of polyester S6 at different concentrations. (B) The intensity ratio $I_{336.5}/I_{333}$ of the excitation spectra of pyrene in aqueous solutions of AIPs-1 versus AIPs-1 concentration.

To determine the critical micelle concentration of the AIPs, excitation spectra of the pyrene-AIP aqueous solutions have been recorded in the wavelength range of 300–360 nm (Figures 3.2 and 3.3). As polymer concentration increases, the red shift of the fluorescence

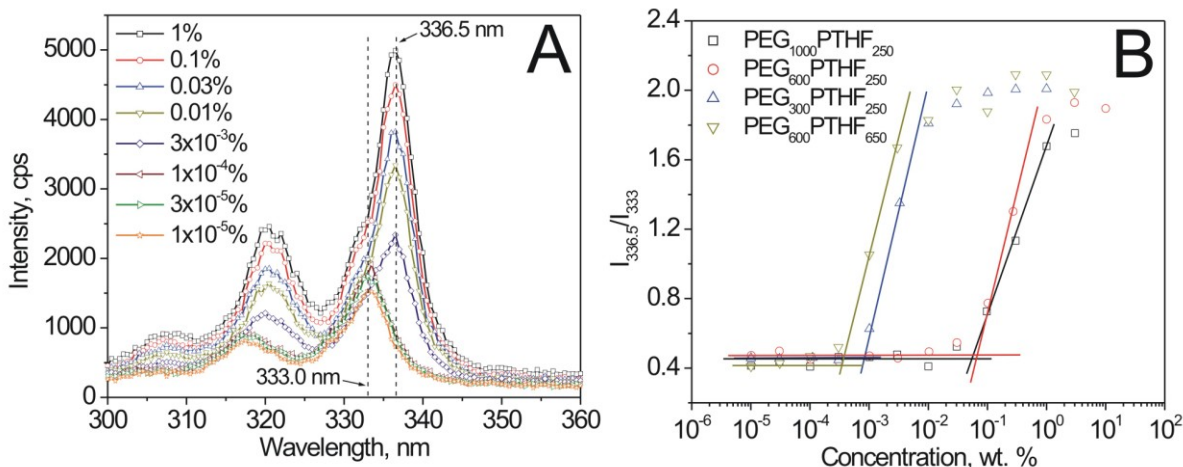


Figure 3.3. (A) Excitation spectra of pyrene in the aqueous solutions of polyester PEG₆₀₀PTHF₆₅₀ at different concentrations. (B) The intensity ratio $I_{336.5}/I_{333}$ of the excitation spectra of pyrene in four aqueous solutions of AIPes-2 versus AIPe-2 concentration.

emission band from 333 nm to 336.5 nm is observed indicating that pyrene molecules are transferred from the polar aqueous environment to the hydrophobic interior of polymer micelles formed via AIP self-organization (Figures 3.2A and 3.3A). Figures 3.2B and 3.3B show the semi-logarithmic plots of intensity ratios $I_{336.5}/I_{333}$ versus log polymer concentration for AIPes-1 based on PEG and aliphatic dicarboxylic acids and PEG-PTHF based AIPes-2, respectively. The sharp increase in the intensity ratio corresponds to the onset of the critical micelle concentration for each polymer. The cmc values determined for all polymers via fitting the semi-logarithmic plots to the sigmoidal curve are given in Table 3.1. The cmc values vary from 3.5 to 680 mg/L and are dependent on both AIPe composition and hydrophilic-lipophilic balance. Such a broad surface activity of the developed polyesters is beneficial, as it is closely associated with the differences in self-assembly behavior. Differences in self-assembly behavior could, in turn, lead to varying AIP micellar capacity for solubilization of poorly soluble materials in water, a feature

useful for the nanoscale drug delivery systems. For both AIPE types, the lowest critical micelle concentration values are observed for the most hydrophobic polymers (10.4 mg/L for D3 and 3.5 mg/L for PEG₆₀₀PTHF₆₅₀). Such a low cmc values indicate that micelles from the more hydrophobic AIPEs would have a very good stability in solution even after a strong dilution by the large volume of water such as after the injection into the systemic blood flow of the human body.

3.4.2. Environment-Dependent Micellization and Responsive Properties of the AIPs in Polar and Nonpolar Media

3.4.2.1. Invertible Micelles from AIPs

¹H NMR spectroscopy has been extensively used to provide researchers with insights into macromolecular conformation of amphiphilic polymers in different media and at wide temperature and concentration range.⁶³⁻⁶⁶ The features of micelle formation have been extensively studied for both low-molecular and polymeric surfactants.⁶⁷⁻⁷⁰ Therefore, in order to further confirm the formation of AIP micelles and their invertible behavior, a broad ¹H NMR spectroscopic study in solvents differing in polarity has been carried out for all AIP types.

¹H NMR spectra of the AIPE-1 polyesters based on PEG and aliphatic dicarboxylic acids have been recorded in D₂O, acetone-*d*₆, CDCl₃, and toluene-*d*₈. The representative local expanded regions of hydrophilic and hydrophobic proton peaks in the ¹H NMR spectra of 1% solutions of the polyester S6 are given in Figure 3.4. The data provided clearly demonstrate that both chemical shifts and appearance of the proton signals are significantly affected by solvent polarity. Thus, S6 proton peaks retain their hyperfine structure in both chloroform-*d* and acetone-*d*₆. The appearance of the peaks as narrow multiplets indicates that both hydrophilic and hydrophobic fragments of the polyester macromolecules can move freely. Hence, S6 molecules

are expanded and no micellization due to polymer self-assembly is observed in these solvents (Figure 3.5A).

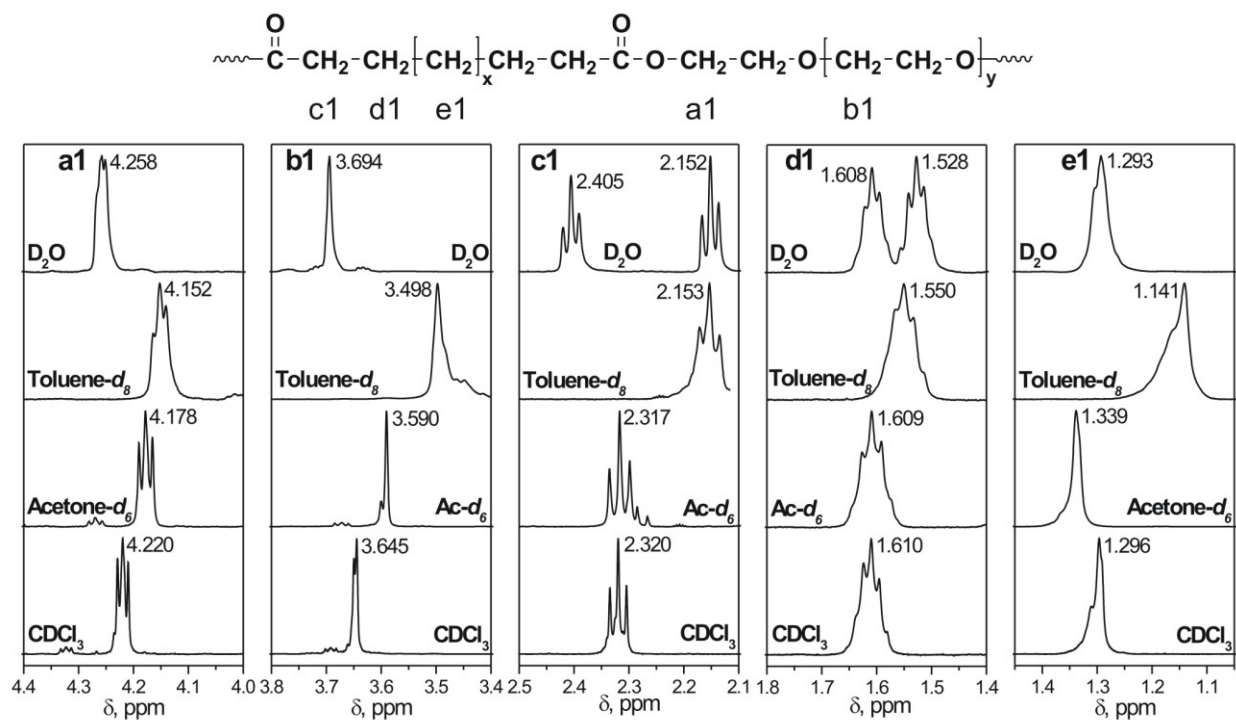


Figure 3.4. Expanded regions of ^1H NMR spectra of the polyester S6 in different solvents.

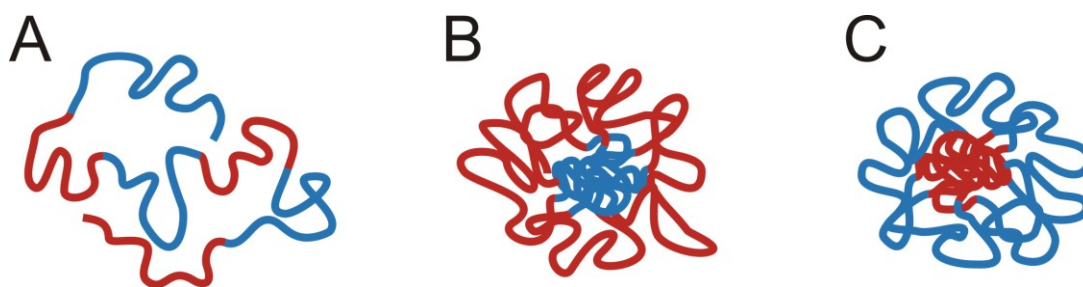


Figure 3.5. Three AIP architectures in solvents differing by polarity: (A) expanded macromolecule, (B) inverse micelle with a hydrophilic interior and a hydrophobic exterior, and (C) micelle with a hydrophobic interior and a hydrophilic exterior.

For the spectra recorded in nonpolar toluene- d_8 , all proton signals exhibit significant upfield shifts arising from the magnetic anisotropy of the aromatic solvent molecules. The

chemical shift is known to be influenced by the chemical nature of the surrounding atoms, therefore interaction of the polyester hydrogen atoms with the aromatic π -electron cloud of the toluene- d_8 molecules gives rise to the ring-current effects causing the so called aromatic solvent induced shift in the ^1H NMR spectrum.^{71,72} NMR signals belonging to the protons of the PEG fragments (peaks a1 and b1) experience broadening in an aromatic solvent. This behavior is assumed to be caused by the development of the microenvironment restricting the mobility of hydrophilic poly(ethylene glycol) chains due to their aggregation. In nonpolar toluene self-assembly of the polyester macromolecules is assumed to give rise to micelles with the tight polar interior consisting of the PEG fragments, while the hydrophobic $-\text{CH}_2-$ chains are believed to form the nonpolar micellar exterior (Figure 3.5B). Noteworthy, peaks of the hydrophobic protons c1, d1, and e1 belonging to the dicarboxylic acid moieties also experience a slight broadening in toluene- d_8 indicating that their motion is hindered. Even though the hydrophobic units form the loose micellar corona, their short length does not allow them to move freely.

As compared to the signals recorded in chloroform- d and acetone- d_6 , the proton peaks of hydrophilic PEG fragments (signals a1 and b1) in D_2O experience a pronounced downfield shift. Shifting PEG proton signals toward higher ppm values indicates the development of the polar microenvironment around these protons caused by formation of the polar micellar exterior. The peaks remain sharp and narrow demonstrating that PEG fragments are able to move freely. In contrast, the width of the polyester proton signals located in the inner part of the nonpolar $-(\text{CH}_2)_n-$ fragment (peak e1) increases in the aqueous medium demonstrating that the mobility of hydrophobic fragments becomes limited as they self-assemble and form a nonpolar micellar interior (Figure 3.5C).

Noteworthy, the methylene protons located in the hydrophobic fragments adjacent to the ester groups (signals c1 and d1) show two different signals in the NMR spectrum of 1% aqueous solution. The considerable downfield shift of one fraction of c1 and d1 (signals at 2.405, and 1.608 ppm, respectively) indicates that the corresponding protons are in direct contact with the polar aqueous environment and are located in the hydrophilic exterior of the micelles. The upfield shift experienced by the remaining part of these protons (peaks at 2.152, and 1.528 ppm, respectively) leads to a conclusion that they are transferred to the nonpolar micellar interior. The observed signal splitting is likely to be caused by the negative inductive effects of the neighboring polar moieties resulting in enhanced polarizability of the C–H bonds adjacent to them.

Hence, in a nonpolar toluene, AIPes-1 based on PEG and aliphatic dicarboxylic acids form micelles with a hydrophilic interior and a hydrophobic exterior (Figure 3.5B). In water, however, polyester macromolecules invert their conformation and build micelles with a hydrophobic inner part and a hydrophilic corona (Figure 3.5C). In contrast, solvents like acetone- d_6 and CDCl_3 are good environments for the amphiphilic polyesters. No micelles are formed in these media (Figure 3.5A).

Due to their low aqueous solubility, micellization behavior of the amphiphilic polyurethanes has been studied by ^1H NMR in benzene- d_6 and mixtures of benzene- d_6 and acetone- d_6 (9 : 1 w/w, respectively), as well as acetone- d_6 and deuterium oxide (9 : 1 w/w). Spectra taken in chloroform- d have been used as a reference. As an example, expanded regions of the spectra of alternating polyurethane based on PEG-1000 and PTHF-1000 in all the solvents employed are depicted in Figure 3.6. The fragments of the spectra show the signals of the protons of polymer hydrophilic (PEG) and hydrophobic (PTHF) chains.

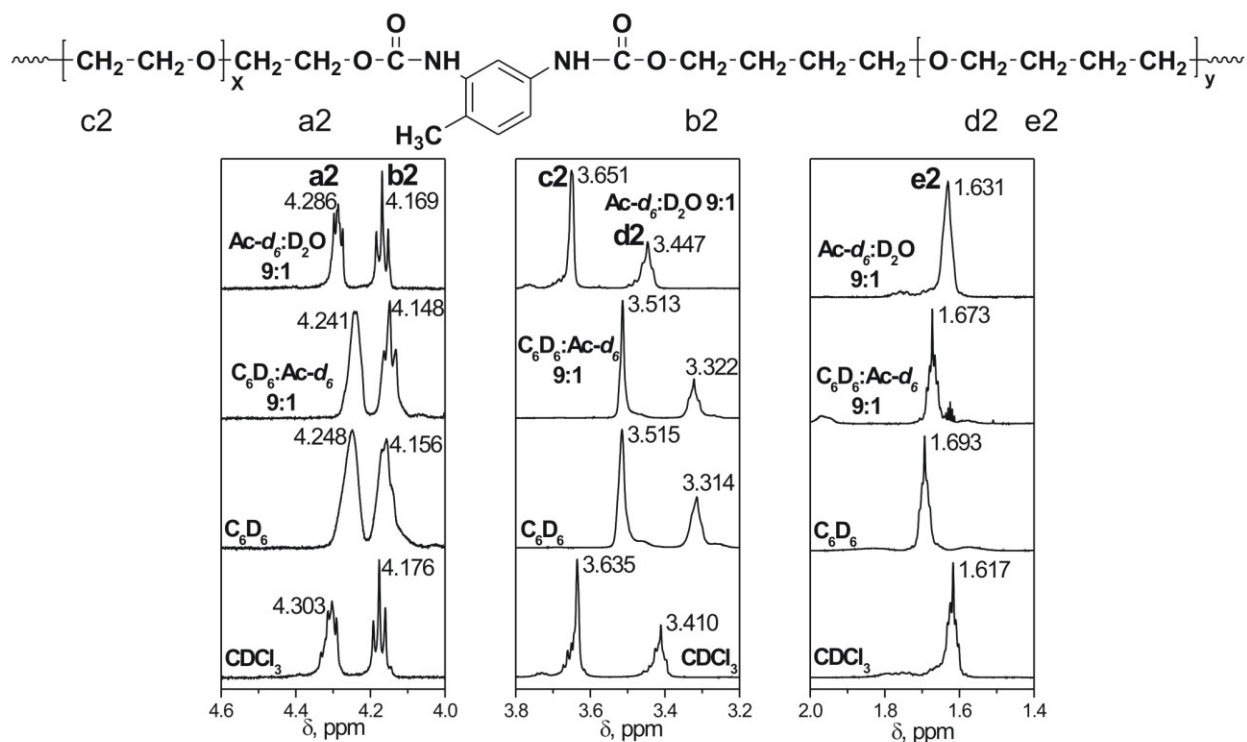


Figure 3.6. Expanded regions of ¹H NMR spectra of the AIPU PEG₁₀₀₀-alt-PTHF₁₀₀₀ in different solvents.

In a polar acetone-*d*₆ – D₂O mixture the signals of both poly(ethylene glycol) and polytetrahydrofuran protons in the α-position to the urethane fragment (signals a2 and b2, respectively) retain their hyperfine structure, which implies that their motions are not hindered. Peak c2, corresponding to the protons in the middle of PEG chain, is narrow, while the signal e2 of the central methylene groups of the tetrahydrofuran fragment appears as a broad singlet, indicating that the mobility of hydrophobic PTHF chains is limited. Remarkably, comparison of spectra recorded in benzene-*d*₆ and in acetone-*d*₆ – D₂O mixture reveals that peak e2 experiences an upfield shift in a polar solvent mixture, indicating that a nonpolar microenvironment consisting of the hydrophobic fragments is formed. The appearance of proton signals in acetone-*d*₆ – D₂O is assumed to be the result of the polymer micellization. Hydrophobic PTHF

chains aggregate and form the dense nonpolar interior of the micelles, while extended poly(ethylene glycol) chains become parts of the micellar exterior (Figure 3.5C).

Comparison of the integral intensity of the signals provides important information about the molecular configuration of amphiphilic polymers. The ratios of numbers of protons in hydrophobic PTHF and in hydrophilic PEG fragments, calculated from the theoretical composition, as well as the integral intensity of the proton signals in the solvents used in the study are shown in Table 3.2.

Table 3.2. PTHF/PEG Proton Ratio of Amphiphilic Invertible Polyurethanes in Different Solvents

Polymer	PTHF/PEG proton ratio				
	Theoretical	CDCl ₃	C ₆ D ₆	C ₆ D ₆ : (CD ₃) ₂ CO 9 : 1	(CD ₃) ₂ CO : D ₂ O 9 : 1
PEG ₁₀₀₀ - <i>alt</i> -PTHF ₆₅₀	0.79	0.85	0.89	0.86	0.75
PEG ₁₀₀₀ - <i>alt</i> -PTHF ₁₀₀₀	1.22	1.26	1.32	1.29	1.17
PEG ₆₀₀ - <i>alt</i> -PTHF ₆₅₀	1.33	1.37	1.46	1.38	1.27
PEG ₆₀₀ - <i>alt</i> -PTHF ₁₀₀₀	2.06	2.11	2.19	2.12	1.99
PEG ₁₀₀₀ - <i>co</i> -PTHF ₆₅₀	0.79	0.84	0.91	0.86	0.79
PEG ₁₀₀₀ - <i>co</i> -PTHF ₁₀₀₀	1.22	1.26	1.33	1.28	1.14
PEG ₆₀₀ - <i>co</i> -PTHF ₆₅₀	1.33	1.38	1.46	1.40	1.29
PEG ₆₀₀ - <i>co</i> -PTHF ₁₀₀₀	2.06	2.02	2.09	2.00	1.89

In chloroform-*d* all proton signals appear as narrow multiplets, suggesting that both hydrophobic and hydrophilic segments of the chains move freely. Moreover, for all polymers PTHF/PEG proton ratio in chloroform is close to the theoretical value, indicating that no segregation of amphiphilic fragments occurs in this solvent (Figure 3.5A). In an acetone-*d*₆ – D₂O mixture, however, the PTHF/PEG proton ratio is significantly lower than that observed in chloroform-*d*. The integral intensity in the NMR spectrum decreases if the protons are buried in the molecular interior and screened by other atoms. Therefore, the data in Table 3.2 demonstrate that the nonpolar PTHF fragments are screened by the polar PEG chains and thus confirm the formation of micelles with a hydrophilic exterior and hydrophobic interior in the polar medium.

All spectra recorded in benzene-*d*₆ show a complete disappearance of the hyperfine structure of hydrophilic PEG proton peaks, accompanied by a broadening of the PTHF proton signals. The absence of any signal splitting in the spectra indicates that the movements of both hydrophilic and hydrophobic units are limited due to steric hindrance. The NMR data are fully consistent with the viscosity measurements (see Chapter 2 for more information), since the lowest viscosity values were measured for AIPU solutions in benzene/toluene. Aromatic solvents are poor solvents for the AIPUs, their molecules are contracted and the polymer chains cannot move freely. It is assumed that the reason for this behavior is the ability of polyurethanes to form intra- and intermolecular hydrogen bonds. Since benzene molecules do not participate in hydrogen bonding, polyurethane –NH– groups can interact only with hydrogen bond acceptors present in the macromolecule, namely, the carbonyl group and oxygen atoms of the PEG and PTHF fragments. This, in turn, impairs the mobility of the polymer chains. Noteworthy, aromatic solvent induced shifts are observed for the AIPU protons a₂–d₂ in benzene.

For all of the AIPUs, the values of the PTHF/PEG protons ratio in benzene- d_6 are higher than those observed in chloroform- d . Nonpolar PTHF segments form the exterior of the polymer micelle, while polar PEG units are located within the micellar interior (Figure 3.5B).

When 10% acetone- d_6 is added to benzene- d_6 , the appearance of NMR signals of hydrophobic protons is changed. Peaks b2 and e2 exhibited a signal splitting which suggested that their mobility had increased. The mobility of hydrophilic PEG chains also became less constrained, as evidenced by the decrease in width of the peak corresponding to protons c2. Since small and mobile acetone molecules possess carbonyl groups that can act as hydrogen bond acceptors, addition of acetone- d_6 is believed to cause cleavage of hydrogen bonds between the AIPU macromolecules, thereby improving mobility of the polyurethane fragments. Since the ratio of hydrophobic to hydrophilic hydrogen atoms in this solvent mixture is similar to that in chloroform- d , neither of these proton types are screened by the other, obviously indicating that no micelles are formed (Figure 3.5A).

Thus, amphiphilic invertible polyurethanes form inverse micelles with a hydrophobic exterior and a hydrophilic interior in 1% solutions in benzene- d_6 . Addition of a small amount of polar acetone- d_6 causes reorganization of the AIPU macromolecular conformation, as the polar inner part of the micelle vanishes and PEG chains become more extended into the medium. Introduction of 10% D₂O to acetone promotes formation of micelles with a hydrophilic outer part and a hydrophobic core.

As the final part of the micellization study, ¹H NMR spectra of PEG-PTHF based polyesters have been recorded in deuterium oxide, toluene- d_8 , and chloroform- d . Figure 3.7 shows the corresponding representative expanded regions of the spectra recorded on PEG₆₀₀PTHF₆₅₀. The changes in chemical shift and appearance of hydrophilic PEG proton

signals similar to those described for the previous AIP types suggest that PEG-PTHF based polyesters also form micelles with a polar exterior and a nonpolar interior in the aqueous medium (Figure 3.5C). Splitting signals of the protons d3 located in the α -position to the PTHF ether oxygen atoms into two peaks (signals at 3.520 and 3.404 ppm) implies that these atoms are divided between the hydrophobic inner part and the hydrophilic corona of the micelle. Polyester macromolecules rearrange themselves in nonpolar toluene- d_8 , giving rise to micelles with the hydrophilic interior and a hydrophobic exterior (Figure 3.5B).

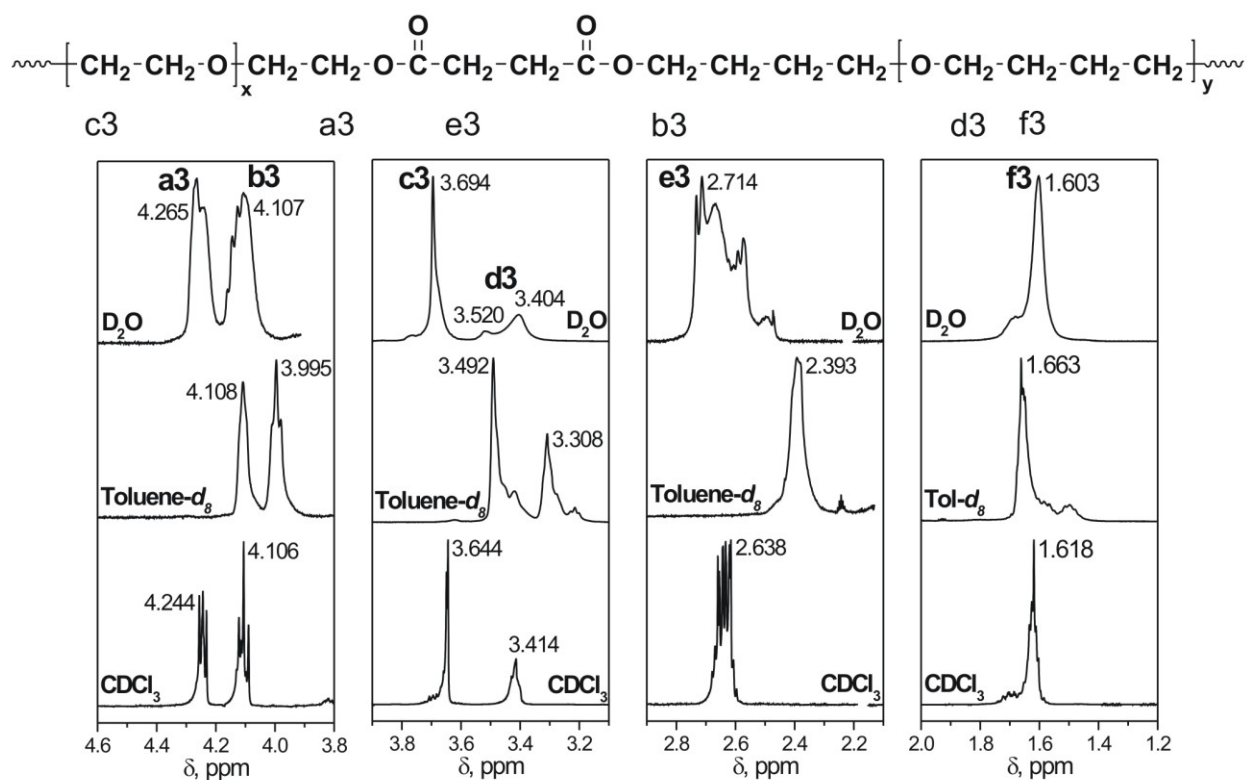


Figure 3.7. Expanded regions of ^1H NMR spectra of $\text{PEG}_{600}\text{PTHF}_{650}$ in different solvents.

Hence, NMR study has clearly confirmed environment-dependent micellization of all types of synthesized amphiphilic invertible polymers. In dilute aqueous solution AIPs build micelles with the polar PEG fragments forming the corona, and hydrophobic chains located in

the interior. In nonpolar aromatic solvents AIPs invert their structure to form micelles with a nonpolar exterior and a polar outer part.

3.4.2.2. Stimuli-Responsive Properties of Thin AIP Films

Measuring contact angles of liquids on the interface between the solid substrate and the air is a simple and rapid test to estimate the surface energy. In order to determine whether the developed amphiphilic invertible polymers are able to adapt to changing polarity of the environment, wetting studies have been carried out. Thin AIPU films have been deposited on the surface of highly polar silicon wafers, less polar poly(2-vinylpyridine), and nonpolar polystyrene. Both PS and PVP have been spin-coated onto silicon wafers and dried. Subsequently, advancing water and diiodomethane contact angles have been measured on the surface of AIPU films (Table 3.3). On the basis of these measurements polar (γ_s^h) and dispersive (γ_s^d) components of surface energy have been calculated in accordance with the Owens-Wendt theory.⁷³

$$1 + \cos \theta = 2 \left[\frac{(\gamma_s^d)^{1/2} (\gamma_l^d)^{1/2}}{\gamma_l} + \frac{(\gamma_s^h)^{1/2} (\gamma_l^h)^{1/2}}{\gamma_l} \right]$$

where θ is the contact angle between the liquid and the solid, degrees; γ_s^d is the dispersive component of the surface energy of solids, mJ/m²; γ_l^d is the dispersive component of the surface tension of the wetting liquid, mJ/m²; γ_s^h is the polar component of the surface energy of solids, mJ/m²; γ_l^h is the polar component of the surface tension of the wetting liquid, mJ/m²; and γ_l is the overall surface tension of the wetting liquid, mJ/m².

The data in Table 3.3 demonstrate that thin AIPU films change the properties of the substrate regardless of its polarity. Water contact angle values measured on the AIPU films deposited on polystyrene surface are lower than those measured on the bare polystyrene substrate

Table 3.3. Advancing Water and Diiodomethane Contact Angles and Surface Energies of Thin Polyurethane Films on Different Substrates

Polymer	On polystyrene				On poly(2-vinylpyridine)				On silica			
	Contact angle, degrees*		Surface energy, mJ/m ²		Contact angle, degrees*		Surface energy, mJ/m ²		Contact angle, degrees*		Surface energy, mJ/m ²	
	H ₂ O	CH ₂ I ₂	γ_s^d	γ_s^h	H ₂ O	CH ₂ I ₂	γ_s^d	γ_s^h	H ₂ O	CH ₂ I ₂	γ_s^d	γ_s^h
PEG ₁₀₀₀ - <i>alt</i> -PTHF ₆₅₀	53±2	18±1	38.7	16.5	40±3	18±1	36.1	25.6	57±2	21±1	38.9	14.4
PEG ₁₀₀₀ - <i>alt</i> -PTHF ₁₀₀₀	70±2	17±1	43.3	6.6	48±5	15±1	38.4	20.0	62±1	19±1	40.6	11.2
PEG ₆₀₀ - <i>alt</i> -PTHF ₆₅₀	34±3	21±2	34.2	30.5	50±3	15±1	38.8	18.6	32±3	21±1	33.9	31.5
PEG ₆₀₀ - <i>alt</i> -PTHF ₁₀₀₀	38±1	18±1	35.8	26.8	41±4	16±1	36.8	25.0	34±1	16±1	35.5	29.6
PEG ₁₀₀₀ - <i>co</i> -PTHF ₆₅₀	23±3	17±1	33.9	36.0	20±2	14±1	34.5	36.5	29±2	17±1	34.7	32.6
PEG ₁₀₀₀ - <i>co</i> -PTHF ₁₀₀₀	36±4	23±1	34.0	29.5	36±2	19±1	35.1	28.6	35±3	20±1	34.8	29.1
PEG ₆₀₀ - <i>co</i> -PTHF ₆₅₀	13±1	18±1	33.0	39.7	36±7	12±1	36.9	27.5	26±1	20±1	33.5	34.5
PEG ₆₀₀ - <i>co</i> -PTHF ₁₀₀₀	30±1	15±1	35.4	31.7	33±2	12±1	36.4	29.3	30±1	15±1	35.4	31.8
No polymer	90±4	26±2	45.9	0.5	49±4	14±1	38.9	19.1	21±2	37±2	26.7	41.8

*All contact angles were measured 30 s after the drop had been placed

demonstrating that thin AIPU films increase the hydrophilicity of the hydrophobic polystyrene. Deposition of thin AIPU films on a highly hydrophilic silica results in the decrease of the diiodomethane contact angle, which obviously indicates that silica surface became more hydrophobic. Exposure to wetting liquids differing by polarity causes changes in the surface energy of the AIPU films due to rearrangement of macromolecular conformation (Table 3.3 and Figure 3.8). When amphiphilic invertible polyurethane layer is in contact with water (a polar solvent), the substrate–wetting liquid interface is enriched with hydrophilic poly(ethylene glycol) chains. If a nonpolar diiodomethane is used as a wetting liquid, AIPU molecules invert their structure and hydrophobic polytetrahydrofuran fragments arrange themselves at the contact surface. This effect is more pronounced in the case of the random amphiphilic invertible polyurethanes due to the presence of segments of several PEG or PTHF units linked together that increase the effective length of hydrophilic and hydrophobic fragments and enhance their flexibility.

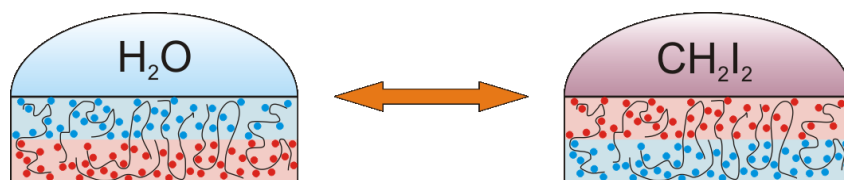


Figure 3.8. Response of the AIP thin film to changing polarity of the medium.

The data in Table 3.3 also demonstrate that the alteration of relative lengths of hydrophilic and hydrophobic segments significantly affects the change of polar component of the surface energy. For example, polar component values vary in the range of 6.6–30.5 mJ/m² for alternating and 29.5–39.7 mJ/m² for random amphiphilic invertible polyurethanes deposited on polystyrene substrate, respectively. Generally, increase in the length of the hydrophobic fragment causes a decrease of the polar component of the surface energy. The value of the polar

component for the random AIPU is typically higher than the corresponding value for the alternating AIPU with the same composition. This fact can be explained by the presence of hard segment domains consisting of 2,4-TDI fragments in the alternating AIPU films which make the structure of the polymer more rigid because of hydrogen bonding (see Section 3.3.3.3 for more information). The presence of numerous hydrogen bonds reduces the mobility of the amphiphilic fragments, thus decreasing the ability of alternating AIPUs to switch their macromolecular conformation leading to the smaller contribution of the polar component into the total surface energy value. In contrast, the values of the dispersive component caused by Wan-der-Waals interactions remain similar for all AIPUs (34.2–43.3 mJ/m² for alternating and 33.0–35.4 mJ/m² for random polyurethanes on polystyrene) indicating that the extent of these interactions in all synthesized AIPUs is comparable regardless of the length of polar and nonpolar fragments.

3.4.3. Self-Assembly of Amphiphilic Invertible Polymers in Polar and Nonpolar Media

A systematic ¹H NMR study has been undertaken to investigate the features of self-assembly of amphiphilic invertible polymers in the media differing by polarity. Effects of AIP composition, concentration and solvent polarity on the structural properties of AIP macromolecules have been evaluated by analyzing ¹H NMR spectra of AIP solutions recorded over the broad range of polymer concentrations in polar and nonpolar solvents.

3.4.3.1. Self-Assembly of Amphiphilic Invertible Polyesters in Water

To study self-assembly of amphiphilic invertible polyesters in water, ¹H NMR spectra of water-soluble AIPs have been recorded at the concentrations ranging from 0.1% to 10%. As an example, the expanded spectral regions of amphiphilic invertible polyesters S6 and

PEG₆₀₀PTHF₆₅₀ recorded in an aqueous solution at 0.1, 1, 5%, and 10% w/w (for S6) are presented in Figures 3.9 and 3.10, respectively.

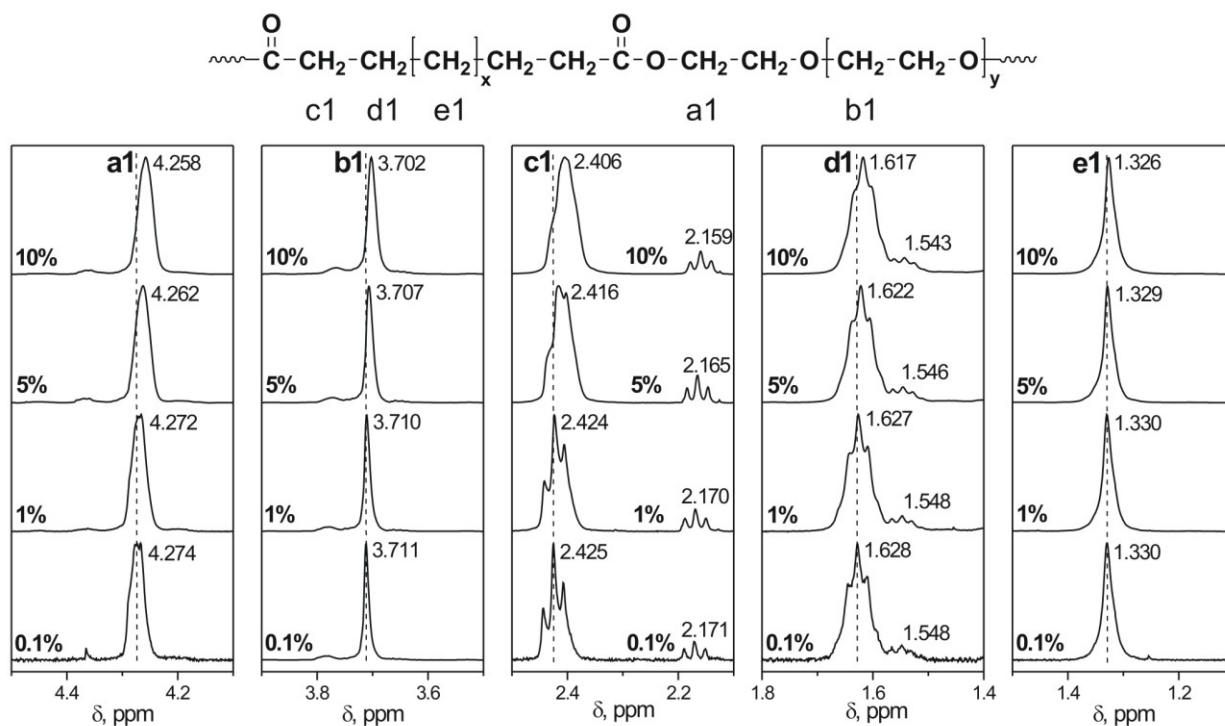


Figure 3.9. Expanded regions of ¹H NMR spectra of S6 recorded in D₂O at different concentrations.

At low concentration in aqueous solution both AIPEs form micelles with a tight nonpolar interior formed by the hydrophobic fragments and a polar exterior formed by the hydrophilic PEG chains. Increasing the AIPE concentration from 0.1 to 5 and 10% leads to the upfield shifts of the majority of the hydrophilic and hydrophobic proton peaks. As polymer concentration increases, AIPE micelles undergo aggregation giving rise to micellar assemblies (Figure 3.11A). The microenvironment in the formed assemblies is less polar than in the individual micelles and, therefore, it causes upfield shifts of the NMR proton peaks.

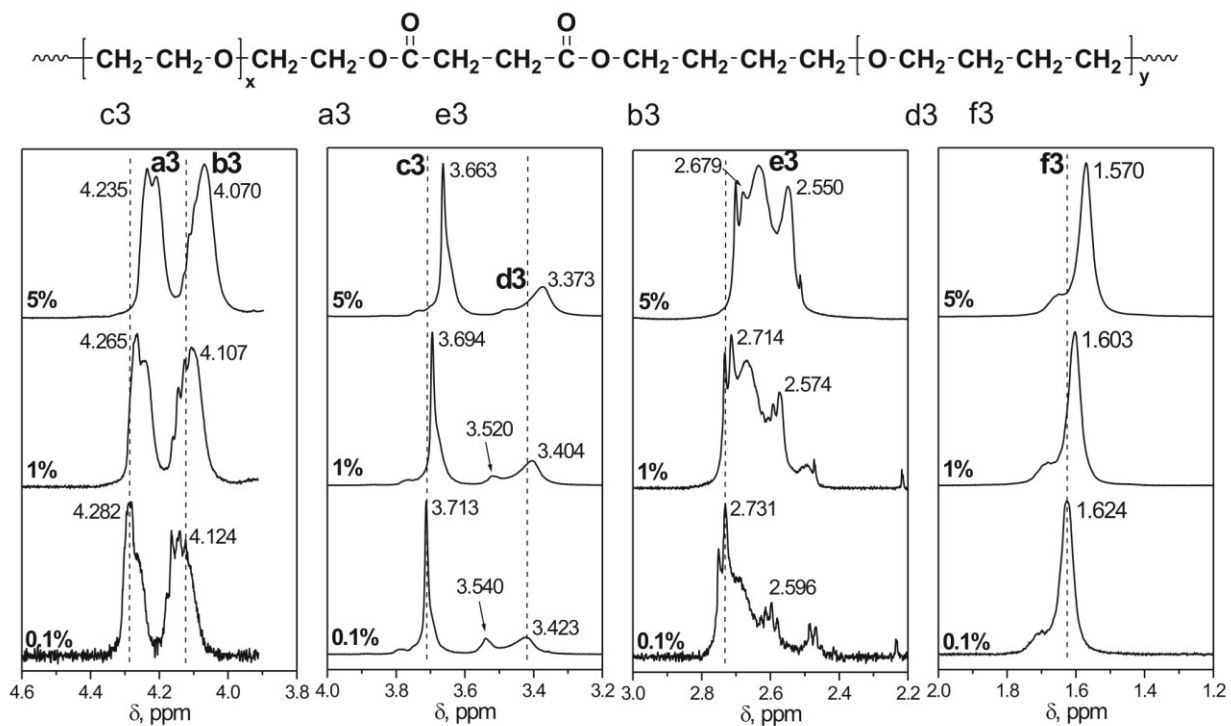


Figure 3.10. Expanded regions of ^1H NMR spectra of $\text{PEG}_{600}\text{PTHF}_{650}$ recorded in D_2O at different concentrations.

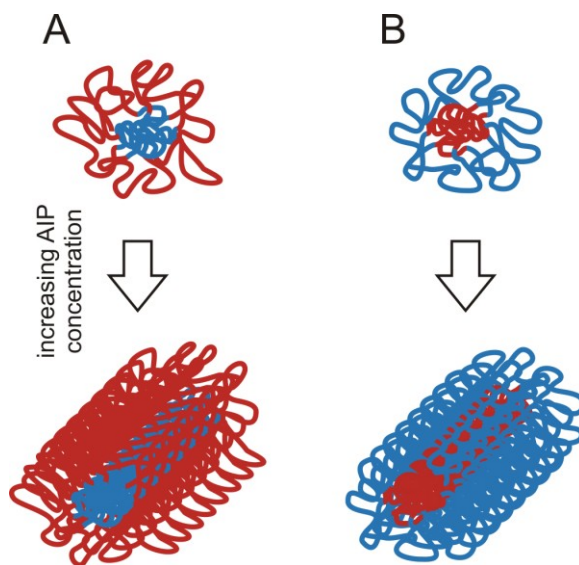


Figure 3.11. Formation of micellar assemblies due to self-assembly of AIP micelles in polar and nonpolar media.

The corresponding ratios of hydrophilic to hydrophobic protons calculated from the integral values of the NMR peaks of both S6 and PEG₆₀₀PTHF₆₅₀ are given in Table 3.4. Even though hydrophilic/hydrophobic proton ratios for all AIP aqueous solutions are higher than the reference values calculated from the spectra recorded in CDCl₃, they decrease with increasing polymer concentration. The aggregation of AIP micelles into micellar assemblies is obviously accompanied with transformation of their “core-shell” morphology and appearance of hydrophilic and hydrophobic domains. Therefore, the domain formation is believed to reduce the extent of screening of the hydrophobic fragments by the hydrophilic ones, thus causing lowering of the ratio of hydrophilic to hydrophobic protons calculated from the NMR integral values.

Table 3.4. The Ratio of Hydrophilic to Hydrophobic Protons Calculated from Integral Intensities of AIPE Proton Signals in ¹H NMR Spectra

Polymer	Hydrophilic : hydrophobic proton ratio*				
	CDCl ₃ (reference)	D ₂ O			
		0.1%	1.0%	5.0%	10.0%
S6	3.309	3.338	3.322	3.317	3.272
PEG ₆₀₀ PTHF ₆₅₀	0.754	0.800	0.798	0.785	0.781

* “Hydrophilic” protons are PEG protons for both S6 and PEG₆₀₀PTHF₆₅₀, “hydrophobic” protons are sebacate CH₂ protons for S6 and PTHF protons for PEG₆₀₀PTHF₆₅₀

Figure 3.12 shows changes in the half-height width of the signals of the protons located in the middle of the hydrophilic (peaks b1 and c3) and hydrophobic (signals e1 and f3) AIPE fragments. Increasing the polymer concentration from 0.1% to 5 and 10% leads to a decreasing

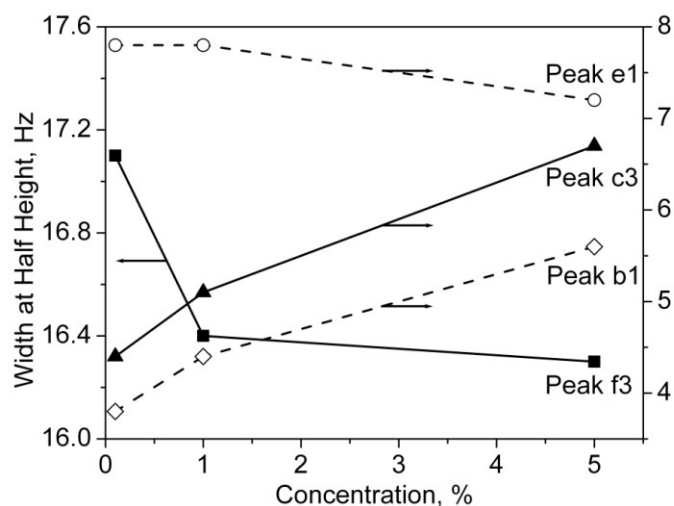


Figure 3.12. Width at half-height of hydrophilic and hydrophobic proton peaks of S6 and PEG₆₀₀PTHF₆₅₀ in D₂O.

half-height width of the hydrogen atoms located in the hydrophobic fragments of S6 and PEG₆₀₀PTHF₆₅₀ (peaks e1 in Figure 3.9 and f3 in Figure 3.10). Narrowing nonpolar proton peaks suggests that the mobility of the nonpolar fragments is enhanced in the big hydrophobic domains of the AIPE micellar assemblies as compared to the tight interior of the smaller micelles. Noteworthy, for PEG₆₀₀PTHF₆₅₀ the rate of peak narrowing greatly decreases in the concentration range of 1–5%, indicating that the minor changes in the packing density of the hydrophobic chains in the nonpolar domains are observed in this concentration range. In the case of S6, increasing concentration causes very small changes in the chemical shifts of the peak e1, showing that the difference in polarity between the hydrophobic interior of the micelle and nonpolar domains of the micellar assembly is insignificant.

On the contrary, broadening of the hydrophilic PEG proton peaks (signals b1 and c3) is observed as AIPE concentration increases. Increased width at half-height of the PEG signals (Figure 3.12) implies that mobility of the poly(ethylene glycol) chains becomes somewhat

hindered because of their close packing in the polar domains. In the case of S6, this suggestion is further supported by the disappearance of the hyperfine structure of methylene protons c1 and d1, located in the hydrophilic region of micellar assemblies, with increasing AIPE concentration.

Remarkably, increasing the AIPE concentration from 0.1% to 5% results in the absolute majority of the PTHF protons d3 (PEG₆₀₀PTHF₆₅₀) being transferred to the hydrophobic domains of the micellar assemblies, as indicated by a drastic reduction of intensity of the peak at ca. 3.5 ppm with the simultaneous increase in the integral intensity of the peak at ca. 3.4 ppm (Figure 3.10).

In summary, at 0.1% concentration AIPEs form micelles with a hydrophilic exterior composed of polar PEG chains and a hydrophobic interior made of nonpolar PTHF (PEG₆₀₀PTHF₆₅₀) or $-(CH_2)_8-$ (S6) fragments in the aqueous solution. Increasing polyester concentration to 1–10% leads to the formation of micellar assemblies composed of hydrophilic and hydrophobic domains due to the aggregation of AIPE micelles.

3.3.3.2. Self-Assembly of Amphiphilic Invertible Polymers in Nonpolar Solvents

Self-assembly behavior of AIPs in a nonpolar medium has been evaluated by recording and analyzing ¹H NMR spectra of amphiphilic invertible polyesters and polyurethanes in aromatic solvents. Two polyesters (D3 and S6) and four polyurethanes including two AIPUs with an alternating distribution of PEG and PTHF constituents (PEG₁₀₀₀-*alt*-PTHF₁₀₀₀ and PEG₆₀₀-*alt*-PTHF₆₅₀) and two AIPUs with a random distribution of PEG and PTHF fragments (PEG₁₀₀₀-*co*-PTHF₁₀₀₀ and PEG₆₀₀-*co*-PTHF₆₅₀) have been chosen for the study and their NMR spectra have been recorded in toluene-*d*₈ (polyesters) and benzene-*d*₆ (polyurethanes) at a concentration of 0.1, 1, 10, and 30%. The representative expanded spectral regions of one

polyester (S6) and one polyurethane (PEG₁₀₀₀-*co*-PTHF₁₀₀₀) are presented in Figures 3.13 and 3.14, respectively.

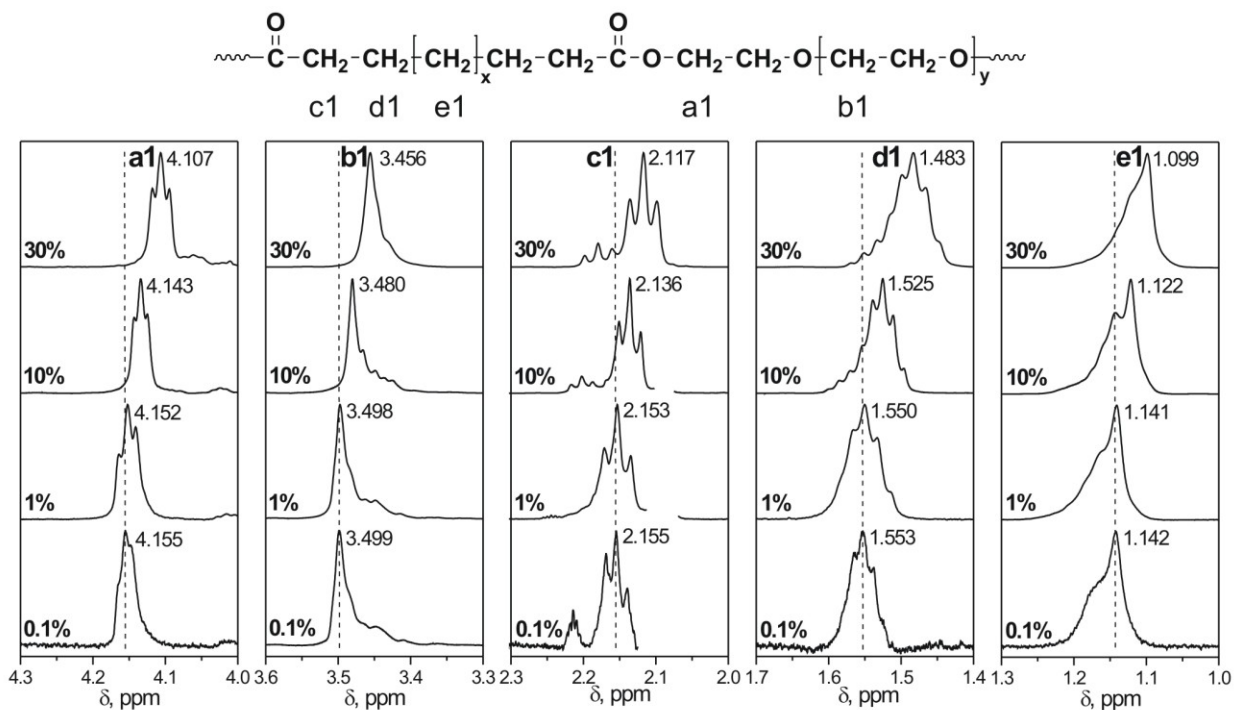


Figure 3.13. Expanded proton regions of ¹H NMR spectra of amphiphilic invertible polyester S6 recorded in toluene-*d*₈ at different concentrations.

Similar to the behavior of AIPE proton peaks in water, signals of both hydrophilic and hydrophobic protons of S6 and PEG₁₀₀₀-*co*-PTHF₁₀₀₀ experience upfield shifts that become even more pronounced for 30% solutions with increasing polymer concentration due to the formation of micellar assemblies (Figures 3.13 and 3.14). The observed shifts toward the lower ppm values are more prominent for hydrophobic proton peaks e1 and e2 compared to hydrophilic PEG protons b1 and c2. The upfield shift of protons e1 and e2 is likely caused by the change of their magnetic susceptibility due to the formation of nonpolar domains. It is concluded that hydrophobic AIP fragments form nonpolar domains in the assemblies as polymer concentration increases.

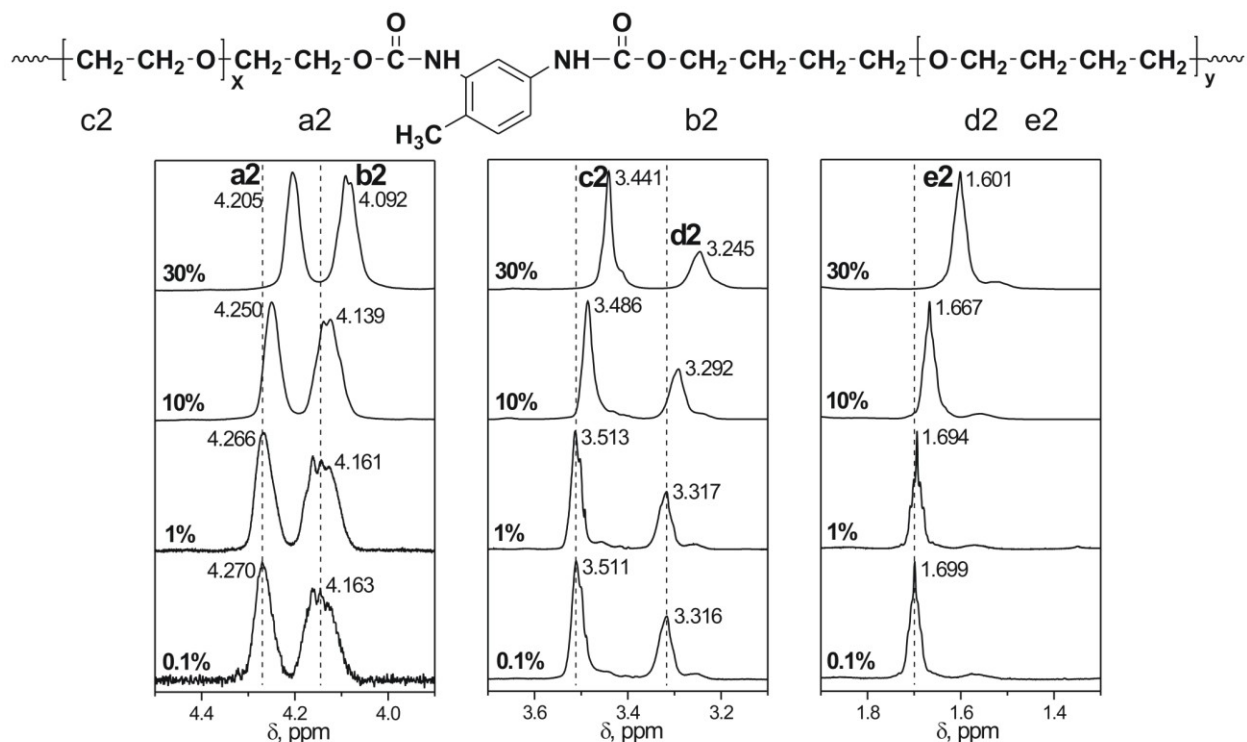


Figure 3.14. Expanded PEG and PTHF proton regions of ^1H NMR spectra of $\text{PEG}_{1000}\text{-co-PTHF}_{1000}$ recorded in benzene- d_6 at different concentrations.

Interestingly, increasing the AIPU concentration from 0.1% to 30% results in a slight narrowing of the signal c2 belonging to PEG protons of the polyurethane $\text{PEG}_{1000}\text{-co-PTHF}_{1000}$ (Figure 3.15). A plausible explanation is the presence of hydrophilic domains formed by the PEG fragments in the polymeric micellar assemblies. Mobility of the polar PEG fragments in the large hydrophilic domain is less limited than in the smaller interior of the micelle,⁷⁰ which leads to narrowing of the PEG proton signal in the ^1H NMR spectra. On the contrary, increasing the AIPU concentration leads to increase in the half-height width of the peaks of PTHF methylene protons d2 and e2 (Figure 3.15). This indicates that the mobility of the PTHF fragments became limited due to their close packing in the hydrophobic domain. The disappearance of the hyperfine structure of the PTHF proton signal e2 at high polymer concentration (Figure 3.14)

supports the idea that the mobility of the nonpolar fragments decreases with increasing AIPU concentration.

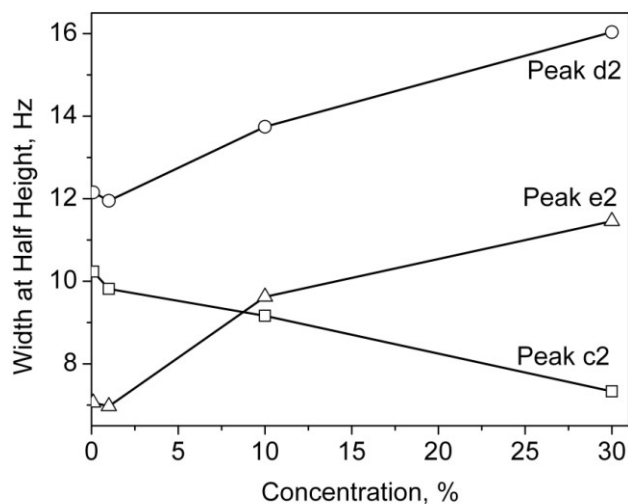


Figure 3.15. Width at half-height of PEG and PTHF proton peaks of the AIPU PEG₁₀₀₀-*co*-PTHF₁₀₀₀ in benzene-*d*₆.

The recorded ¹H NMR data clearly indicate that increasing the concentration of amphiphilic invertible polyesters and polyurethanes in nonpolar aromatic solvents leads to the formation of micellar assemblies with hydrophilic and hydrophobic domains as a result of the self-assembly of AIP micelles (Figure 3.11B).

3.3.3.3. Microphase Structure of the Amphiphilic Invertible Polyurethanes in the Solid State

Despite the similarity of the chemical composition, a difference in physical properties has been observed between amphiphilic invertible polyurethanes with a random and an alternating distribution of the hydrophilic and hydrophobic fragments. For example, while all AIPUs are soluble in acetone, carbon tetrachloride, and aromatic solvents, amphiphilic invertible polyurethanes with a random distribution of the hydrophilic and hydrophobic fragments are soluble in water, whereas the ones with alternating distribution do not dissolve readily.

Molecules of both random and alternating AIPUs consist of the so called hard (2,4-TDI) and soft (PEG and PTHF) segments. The physical and chemical properties of segmented polyurethanes are known to be influenced by microphase separation in the solid state.⁷⁴ Therefore, in order to recognize the possible reason for different AIPU solubility and determine the microphase structure of amphiphilic invertible polyurethanes in the bulk, a modulated differential scanning calorimetry study has been undertaken.

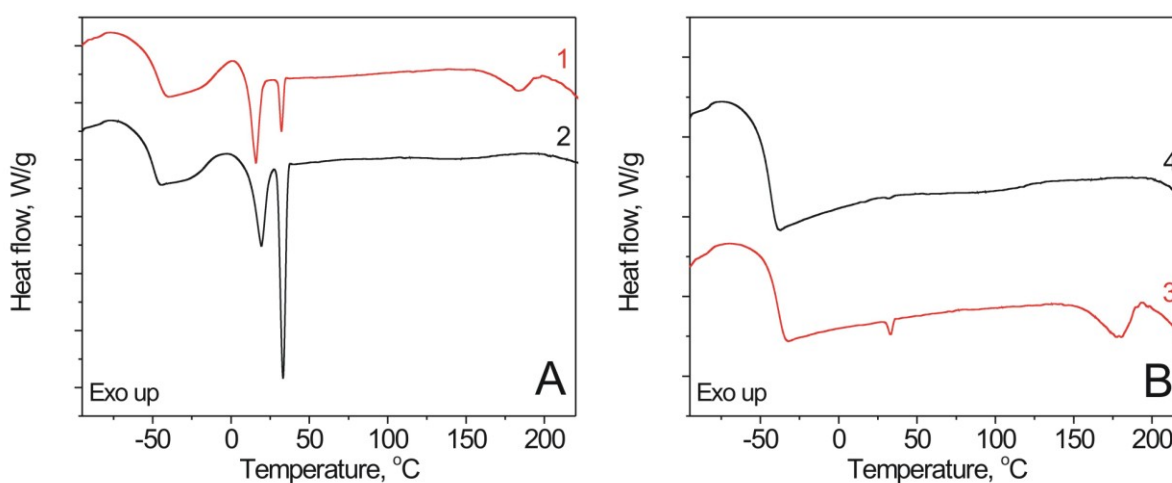


Figure 3.16. Representative MDSC thermograms of the amphiphilic invertible polyurethanes with (A) long hydrophilic and hydrophobic fragments: (1) PEG₆₀₀-*alt*-PTHF₁₀₀₀, (2) PEG₁₀₀₀-*co*-PTHF₁₀₀₀ and (B) short hydrophilic and hydrophobic fragments: (3) PEG₆₀₀-*alt*-PTHF₆₅₀, (4) PEG₆₀₀-*co*-PTHF₆₅₀.

To this end, MDSC thermograms of amphiphilic invertible polyurethanes have been recorded in the temperature range from -100 °C to 225 °C. A typical thermogram of the alternating AIPU is depicted in Figure 3.16A (curve 1, only the total heat flow is given). A well pronounced break is clearly seen at ca. -45 °C, indicating the glass transition of the flexible polyol (PEG and PTHF) segments. The glassy state of the soft segments is followed by the

development of a semicrystalline state that appears as an exothermic peak at about 0 °C. This process, frequently referred to as “cold crystallization”, is a result of the rearrangement and ordering of nearby segments in the amorphous regions of the polyurethanes in bulk and, obviously, is not accompanied by the ordering of the macromolecules. A further increase in temperature results in the appearance of two endothermic peaks at 16 °C and 32 °C due to melting of crystallites of the soft polyol segments. These two peaks either imply the melting of two diverse crystalline regions or this can be explained by a different degree of soft segment ordering in the crystallites. The former is more likely – a separate experiment has demonstrated that a mixture of PEG and PTHF showed two similar peaks in the same region. The endothermal peak appearing at 185 °C is attributed to the melting of the polyurethane hard segment domains formed by 2,4-TDI moieties linked together by hydrogen bonding between the urethane groups. Therefore, microphase separation in the alternating AIPUs results in appearance of three microphases as schematically shown in Figure 3.17A.

Thermograms of the AIPUs with a random distribution of the hydrophilic and hydrophobic fragments (Figure 3.16A, curve 2) are similar to those of the alternating polyurethanes except for the absence of an endothermic peak at 170–200 °C. Hence, hard 2,4-TDI segments do not form separate domains in the bulk material. Obviously, the reason for this type of behavior is the configuration of the random AIPUs whose macromolecules contain different types of segments. As a result of random distribution, segments consisting of several PEG fragments and segments with several PTHF fragments are found in the structure of these polymers. These segments apparently form two different crystalline regions (PEG and PTHF domains) with “inclusions” of the hard segments as suggested in Figure 3.17B.

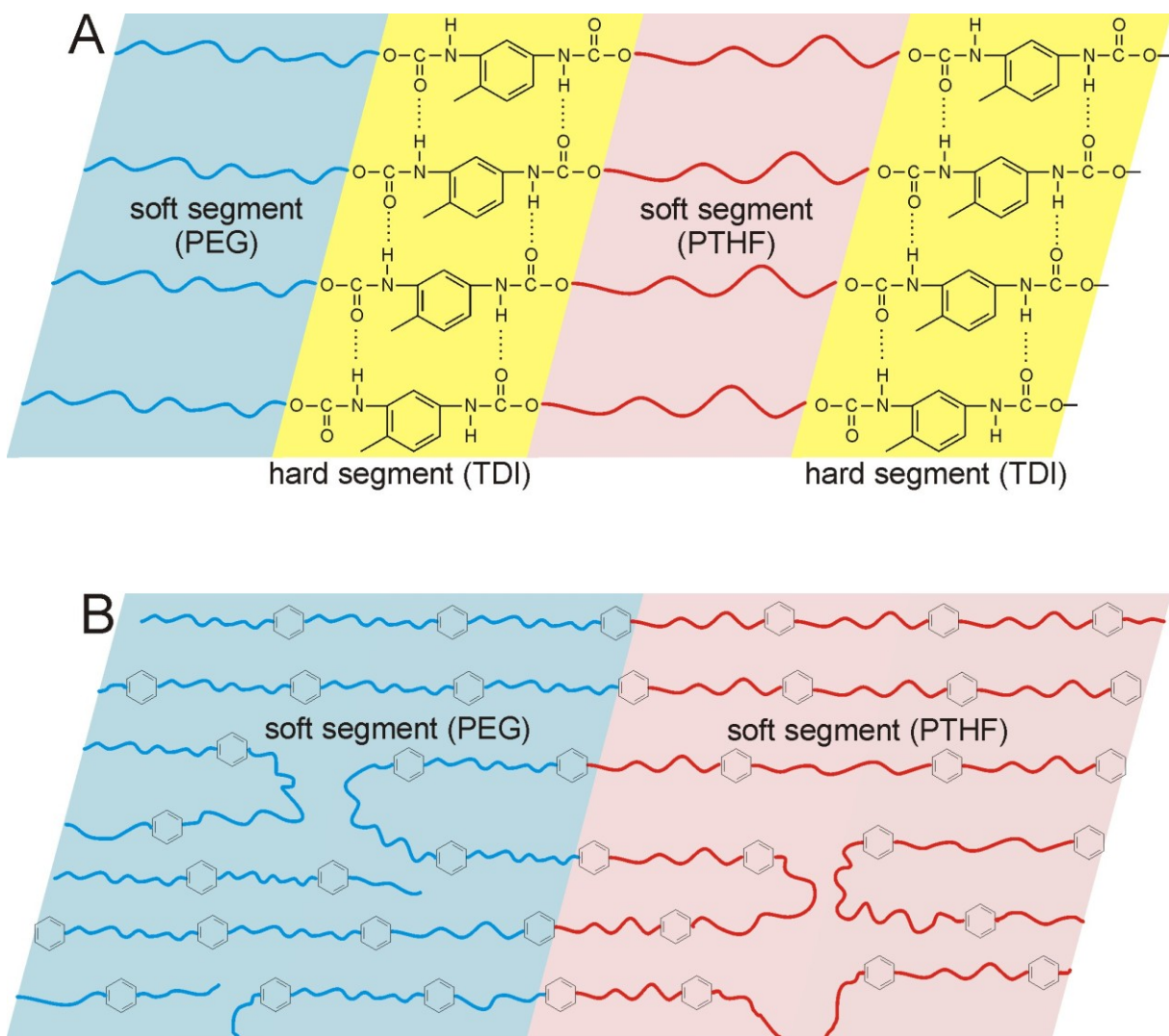


Figure 3.17. A schematic representation of the microphase separation in the AIPUs with (A) alternating and (B) random distribution of hydrophilic PEG and hydrophobic PTHF fragments.

Two AIPUs (namely PEG₆₀₀-*alt*-PTHF₆₅₀ and PEG₆₀₀-*co*-PTHF₆₅₀) do not undergo cold crystallization. The MDSC thermograms (Figure 3.16B) show that the soft polyol segments of these polyurethanes form an amorphous phase. Both AIPUs are based on two short-chain polyols and it is a small length of the PEG-600 and PTHF-650 segments that apparently causes such a behavior. Nevertheless, the endothermic peak at 178 °C indicates the presence of hard segment domains in the alternating AIPU PEG₆₀₀-*alt*-PTHF₆₅₀ (Figure 3.18A).

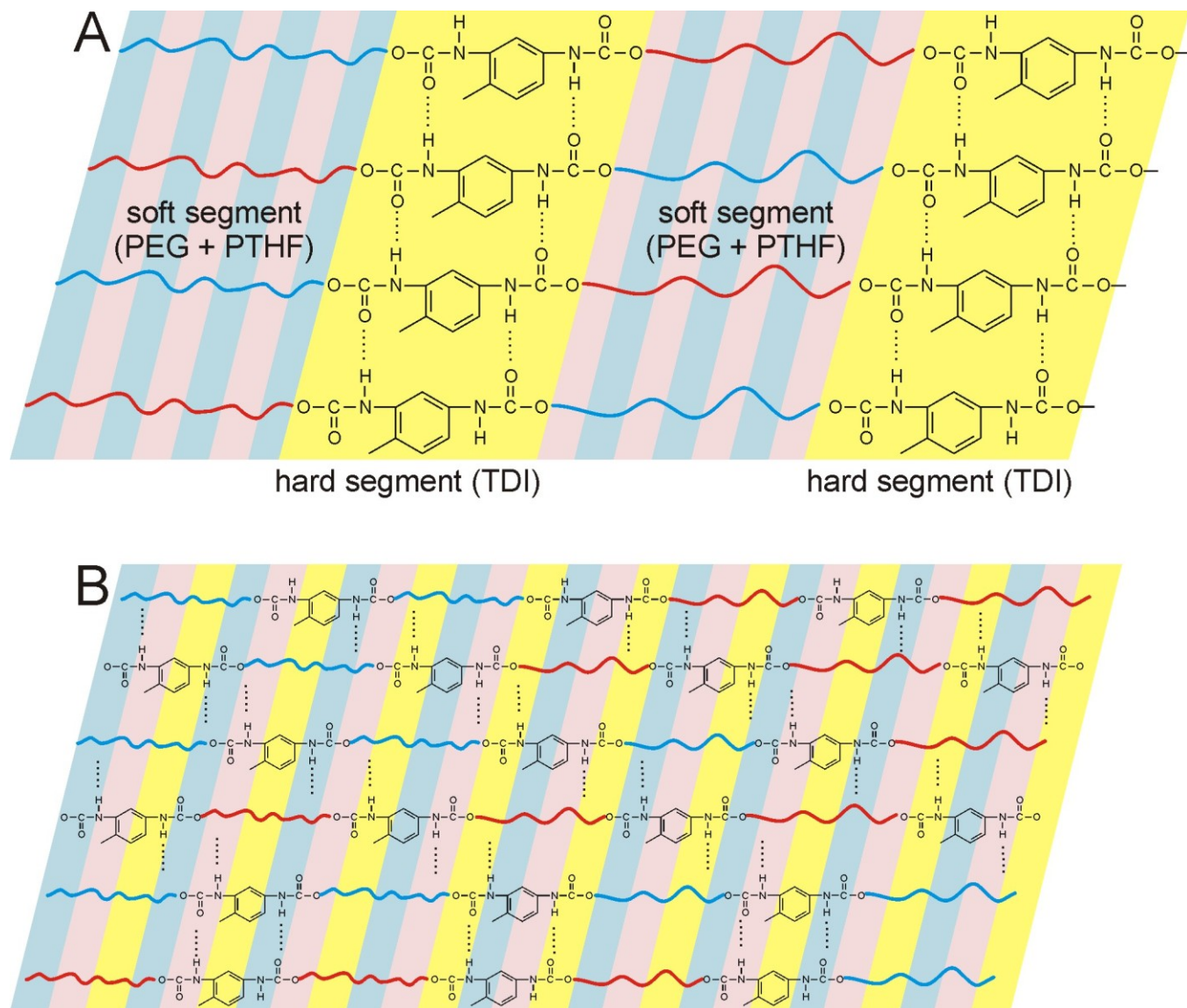


Figure 3.18. A schematic representation of the microphase separation in the AIPUs based on short-chain polyols: (A) PEG₆₀₀-*alt*-PTHF₆₅₀ with an alternating and (B) PEG₆₀₀-*co*-PTHF₆₅₀ with a random distribution of hydrophilic PEG and hydrophobic PTHF fragments.

Thus, the MDSC study has clearly shown that an alternating distribution of the hydrophilic and hydrophobic fragments in the AIPUs results in formation of hard segment domains (crystallites) in the bulk material. Strong intermolecular hydrogen bonding between the

urethane groups within these crystallites is the reason for insolubility of alternating AIPUs in water.

3.4.4. Morphological Study of AIP Micelles and Micellar Assemblies

Possible application of polymeric micelles and micellar assemblies is to a great extent determined by their size and shape. Hence, a systematic morphological study of micellar assemblies developed from amphiphilic invertible polyesters in the aqueous medium has been undertaken using a combination of transmission electron microscopy, small angle neutron scattering, and dynamic light scattering.

Small angle neutron scattering is widely used for examining morphology of different nanosized systems, including micelle-like structures.⁷⁵ The examined structures could vary in size from the atomic level to the near micrometer scale – a feature that makes SANS a tool of choice for analyzing polymer micelles and micellar assemblies.⁷⁶ The shape of the scattering curves is known to be determined by the shape, size, and polydispersity of the scattering objects, as well as by their contrast with respect to the solvent.⁷⁷ Since a very significant number of micelles is probed at the same time, SANS experiments provide reasonable averages over the structure of the micelles and their interactions.⁷⁸ Due to the sensitivity of the technique to the internal structure of the scattering objects, polymer micelles can be described in a very detailed way. For example, given the necessary contrast between the hydrophilic and hydrophobic fragments in the micelle, the properties of the micellar hydrophobic interior and the hydrophilic exterior can be studied.⁷⁹

To this end, SANS patterns on the solutions of four amphiphilic invertible polyesters (D3, S6, PEG₆₀₀PTHF₂₅₀ and PEG₆₀₀PTHF₆₅₀) in deuterium oxide at three concentrations (0.1, 1, and 5% w/w) have been recorded. The SANS data were corrected to allow for sample

transmission, detector response, empty cell, and background (solvent) scattering. Deuterated solvent has been used for scattering experiments to create the necessary contrast between the micelles and the solvent medium.

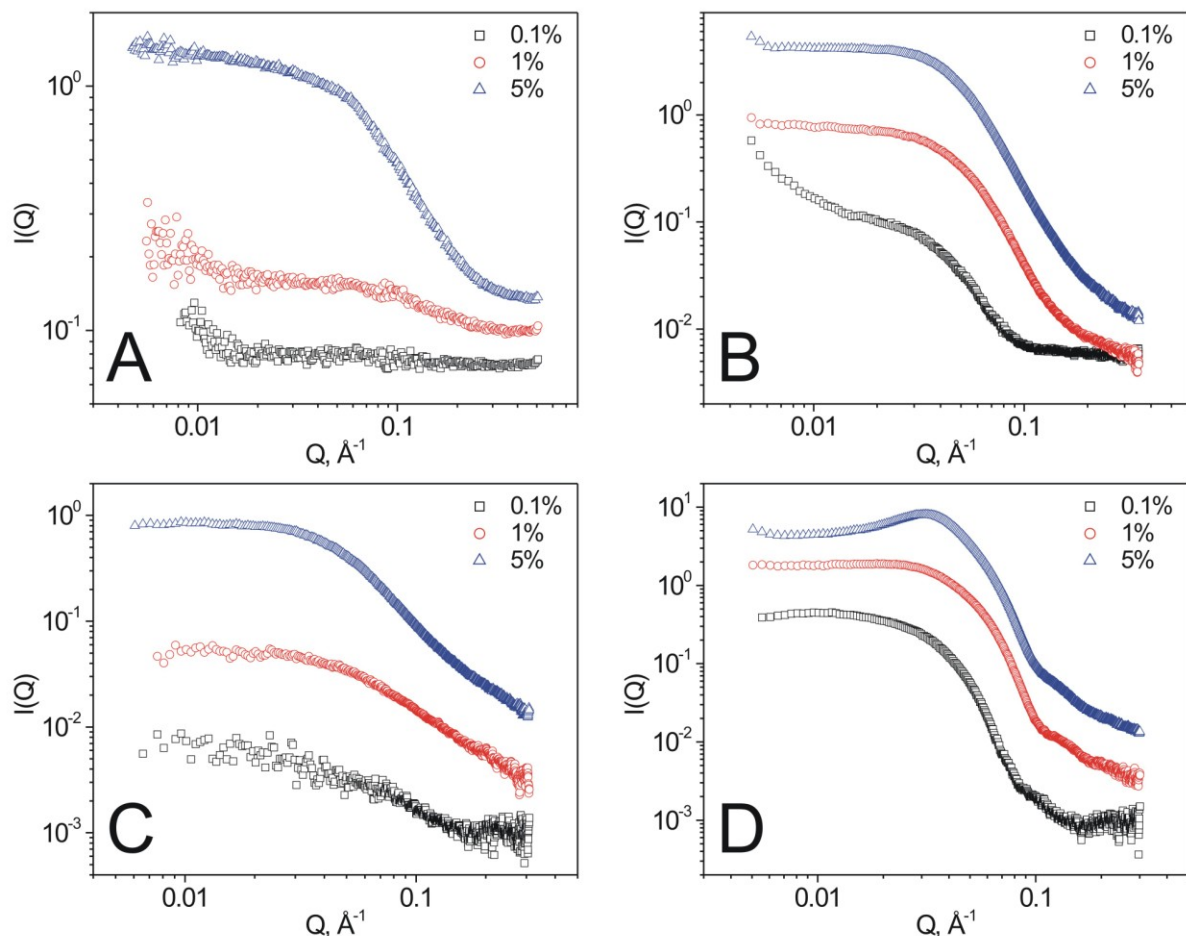


Figure 3.19. SANS patterns recorded on aqueous solutions of amphiphilic invertible polyesters S6 (A), D3 (B), PEG₆₀₀PTHF₂₅₀ (C), and PEG₆₀₀PTHF₆₅₀ (D) at different concentrations.

Figure 3.19 shows SANS spectra of the AIPE aqueous micellar solutions. A strong dependence of the scattering intensity $I(Q)$ on the values of scattering vector (Q) indicates the presence of the scattering objects, i.e. AIPE micelles. In turn, increasing AIPE concentration leads to dramatic changes in the scattering pattern for all polymers due to the aggregation of

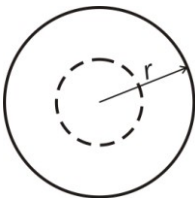
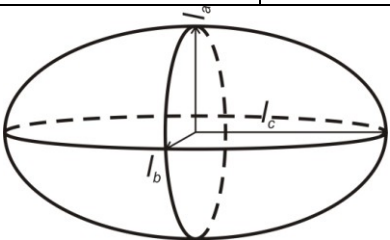
micelles into micellar assemblies. In this way, neutron scattering data confirm results of the NMR experiments that AIPs form micelles with a hydrophilic exterior and a hydrophobic interior in dilute aqueous solutions that self-assemble into micellar assemblies as concentration increases.

The information about the structure, morphology and phase transitions in the sample could be determined from its scattering intensity in accordance with the following equation:⁷⁶

$$I(Q) = nP(Q)S(Q),$$

where n is the number density of the scattering particles; $P(Q)$ is the form factor determining the shape and morphology of the particles; and $S(Q)$ is the structure factor containing information about the ordering of the particles and the interparticle interactions. By fitting the appropriate form and structure factors to the experimental scattering curves, dimensional parameters for AIP micelles have been calculated.

Table 3.5. Geometric Parameters of Micelles of PEG₆₀₀PTHF₂₅₀ at Different Concentrations

Concentration, %		0.1	1.0		5.0
Micellar geometry					
Geometric parameters, Å	r	25.4±0.4	l_a	6.3±0.2	8.2±0.1
			l_b	20.9±0.3	41.1±0.1
			l_c	56.3±0.7	58.8±0.3

The geometric parameters of the AIP micelles at all concentrations calculated from SANS patterns are given in Tables 3.5–3.8. Furthermore, the morphology of the AIP micelles

Table 3.6. Geometric Parameters of Micelles of PEG₆₀₀PTHF₆₅₀ at Different Concentrations

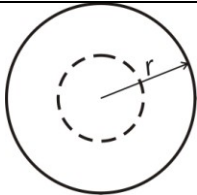
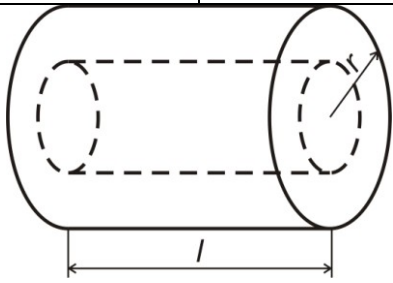
Concentration, %		0.1	1.0	5.0
Micellar geometry				
Geometric parameters, Å	<i>r</i>	52.4±0.1	41.2±0.1	42.1±0.1

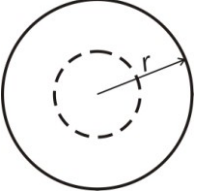
Table 3.7. Geometric Parameters of Micelles of S6 at Different Concentrations

Concentration, %		1.0	5.0
Micellar geometry			
Geometric parameters, Å	<i>r</i>	5.5±0.2	10.2±0.2
	<i>l</i>	30.4±2.3	50.4±0.1

has been visualized by means of transmission electron microscopy. TEM images recorded on the AIP micelles deposited from 1% aqueous solution and stained with phosphotungstic acid are presented in Figure 3.20. As evidenced by the data in Figure 3.20 and Tables 3.5–3.8, a reasonable correlation exists between SANS and TEM data in terms of both micellar size and shape. Depending on chemical composition, different micellar morphologies are developed from the amphiphilic invertible polymers: PEG₆₀₀PTHF₆₅₀ and D3 build spherical micelles, PEG₆₀₀PTHF₂₅₀ forms ellipsoids, while micelles developed from S6 are cylindrical in shape. Noteworthy, both SANS and TEM data are in a good agreement with the particle size data

measured on spherical D3 and PEG₆₀₀PTHF₆₅₀ micelles using dynamic light scattering (Figure .21).

Table 3.8. Geometric Parameters of Micelles of D3 at Different Concentrations

Concentration, %		0.1	1.0	5.0
Micellar geometry				
Geometric parameters, Å	<i>r</i>	36.4±0.2	24.7±0.1	18.9±0.1

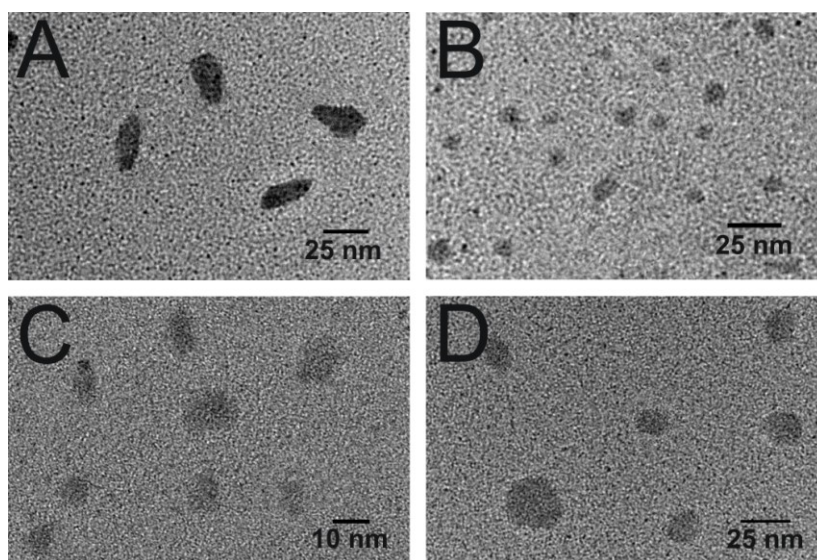


Figure 3.20. TEM images of the micelles of S6 (A), D3 (B), PEG₆₀₀PTHF₂₅₀ (C), and PEG₆₀₀PTHF₆₅₀ (D).

The data in Tables 3.5–3.8 imply that AIPE micellar morphologies exhibit strong concentration dependence. As confirmed by the NMR study, concentration increase leads to the transformation of AIPE micelles into micellar assemblies with hydrophilic and hydrophobic domains. Hence, rising polymer concentration from 0.1 to 5% leads to flattening of the

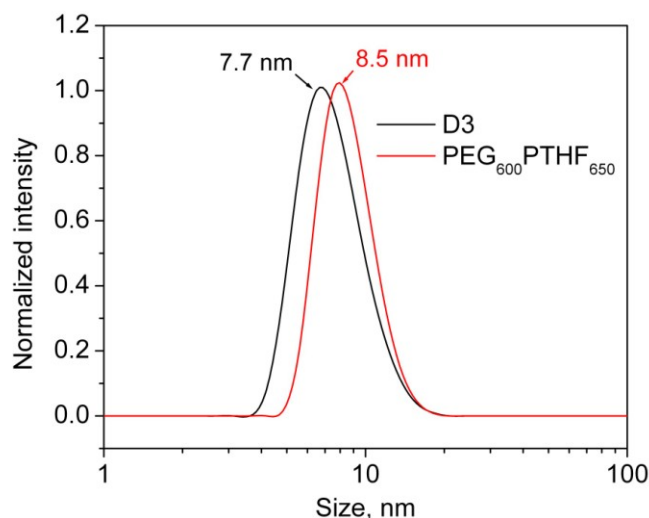


Figure 3.21. Particle size distribution of spherical micelles made from D3 and PEG₆₀₀PTHF₆₅₀ as determined by DLS at 1% w/w.

PEG₆₀₀PTHF₂₅₀ micelles and increase in the size of S6 cylinders. Spherical micelles of PEG₆₀₀PTHF₆₅₀ and D3, however, experience a decrease in radius with growing AIPE concentration from 1 to 5%. A plausible explanation is that increased interparticle interactions in concentrated solutions cause a decrease in size of the micellar assemblies. Moreover, more dense packing of poly(ethylene glycol) chains in the hydrophilic domains in 1 and 5% solutions (as compared to the micellar corona at 0.1% w/w) could also lead to decreasing size of the micellar assemblies.

3.5. Conclusions

Macromolecules of amphiphilic invertible polymers have been demonstrated to build micelles in solvents differing by polarity. Micelles with a hydrophilic exterior consisting of PEG fragments and a hydrophobic inner part are formed in a polar aqueous medium. The conformation of AIP macromolecules is inverted in nonpolar aromatic solvents leading to

formation of micelles with a hydrophobic exterior and a hydrophilic interior. Increasing AIP concentration in both polar and nonpolar media causes the self-assembly of amphiphilic invertible micelles into micellar assemblies with hydrophilic and hydrophobic domains. Depending on the AIP chemical composition and concentration, different micellar morphologies (i.e., spheres, cylinders, and ellipsoids) are formed.

Thin AIP films have been shown to change the surface energy of the substrate regardless of its polarity: nonpolar substrates become more hydrophilic, while polar ones become more hydrophobic. In turn, exposure to liquids differing by polarity causes changes in the surface energy of the AIP film. If AIP film is in contact with water, the contact interface is enriched with hydrophilic PEG chains. Upon exposure to the nonpolar diiodomethane, amphiphilic macromolecules invert their structure and hydrophobic fragments assemble at the surface.

The responsive properties of amphiphilic invertible polymers are assumed to form the basis for new invertible architectures, both in solution and on the surface, which have potential in a broad range of applications.

3.6. References

1. Wu, X.; Qiao, Y.; Yang, H.; Wang, J. *J. Colloid Interface Sci.* **2010**, *349*, 560–564.
2. Almgren, M.; Brown, W.; Hvidt, S. *Colloid Polym. Sci.* **1995**, *273*, 2–15.
3. Lim, K.T.; Lee, M.Y.; Moon, M.J.; Lee, G.D.; Hong, S.S.; Dickson, J.L.; Johnston, K.P. *Polymer* **2002**, *43*, 7043–7049.
4. Lee, M.Y.; Kim, S.H.; Kim, J.T.; Kim, S.W.; Lim, K.T. *J. Nanosci. Nanotechnol.* **2008**, *8*, 4864–4868.
5. Lee, M.Y.; Jeong, Y.T.; Lim, K.T.; Choi, B.-C.; Kim, H.G.; Gal, Y.S. *Mol. Cryst. Liq. Cryst.* **2009**, *508*, 173–182.

6. Sorrells, J.L.; Tsai, Y.-H.; Wooley, K.L. *J. Polym. Sci. Part A Polym. Chem.* **2010**, *48*, 4465–4472.
7. Laurent, B.A.; Grayson, S.M. *Polym. Chem.* **2012**, *3*, 1846–1855.
8. Riess, G. *Prog. Polym. Sci.* **2003**, *28*, 1107–1170.
9. Zhang, L.; Eisenberg, A. *Science* **1995**, *268*, 1728–1731.
10. Basu, S.; Vutukuri, D.R.; Thayumanavan, S. *J. Am. Chem. Soc.* **2005**, *127*, 16794–16795.
11. Discher, D.E.; Eisenberg, A. *Science* **2002**, *297*, 967–973.
12. Mortensen, K. *Curr. Opin. Coll. Interface Sci.* **1998**, *3*, 12–19.
13. Wang, X.; Guerin, G.; Wang, H.; Wang, Y.; Manners, I.; Winnik, M.A. *Science* **2007**, *317*, 644–647.
14. Li, M.-H.; Keller, P. *Soft Matter* **2009**, *5*, 927–937.
15. Del Barrio, J.; Oriol, L.; Sánchez, C.; Serrano, J.L.; Di Cicco, A.; Keller, P.; Li, M.H. *J. Am. Chem. Soc.* **2010**, *132*, 3762–3769.
16. Sin, S.L.; Gan, L.H.; Hu, X.; Tam, K.C.; Gan, Y.Y. *Macromolecules* **2005**, *38*, 3943–3948.
17. Hajduk, D.A.; Kossuth, M.B.; Hillmyer, M.A.; Bates, F.S. *J. Phys. Chem. B* **1998**, *102*, 4269–4276.
18. Maestro, A.; Acharya, D.P.; Furukawa, H.; Gutiérrez, J.M.; López-Quintela, M.A.; Ishitobi, M.; Kunieda, H. *J. Phys. Chem. B* **2004**, *108*, 14009–14016.
19. Stoykovich, M.P.; Kang, H.; Daoulas, K.C.; Liu, G.; Liu, C.-C.; de Pablo, J.J.; Müller, M.; Nealy, P.F. *ACS Nano* **2007**, *1*, 168–175.
20. Husemann, M.; Mecerreyes, D.; Hawker, C.J.; Hedrick, J.L.; Shah, R.; Abbott, N.L. *Angew. Chem. Int. Ed.* **1999**, *38*, 647–649.

21. Thurn-Albrecht, T.; Steiner, R.; DeRouchey, J.; Stafford, C.M.; Huang, E.; Bal, M.; Tuominen, M.; Hawker, C.J.; Russell, T.P. *Adv. Mater.* **2000**, *12*, 787–791.
22. Black, C.T. *ACS Nano* **2007**, *1*, 147–150.
23. Cheng, J.Y.; Ross, C.A.; Smith, H.I.; Thomas, E.L. *Adv. Mater.* **2006**, *18*, 2505–2521.
24. Ahmed, F.; Pakunlu, R.I.; Srinivas, G.; Brannan, A.; Bates, F.; Klein, M.L.; Minko, T.; Discher, D.E. *Mol Pharm* **2006**, *3*, 340–350.
25. Malam, Y.; Loizidou, M.; Seifalian, A.M. *Trends Pharmacol. Sci.* **2009**, *30*, 592–599.
26. Du, W.; Xu, Z.; Nyström, A.M.; Zhang, K.; Leonard, J.R.; Wooley, K.L. *Bioconjugate Chem.* **2008**, *19*, 2492–2498.
27. Cabral, H.; Nishiyama, N.; Kataoka, K. *J. Controlled Release* **2007**, *121*, 146–155.
28. Du, J.; O'Reilly, R.K. *Soft Matter* **2009**, *5*, 3544–3561.
29. Du, W.; Nyström, A.M.; Zhang, L.; Powell, K.T.; Li, Y.; Cheng, C.; Wickline, S.A.; Wooley, K.L. *Biomacromolecules* **2008**, *9*, 2826–2833.
30. Bawarski, W.E.; Chidlow, E.; Bharali, D.J.; Mousa, S.A. *Nanotechnol. Biol. Med.* **2008**, *4*, 273–282.
31. Doshi, N.; Mitragotri, S. *Adv. Funct. Mater.* **2009**, *19*, 3843–3854.
32. Liu, J.; Liu, H.; Boyer, C.; Bulmus, V.; Davis, T.P. *J. Polym. Sci. Part A: Polym. Chem.* **2009**, *47*, 899–912.
33. Lodge, T.P. *Science* **2008**, *321*, 50–51.
34. Savić, R.; Eisenberg, A.; Maysinger, D. *J. Drug Targeting* **2006**, *14*, 343–355.
35. Alexandridis, P.; Hatton, T.A. *Colloids Surf. A* **1995**, *96*, 1–46.
36. Zhang, W.; He, J.; Liu, Z.; Ni, P.; Zhu, X. *J. Polym. Sci. Part A Polym. Chem.* **2010**, *48*, 1079–1091.

37. Wang, J.; Xu, W.; Cheng, Z.; Zhu, X.; Zhang, Z.; Zhu, J.; Zhang, W. *J. Polym. Sci. Part A Polym. Chem.* **2008**, *46*, 7690–7701.
38. Basu, S.; Vutukuri, D.R.; Shyamroy, S.; Sandanaraj, B.S.; Thayumanavan, S. Invertible Amphiphilic Homopolymers. *J. Am. Chem. Soc.* **2004**, *126*, 9890–9891.
39. Montazeri, H.; Lavasanifar, A. *Expert Opin. Drug Delivery* **2006**, *3*, 139–162.
40. Torchilin, V.P. *Pharm. Res.* **2007**, *24*, 1–16.
41. Gratton, S.E.A.; Ropp, P.A.; Pohlhaus, P.D.; Luft, J.C.; Madden, V.J.; Napier, M.E.; DeSimone, J.M. *Proc. Natl. Acad. Sci. USA* **2008**, *105*, 11613–11618.
42. Zhang, K.; Fang, H.; Chen, Z.; Taylor, J.-S.A.; Wooley, K.L. *Bioconjugate Chem.* **2008**, *19*, 1880–1887.
43. Kline, S. *J. Appl. Crystallogr.* **2000**, *33*, 618–622.
44. Kline, S. R. *Langmuir* **1999**, *15*, 2726–2732.
45. Wang, X.S.; Wang, H.; Coombs, N.; Winnik, M.A.; Manners I. *J. Am. Chem. Soc.* **2005**, *127*, 8924–8925.
46. Lin, Z.Q.; Zakin, J.L.; Zheng, Y.; Davis, H.T.; Scriven, L.E.; Talmon, Y. *J. Rheol.* **2001**; *45*, 963–981.
47. Walker, L.M. *Curr. Opin. Colloid Interface Sci.* **2001**, *6*, 451–456.
48. Daripa, P.; Pasa, G. *Int. J. Eng. Sci.* **2004**, *42*, 2029–2039.
49. Won, Y.-Y.; Bates, F.S. *Surfactant Sci. Ser.* **2007**, *140*, 417–451.
50. Schmitt, A.L.; Repollet-Pedrosa, M.H.; Mahanthappa, M.K. *ACS Macro Lett.* **2012**, *1*, 300–304.
51. Bosman, A.W.; Heumann, A.; Klaerner, G.; Benoit, D.; Fréchet, J.M.J.; Hawker, C.J. *J. Am. Chem. Soc.* **2001**, *123*, 6461–6462.

52. Zhang, Y.; Guo, S.; Lu, C.; Liu, L.; Li, Z.; Gu, J. *J. Polym. Sci. Part A Polym. Chem.* **2007**, *45*, 605–613.
53. Liu, F.; Eisenberg, A. *J. Am. Chem. Soc.* **2003**, *125*, 15059–15064.
54. Sundararaman, A.; Stephan, T.; Grubbs, R.B. *J. Am. Chem. Soc.* **2008**, *130*, 12264–12265.
55. Li, Z.; Chen, Z.; Cui, H.; Hales, K.; Qi, K.; Wooley, K.L.; Pochan, D.J. *Langmuir* **2005**, *21*, 7533–7539.
56. Zhong, S.; Cui, H.; Chen, Z.; Wooley, K.L.; Pochan, D.J. *Soft Matter* **2008**, *4*, 90–93.
57. Pochan, D.J.; Chen, Z.; Cui, H.; Hales, K.; Qi, K.; Wooley, K.L. *Science* **2004**, *306*, 94–97.
58. Li, Z.; Chen, Z.; Cui, H.; Hales, K.; Wooley, K.L.; Pochan, D.J. *Langmuir* **2007**, *23*, 4689–4694.
59. Sadron, C. *Angew. Chem. Int. Ed.* **1963**, *2*, 5. 248–250.
60. Tuzar, Z.; Kratochvil, P. *Adv. Colloid Interface Sci.* **1976**, *6*, 201–232.
61. Voronov, A.; Vasylyev, S.; Kohut, A.; Peukert, W. *J. Colloid Interface Sci.* **2008**, *323*, 379–385.
62. Sieburg, L.; Kohut, A.; Kislenko, V.; Voronov, A. *J. Colloid Interface Sci.* **2010**, *35*, 116–121.
63. Holmqvist, P.; Nilsson, S.; Tiberg, F. *Colloid Polym. Sci.* **1997**, *275*, 467–473.
64. Kriz, J.; Brus, J.; Plestil, J.; Kurkova, D.; Masar, B.; Dybal, J.; Zune, C.; Jerome, R. *Macromolecules* **2000**, *33*, 4108–4115.
65. Ma, J.-H.; Guo, C.; Tang, Y.-L.; Liu, H.-Z. *Langmuir* **2007**, *23*, 9596–9605.
66. Walderhaug, H.; Söderman, O. *Curr. Opin. Colloid Interface Sci.* **2009**, *14*, 171–177.

67. He, Y.; Zhang, Y.; Gu, C.; Dai, W.; Lang, M. *J. Mater. Sci. Mater. Med.* **2010**, *21*, 567–574.
68. Barhoum, S.; Yethiraj, A. *J. Chem. Phys.* **2010**, *132*, 024909/1–024909/9.
69. Wilmes, G.M.; Arnold, D.J.; Kawchak, K.S. *J. Polym. Res.* **2011**, *18*, 1787–1797.
70. Kohut, A.; Voronov, A. *Langmuir* **2009**, *25*, 4356–4360.
71. Onak, T.; Inman, W.; Rosendo, H.; DiStefano, E.W.; Nurse, J. *J. Am. Chem. Soc.* **1977**, *99*, 6488–6492.
72. Stamm, H.; Jaeckel, H. *J. Am. Chem. Soc.* **1989**, *111*, 6544–6550.
73. Van Krevelen, D.W. *Properties of Polymers: Correlations with Chemical Structure*; Elsevier: London, 1972; p 412.
74. Król, P. *Prog. Mater. Sci.* **2007**, *52*, 915–1015.
75. Hammouda, B. *J. Macromol. Sci. Part C Polym. Rev.* **2010**, *50*, 14–39.
76. Melnichenko, Y.B.; Wignall, G.D. *J. Appl. Phys.* **2007**, *102*, 021101/1–021101/24.
77. Skov Pedersen, J. *Adv. Colloid Interface Sci.* **1997**, *70*, 171–201.
78. Skov Pedersen, J. *Curr. Opin. Colloid Interface Sci.* **2002**, *7*, 158–166.
79. Caba, B.L.; Zhang, Q.; Carroll, M.R.J.; Woodward, R.C.; St. Pierre, T.G.; Gilbert, E.P.; Riffle, J.S.; Davis, R.M. *J. Colloid Interface Sci.* **2010**, *344*, 81–89.

CHAPTER 4. FUNCTIONAL SELF-ASSEMBLY OF AMPHIPHILIC INVERTIBLE POLYMERS IN POLAR MEDIUM: NANOCONTAINERS AND STIMULI- RESPONSIVE DRUG DELIVERY SYSTEM

4.1. Abstract

Micellar assemblies based on amphiphilic invertible polyesters solubilize poorly water-soluble cargo molecules and transfer their payload into a nonpolar phase by inverting their macromolecular conformation in response to changes in the polarity of the local environment. The amount of material transferred depends primarily on micellar loading capacity and increases with increasing AIPE lipophilicity. The unique ability of AIPEs to invert the molecular conformation depending on the polarity of the environment can be a decisive factor in establishing the novel stimuli-responsive mechanism of solubilized drug release that is induced in response to a change of the environmental polarity. Drug-loaded AIPE micellar assemblies have been shown to deliver poorly water-soluble curcumin to carcinoma cells. The release of curcumin from the AIPE micellar assemblies is primarily caused by macromolecular inversion due to changing local environmental polarity and can be controlled by AIPE structure and concentration. On the other hand, the curcumin-loaded AIPE micelles are cytotoxic to breast carcinoma cells while remaining nontoxic to human cells at a polymer concentration of 10 $\mu\text{g/mL}$. An additional advantage of the AIPE-based vehicles is their ability to stabilize curcumin molecules against chemical decomposition. The obtained results demonstrate the potential of AIPE-based responsive vehicles as a promising platform for controlled delivery of poorly water-soluble drug candidates by means of new stimuli-responsive release mechanism.

4.2. Introduction

PEG-based amphiphilic polymers such as Pluronic® are widely used for various practical applications in the aqueous medium. These polymers build micelles with a polar corona and a nonpolar core that is capable of sequestering nonpolar molecules. The ability of amphiphilic polymers to form micelles in an aqueous medium makes them useful in a number of practical applications as detergents, emulsifiers, defoaming agents or dispersants,¹ along with more specialized applications in pharmaceuticals, bio-processing, and separation.^{2,3} In particular, amphiphilic polymer micelles may act as nanocontainers and nanocarriers that have potential in controlled and targeted delivery of drugs that are poorly soluble in water.⁴⁻⁸ Solubility of hydrophobic drugs can be significantly increased by drug solubilization within the micellar hydrophobic interior by physical (non-covalent) interaction.⁹ The advantage of the incorporation strategy over the alternative approaches that include covalent attachment of the drug molecules to the carrier is that the drug molecules remain chemically intact – a feature that leads to higher drug activity and improved release profile.¹⁰ The unique attribute that differentiates polymer micelles from alternative potential nanoscale therapeutics is the chemical flexibility of micellar structure, which permits the design of custom made carriers that can be developed individually with respect to drug properties, site of action, and administration pathway.¹¹ Although the utility of polymer micelles in pharmaceutical formulations is now well recognized, their thermodynamic stability in biological media often complicates the release of the active agents.¹² The release of physically incorporated drug molecules from the polymeric micellar containers usually occurs by diffusion (Figure 4.1A).¹¹ However, it is desirable that upon entering the action site the solubilized drug be released in a controlled fashion in order to reach the appropriate therapeutic efficacy. The introduction of stimuli-responsive fragments to the polymer structure

may be used to provide an instant or pulsed mode of drug delivery, and a controlled rate of drug release toward the release profile of micellar delivery systems. Recently, several smart polymeric micellar platforms have been established to trigger drug release from the delivery system through a stimuli-sensitivity mechanism. Among the ways to achieve the stimuli-responsive drug release, there are strategies including pH,¹³⁻¹⁶ temperature,^{17,18} and ultrasound-stimulated release.¹⁹⁻²¹

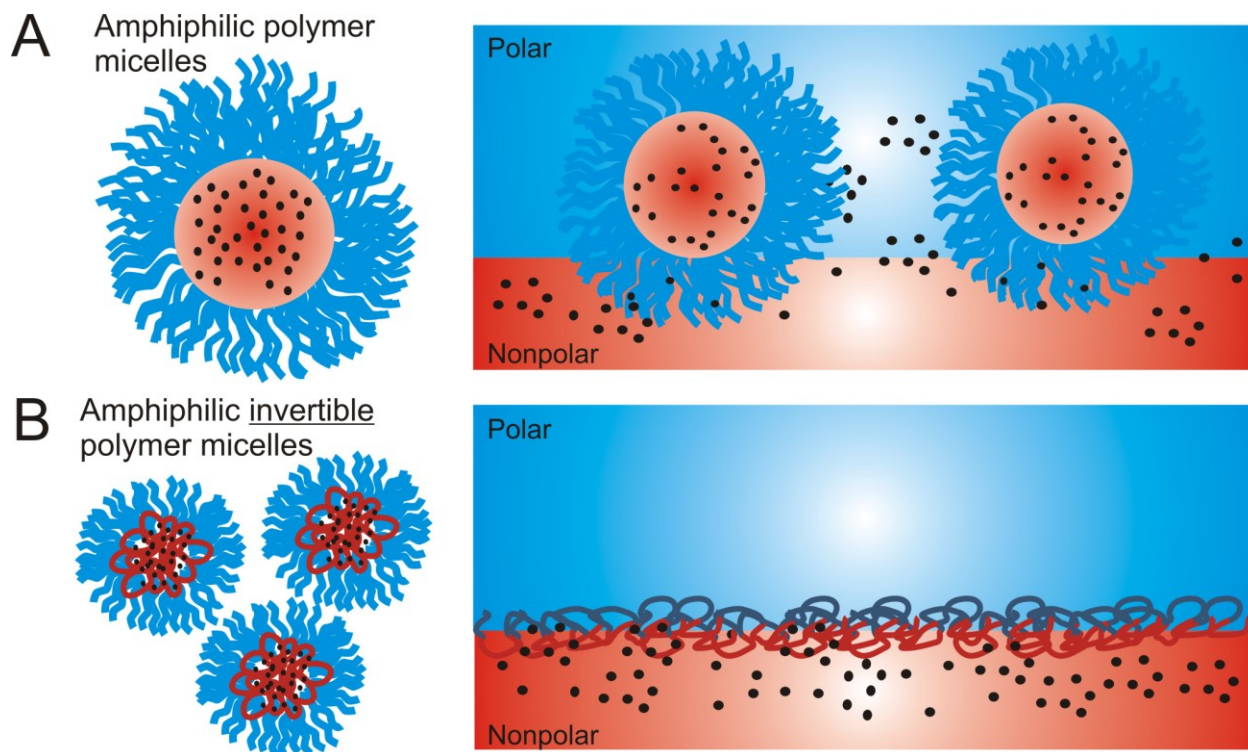


Figure 4.1. Diffusion mechanism (A) and stimuli-responsive (inversion) mechanism (B) for delivery of poorly water-soluble drugs using polymeric micellar platforms.

The use of amphiphilic invertible polymer micelles loaded with hydrophobic agents as nanocontainers and nanocarriers is a novel approach to drug delivery targeted in the current work based on the use of polarity of the medium as a stimulus to induce the release of the solubilized hydrophobic drug. Adsorption of drug-loaded micellar assemblies onto the cell membrane which is essentially a lipid matrix consisting of a phospholipid bilayer with inwardly oriented

hydrophobic hydrocarbons and outwardly oriented hydrophilic heads²² would be expected to change the conformation of amphiphilic invertible polymers. This could result in an enhancement of interactions between the polymer and membrane and subsequent release of the drug molecules. In such a way, polymeric micellar assemblies loaded with a water-insoluble drug can successfully transfer drug molecules from an aqueous medium to a polar/nonpolar interface, and release the payload upon inverting the macromolecular conformation by entering or contacting the less polar medium (Figure 4.1B). In this way, two critical drug performance parameters, namely enhanced solubility and promoted release, are simultaneously achieved using the responsive polymeric micellar assemblies.

As a first part of the study, nanocontainer properties of amphiphilic invertible polyesters (AIPes) have been probed in the aqueous medium on a model system by loading AIPe micellar assemblies with lipophilic insoluble dye molecules. Subsequently, modeling of a drug transfer through a polar/nonpolar interface has been carried out to demonstrate the AIPe capability to release the payload using stimuli-responsive inversion of macromolecules.

4.3. Experimental

4.3.1. Materials

Solvents (toluene and 1-octanol, ACS grade), curcumin, and Nile red were all purchased from VWR International. Sudan Red B was purchased from Aldrich. All reagents and materials were used as received.

Amphiphilic invertible polyesters were synthesized from PEG and aliphatic dicarboxylic acids (AIPes-1) and PEG, PTHF and succinic anhydride (AIPes-2) as described in Chapter 2.

4.3.2. Characterization

Size distribution and zeta potential of blank and loaded AIPE micelles were measured using Malvern Zetasizer Nano-ZS90 at 25 °C. The final numbers represent an average of a minimum of five (size) or ten (zeta potential) individual measurements.

4.3.3. Loading and Release Study

4.3.3.1. Preparation of Loaded AIPE Micellar Assemblies

Loaded AIPE micellar assemblies were prepared using a thin film method.²³ Following this method, polymer (0.1 g) and methanol solution of nonpolar cargo molecules (Sudan Red B, Nile red or curcumin, 0.5 mL, 1 mg/mL) were dissolved in carbon tetrachloride (10 mL). The solvent was removed by rotary evaporation at 60 °C for 1 h to obtain a solid cargo/AIPE matrix. Residual carbon tetrachloride remaining in the cargo/AIP matrix was evaporated overnight *in vacuo*. The resultant thin film was hydrated with Millipore water (10 mL), and unincorporated nonpolar cargo aggregates were removed by filtration through 0.45 and 0.2 µm filters.

4.3.3.2. Release Behavior and Chemical Stability of Curcumin-Loaded AIPE Micellar Assemblies

Drug release from curcumin-loaded micelles was studied by dialyzing those using 15 mL Slide-A-Lyzer dialysis cassettes (Thermo Scientific, molecular-weight cutoff of 3,500 Da) against 700 mL of Millipore water at room temperature with water exchange every 6 h. The released curcumin content was measured by UV-vis spectroscopy.

Chemical stability of curcumin-loaded micellar assemblies was evaluated using UV-vis spectroscopy. The decrease in absorbance of micellar solutions was monitored with time at room temperature.

4.3.4. Phase Transfer Study

4.3.4.1. Study of AIPE-Mediated Phase Transfer

For phase transfer, loaded aqueous AIPE solutions (3 mL) were mixed with an equal volume of a nonpolar solvent (toluene or 1-octanol). To reach equilibrium, the mixtures were stirred for 10 min. Subsequently, the aqueous phase was separated from the organic phase by centrifugation.

4.3.4.2. Determination of the Curcumin Concentration in Aqueous and 1-Octanol Phase

The initial concentration of the curcumin in aqueous solution was estimated using UV-vis spectroscopy. UV-Vis spectra were recorded on a Cary 5000 UV-Vis-NIR spectrophotometer (Varian, Inc.). The absorbance values were measured in the range of 350–800 nm. The height of the curcumin adsorption peak at 425–430 nm was attributed to a particular drug concentration using the calibration method. If necessary, curcumin-loaded solution samples were diluted with the corresponding 1% aqueous AIPE solution to maintain measurable absorbance. To build a calibration curve, sets of 1% micellar solutions for each amphiphilic invertible polymer containing known amounts of solubilized curcumin were prepared and their UV-vis spectra were recorded. The final concentration of the drug in 1-octanol phase after the experiment was determined using UV-vis spectroscopy (samples were diluted with 1-octanol if necessary). The calibration curves were built after recording the UV-vis spectra of a set of curcumin solutions of known concentration in the 1-octanol.

4.3.4.3. Study of the AIPE Transfer to 1-Octanol

1% AIPE aqueous solution (3 mL) was mixed with an equal volume of 1-octanol and stirred for 10 min. Subsequently, two phases were separated by centrifugation, both solvents were evaporated, and the amount of polymer in each phase was estimated gravimetrically.

The fraction of polymer transferred to the organic phase was calculated as follows:

$$x = \frac{[AIPE_{org}]}{[AIPE_{aq}]_0} = \frac{m(AIPE_{org})}{m_0(AIPE_{aq})},$$

where $[AIPE_{org}]$ and $[AIPE_{aq}]_0$ comprise the final AIPE concentration in the organic phase and initial AIPE concentration in the aqueous phase, mol/L; $m(AIPE_{org})$ and $m_0(AIPE_{aq})$ is the weight of the AIPE in the organic phase after the experiment and the weight of the AIPE in the initial aqueous solution, respectively, g.

4.3.5. Cytotoxicity Study

4.3.5.1. Cytotoxicity of AIPE Micellar Assemblies against Human Embryonic Kidney 293 Cells

Cytotoxicity of AIPE micellar assemblies against human living cells was tested using MTT assay. Human embryonic kidney cells (HEK 293) were grown and maintained in the DMEM medium supplemented with 10% fetal bovine serum, penicillin (100 U/mL), and streptomycin (100 µg/mL) at 37 °C in a humidified incubator in an atmosphere of 5% CO₂. The cells were plated in a 96-well plate at density of 1×10^4 cells/well 24 h prior to addition of polymers. Following this, micellar assemblies developed from the aqueous solutions of S10, D10, PEG₆₀₀PTHF₆₅₀, and PEG₃₀₀PTHF₂₅₀ at different concentrations above the cmc were added to the cells and incubated for another 24 h. After 24 h, a 2 mg/mL solution of MTT (3-[4,5-dimethylthiazol-2-yl]-2,5-diphenyltetrazolium bromide) in Hank's balanced salt solution (HBSS) was added to all the wells (25 µL/well) and the plate was re-incubated for 6 h in an incubator to allow for the formation of formazan crystals. After incubation, the media were discarded carefully from the wells and dimethyl sulfoxide (DMSO, 100 µL) was added to solubilize the formazan crystals that formed. The absorbance was measured in each well at 570 nm using

microplate spectrophotometer. Untreated cells were used as controls and Triton-100 (at 0.025 and 0.015%) was used as positive control.

4.3.5.2. Cytotoxicity of Curcumin-loaded AIPE Micellar Assemblies against Breast Carcinoma Cells

The curcumin-loaded AIPE micellar assemblies were evaluated for cytotoxicity toward the breast carcinoma cell line T47D (CRL-2865) obtained from the American Type Culture Collection (Rockville, MD).²⁴ The T47D cells were maintained in Dulbecco's Modified Eagle Medium (DMEM) supplemented with 10% fetal bovine serum (FBS), penicillin (100 U/mL), streptomycin (100 µg/mL), and glutamine (2 mM). The cells were trypsinized, resuspended into fresh DMEM, and then seeded into 96-well Poly-*L*-Lysine plates at an inoculum density of 2×10^4 cells/well. The plates were incubated for 24 h at 37 °C (5% CO₂) and then the DMEM was carefully removed from each well using an 8-channel pipette.

Each curcumin-loaded AIPE sample (0.150 mL) was transferred to five replicate wells containing attached T47D cells. The samples were prepared in DMEM by adding Na₂CO₃ solution to adjust pH to 7.2. In addition to the curcumin-loaded polymer micelle samples, a set of Triton X-100 cytotoxic controls (0.01% and 0.001% v/v) were also prepared in DMEM and added to five replicate wells. A growth positive (i.e., non-cytotoxic) control was included by adding fresh DMEM to the wells only (i.e., without curcumin-loaded polymer micelles or Triton X-100). The plates were then transferred to a 37 °C growth chamber (5% CO₂) and incubated for 3 h. Following the 3-h incubation period, the curcumin-loaded polymer micelle and control samples were discarded and the entire plate was rinsed three times with DMEM (0.150 mL). Subsequently, fresh DMEM (0.3 mL) was added to each well and the plates were placed back into the growth chamber and incubated at 37 °C (5% CO₂).

T47D cell viability was determined after 18, 42, and 66 h of incubation using an MTT colorimetric assay.²⁵ In particular, a 0.5 g/L solution of MTT in HBSS (0.033 mL) was added to each well of the plate and then incubated for 4 h at 37 °C. Following the 4 h incubation period, the MTT solution was removed from each well and DMSO (0.150 mL) was added. The plates were then placed on an orbital shaker for 15 min (150 rpm; ambient laboratory temperature) to lyse the cells and solubilize the MTT dye. The plates were transferred to a multi-well plate spectrophotometer and the absorbance values were measured at 570 nm. The mean absorbance values reported ($n = 5$) were considered to be directly proportional to the number of viable cells that survived after the curcumin-loaded polymer micelle and control sample treatments. Error bars represent one standard deviation of the mean absorbance values.

4.4. Results and Discussion

4.4.1. AIPE Micellar Assemblies as Nanocontainers for Insoluble Molecules

Macromolecules of amphiphilic invertible polyesters build micelles with a hydrophilic exterior and a hydrophobic interior that self-assemble into micellar assemblies with increasing AIPE concentration in aqueous solution (see Chapter 3 for more information). Polymeric micelles are known to sequester poorly soluble substances in their interior, i.e. they act as nanocontainers.²⁶ Nanocontainer properties of polymeric micelles have found their use in biomedical applications.^{27,28} The ability of amphiphilic invertible polyesters to serve as nanocontainers by sequestering poorly soluble lipophilic molecules in water has been studied using dye solubilization. Nonpolar dyes such as Sudan Red B or Nile red are known to be sparingly soluble in water. However, addition of the solid dye to the colorless aqueous solution of amphiphilic invertible polyesters (both AIPes-1 and AIPes-2) has resulted in the dye entering the solvent phase, which was indicated by the change of solution color to red (Figure 4.2). The

color does not disappear after removal of the residual solid dye by centrifugation and filtering solution through a filter with an average pore size of 200 μm . Hence, the hydrophobic dye molecules diffuse into the AIPE micelles and become solubilized in the nonpolar micellar interior.

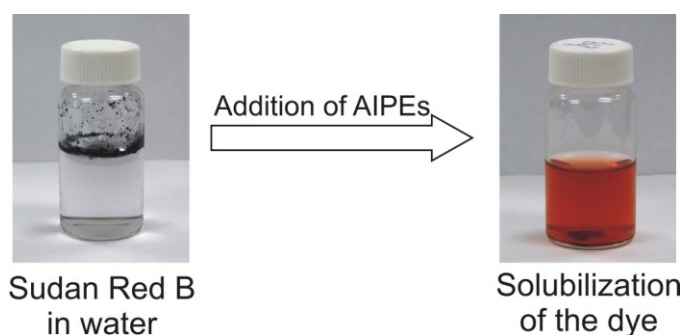


Figure 4.2. Solubilization of Sudan Red B by AIPE aqueous solutions.

UV-Vis spectra of Sudan Red B solubilized by AIPE-1 S6 based on PEG-600 and sebacic acid at different polyester concentrations are presented in Figure 4.3. Increasing S6 concentration

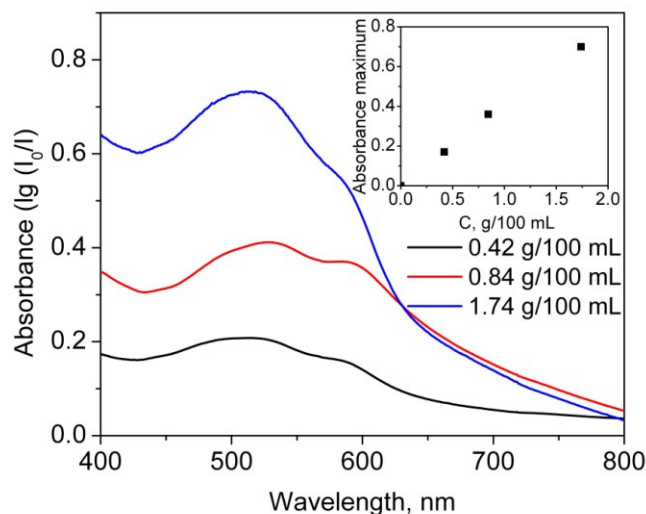


Figure 4.3. UV-Vis spectra of Sudan Red B solubilized by aqueous solution of polyester S6 at different polyester concentrations.

leads to a higher intensity of the Sudan Red B absorption peak at 514 nm. In the concentration range of 0.5–2% the peak height is directly proportional to the polyester concentration, as increasing S6 concentration in the aqueous solution leads to an increase of the total number of hydrophobic fragments capable of dye solubilization.

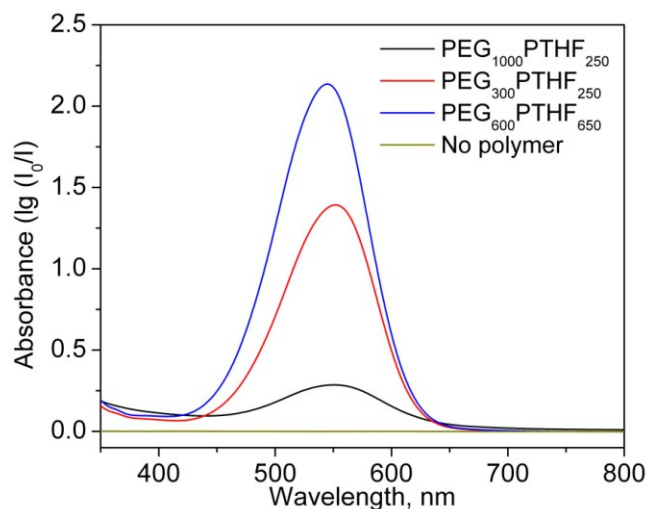


Figure 4.4. UV-Vis spectra of 1% aqueous solutions of AIPE-2 micelles loaded with Nile red.

Solubilization of Nile red (7-diethylamino-3,4-benzophenoxazine-2-one), a lipophilic dye that demonstrates solvatochromic behavior over a wide wavelength range,²⁹ has been carried out by three AIPE-2 polyesters differing in hydrophilic-lipophilic balance (PEG₁₀₀₀PTHF₂₅₀, PEG₃₀₀PTHF₂₅₀, and PEG₆₀₀PTHF₆₅₀).²⁹ Since Nile red is poorly soluble in water, it shows no absorption in UV-vis spectroscopy measurements. However, the dye was solubilized in water by AIPEs-2 macromolecules that provided a microenvironment capable of sequestering hydrophobic molecules. UV-Vis spectra of the 1% aqueous solutions of AIPE-2 micelles saturated with Nile red are depicted in Figure 4.4. Significantly lower absorption intensity of Nile red solubilized by PEG₁₀₀₀PTHF₂₅₀ has been observed as compared to polymers PEG₃₀₀PTHF₂₅₀, and PEG₆₀₀PTHF₆₅₀. Although macromolecules of PEG₁₀₀₀PTHF₂₅₀ did

sequester the dye, a smaller number of hydrophobic molecules were solubilized. The latter effect can be explained by the higher hydrophobicity of polyesters PEG₃₀₀PTHF₂₅₀ and PEG₆₀₀PTHF₆₅₀ in comparison to the more hydrophilic PEG₁₀₀₀PTHF₂₅₀. The differences in HLB values also explain the marked difference in absorption intensity observed in dye sequestration by PEG₃₀₀PTHF₂₅₀ compared to PEG₆₀₀PTHF₆₅₀: the intensity was significantly higher when dye was solubilized by macromolecules with a lower HLB value. The data on sequestration of Nile red by AIPES-2 follow the same trend as the cmc values of these polymers do: higher surface activity and stronger micellization observed for AIPES-2 with lower HLB values explain their better capacity for solubilizing hydrophobic molecules in aqueous solutions.

Hence, amphiphilic invertible polyesters have been shown to solubilize nonpolar substances in their micellar interior in the aqueous solution and, therefore, act as nanocontainers for hydrophobic cargos. Nanocontainer properties of the AIPs have been further exploited by probing them as potential drug delivery vehicles for the delivery of hydrophobic drugs.

4.4.2. Amphiphilic Invertible Polymers as Potential Responsive Drug Delivery Systems: Model Dye Experiments

The invertibility and responsive properties of amphiphilic invertible polymers are especially promising for controlled self-assembly in applications that require the use of micellar nanoassemblies simultaneously in polar and nonpolar media, such as drug delivery. The process of delivery of poorly soluble drugs to the target cell involves interaction of drug delivery vehicle with the amphiphilic cell membrane. This interaction is expected to change the AIP conformation causing the release of the solubilized drug. Probing this possibility requires that micellar assemblies be confirmed to transfer these molecules through a polar/nonpolar interface.

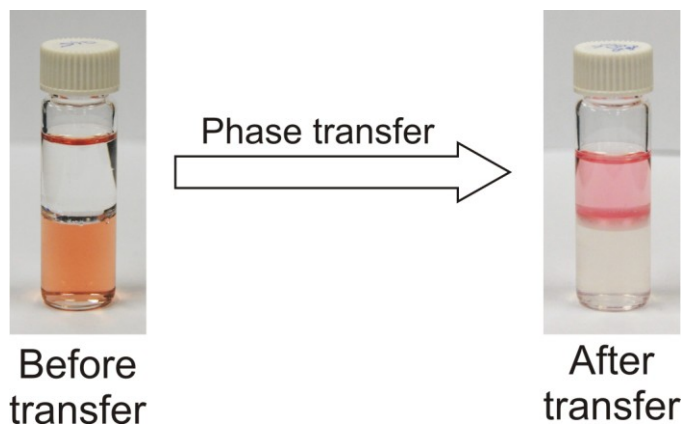


Figure 4.5. Appearance of the two-phase system consisting of 1% aqueous solution of AIPE-2 micellar assemblies loaded with Nile red and toluene before (left) and after the polymer-mediated transfer (right).

To probe the transfer of dye-loaded polymeric micelles through a polar/nonpolar interface, a model system consisting of a 1% aqueous solution of AIPE-2 micellar assemblies loaded with Nile red and two nonpolar solvents (toluene and 1-octanol) that are immiscible with water. The nonpolar solvent was added to the top of an aqueous solution containing dye-loaded polymeric micelles (Figure 4.5). The goal was to study the behavior of these micelles in the presence of two solvents with opposite polarity, and to answer the question whether the hydrophobic payload could be delivered from the aqueous phase to the nonpolar organic phase. Being more polar than toluene, 1-octanol has been used in the transfer experiments as the most valid hydrophobicity scale model system to study partitioning in a biomembrane. Experimental mixtures have been shaken for ten minutes and then allowed to separate (Figure 4.5). The polymer-sequestered Nile red, normally insoluble in water, has been successfully delivered to both toluene and 1-octanol using three AIPE-2 polyesters, PEG₁₀₀₀PTHF₂₅₀, PEG₃₀₀PTHF₂₅₀, and PEG₆₀₀PTHF₆₅₀. All three AIPEs were capable of transferring dye molecules from water to an

organic medium of opposite polarity that is seen by top (organic) phase color appearance (Figures 4.6A and 4.6B).

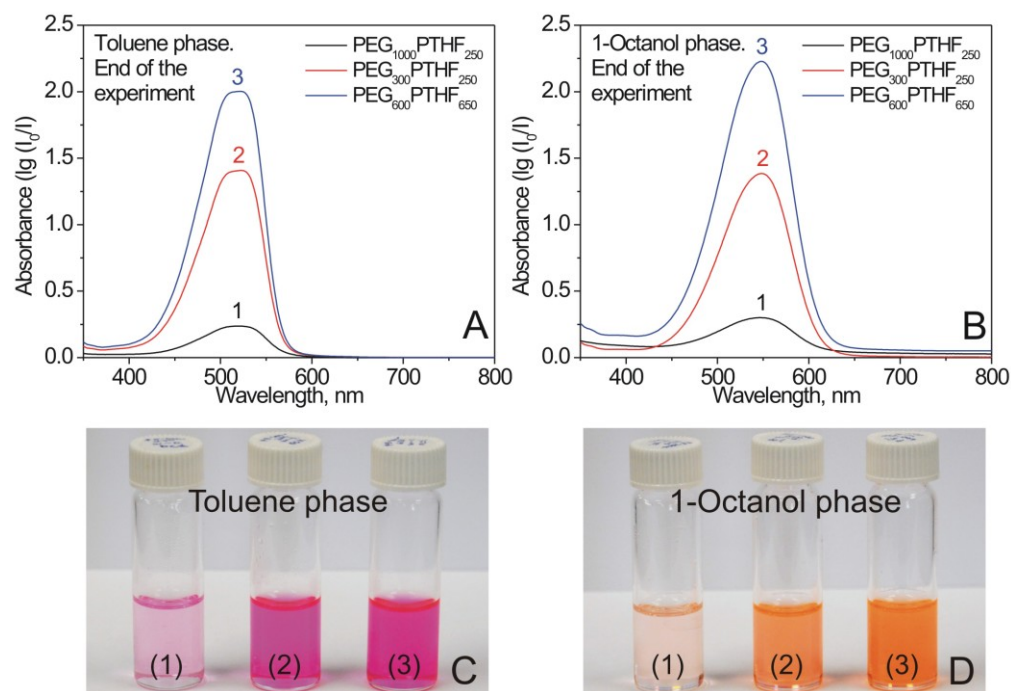


Figure 4.6. UV-Vis spectra of Nile red solutions transferred by AIPES-2 to toluene (A) and 1-octanol (B). Appearance of dye solutions in toluene (C) and 1-octanol (D) after the transfer.

Due to the solvatochromic nature of Nile red, the differences in transferred dye solution color in toluene (pink) and 1-octanol (orange) are noticeable (Figures 4.6C and 4.6D). In addition, a significant difference in dye solution color intensity has been noted, both in 1-octanol and toluene, when different polymers were used for the transfer. The differences in color intensity of the dye solution can be attributed either to: (1) different loading capacity of polymeric micelles (ability to bind dye molecules in aqueous medium) and/or (2) different transfer efficiency of the polymeric micelles (ability to deliver and release dye molecules from aqueous to organic nonpolar phase). The effect of these two factors has been determined by comparing an initial concentration of the polymer-solubilized dye in water with the final Nile red

concentration in toluene and 1-octanol after the transfer, measured by UV-vis spectroscopy. Analysis of the dye concentration in aqueous (before the transfer) and organic (after the transfer) phases has revealed that vast majority of the dye molecules has been transferred to the toluene and 1-octanol (Table 4.1). This observation obviously rules out the factor of different transfer efficiency of polymeric micelles. The ability of the polymer to bind dye molecules in water (loading capacity) was the major determinant of the extent of transfer of Nile red by polymeric micelles through the polar/nonpolar interface.

Table 4.1. Transfer of Nile Red and AIPES-2 from the Aqueous to the Nonpolar Media

Polymer	Davies HLB	Nile red transferred, %	
		to toluene	to 1-octanol
PEG ₁₀₀₀ PTHF ₂₅₀	20.1	84 ± 3	86 ± 2
PEG ₃₀₀ PTHF ₂₅₀	14.9	98 ± 4	81 ± 4
PEG ₆₀₀ PTHF ₆₅₀	13.8	97 ± 3	86 ± 3

In summary, model phase transfer experiments using Nile red have shown that: (1) AIPE polymeric micelles can sequester hydrophobic molecules in aqueous solutions, cross polar/nonpolar liquid interface and transfer their payload to the nonpolar phase of an immiscible solvent mixture. The micelles are stable in water and exhibit both container and carrier properties while transferring the material; and (2) the amount of transferred material depends mainly on micellar loading capacity (the ability of the AIPE macromolecules making up the micelles to bind guest molecules). Increasing the lipophilicity of the AIPES increases the amount of transferred material.

4.4.3. Amphiphilic Invertible Polymers as Potential Responsive Drug Delivery

Systems: Curcumin Transfer

After initial studies on transfer of the model dye, Nile red, experiments with curcumin, a poorly water-soluble phytochemical agent have been carried out. Curcumin, a potential therapeutic agent, has low intrinsic toxicity but possesses a great potential in the treatment of diverse diseases including cancer, arthritis, Alzheimer's disease etc.,³⁰ due to broad biological activity such as anti-oxidant, anti-inflammatory, and anti-tumor activity at the molecular level, following oral or topical administration.³¹ Curcumin has been subjected to several clinical trials for the development of therapeutic agents for various diseases, which include cancer,³² but its clinical development has been hindered due to the insolubility of the curcumin in water, restricting the use of the drug.³³ Therefore, curcumin solubilization by AIPE micellar assemblies is seen as a tool to address this issue by improving the aqueous solubility of this therapeutic agent.

Table 4.2. Physical Properties of Blank and Curcumin-Loaded AIPE Micellar Assemblies at 1% Concentration

Polymer	Davies HLB	Drug loading, % w/w	Size, nm (blank)	Size, nm (loaded)	ζ-potential, mV (blank)	ζ-potential, mV (loaded)
PEG ₃₀₀ PTHF ₂₅₀	14.9	3.6±0.3	12.4±0.2	18.4 ±1.1	-43.0±2.3	-42.6±1.5
PEG ₆₀₀ PTHF ₆₅₀	13.8	10.3±0.4	12.0±0.2	17.5±2.6	-24.2±3.8	-18.2±0.6
S10	15.4	0.14±0.03	3.3±0.5	3.6±0.2	-7.1±0.3	-6.7±0.9
D10	14.4	1.9±0.3	6.3±0.3	7.8±0.6	-10.3±0.9	-7.4±0.3

Four amphiphilic invertible polyesters including two AIPES-1 (D10, S10) and two AIPES-2 (PEG₃₀₀PTHF₂₅₀, PEG₆₀₀PTHF₆₅₀) have been chosen to be loaded with curcumin. Curcumin-loaded AIFE micelles were prepared using 1% polymer solutions. At this concentration, the micelles have self-assembled into invertible micellar assemblies, and the hydrophobic curcumin has been solubilized through physical interactions with the polymer hydrophobic fragments of the micellar interior. To determine loading, UV-vis spectroscopy measurements have been carried out. Table 4.2 shows the curcumin loading content for each AIFE micellar formulation.

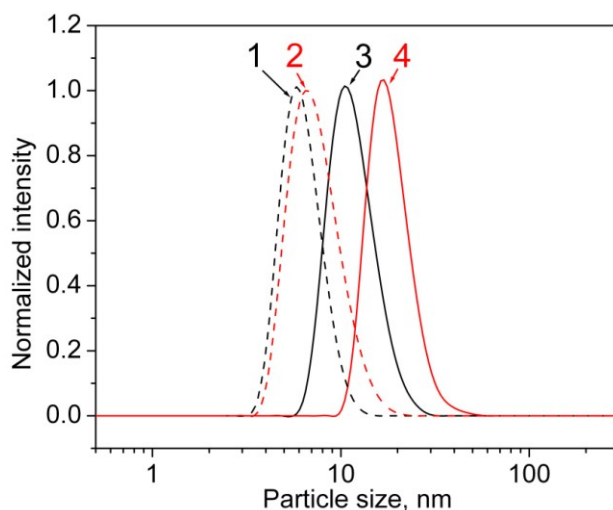


Figure 4.7. The size of blank and curcumin-loaded AIFE micellar assemblies as determined by dynamic light scattering: (1) D10, (2) curcumin–D10, (3) PEG₆₀₀PTHF₆₅₀, and (4) curcumin–PEG₆₀₀PTHF₆₅₀.

Hydrodynamic diameters of the AIFE micellar assemblies have been compared for amphiphilic invertible polyesters with different HLB, before and after the curcumin loading. Figure 4.7 shows the characteristic average diameter and size distribution of blank and drug-loaded micellar assemblies from D10 and PEG₆₀₀PTHF₆₅₀. The diameters of micellar assemblies

vary between 4.7 ± 0.2 nm and 12 ± 0.6 nm for chosen polymers and become larger for macromolecules with higher HLB. The loaded micellar assemblies showed a higher diameter value in comparison with the blank ones, which confirms the incorporation of curcumin into the micellar interior. Small size and narrow unimodal size distribution indicate that AIPE micellar assemblies possess good physical properties for being considered as nanocarriers for poorly water-soluble drugs.

Analysis of the zeta potential for blank and drug-loaded micellar assemblies showed that all polymer formulations have negative surface charge at room temperature (Table 4.2). The zeta potentials of loaded micelles decrease but still remain negative after the solubilization of curcumin. The negative zeta potentials indicate that AIPE micellar assemblies can provide an enhanced adhesion and interactions with gastrointestinal mucus and cellular linings and, thus, facilitate the bioadhesion between the micellar carriers and intestinal epithelial cells.³⁴

The obtained results demonstrate that amount of solubilized curcumin in the AIPE micellar assemblies is the highest for the most hydrophobic PEG₆₀₀PTHF₆₅₀ (HLB = 13.8). The loading capacity of micellar assemblies is essentially smaller for PEG₃₀₀PTHF₂₅₀, a polymer with shorter hydrophobic fragments. Much less curcumin was loaded in AIPE micellar assemblies developed from the more hydrophilic D10 and S10 (HLB = 14.4 and 15.4, respectively). However, all four polymers were chosen for further experiments on the chemical stability of micellar curcumin and phase transfer study.

While curcumin is known to be stable at acidic pH, it is transformed into (4'-hydroxy-3'-methoxyphenyl)-2,4-dioxo-5-hexanal, ferulic acid, and feruloyl methane at neutral and basic pH in the aqueous solution.³⁵ More than 90% of the curcumin rapidly decomposes within 30 minutes of placement in phosphate-buffered saline at pH 7.2. The stability of curcumin loaded in the

AIPE micellar assemblies has been monitored by UV-vis spectroscopy in the aqueous medium at pH 7 (Figure 4.8). The data show that the change in curcumin absorbance with time was negligibly small for micellar assemblies based on AIPes with lower HLB, confirming the very good stability of micellar curcumin. In particular, extremely low curcumin decomposition rate has been observed for micellar formulation based on PEG₆₀₀PTHF₆₅₀ and PEG₃₀₀PTHF₂₅₀. Lower stability has been demonstrated by curcumin samples solubilized in micelles formed from more hydrophilic AIPes, yet more than 50% of the loaded drug remained intact after 10 days of the experiment for the most hydrophilic S10. Therefore, curcumin-loaded AIPE micellar assemblies from four polymers have been subject to the phase transfer study.

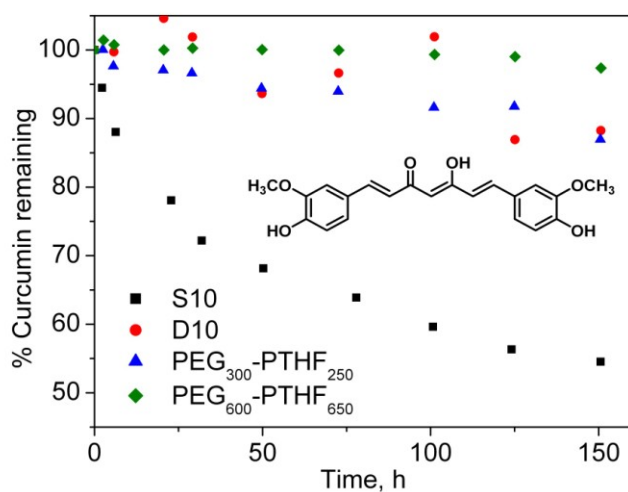


Figure 4.8. Chemical stability of curcumin in AIPE micellar assemblies in the aqueous medium with time.

To probe the AIPE-mediated drug transfer through a polar/nonpolar interface, 1-octanol was added to the top of an aqueous solution containing curcumin-loaded micellar assemblies, the mixtures were shaken for ten minutes and then allowed to separate. All chosen polymeric micellar formulations were capable of transferring sequestered curcumin molecules from water

to an organic medium of opposite polarity as detected via UV-vis spectroscopy measurements (Figure 4.9).

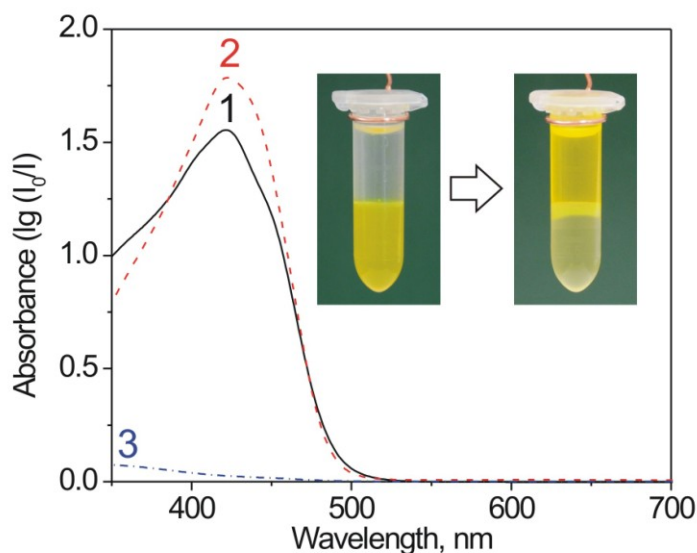


Figure 4.9. Representative UV-vis spectra of curcumin in (1) aqueous phase before the transfer, as well as in (2) 1-octanol and (3) aqueous phase after the transfer from water to 1-octanol. Inset: appearance of water-octanol mixture before (left-side tube) and after (right-side tube) the polymer-mediated transfer of curcumin from water (bottom phase) to 1-octanol (top phase).

This observation indicates that AIPE micellar assemblies have been efficient in transferring cargo molecules. Analysis of the curcumin concentration in aqueous (before the transfer) and 1-octanol (after the transfer) phases revealed that the vast majority of the drug molecules have been transferred to the 1-octanol (Table 4.3). The latter demonstrates that the major determinant of the extent of AIPE-mediated drug transfer through the polar/nonpolar interface is the ability of the AIPE micellar assemblies to bind curcumin molecules in water, i.e. the AIPE loading capacity.

Table 4.3. Phase Transfer Characteristics of Curcumin-Loaded AIPE Micellar Assemblies at 1% Concentration

Polymer	Curcumin transferred, %	Curcumin released in dialysis, %	AIPE transferred to 1-octanol,%
PEG ₆₀₀ PTHF ₆₅₀	89±3	1.4±0.7	14±2
PEG ₃₀₀ PTHF ₂₅₀	91±3	0.3±0.5	26±2
D10	99±2	16±2	21±3
S10	96±3	49±2	13±1

With the AIPE-mediated drug transfer established, a mechanism of release of the hydrophobic substance from micellar assemblies was considered next. Obviously, three different possibilities exist to explain how curcumin molecules could cross a polar/nonpolar interface. One of these assumes that molecules that are poorly soluble in water can be partitioned between the micellar interior and bulk water due to their limited aqueous solubility.³⁶ At the beginning of the experiment, curcumin molecules are distributed between the bulk water and the AIP micellar assemblies, which act as containers for poorly soluble material. The limited solubility of drug in water, and thus, its low concentration in the aqueous phase, is obviously sufficient to transfer the drug from the micellar interior, first to water and then from water to the nonpolar phase (Figure 4.10A).³⁷ At the same time, the curcumin-loaded micellar containers can migrate from the aqueous phase to the polar/nonpolar interface, change their conformation due to the macromolecular inversion upon changing polarity of local environment, disassemble (lose their container properties), and release curcumin into the 1-octanol, where the drug is soluble

(Figure 4.10B). Finally, the loaded micellar assemblies can undergo thermodynamically driven distribution between the aqueous and 1-octanol phases. This can happen when drug-loaded micelles cross the interface, invert their conformation, and form new micelles in the 1-octanol (Figure 4.10C). If this mechanism works, then curcumin-loaded assemblies can act as responsive carriers for solubilized drug molecules and release the drug upon inversion within a nonpolar phase.

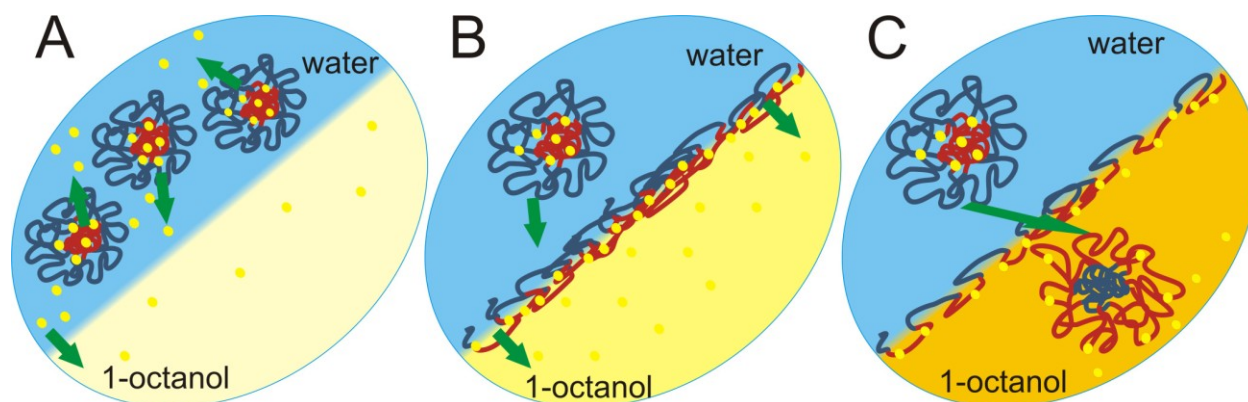


Figure 4.10. Possible mechanisms of AIPE-mediated curcumin delivery from water to 1-octanol.

To distinguish between three possible mechanisms and their contributions to the established AIPE-mediated curcumin transfer, two additional experiments have been carried out. Firstly, the presence of AIPE macromolecules in 1-octanol was analyzed to confirm crossing the interface by polymer and, thus, the possibility for the AIPE micellar assemblies to deliver curcumin to 1-octanol using the mechanism shown in Figure 4.10C. Secondly, release of curcumin from micellar assemblies was studied using conventional dialysis membrane to evaluate the potential contribution of anticipated partitioning of curcumin between the micellar interior and the aqueous phase due to the limited solubility of the drug in water (Figure 4.10A).

Table 4.3 shows that polyester macromolecules were detected in 1-octanol for each polymer employed in the AIPE-mediated curcumin transfer experiment, indicating that all the

polyesters have been able to cross the interface between water and 1-octanol during the experiment. Interestingly, the hydrophilic-lipophilic balance of the polyesters does not show a great influence on the amount of the transferred AIPE. In turn, curcumin release in dialysis differs greatly for AIPEs with different HLB values. To this end, almost no release was detected for drug molecules loaded in PEG₆₀₀PTHF₆₅₀ and PEG₃₀₀PTHF₂₅₀. In turn, the release of curcumin from the more hydrophilic polyesters (especially, S10) is much higher, which demonstrates differences in the thermodynamic stability of loaded micelles and the significant influence of HLB on the contribution of the partitioning mechanism (Figure 4.10A) to the transfer.

Quantitative analysis of data in Table 4.3 indicates that most of the micellar curcumin was delivered to 1-octanol using the conformational change of macromolecules that is induced in response to the changing polarity of the environment (Figure 4.10B). The total amount of transferred curcumin suggests that micellar assemblies developed from the AIPEs are superior in curcumin delivery from water to 1-octanol, and the drug was efficiently transferred through the polar/nonpolar interface predominantly using the inversion mechanism. To further investigate the potential of AIPE formulations in cellular uptake, the cytotoxicity of curcumin-loaded micellar assemblies has been evaluated against human embryonic kidney cells and breast carcinoma cells.

Prior to studying the cytotoxicity of curcumin-loaded micellar assemblies against carcinoma cells, the cell viability of human embryonic kidney cells (HEK 293) in the presence of blank AIPE micellar assemblies was examined using standard MTT assay. As a potential drug-delivering carrier, the material has to be nontoxic to human cells and highly biocompatible.

The AIPE micellar assemblies exhibit no cytotoxicity against living human cells at concentrations of 2×10^{-3} – $10 \mu\text{g/mL}$ (Figure 4.11). Three different polymers are comparable on the cell viability of HEK 293 cells.

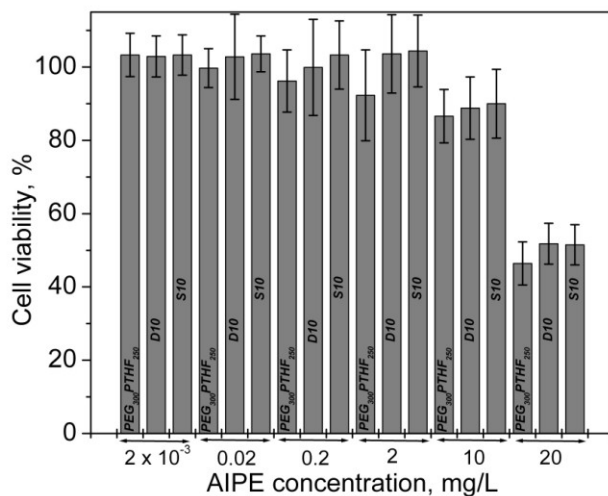


Figure 4.11. Cell viability of HEK 293 cells treated with various concentrations of blank AIPE micellar assemblies.

The efficiency of curcumin-loaded AIPE micellar assemblies on the viability of T47D breast carcinoma cells was assessed using MTT assay for S10 and PEG₆₀₀PTHF₆₅₀ formulations at concentration of $10 \mu\text{g/mL}$ and maximum curcumin loading. Both formulations showed high efficiency in the phase transfer experiment, while they are, obviously, significantly different in terms of releasing mechanism. The very small amount of drug was released through dialysis from PEG₆₀₀PTHF₆₅₀-based formulation, while almost half of the drug amount was released in the same experiment from the S10-based formulation (Table 4.3).

Figure 4.12 shows the *in vitro* viability of T47D breast carcinoma cells after 18, 42, and 66 hours treatment with curcumin solubilized in the AIPE micellar assemblies at maximum loading. Several general conclusions can be drawn from Figure 4.12. First, the AIPE-based

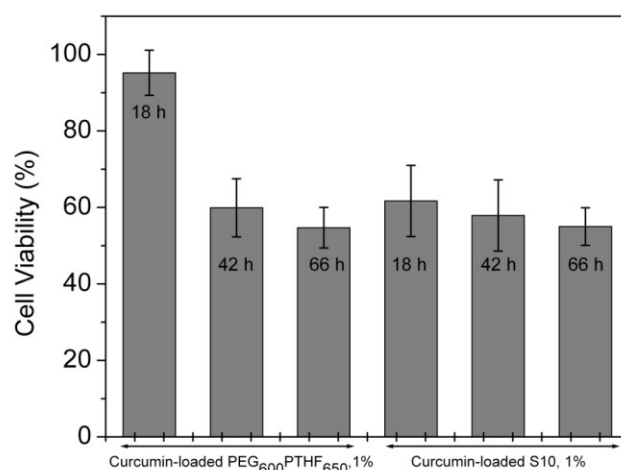


Figure 4.12. Cytotoxicity of curcumin-loaded AIPE micellar assemblies on T47D breast carcinoma cells after 18, 42, and 66 h incubation.

curcumin-loaded drug delivery vehicles are cytotoxic against the carcinoma cells, which confirms their successful administration and/or curcumin delivery to the cells. Second, the micellar curcumin remains stable for at least 66 h under conditions that (without solubilization in micelles) facilitate its rapid chemical decomposition with water, which indicates the improved bioavailability of micellar curcumin for the cellular uptake. Thirdly, the cytotoxicity results demonstrate that two AIPE formulations obviously exhibit different profiles of carcinoma cell viability in time, which may be due to variations in the mechanism of drug release. For the formulation based on PEG₆₀₀PTHF₆₅₀, the cytotoxic effect is small after 18 h, but it improves with an increasing time of incubation. In case of curcumin-loaded S10 assemblies, the cell viability significantly decreases after 18 h, and remains almost constant during further incubation. This difference could be related to the fact that the polymer-based formulations have different profiles for releasing curcumin. The results from the phase transfer study indicate that a large portion of S10-loaded curcumin could be released by diffusion (Figure 4.10A), while this

mechanism is almost negligible in the case of highly thermodynamically stable PEG₆₀₀PTHF₆₅₀ formulation (Table 4.3). However, although the micellar assemblies developed from PEG₆₀₀PTHF₆₅₀ remain stable in a homogenous environment, they can rapidly invert conformation due to a subtle change in polarity of the medium. Thus, once the curcumin-loaded micellar assemblies developed from PEG₆₀₀PTHF₆₅₀ reach the cell sites, the drug release can be induced by rapid inversion of the macromolecular conformation. As a result, the cytotoxicity of curcumin-loaded PEG₆₀₀PTHF₆₅₀ assemblies becomes comparable to the cytotoxicity of the formulation made from S10 already after 42 hours and further remains constant. This behavior of PEG₆₀₀PTHF₆₅₀ formulation demonstrates the promising ability of the AIPE micellar assemblies to remain stable in a homogenous environment, but then rapidly undergo inverse conformation due to changes in environmental polarity.

4.5. Conclusions

To summarize, the ability of AIPE-based micellar formulations to solubilize poorly water-soluble cargo molecules and transfer their payload into a nonpolar phase by inverting their macromolecular conformation in response to changes in the polarity of the local environment has been demonstrated. The amount of material transferred depends primarily on micellar loading capacity. Increasing the lipophilicity of the AIPE composition increases the amount of material transferred. The unique ability of AIPEs to invert the molecular conformation depending on the polarity of the environment can be a decisive factor in establishing the novel stimuli-responsive mechanism of solubilized drug release that is induced in response to a change of the environmental polarity. Drug-loaded AIPE micellar assemblies have been shown to deliver poorly water-soluble curcumin to carcinoma cells. The release of curcumin from AIPE micellar assemblies is primarily caused by macromolecular inversion due to changing local

environmental polarity and can be controlled by the AIPE structure and concentration. The AIPE micellar assemblies are shown to be nontoxic against human cells up to a concentration of 10 $\mu\text{g/mL}$, while they show cytotoxicity against T47D breast carcinoma cells at this concentration. An additional advantage of AIPE-based vehicles is their ability to stabilize curcumin molecules against chemical decomposition. The obtained results demonstrate the potential of AIPE-based responsive vehicles as a promising platform for controlled delivery of poorly water-soluble drug candidates by means of new stimuli-responsive release mechanism.

4.6. References

1. Schmolka, I.R. *J. Am. Oil Chem. Soc.* **1977**, *54*, 110–116.
2. Alexandridis, P.; Hatton, T.A. *Colloids Surf. A.* **1995**, *96*, 1–46.
3. Adams, M.L.; Lavasanifar, A.; Kwon, G.S. *J. Pharm. Sci.* **2003**, *92*, 1343–1355.
4. Croy S.R.; Kwon, G.S. *Curr. Pharm. Des.* **2006**, *12*, 4669–4684.
5. Nishiyama N.; Kataoka, K. *Pharmacol. Ther.* **2006**, *112*, 630–648.
6. Torchilin, V.P. *Pharm. Res.* **2007**, *24*, 1–16.
7. Yokoyama, M. *Expert Opin. Drug Delivery* **2010**, *7*, 145–158.
8. Ghosh, S.; Irvin K.; Thayumanavan, S. *Langmuir* **2007**, *23*, 7916–7919.
9. Montazeri H.; Lavasanifar, A. *Expert Opin. Drug Delivery* **2006**, *3*, 139–162.
10. Kwon, G. *Crit. Rev. Ther. Drug Carrier Syst.* **2003**, *20*, 357–403.
11. Aliabadi, H.M.; Lavasanifar, A. *Expert Opin. Drug Delivery* **2006**, *3*, 139–162.
12. Bawarski, W.E.; Chidlow, E.; Bharali, D.J.; Mousa, S.A. *Nanomedicine: NBM* **2008**, *4*, 273–282.
13. Bae, Y.; Nishiyama, N.; Fukushima, S.; Koyama, H.; Yasuhiro, M.; Kataoka, K. *Bioconjug. Chem.* **2005**, *16*, 122–130.

14. Potineni, A.; Lynn, D.M.; Langer, R.; Amiji, M.M. *J. Controlled Release* **2003**, *86*, 223–234.
15. Stapert, H.R.; Nishiyama, N.; Jiang, D.-L.; Aida, T.; Kataoka, K. *Langmuir* **2000**, *16*, 8182–8188.
16. Tang, Y.; Liu, S.Y.; Armes, S.P.; Billingham, N.C. *Biomacromolecules* **2003**, *4*, 1636–1645.
17. Liu, S.Q.; Tong, Y.W.; Yang, Y.Y. *Mol. Biosyst.* **2005**, *1*, 158–165.
18. Chung, J.E.; Yokoyama, M.; Yamato, M.; Aoyagi, T.; Sakurai, Y.; Okano, T. *J. Controlled Release* **1999**, *62*, 115–127.
19. Mitragotri, S. *Nat. Rev. Drug Discov.* **2005**, *4*, 255–260.
20. Gao, Z.-G.; Fain, H.D.; Rapoport, N. *J. Controlled Release* **2005**, *102*, 203–222.
21. Priutt, J.D.; Pitt, W.G. *Drug Delivery* **2002**, *9*, 253–258.
22. Singer, S.J.; Nicolson, G.L. *Science* **1972**, *175*, 720–731.
23. Zhang, X.; Jackson, J.K.; Burt, H.M. *Int. J. Pharm.* **1996**, *132*, 195–206.
24. Stumm, S.; Meyer, A.; Lindne, M.; Baster, G.; Wallwiener, D.; Guckel, B. *Oncology* **2004**, *66*, 101–111.
25. Wang, Y.; Yu, L.; Han, L.; Sha, X.; Fang, X. *Int. J. Pharm.* **2007**, *337*, 63–73.
26. Kale, T.S.; Klaikherd, A.; Popere, B.; Thayumanavan, S. *Langmuir* **2009**, *25*, 9660–9670.
27. Kabanov, A.V.; Batrakova, E.V.; Melik-Nubarov, N.S.; Fedoseev, N.A.; Dorodnich, T.Yu.; Alakhov, V.Yu.; Chekhonin, V.P.; Nazarova, I.R.; Kabanov, V.A. *J. Controlled Release* **1992**, *22*, 141–157.
28. Rapoport, N.Y.; Herron, J.N.; Pitt, W.G.; Pitina, L. *J. Controlled Release* **1999**, *58*, 153–162.

29. Deye, J.F.; Berger, T.A. *Anal. Chem.* **1990**, *62*, 615–622.
30. Aggarwal, B.B.; Harikumar, K.B. *Int. J. Biochem. Cell Biol.* **2009**, *41*, 40–59.
31. Maheshwari, R.K.; Singh, A.K.; Gaddipati, J.; Srimal, R.C. *Life Sci.* **2006**, *78*, 2081–2087.
32. Goel, A.; Kunnumakkara, A.B.; Aggarwal, B.B. *Biochem. Pharmacol.* **2008**, *75*, 787–809.
33. Sharma, R.A.; Gescher, A.J.; Steward, W.P. *Eur. J. Cancer* **2005**, *41*, 1955–1968.
34. Lo, C.L.; Lin, K.M.; Huang, C.K.; Hsiue, G.H. *Adv. Funct. Mater.* **2006**, *16*, 2309–2316.
35. Kumar, A.; Ahuja, A.; Ali, J.; Baboota, S. *Crit. Rev. Ther. Drug Carrier Syst.* **2010**, *27*, 279–312.
36. Berthod, A.; Garcia-Alvarez-Coque, C. *Micellar Liquid Chromatography*; Chromatographic Science Series, Vol. 83; Marcel Dekker: New York, NY, 2000.
37. Basu, S.; Vutukuri, D. R.; Thayumanavan, S. *J. Am. Chem. Soc.* **2005**, *127*, 16794–16795.

CHAPTER 5. FUNCTIONAL SELF-ASSEMBLY OF AMPHIPHILIC INVERTIBLE POLYMERS IN NONPOLAR MEDIUM: NANOREACTORS FOR NANOPARTICLE DEVELOPMENT

5.1. Abstract

A size-controlled synthesis of silver nanoparticles dispersible in polar and nonpolar media has been carried out in micellar assemblies from amphiphilic invertible polyurethanes (AIPUs) based on poly(ethylene glycol) as a hydrophilic constituent and polytetrahydrofuran as a hydrophobic constituent. Amphiphilic invertible polyurethanes self-assemble into micellar assemblies with hydrophilic interior and hydrophobic exterior domains in a nonpolar benzene medium at high concentration. AIPU micellar assemblies can be applied simultaneously as nanoreactors and colloidal stabilizers to synthesize size-controlled batches of silver nanoparticles. Size tuning and narrow particle size distribution can be facilitated by changes in the AIPU composition, macromolecular configuration, and concentration of the polymer solution. Depending on the length of polymer hydrophilic and hydrophobic constituent and fragment distribution along the macromolecule, the size of the fabricated nanoparticles can be varied from 6 to 14 nm. Due to the invertible properties of polyurethanes, the synthesized silver nanoparticles can be successfully dispersed in either polar or nonpolar media, where they form stable colloidal solutions. Silver nanoparticles developed in nanoreactors of the AIPU PEG₁₀₀₀-co-PTHF₆₅₀ have been successfully used as the seeds to aid anisotropic growth of the cadmium selenide semiconductor nanoparticles using the modified solution-liquid-solid method. As a result, a population of the monodisperse semiconductor nanoparticles with an average particle size of ca. 5 nm has been developed. Cadmium selenide nanoparticles developed in such a way have potential in a variety of applications ranging from physics to medicine.

5.2. Introduction

Development and characterization of nanoparticles have recently received considerable interest due to their properties and potential for use in a variety of applications.¹⁻⁵ Nanoparticle applications depend strongly on physical and chemical properties related to their size, which is essential for many advanced applications⁶ including optical,⁷ electronic,⁸ magnetic,⁹ catalytic,¹⁰ and antibacterial properties.¹¹ It is very important that successful applications apply nanoparticles fractionated in size or fabricated in size-selective syntheses.

Among the different methods for nanoparticle synthesis, polymer-assisted or polymer template synthesis has received considerable attention because of (1) small polymer concentration required to effectively stabilize formed nanoparticles via steric stabilization, (2) the possibility to tune the nanoparticle size and morphology by varying polymer composition and polymer : nanoparticle precursor ratio, (3) the ability of polymers to be used as both reagents and stabilizers in the nanoparticle synthesis, and (4) the possibility to develop novel metal-polymer nanocomposites.¹²⁻¹⁴

The methods used to develop polymer-stabilized nanoparticles include electrochemical techniques, a chemical or a photochemical reduction, a polyol process, and radiolytic methods.¹⁵⁻¹⁸ Even though the majority of approaches to nanoparticle development are successful, scalable synthesis of nanoparticles with a controlled size, a narrow size distribution, and a good stability in different dispersion media is still an issue to be solved. Furthermore, most of the methods of nanoparticle development suffer from particle agglomeration during the synthesis caused by van der Waals interactions. The use of polymers as steric stabilizers is considered a promising approach to develop stable nanoparticle dispersions.¹⁹

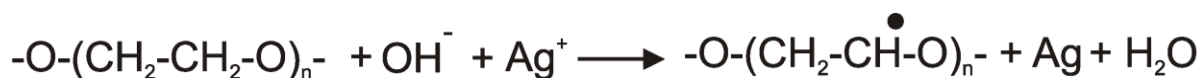
Poly(ethylene glycol) and PEG-containing polymers are widely used for the development of metal nanoparticles from metal salt precursors.^{20,21} Poly(ethylene glycol) chains are known to form cavities or pseudo-crown ether structures that can bind metal ions.^{22,23} The reason for PEG adopting the conformation similar to crown ethers is the ion-dipole interaction between the metal ion and the electron pair of the poly(ethylene oxide) fragments. Poly(ethylene glycol) chains are then able to reduce metal ions from the precursors bound to pseudo-crown PEG ether structures.

Amphiphilic invertible polyesters based on PEG and aliphatic dicarboxylic acids (AIPEs-1) have been recently used for the development of silver nanoparticles in a nonpolar solvent, benzene.^{6,24,25} At high polymer concentration in benzene AIPEs-1 form micellar assemblies with hydrophilic and hydrophobic domains serving as nanoreactors for nanoparticle synthesis. After being dispersed in a concentrated solution of amphiphilic invertible polyester, an aqueous solution of a silver precursor, $[\text{Ag}(\text{NH}_3)_2]\text{OH}$, has been accommodated in the hydrophilic domains of the micellar assemblies and reduced by polyester PEG fragments. The most prominent advantages of the proposed methodology are (1) spontaneous formation of silver nanoparticles at room temperature, (2) synthesis of a ready-to-use colloidal solution with an enhanced silver nanoparticle concentration, and (3) formation of surface-modified nanoparticles dispersible in both polar and nonpolar medium.⁶

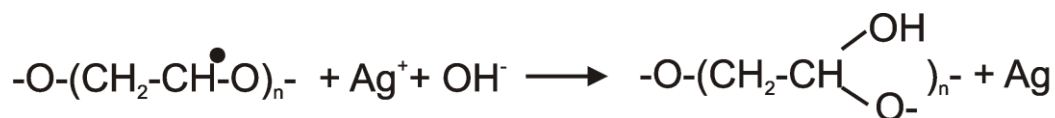
The mechanism of the AIPE-assisted silver reduction process has been proposed.⁶ After dissociation of the $[\text{Ag}(\text{NH}_3)_2]\text{OH}$ precursor, silver-containing cations $[\text{Ag}(\text{NH}_3)_2]^+$ become sequestered by pseudo-crown ether PEG structures with subsequent detachment of the ammonia molecules leading to an increase in the redox potential of the silver cation.²⁶ Hydroxyl OH^- anions formed in dissociation are non-solvated or “bare” that results in a significant increase of their basic properties, reactivity and nucleophilicity.²⁷

Reduction of the silver cations occurs according to the one-electron reduction mechanism that involves (1) interaction of Ag^+ with a mobile hydrogen atom of PEG chain yielding a macroradical, (2) proton generation, and (3) reduction of silver cations to Ag^0 .²⁸

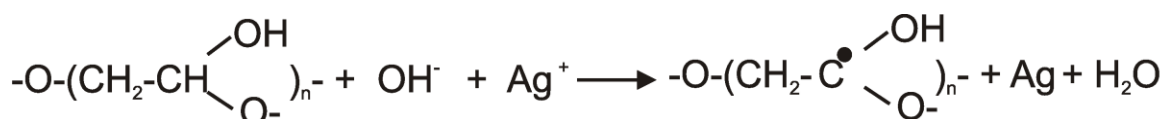
First, the silver cation, serving as an oxidation agent, reacts with a mobile PEG methylene hydrogen (reducing agent) in the presence of highly basic “bare” OH^- anions giving the reduced silver, PEG macroradical, and water:



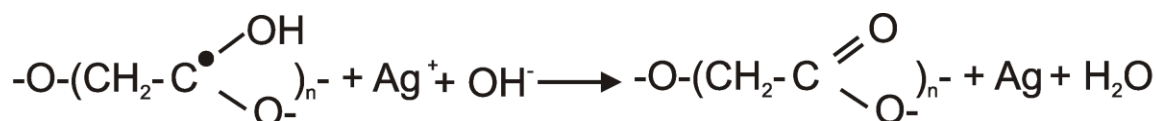
Next, Ag^+ cations receive an electron from PEG macroradicals and are therefore reduced to Ag^0 . The macroradicals are transformed into carbocations that, in turn, interact with the OH^- anion yielding hydroxyl-containing PEG fragments:



Subsequently, the silver cations react with mobile tertiary hydrogen atoms formed in the above reaction to give reduced silver and new macroradicals:



As a final step of the PEG transformation, the macroradical hydroxyl groups interact with Ag^+ . The reaction results in silver reduction, proton release and formation of an ester fragment:⁶



Even though silver reduction in AIPE-1 nanoreactors has yielded silver nanoparticles with a narrow particle size distribution, almost no variation in nanoparticle size has been observed, regardless of the polyester concentration, composition, and HLB. In fact, the use of

amphiphilic invertible polyesters with different length of hydrophilic and hydrophobic constituents has resulted in development of spherical silver nanoparticles ca. 10 nm in size.⁶

The research described in this chapter is aimed at probing self-organized micellar assemblies from the amphiphilic invertible polyurethanes based on poly(ethylene glycol) and polytetrahydrofuran for the development of nanoparticles in a nonpolar medium. In nonpolar solvents, AIPU forms micelles and micellar assemblies with a hydrophobic exterior and a hydrophilic interior made up of PEG fragments. By changing polyurethane hydrophilic-lipophilic balance, chain configuration, and solution concentration the ability to vary the size of silver nanoparticles in a controlled way has been targeted in the study. Subsequently, silver nanoparticles developed in AIPU nanoreactors have been used as the nucleation centers (seeds) in the development of cadmium selenide semiconductor nanoparticles. Hence, the use of AIPU micelles and micellar assemblies for nanoparticle synthesis makes them promising materials for the nanochemistry applications.

5.3. Experimental

5.3.1. Materials

Solvents (acetone, benzene, hexane, and diphenyl ether, all ACS grade), sodium hydroxide, ammonium hydroxide (30% aqueous solution), selenium powder, and cadmium oxide were all purchased from VWR International. Trioctylphosphine, Malachite green, and silver nitrate were purchased from Aldrich. All reagents and materials were used as received.

Amphiphilic invertible polyurethanes were synthesized from PEG, PTHF and 2,4-TDI as described in Chapter 2.

5.3.2. Characterization

UV-Vis spectra were recorded on a Varian Cary 5000 UV-Vis-NIR spectrophotometer. The absorbance values were measured in the range of 350–800 nm.

Particle size distribution of the nanoparticle dispersions was measured by dynamic light scattering (DLS) on Malvern Zetasizer Nano-ZS90 at 25 °C. The final numbers represent an average of a minimum of five individual measurements.

Transmission electron microscopy (TEM) images were taken using a JEOL JEM-2100 analytical transmission electron microscope. For the TEM measurements, a drop of nanoparticle dispersions prepared for DLS measurements was placed onto a copper mesh covered with a thin carbon film.

The presence of metallic silver in silver nanoparticles and phase characterization of cadmium selenide crystals were studied by X-ray diffraction (XRD) using Phillips X'Pert-MPD diffractometer (45 kV, 40 mA) equipped with a vertically mounted goniometer and a Cu X-ray source. XRD patterns were obtained for 30-80° (2θ) in a continuous scanning mode with a step size of 0.05°.

5.3.3. Solubilization Study

To prepare initial polyurethane solutions (0.1%, 0.5%, and 1.0% concentration), AIPUs (0.02 g, 0.1 g, and 0.2 g, respectively) were dissolved in the appropriate amount of benzene. After overnight equilibration, Malachite green (5 mg) was added, and the suspensions were stirred for 24 h. Prior to recording UV-vis spectra, excess dye was removed by filtration through 0.45 μm PTFE filters.

5.3.4. Synthesis of Silver Nanoparticles

Silver precursor $[\text{Ag}(\text{NH}_3)_2]\text{OH}$ was developed by adding an aqueous solution of sodium hydroxide (0.2 g NaOH/1 mL H_2O) to an aqueous solution of silver nitrate (0.12 g AgNO_3 /1 mL H_2O) to yield a brown precipitate of silver oxide. The latter was filtered off after washing with Millipore water to pH 8–9. Subsequently, the precipitate was completely dissolved in 30% ammonia solution (0.26 mL) to form a precursor solution.

Amphiphilic polyurethane nanoreactors for nanoparticle synthesis were prepared by dissolution of the corresponding polyurethane in benzene (0.4 g polymer in 1.6 g benzene for a 20% solution or 0.6 g polymer in 1.4 g benzene for a 30% solution). The solutions were left to equilibrate overnight under stirring at ambient conditions.

Silver nanoparticles were synthesized by adding a silver precursor solution (30 μL) to a benzene solution of polymer nanoreactors (2.0 g). The resulting mixture was stirred for 24 h. For UV-vis and TEM analyses, silver nanoparticle dispersions were prepared by diluting the resultant mixture with acetone (reactive mixture : solvent as 1:100).

5.3.5. Synthesis of Cadmium Selenide Nanoparticles

A suspension of cadmium oxide (0.128 g, 1 mmol) and AIPU PEG_{1000-co}-PTHF₆₅₀ (1.270 g) in diphenyl ether (15 mL) was mixed with a stock dispersion of silver nanoparticles developed in 30% solution of PEG_{1000-co}-PTHF₆₅₀ in benzene (1.000 g) in a three-necked flask. The reaction mixture was slowly heated to 220 °C under a nitrogen atmosphere with a needle outlet that allows solvent to evaporate. After 20 min of heating, the valve was removed, the reactive mixture was maintained at 220 °C for another 20 min and then 0.5 mL of 1 M solution of TOPSe prepared *in situ* from selenium (0.0395 g, 0.5 mmol) in triphenylphosphine (0.400 g, 1.1 mmol) was rapidly injected. After a certain reaction time (5, 10, 15, or 20 min), the reactive

mixture was quenched with hexane (ca. 10 mL). The resulting dispersion was washed and precipitated twice with benzene followed by centrifugation to remove the reaction solvent and excess AIPU. The precipitate was then redispersed in hexane and centrifuged. Cadmium selenide nanoparticles were contained in the supernatant.

5.4. Results and Discussion

5.4.1. Solubilization of Malachite Green by AIPU Micelles

Micelles and micellar assemblies from amphiphilic polymers are known to be able to accommodate insoluble substances in their interior.²⁹⁻³¹ Amphiphilic invertible polyurethanes have been shown to form micelles with an exterior consisting of lipophilic PTHF fragments and an interior made up of the polar PEG fragments in a nonpolar environment (benzene-*d*₆). As AIPU concentration increases, micelles self-assemble into micellar assemblies with hydrophilic PEG and hydrophobic PTHF domains (see Chapter 3 for more information).

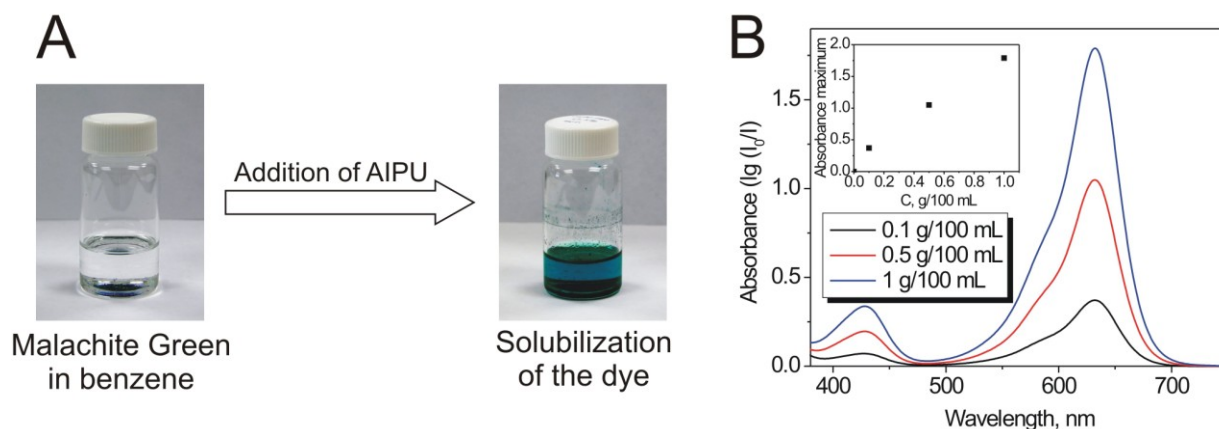


Figure 5.1. (A) Photographs of Malachite green in toluene (left) and solubilized in the AIPU micellar solution (right). (B) UV-vis spectra of Malachite green solubilized in benzene by different concentrations of PEG₁₀₀₀-*alt*-PTHF₆₅₀.

To confirm the capability of amphiphilic invertible polyurethane micelles to solubilize polar substances in a nonpolar medium and study the effect of polymer concentration, composition, and configuration on loading capacity of the micelles, an experiment on dye extraction by amphiphilic macromolecules has been carried out first (Figure 5.1A). Malachite green dye is known to be poorly soluble in benzene. However, addition of the solid dye to the benzene solution of amphiphilic invertible polyurethane has resulted in the dye entering the solvent phase, which was indicated by the change of solution color to green as in the UV-vis spectra shown in Figures 5.1B and 5.2. This observation can be explained by the solubilization of Malachite green by the AIPU macromolecules. As shown in the inset in Figure 5.1B, the absorbance maximum recorded at 632 nm, and, thus, the amount of solubilized dye linearly increases with polymer concentration. Higher polymer concentration in benzene leads to an increase in the number of macromolecules capable of dye solubilization.

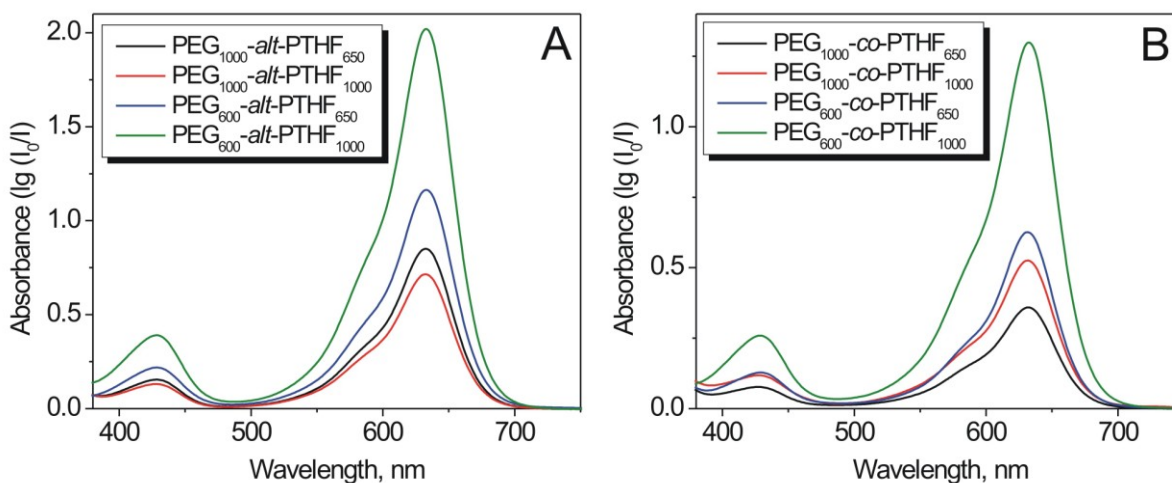


Figure 5.2. UV-Vis spectra of Malachite green solubilized in benzene by (A) alternating AIPUs and (B) random AIPUs (0.5 g/100 mL).

The solubilizing capacity of AIPUs increases with decreasing polyurethane HLB, indicating that macromolecules having a more hydrophobic composition accommodate higher amounts of insoluble dye within the micelles (Figure 5.2). This trend seems surprising, primarily because longer hydrophilic fragments of the polymers have been expected to provide more sites to solubilize polar dye molecules in the micellar interior. A reasonable explanation is that obviously the PTHF units of the macromolecules also possess the affinity for Malachite green. Indeed, a separate experiment confirmed the solubility of this dye in molten PTHF. Therefore, upon contact with the AIPU micellar benzene solution, the dye molecules were accommodated by both the interior and the exterior of the micelles. The loading capacity of the invertible micelles in terms of Malachite green is higher for alternating amphiphilic invertible polyurethanes than for the random ones, since the adsorption maxima in UV-vis spectra are systematically higher for the alternating macromolecules compared with the corresponding random AIPUs (Figures 5.2).

Hence, AIPU micelles are able to solubilize otherwise insoluble polar compounds in a nonpolar medium and loading capacity of the polymers could be correlated to their composition, chain configuration, and concentration.

5.4.2. Development of Silver Nanoparticles in AIPU Nanoreactors

After establishing the ability of the AIPUs to solubilize insoluble molecules in the micellar interior, experiments on the development of silver nanoparticles in the AIPU nanoreactors in a nonpolar solvent have been carried out. Silver nanoparticles have been formed by adding $[\text{Ag}(\text{NH}_3)_2]\text{OH}$ precursor to a concentrated AIPU solution in benzene (at polymer concentration of 20 and 30% w/w). Dispersed in benzene, an aqueous solution of a silver precursor is transferred through the solvent into the AIPU micellar assemblies by a liquid–liquid

phase transfer. The precursor is trapped in the hydrophilic PEG domains and is directly reduced therein. The scheme of the AIPU-assisted development of silver nanoparticles is shown in Figure 5.3.

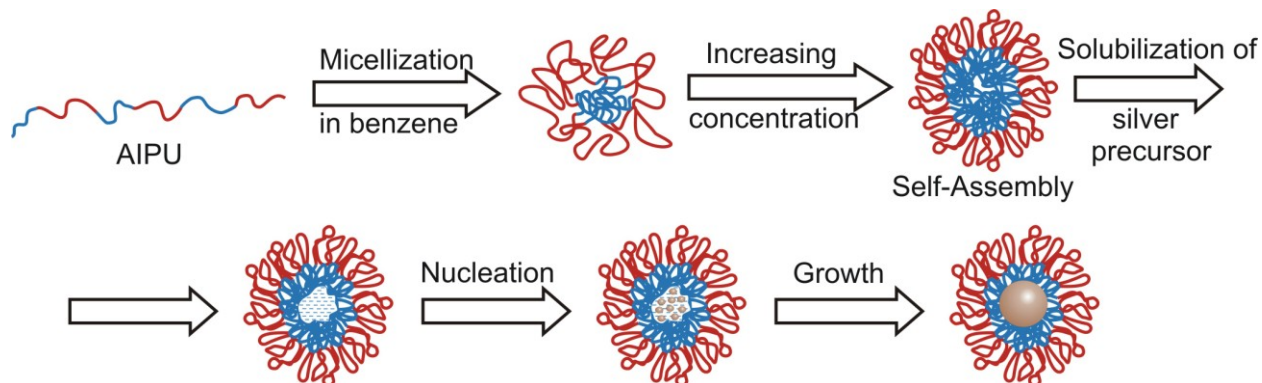


Figure 5.3. Development of silver nanoparticles in the AIPU nanoreactors.

The formation of silver nanoparticles has been monitored by UV-vis spectroscopy and further confirmed in X-ray diffraction study. UV-Vis spectra have been recorded on the reactive mixtures after diluting them with acetone (Figure 5.4). Distinct absorption bands with the maximum at ca. 420 nm corresponding to surface plasmon resonance of silver nanoparticles have been observed in the UV-vis spectra for all PEG-1000 based amphiphilic invertible polyurethanes, as well as for PEG₆₀₀-*co*-PTHF₆₅₀. Reactive mixtures have been further analyzed using XRD. A pattern recorded on the dried silver-PEG₁₀₀₀-*alt*-PTHF₆₅₀ nanocomposite is shown in Figure 5.5. The diffraction maxima at $2\lambda = 38.2, 44.3, 64.5,$ and 77.5° correspond to the (111), (200), (220), and (311) planes of the face-centered cubic (fcc) silver, respectively,^{32,33} and confirm the presence of Ag in the nanoparticles.

As Figure 5.4 shows, the maximum surface plasmon resonance bands have been observed for the silver nanoparticles synthesized using AIPUs based on PEG-1000. The reduction of the [Ag(NH₃)₂]OH precursor and formation of nanoparticles are concluded to be facilitated by an

increasing length of the hydrophilic PEG constituents at the fixed concentration of the precursor and the polymer. PEG chains form cavities or pseudo-crown ether structures capable of binding metal ions, subsequently reducing them to metal nanoparticles.⁶ The higher efficiency of PEG-1000-based AIPUs is most likely because of their higher loading capacity and metal ion reducing activity caused by longer poly(ethylene glycol) fragments. The similar behavior has

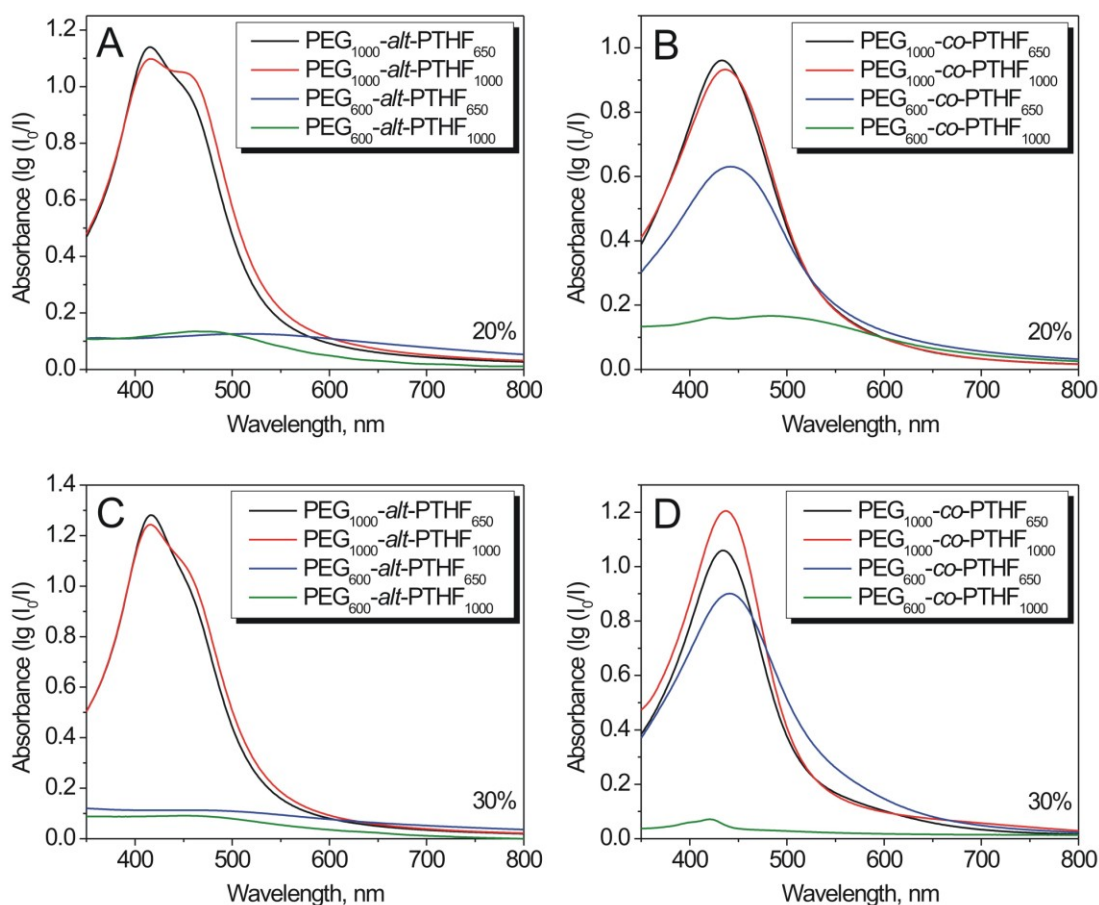


Figure 5.4. UV-Vis spectra of silver nanoparticles synthesized in 20% w/w benzene solutions of (A) alternating and (B) random AIPUs and 30% w/w benzene solutions of (C) alternating and (D) random AIPUs. All samples were dispersed in acetone after the synthesis (reactive mixture : acetone ratio as 1 : 100).

been previously reported for amphiphilic invertible polyesters where the reduction of $[\text{Ag}(\text{NH}_3)_2]^+$ ions and formation of silver nanoparticles has been enhanced by increasing length of the hydrophilic poly(ethylene glycol) moieties.⁶ In the case of AIPUs this tendency is even more pronounced, as no formation of silver nanoparticles has been observed in benzene solutions of the most hydrophobic polymer samples based on PEG-600 and PTHF-1000 (i.e. $\text{PEG}_{600}\text{-alt-PTHF}_{1000}$ and $\text{PEG}_{600}\text{-co-PTHF}_{1000}$).

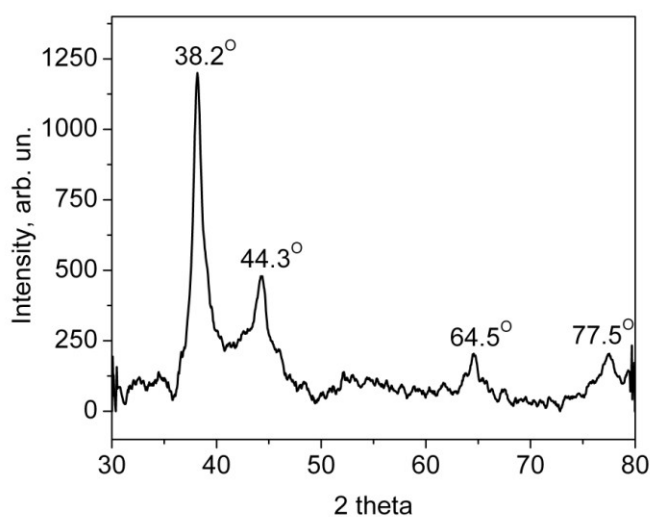


Figure 5.5. X-ray diffraction pattern of silver nanoparticles synthesized in 30% w/w benzene solution of $\text{PEG}_{1000}\text{-alt-PTHF}_{650}$.

A drastic difference in the efficiency of silver reduction was observed for nanoreactors composed of shorter PEG fragments, $\text{PEG}_{600}\text{-alt-PTHF}_{650}$ and $\text{PEG}_{600}\text{-co-PTHF}_{650}$ (Figure 5.4), i.e. polymers having the same composition but differing in configuration. The precursor undergoes the reduction in the random macromolecules, while no silver nanoparticles are formed in the alternating ones. It is the presence of macromolecular sequences composed of several PEG units linked with 2,4-TDI moieties in the macromolecules of a random AIPU that could be the

key reason for this behavior. It increases an effective length of the hydrophilic fragments in the macromolecules and makes the reduction possible (Figure 5.6).

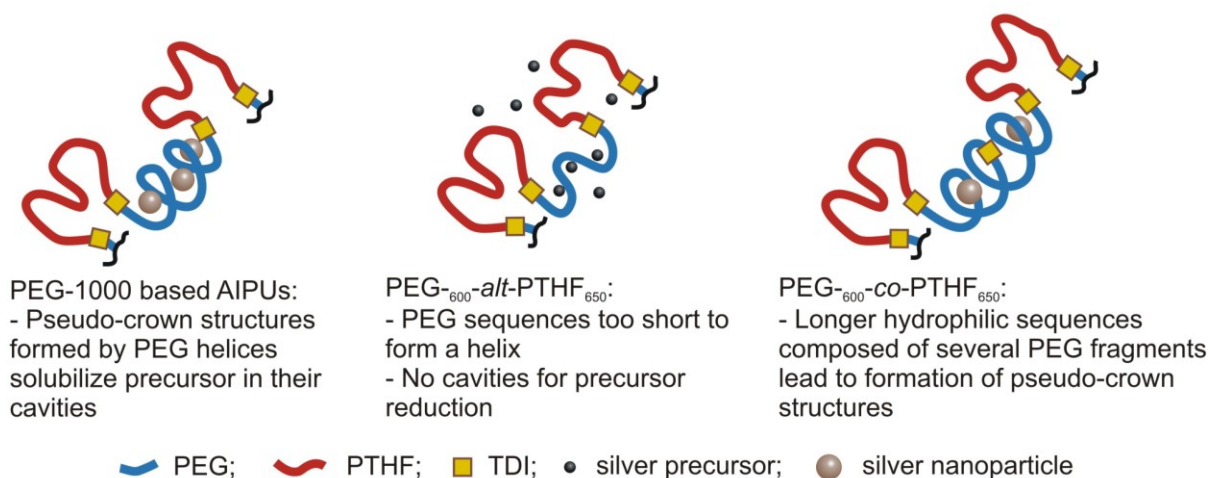


Figure 5.6. Dependence of precursor solubilization on the AIPU hydrophilic fragment length.

Interestingly, the absorption maxima of the silver nanoparticles synthesized in random AIPUs (Figures 5.4B and 5.4D) are red-shifted compared with the alternating AIPUs (Figures 5.4A and 5.4C). A reason for the red shift of the surface plasmon resonance peaks of silver nanoparticles is the presence of silver oxide,³⁴ an intermediate product formed in the reduction reaction of an $[\text{Ag}(\text{NH}_3)_2]^+$ complex to Ag^0 by PEG fragments.³⁵ Indeed, a diffraction maximum at $2\lambda = 32.5^\circ$ and a shoulder peak at 37.8° corresponding to (111) and (200) planes of the cubic crystal structure of silver oxide, respectively, have been found in the XRD patterns in case of the random AIPUs (Figure 5.7), revealing the presence of silver oxide along with metallic silver. In contrast to the random amphiphilic invertible polyurethanes, no silver oxide signals have been detected in XRD patterns of silver nanoparticles developed in the alternating AIPUs, which suggests that complete conversion of Ag_2O to Ag^0 is achieved in the latter case.

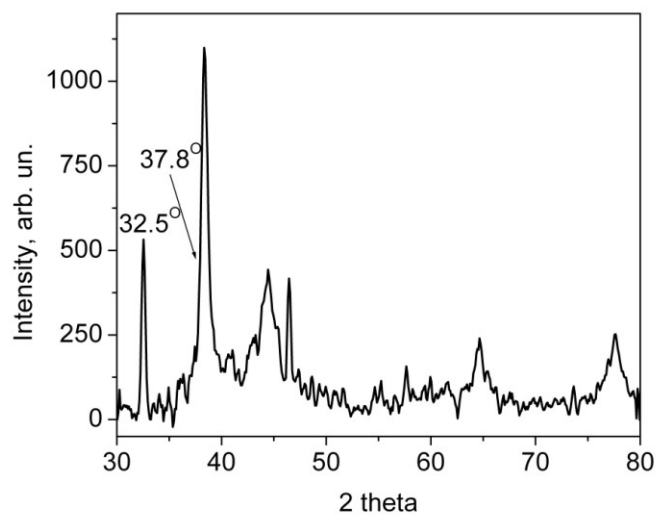


Figure 5.7. X-ray diffraction pattern of silver nanoparticles synthesized in 30% benzene solution of PEG₁₀₀₀-*co*-PTHF₆₅₀ revealing the presence of the silver oxide.

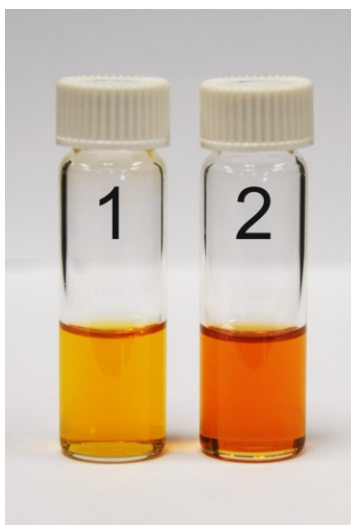


Figure 5.8. Photograph of silver nanoparticles developed in nanoreactors made from PEG₁₀₀₀-*co*-PTHF₁₀₀₀ dispersed in (1) acetone (a polar solvent) and (2) benzene (a nonpolar solvent).

As expected, due to the presence of hydrophilic and hydrophobic fragments in AIPU macromolecules, the synthesized silver nanoparticles were found to be dispersible in polar and

nonpolar media. They formed stable colloidal solutions in acetone and benzene upon diluting the concentrated reactive mixture (Figure 5.8). Colloidal solutions of nanosilver remained stable in acetone and benzene for a few weeks.

Particle size distribution of the synthesized silver nanoparticles dispersed in acetone has been determined by dynamic light scattering measurements. The data provided for silver nanoparticles developed in 20% w/w (Figure 5.9A) and 30% w/w (Figure 5.9B) AIPU solutions in benzene indicate that nanoparticles with a narrow size distribution have been successfully developed. Colloidal silver with an average particle size between 6 and 14 nm has been synthesized using polymeric nanoreactors based on micellar assemblies made from AIPUs of various macromolecular configuration and concentration (Table 5.1). The calculated polydispersity indices (PDI) for the synthesized silver nanoparticles are generally lower for nanosilver synthesized in nanoreactors based on PEG-*co*-PTHF polyurethanes.

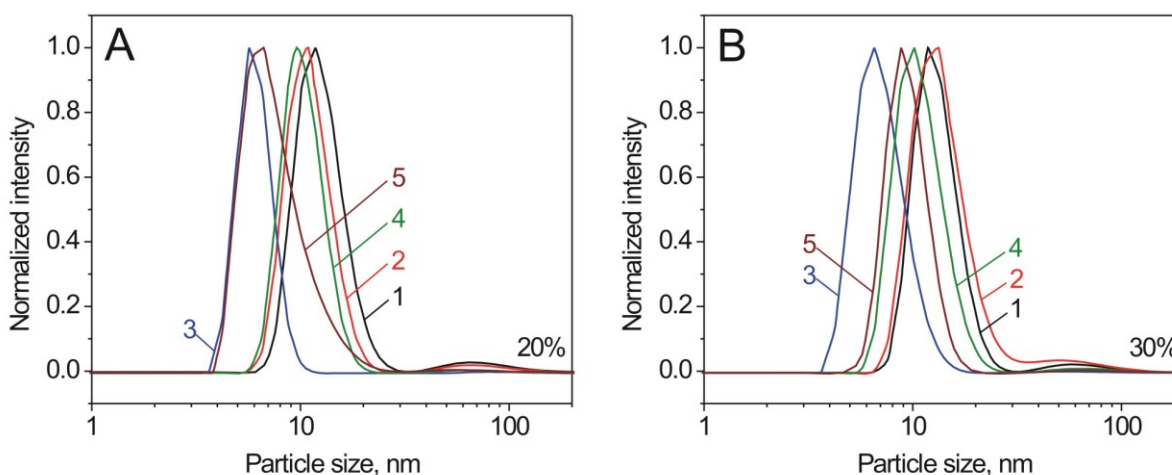


Figure 5.9. Size distribution of silver nanoparticles prepared in (A) 20% and (B) 30% AIPU solutions: (1) PEG₁₀₀₀-*alt*-PTHF₆₅₀, (2) PEG₁₀₀₀-*alt*-PTHF₁₀₀₀, (3) PEG₁₀₀₀-*co*-PTHF₆₅₀, (4) PEG₁₀₀₀-*co*-PTHF₁₀₀₀, (5) PEG₆₀₀-*co*-PTHF₆₅₀.

Table 5.1. Particle Size and Polydispersity Indices of Silver Nanoparticles Developed in 20% and 30% AIPU Solutions

Polymer	20%		30%	
	Mean particle size, nm	PDI	Mean particle size, nm	PDI
PEG ₁₀₀₀ - <i>alt</i> -PTHF ₆₅₀	12 ± 1	0.34	13 ± 1	0.31
PEG ₁₀₀₀ - <i>alt</i> -PTHF ₁₀₀₀	11 ± 2	0.31	14 ± 2	0.46
PEG ₁₀₀₀ - <i>co</i> -PTHF ₆₅₀	6 ± 1	0.11	7 ± 1	0.23
PEG ₁₀₀₀ - <i>co</i> -PTHF ₁₀₀₀	10 ± 1	0.25	11 ± 1	0.33
PEG ₆₀₀ - <i>co</i> -PTHF ₆₅₀	8 ± 1	0.31	9 ± 1	0.21

A representative TEM micrograph of synthesized nanosilver is shown in Figure 5.10. It confirms the formation of spherical silver nanoparticles in PEG₁₀₀₀-*co*-PTHF₆₅₀ micellar assemblies (plot 3 in Figure 5.9B). The average nanoparticle diameter (about 7 nm) corresponds to the data recorded in DLS measurements.

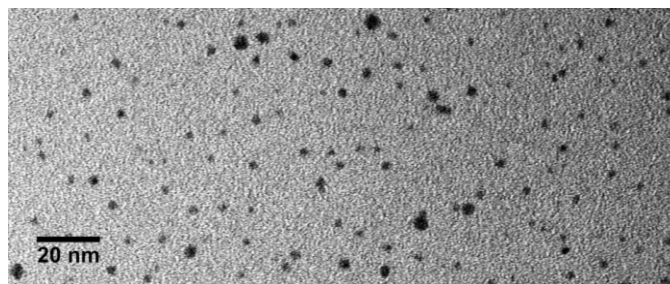


Figure 5.10. TEM micrograph of silver nanoparticles developed in nanoreactors prepared from 30% solution of PEG₁₀₀₀-*co*-PTHF₆₅₀.

According to Figure 5.9, the average size of silver nanoparticles is systematically smaller if the nanoreactors from more hydrophilic AIPUs based on PTHF-650 are used, compared with the more hydrophobic ones based on PTHF-1000. It is evident that the weight fraction of PEG

fragments in AIPU macromolecules is higher for PEG₁₀₀₀-PTHF₆₅₀ in comparison with PEG₁₀₀₀-PTHF₁₀₀₀. The higher content of PEG (i.e., CH₂CH₂O ethylene oxide units) in the AIPU macromolecules is assumed to provide more reaction sites for the precursor reduction in the PEG₁₀₀₀-PTHF₆₅₀, which obviously results in the formation of smaller silver nanoparticles.

Larger nanoparticles with a higher PDI value were synthesized in nanoreactors from alternating AIPU macromolecules compared with the random amphiphilic invertible polyurethanes. Due to the alternating distribution of hydrophilic and hydrophobic fragments, PEG-*alt*-PTHF compositions are assumed to form micellar assemblies with more distinct domains of hydrophilic and hydrophobic fragments. This implies that the hydrophilic domains in alternating amphiphilic invertible polyurethanes have a higher loading capacity of the silver precursor compared with random AIPUs, and therefore, larger particles are formed.

Raising the polymer concentration from 20% w/w to 30% w/w results in a slight increase in diameter of the synthesized nanoparticles and does not significantly impact the PDI value. Comparison of the corresponding UV-vis spectra (Figure 5.4) reveals that the absorption maxima, and thus the content of silver nanoparticles increases with an increasing polymer concentration. Based on the solubilization data, the amount of the silver precursor accommodated in micellar assemblies is believed to increase with an increasing polymer concentration. Therefore, both of the aforementioned trends can be explained by the increased loading capacity in 30% w/w polymer solutions compared with 20% w/w solutions.

Thus, the self-assembled micellar assemblies from amphiphilic invertible polyurethanes serve simultaneously as nanoreactors and stabilizers in the synthesis of silver nanoparticles in a nonpolar media. The size of the synthesized nanosilver appears to be varied between 6 and 14 nm and depends on the polymer composition, chain configuration, and concentration. The latter

observation distinguishes the amphiphilic invertible polyurethanes from the amphiphilic invertible polyesters, where the reaction leads to almost exclusively ca. 10 nm-sized nanosilver.^{6,24} The use of PTHF as a hydrophobic fragment in amphiphilic invertible polymers is beneficial in terms of varying of AIPU HLB, and thus, the size of the resultant nanoparticles.

5.4.3. Development of Semiconductor Nanoparticles Using AIPU-Stabilized Nanosilver Seeds

One of the possible applications of nanosilver in nanotechnological applications is their use as nucleation centers (seeds) in nanoparticle synthesis.^{36,37} In this study, silver nanoparticles have been used to develop semiconductor crystals. Semiconductor nanoparticles have attracted much attention due to their distinctive electronic and optical properties that arise from quantum size effects that are useful for a wide range of applications. They have shown potential as active components in chemical sensors,³⁸ biological labels,³⁹⁻⁴¹ solar cells,⁴² optoelectronic devices,⁴³ in nanoelectronics⁴⁴⁻⁴⁶ and functional nanocomposites.⁴⁷ Optoelectronic and physical properties of semiconductor nanoparticles are known to be strongly influenced by their size and shape.^{48,49} In recent years, significant effort has been put into development and application of monodisperse spherical semiconductor nanocrystals or quantum dots. One-dimensional quantum nanorods or nanowires, however, are known to have several advantages over the zero-dimensional quantum dots and can offer new possibilities for tuning semiconductor properties.⁵⁰ Thus, magnetic quantum wires have been demonstrated to have higher blocking temperatures and magnetization than quantum dots. Moreover, CdSe quantum rods have been shown to polarize light linearly along the crystallite c-axis, the degree of polarization being dependent on the nanorod aspect ratio.⁵¹ These unique properties render one-dimensional semiconductor nanocrystals useful for improving performance of memory and optoelectronic devices.³⁷

To develop nonspherical CdSe nanoparticles, a variation of a solution-liquid-solid method using metallic nanoparticles as seeds to promote anisotropic crystal growth has been used.^{37,52} According to this technique, the reaction mixture is heated to the temperature at which metal nanoparticles form a quasi-molten surface layer. Thus, metal liquefied surface serves as a sink for the reagent molecules and semiconductor crystal grows from the nanoparticle surface (Figure 5.11). This method is known to provide a lower energy path to nucleation than homogeneous nucleation in the vapor or solution phase.³⁷

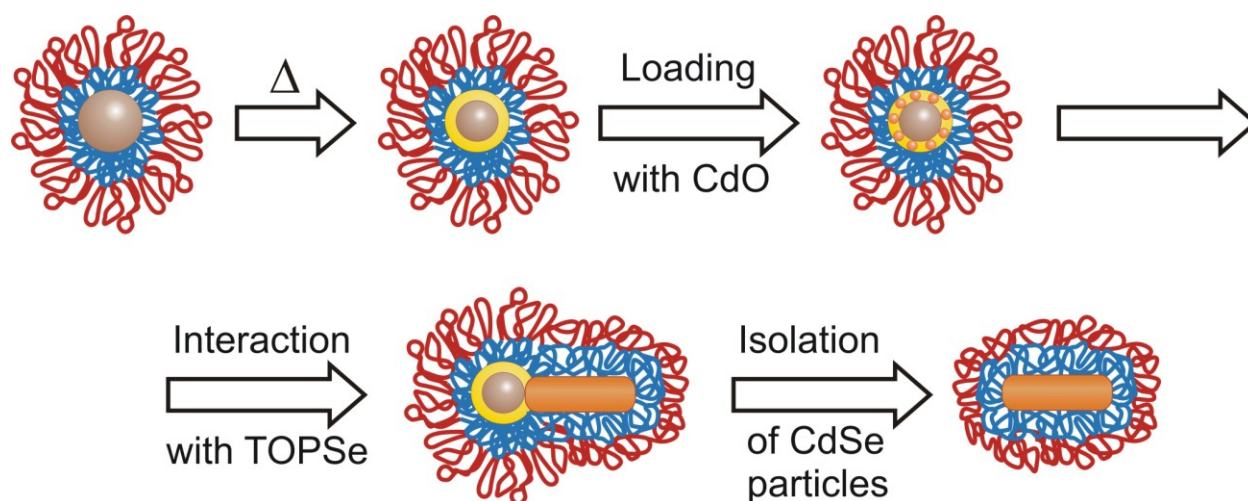


Figure 5.11. Development of cadmium selenide nanoparticles using silver nanoparticle seeds stabilized by AIPUs.

The reaction mixture consists of three major component types: precursor reagents, metal nanoparticle seeds, and a polymeric stabilizer dispersed in a high-boiling nonpolar solvent, diphenyl ether. Cadmium selenide is synthesized during interaction between the two precursors: cadmium oxide and trioctylphosphine selenide (TOPSe), while nanosilver developed in 30% solution of the AIPU PEG₁₀₀₀-*co*-PTHF₆₅₀ serves as the seeds for growing cadmium selenide particles. Before the reaction, a dispersion of cadmium oxide precursor and silver nanoparticle seeds stabilized by the AIPU is heated to 220 °C, a temperature which is lower than the melting

temperature of silver nanoparticles, but at which a quasi-molten surface layer is formed on the nanoparticle surface. The reaction is started by injecting TOPSe, a second precursor, into the dispersion. During the reaction, silver nanoparticles are used as seeding agents to aid anisotropic growth of semiconductor nanoparticles. The reaction starts in the quasi-molten surface layer of nanosilver and CdSe crystal growth occurs from the silver surface (Figure 5.11). During the process, AIPU macromolecules provide stabilization for both silver nanoparticle seeds and cadmium selenide crystals. After the reaction, cadmium selenide nanocrystals have been separated from the reactive mixture, including the nanosilver seeds, by hexane extraction.

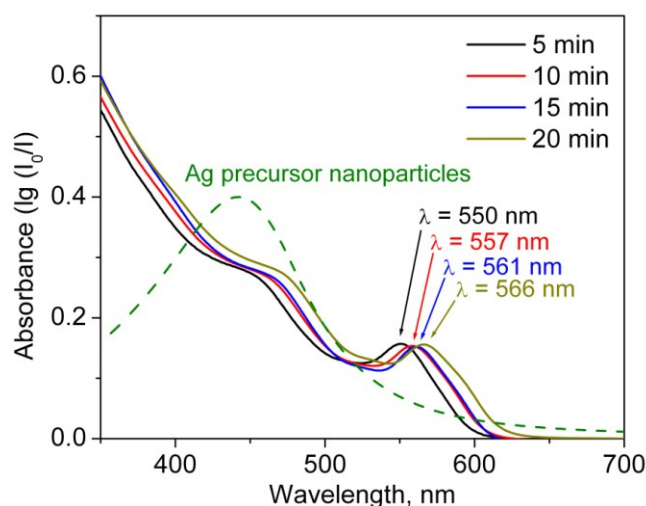


Figure 5.12. UV-Vis spectra of CdSe nanoparticles recovered at different reaction times.

UV-Vis spectra of the nanoparticles recovered from the reactive mixture at different reaction times are given in Figure 5.12. The presence of the adsorption peak at 550-570 nm clearly confirms the presence of cadmium selenide nanoparticles in the mixture. As the reaction time increases from 5 to 20 min, the adsorption peak of CdSe nanoparticles experiences a red shift from 550 to 566 nm. The adsorption maximum of CdSe particles is known to be strongly

dependent on the particle size – increasing size causes a red shift of the peak maximum.

Therefore, UV-vis data show a steady growth of the nanoparticle dimensions with reaction time.

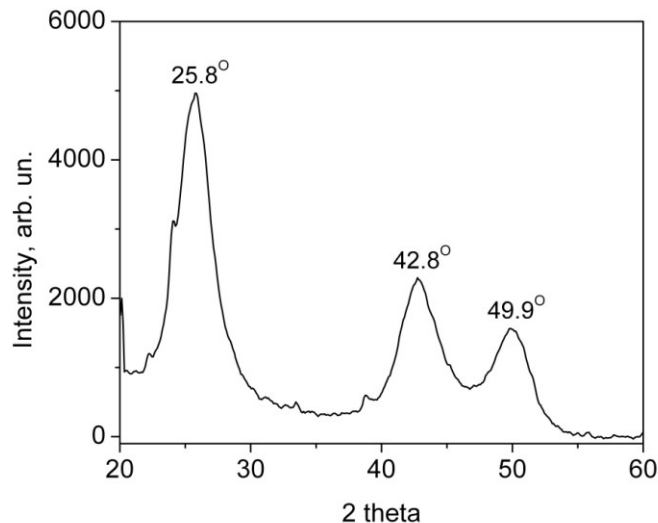


Figure 5.13. A representative X-ray diffraction pattern of cadmium selenide nanoparticles synthesized using nanosilver seeds.

The phase composition of the developed nanoparticles has been studied by X-ray diffraction. A pattern recorded on the CdSe powder is shown in Figure 5.13. Cadmium selenide is found in three crystal forms: hexagonal wurzite, as well as cubic sphalerite and rock-salt structures. Among the three, wurzite structure, being anisotropic by nature, is most likely to give nonspherical particles as a result of anisotropic crystal growth. However, the diffraction maxima at $2\lambda = 26.2, 42.3, \text{ and } 49.5^\circ$ found in the XRD pattern correspond to the (111), (220) and (311) planes of the cubic cadmium selenide, respectively.⁵³ No peaks due to the silver nanoparticle seeds are present in the pattern, since a negligible amount of silver remains in the semiconductor nanoparticles after purification. This is obviously due to the detachment of the silver nanoparticles from CdSe after the reaction is complete.

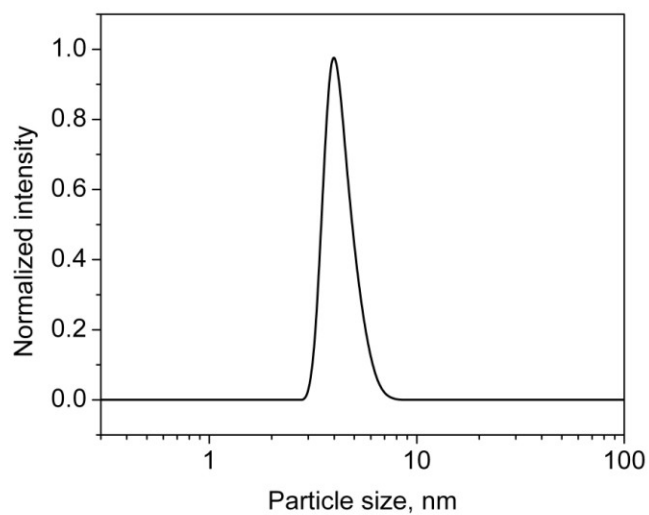


Figure 5.14. Size distribution of cadmium selenide nanoparticles developed using nanosilver seeds.

Particle size distribution of produced CdSe nanoparticles dispersed in hexane measured by DLS is given in Figure 5.14. The presented data indicate that nanoparticles with an average particle size of 4.2 ± 0.6 nm and a narrow size distribution have been successfully synthesized.

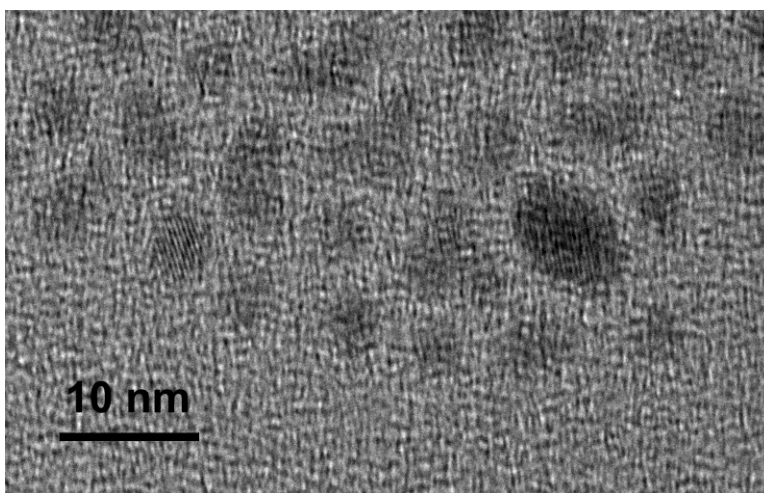


Figure 5.15. TEM micrograph of cadmium selenide nanoparticles.

A representative TEM micrograph of cadmium selenide is shown in Figure 5.15. It confirms the presence of nanoparticles with the average size of ca. 5 nm which is in a good correlation with the DLS data. A mixture of both spherical and elongated ellipsoid structures is seen in the micrograph indicating that despite CdSe crystallization in a cubic form, the process yielded a population of nonspherical semiconductor nanoparticles.

Therefore, the possibility of fabricating nonspherical CdSe nanoparticles using nanosilver synthesized in AIPU nanoreactors has been demonstrated. Semiconductor nanocrystals developed in such a way might be useful in applications ranging from physics to medicine, for example, as biological markers or components of photodetector and photovoltaic devices.³⁷

5.5. Conclusions

A facile way to perform a size-controlled synthesis of silver nanoparticles dispersible in polar and nonpolar media using micellar assemblies from amphiphilic invertible polyurethanes based on poly(ethylene glycol) as a hydrophilic constituent and polytetrahydrofuran as a hydrophobic constituent has been demonstrated. Two different types of copolymers were used in the work for silver nanoparticle synthesis: alternating and random. The invertible polyurethanes undergo self-assembly upon increasing their concentration in solution and form micellar assemblies with hydrophilic interior and hydrophobic exterior domains. AIPU micellar assemblies were applied as both nanoreactors and stabilizers to synthesize silver nanoparticles. Depending on the length of polymer hydrophilic and hydrophobic fragments and fragment distribution along the macromolecule, the size of nanoparticles appears to be varied between 6 and 14 nm. Due to the invertible properties of polyurethanes, the synthesized silver nanoparticles can be successfully dispersed in either polar or nonpolar media, where they form stable colloidal solutions. Since the applications of nanosilver depend strongly on physical and chemical

properties strongly related to the size (surface area) of nanoparticles, different chemical and biomedical applications can benefit from the approach described in this study. The nanosilver developed in nanoreactors from the AIPU PEG₁₀₀₀-*co*-PTHF₆₅₀ has been successfully used as seeds to aid anisotropic growth of cadmium selenide semiconductor nanoparticles using the modified solution-liquid-solid method of nanoparticle synthesis. As a result, a population of monodisperse semiconductor nanoparticles with an average particle size of ca. 5 nm has been developed. Cadmium selenide nanoparticles developed in such a way have potential in a variety of applications ranging from physics to medicine.

5.6. References

1. Bajpai, S.K.; Murali Mohan, Y.; Bajpai, M.; Tankhiwale, R.; Thomas, Y. *J. Nanosci. Nanotechnol.* **2007**, *7*, 2994–3010.
2. Shon, Y.-S.; Cutler, E. *Langmuir* **2004**, *20*, 6626–6630.
3. Sun, Y.G.; Xia, Y.N. *Science* **2002**, *298*, 2176–2179.
4. Hashmi, A.S.K.; Hutchings, G.J. *Angew. Chem. Int. Ed.* **2006**, *45*, 7896–7936.
5. Sau, T.K.; Murphy, C.J. *J. Am. Chem. Soc.* **2004**, *126*, 8648–8649.
6. Voronov, S.; Kohut, A.; Vasylyev, S.; Peukert, W. *Langmuir* **2008**, *24*, 12587–12594.
7. Jin, R.; Cao, Y.; Mirkin, C.A.; Kelley, K.L.; Schatz, G.C.; Zheng, J.G. *Science* **2001**, *294*, 1901–1903.
8. Banin, U.; Millo, O. In *Nanoparticles: From Theory to Applications*; Schmid, G., Ed.; Wiley-VCH: Weinheim, 2004, pp 305–367.
9. Bradley, J.S.; Schmid, G.; Talapin, D.V.; Shevchenko, E.V.; Weller, H.; In *Nanoparticles: From Theory to Applications*; Schmid, G., Ed.; Wiley-VCH: Weinheim, 2004, pp 185–238.

10. Narayanan, R.; El-Sayed, M.A. *J. Am. Chem. Soc.* **2003**, *125*, 8340–8347.
11. Dal Lago, V.; de Oliveira, L.F.; de Almeida Goncalves, K.; Kobarg, J.; Cardoso, M.B. *J. Mater. Chem.* **2011**, *21*, 12267–12273.
12. Malynych, S.; Chumanov, G. *J. Am. Chem. Soc.* **2003**, *125*, 2896–2898.
13. Thomas, V.; Namdeo, M.; Murali Mohan, Y.; Bajpai, S.K.; Bajpai, M.J. *Macromol. Sci. Part A Pure Appl. Chem.* **2008**, *45*, 107–119.
14. Jewerajka, S.K.; Chatterjee, U.J. *Polym. Sci. Part A Polym. Chem.* **2006**, *44*, 1841–1854.
15. Yin, Y.; Xu, X.; Xia, C.; Ge, X.; Zhang, Z. *Chem. Commun.* **1998**, 941–942.
16. Chou, K.S.; Ren, C.Y. *Mater. Chem. Phys.* **2000**, *64*, 241–246.
17. Silvert, P.V.; Urbina, R.H.; Elhisissen, K.T. *J. Mater. Chem.* **1997**, *7*, 293–299.
18. Zhu, Y.; Qian, Y.; Li, X.; Zhang, M. *Chem. Commun.* **1997**, 1081–1082.
19. Bossel, C.; Dutta, J.; Houriet, R.; Hilborn, J.; Hofmann, H. *Mater. Sci. Eng. A* **1995**, *204*, 107–112.
20. Longenberger, L.; Mills, G. *J. Phys. Chem.* **1995**, *99*, 475–478.
21. Iwamoto, M.; Kuroba, K.; Zaporozhchenko, V.; Hayashi, S.; Faupel, F. *Eur. Phys. J. D* **2003**, *24*, 365–367.
22. Adams, M.D.; Wade, P.W.; Hancock, R.D. *Talanta* **1990**, *37*, 875–883.
23. Warshawsky, A.; Kalir, R.; Deshe, A.; Berkovitz, H.; Patchornik, A. *J. Am. Chem. Soc.* **1979**, *101*, 4249–4258.
24. Voronov, A.; Kohut, A.; Peukert, W. *Langmuir* **2007**, *23*, 360–363.
25. Kohut, A.; Voronov, A.; Samaryk, V.; Peukert, W. *Macromol. Rapid Commun.* **2007**, *28*, 1410–1414.
26. Ohno, I.; Haruyama, S. *Bull. Jap. Inst. Metals* **1981**, *20*, 12, 986.

27. Hiraoka, M. *Crown Compounds. Their Characteristics and Applications*; Elsevier: London, 1982; 350 p.
28. Berlin, A.A.; Kislenco, V.N. *Prog. Polym.Sci.* **1992**, *17*, 765–825.
29. Kellermann, M.; Bauer, W.; Hirsch, A.; Schade, B.; Ludwig, K.; Böttcher, C. *Angew. Chem. Int. Ed.* **2004**, *43*, 2959–2962.
30. Jeong, B.; Bae, Y.H.; Lee, D.S.; Kim, S.W. *Nature* **1998**, *388*, 860–862.
31. Aliabadi, H.M.; Lavasanifar, A. *Expert Opin. Drug Delivery* **2006**, *3*, 139–162.
32. Bajpai, S.K.; Johnson, S. *React. Funct. Polym.* **2005**, *62*, 271–283.
33. Thomas, V.; Murali Mohan, Y.; Sreedharm, B.; Bajpai, S.K. *J. Colloid Interface Sci.* **2007**, *315*, 389–395.
34. Krylova, G.; Eremenko, A.; Smirnova, N.; Eustis, S. *Int. J. Photoenergy* **2005**, *7*, 193–198.
35. Zhang, L.; Yu, J.C.; Yip, H.Y.; Li, Q.; Kwong, K.W.; Xu, A.-W.; Wong, P.K. *Langmuir* **2003**, *19*, 10372–10380.
36. Xu, Z.-C.; Shen, C.-M.; Xiao, C.-W.; Yang, T.-Z.; Zhang, H.-R.; Li, J.-Q.; Li, H.-L.; Gao, H.-J. *Nanotechnol.* **2007**, *18*, 115608/1–115608/5.
37. Yong, K.-T.; Sahoo, Y.; Swihart, M.; Prasad, P. U.S. Patent 20070186846, August 16, 2007.
38. Kong, J.; Franklin, N.R.; Zhou, C.; Chapline, M.G.; Peng, S.; Cho, K.; Dai, H. *Science* **2000**, *287*, 622–625.
39. Bruchez, M., Jr.; Moronne, M.; Gin, P.; Weiss, S.; Alivisatos, A.P. *Science* **1998**, *281*, 2013.

40. Mattoussi, H.; Mauro, J.M.; Goldman, E.R.; Anderson, G.P.; Sundar, V.C.; Mikulec, F. V.; Bawendi, M.G. *J. Am. Chem. Soc.* **2000**, *122*, 12142–12150.
41. Chan, W.C.; Nie, S.M. *Science* **1998**, *281*, 2016–2018.
42. Yu, P.; Zhu, K.; Norman, A.G.; Ferrere, S.; Frank, A.J.; Nozik, A.J. *J. Phys. Chem. B* **2006**, *110*, 25451–25454.
43. Bhattacharya, P.; Ghosh, S.; Stiff-Roberts, A.D. *Annu. Rev. Mater. Res.* **2004**, *34*, 1–40.
44. Banin, U.; Cao, Y.; Katz, D.; Millo, O. *Nature* **1999**, *400*, 542–544.
45. Gudixsen, M.S.; Lauhon, L.J.; Wang, J.; Smith, D.C.; Lieber, C.M. *Nature* **2002**, *415*, 617–620.
46. Duan, X.; Huang, Y.; Cui, Y.; Wang, J.; Lieber, C.M. *Nature* **2001**, *409*, 66–69.
47. Morris, C.A.; Anderson, M.L.; Stroud, R.M.; Merzbacher, C.I.; Rolison, D.R. *Science* **1999**, *284*, 622–624.
48. Lieber, C.M. *Solid State Commun.* **1998**, *107*, 607–616.
49. Smalley, R.E.; Yakobson, B.I. *Solid State Commun.* **1998**, *107*, 597–606.
50. Huynh, W.U.; Dittmer, J.J.; Alivisatos, A.P. *Science* **2002**, *295*, 2425–2427.
51. Peng, X.; Manna, L.; Yang, W.; Wickham, J.; Scher, E.; Kadavanich, A.; Alivisatos, A.P. *Nature* **2000**, *404*, 59–61.
52. Kan, S.; Mokari, T.; Rothenberg, E.; Banin, U. *Nat. Mater.* **2003**, *2*, 155–158.
53. Girija, K.; Thirumalairajan, S.; Mohan, S.M.; Chandrasekaran, J. *Chalcogenide Lett.* **2009**, *8*, 351–357.

**CHAPTER 6. FUNCTIONAL SELF-ASSEMBLY OF AMPHIPHILIC INVERTIBLE
POLYMERS ON THE SURFACES AND AT THE INTERFACES:
ADSOLUBILIZATION AND DEVELOPMENT OF SILICON NANOWIRES**

6.1. Abstract

Amphiphilic invertible polyesters based on poly(ethylene glycol) and aliphatic dicarboxylic acids (AIPes-1) have been successfully adsorbed on the surface of both hydrophilic and hydrophobized silica nanoparticles and adsolubilized sparingly water-soluble 2-naphthol in the adsorbed polymer layer. While AIPe adsorption on the hydrophilic silica is mainly governed by to the interaction between the hydrophilic polyester PEG fragments and the polar substrate, adsorption of the amphiphilic invertible polyesters on the hydrophobized silica occurs due to the hydrophobic interactions between the hydrophobized surface and the AIPe $-(CH_2)_n-$ chains. The amount of adsolubilized 2-naphthol does not depend on the nature of the substrate silica and the length of the AIPe hydrophobic constituent and increases with increasing amount of the adsorbed AIPes.

Amphiphilic invertible polyester S6 has been used as a functional additive in fabrication of the electrospun silicon wires on the basis of cyclohexasilane (CHS), a liquid silicon precursor. The use of the AIPe in the electrospinning ink formulation has allowed to significantly improve wire appearance by drastically reducing the number of globules formed during electrospinning. Electrospinning AIPe-containing formulation with subsequent UV-induced conversion of CHS into polydihydrosilane has resulted in development of the “strawberry-like” wire morphology, that has not been detected during electrospinning non-AIPe containing inks. The appearance of the “strawberry-like” morphology has been attributed to microphase separation of the AIPe layer on the air/wire interface. AIPe-assisted fabrication of silicon wires from the liquid

cyclohexasilane precursor could find application as a method for developing electronic functional materials.

6.2. Introduction

Since material performance in a specific environment is often determined not only by its bulk characteristics, but also by the surface properties,¹ modification of material surface with amphiphilic polymer molecules is known to be a promising way to tailor the material properties for specific applications.²⁻⁴ During interaction of amphiphilic polymer solutions with solid surfaces, polymer adsorbed layers are formed at the solid-liquid interface. The adsorption of polymeric surfactants at the solid-liquid interface is useful in numerous applications such as in detergency, wetting and mineral flotation, as well as in the newer fields of templated surfaces and nanotechnology.⁵⁻⁸

Being adsorbed at the solid-liquid interface, amphiphilic polymer layers are able to solubilize sparingly soluble organic molecules (solutes), even if the solutes themselves hardly adsorb at the interface, a process called adsolubilization.⁹ For example, when a polymer layer is adsorbed at the solid-aqueous solution interface, the interior of the adsorbed polymer aggregates (also called admicelles) provides hydrophobic regions in which poorly water-soluble substances may be sequestered. The adsolubilization phenomenon has opened up a variety of applications in separation, reaction processes, surface engineering and nanotechnology.¹⁰⁻¹³ Thus, this process is used in the development of different industrial products such as pharmaceuticals,¹⁴ paints,¹⁵ surface coatings,¹⁶ cosmetics and health care products,¹⁷ etc.

The presence of both hydrophilic and hydrophobic fragments in amphiphilic invertible polymers is assumed to allow polymer interaction with surfaces greatly differing by polarity. Hence, AIPE-modified silica nanoparticles have been prepared by adsorption of the two

amphiphilic invertible polyesters, D10 and S10, on the surface of both hydrophilic and hydrophobized silica nanoparticles. The modified silica nanoparticles could be potentially used as hybrid adsorbents for water purification, biomedical and agricultural applications, drug delivery, etc. To demonstrate the ability of AIPE layers adsorbed on the nanoparticulate substrate to adsolubilize poorly water-soluble compounds, adsolubilization of 2-naphthol has been carried out by both AIPES and the relationship between the polymer composition and adsorption/adsolubilization behavior has been studied. Due to the high hydrophilicity of the amphiphilic invertible polyesters used in the study (HLB values are 14.4 and 15.4 for D10 and S10, respectively), AIPE-modified silica nanoparticles are likely to demonstrate enhanced performance in the applications related to the aqueous medium, for example they can be utilized as the basis for development of enterosorbents (amphiphilic adsorbents) for selective removal of toxins such as bilirubin.¹⁸

Having hydrophilic and hydrophobic fragments distributed along the main backbone, amphiphilic invertible polymer macromolecules also have a potential as functional additives that improve dispersion and adhesion of two poorly miscible materials in a blend. In general, the use of amphiphilic polymers as functional additives to improve the miscibility of the blend is an effective and commonly used method.^{19,20} Thus, amphiphilic invertible polyester S6 has been used as a functional additive to improve the properties of the electrospun wires from poly(methyl methacrylate) (PMMA) and cyclohexasilane, a novel liquid silicon precursor. The developed wires could find their application in a variety of electronic and nanoelectronic devices, such as in the development of next-generation batteries, nanosensors, light-emitting diodes, solar batteries, etc.²¹⁻²⁶

6.3. Experimental

6.3.1. Materials

Toluene and dichloromethane, ACS grade, were purchased from VWR International. Tannic acid, 2-naphthol, and poly(methyl methacrylate) (M_w 350,000 g/mol) were purchased from Sigma-Aldrich. Hydrophilic fumed silica AEROSIL® OX50 and hydrophobized silica AEROSIL® NAX50, treated with HMDS, were kindly supplied by Evonik Degussa Corporation. The average primary particle size and specific surface area of AEROSIL® OX50 experimentally estimated in accordance with the BET theory are 40 nm and 50 ± 15 m²/g, respectively, as reported by the supplier. The specific surface area (BET) of AEROSIL® NAX50 is 30–50 m²/g. All reagents and materials were used as received.

Amphiphilic invertible polyesters were synthesized from PEG and aliphatic dicarboxylic acids as described in Chapter 2.

Cyclohexasilane (Si₆H₁₂) was synthesized by Kenneth Anderson (NDSU Center for Nanoscale Science and Engineering) according to a known technique.²⁷ All experiments with cyclohexasilane were carried out in a dry nitrogen atmosphere using a glovebox.

6.3.2. Characterization

Raman spectra were recorded using a LabRAM ARAMIS confocal Raman microscope (Jobin Yvon Horiba). Phase analysis was performed by analyzing transverse orthogonal (TO) mode.

The morphology of silicon containing wires was studied by scanning electron microscopy (SEM) using a JEOL JSM-6490LV microscope.

6.3.3. Adsorption Study

6.3.3.1. AIPE Adsorption on Silica

Silica particles (0.1 g) were shaken with 10 mL of polyester solutions of various concentrations for 24 h to achieve adsorption equilibrium. The silica particles were separated by centrifugation (60 min, 9000 rpm). The polyester concentration in the supernatant was measured using the tannic acid method, and the adsorbed amount of the polyester was calculated from the difference in the concentration before and after adsorption.

6.3.3.2. Measurements of AIPE Concentration in Supernatant (Tannic Method)

This method is based on a principle that turbidity caused by complexation between tannic acid and PEG chains of the polyesters S10 and D10 becomes proportional to the concentration of a particular polyester.²⁸ A linear calibration equation of the absorbency of the polyester and tannic acid complex as a function of the polyester concentration was obtained first in the following manner: 3 mL of the polyester solution of different concentrations was added into a 7 mL glass vial containing 1 mL of water. A 0.5 mL volume of 1 M NaCl solution was added, and the vial was shaken up and down 20 times. A 0.5 mL volume of 2 g/L tannic acid was added to give a total volume of 5.0 mL. The vial was shaken for 10 sec, and the absorbency of the polyester and tannic acid complex was measured immediately with a Varian Cary 5000 UV-Vis-NIR spectrophotometer at a wavelength of 600 nm. The amount of free polyester in the supernatant was measured by the absorbance of the polyester and tannic acid complex.

6.3.4. Adsolubilization Study

After equilibration of the polyester adsorption on silica, the supernatant was replaced by 10 mL of a 0.4 mM aqueous solution of 2-naphthol, and the resulting suspension was shaken for 24 h. The silica particles were separated by centrifugation (60 min, 9000 rpm). The concentration

of 2-naphthol in the supernatant was determined by measuring the absorbance at 328 nm using a Varian Cary 5000 UV-Vis-NIR spectrophotometer. The adsolubilized amount of 2-naphthol was calculated from the difference in the concentration before and after adsolubilization.

6.3.5. Desorption Study

The desorbed amount of the polyester was calculated from the concentration of free polyester in the supernatant after the adsolubilization stage (e.g., after the supernatant replacement). The concentration of free polyester was measured in a manner similar to that mentioned above.

6.3.6. AIPE-Assisted Electrospinning of Silicon Wires

6.3.6.1. Preparation of Electrospinning Inks

The inks were prepared inside a nitrogen purged glovebox. Polyester S6 (0.150 g for ink 1 or 0.075 g for ink 2) was dissolved in the appropriate solvent (toluene or dichloromethane, 3 mL) and the formed solution was stirred for ca. 70 h. At the same time, two portions of 12.5% w/v solution of PMMA (1 g) in the same solvent (8 mL) have been prepared and stirred for ca. 70 h. A portion of CHS (750 μ L) was then added dropwise to each of the two S6 solutions while stirring and new solutions were allowed to stir for the next 16 h. Next, the two developed CHS-S6 solutions (2 mL each) were dropwise added to the two 12.5% w/v PMMA solutions and stirred for another 16 h before electrospinning.

6.3.6.2. Fabrication of Silicon Wires by Electrospinning

Electrospinning and post-treatment procedures were carried out inside a nitrogen purged glovebox. The inks were drawn up into a 1 mL HDPE syringe fitted with a blunt-nosed 21 gauge stainless steel needle 1.5 inches in length. The syringe was loaded onto an automatic syringe pump. A 2'' \times 2'' square sheet of aluminum foil was placed on a grounding pad with a standoff

distance of ca. 10 cm from the needle tip. A high voltage source (Gamma High Voltage Research Inc. model ES40P-12W/DDPM) was connected with the positive terminal on the needle and the negative (ground) on the aluminum foil. The syringe pump was set to a flow rate of 0.5 mL/h and allowed to run until the needle was primed with liquid. Once a droplet formed on the outside of the needle, the power source was adjusted to 14 kV to start electrospinning process. After electrospinning, aluminum substrate with Si containing deposits was cut into four equal pieces; each piece subject to different post-treatment processes.

Photopolymerization of CHS was carried out by irradiation the sample using a UV lamp/fiber optic for 5 min using 1.10 W output power.

Thermal treatment was carried out by heating foil substrate on a hotplate to 350 °C with a ramp rate of 250 °C/h and maintaining this temperature for additional 20 min.

6.4. Results and Discussion

6.4.1. The Use of AIPes for Modification of Silica Nanoparticles Differing by Polarity

Modification of silica nanoparticles has been carried out by adsorbing amphiphilic invertible polyesters S10 and D10 from the aqueous solution at different concentrations. Figure 6.1 shows the adsorption isotherms of S10 and D10 on hydrophilic fumed silica (AEROSIL® OX50) and hydrophobized silica nanoparticles (AEROSIL® NAX50, treated with HMDS), respectively. Silica particles have been shaken with polymer solutions of various concentrations and separated by centrifugation. The polymer concentration in the supernatant has been subsequently evaluated using the tannic acid method, and the amount of adsorbed polymer has been calculated from the difference in the concentration before and after the adsorption.

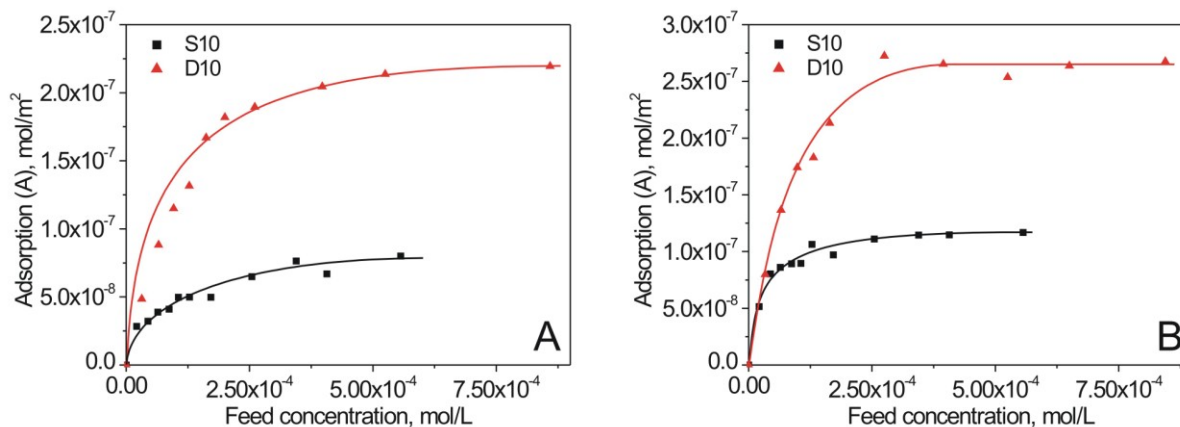


Figure 6.1. Adsorption isotherm of S10 and D10 on hydrophilic (A) and hydrophobized (B) silica nanoparticles.

The data presented in Figure 6.1 demonstrate that AIPE macromolecules readily adsorb onto the both hydrophilic and hydrophobic substrates. Noteworthy, hydrophobized silica nanoparticles cannot be dispersed in water and remains floating at the air/water interface. However, a stable aqueous dispersion of silica nanoparticles was formed within 24 h after adding them to the AIPE aqueous solution upon agitation.

For both hydrophilic and hydrophobized silica, the amount of adsorbed AIPEs increases with increasing polymer concentration and then reaches a plateau. Comparing the amount of the adsorbed polymer for each of the two AIPEs suggests that the chemical composition plays a significant role in the AIPE adsorption efficiency. The adsorption of PEG-based surfactants on the oxide surfaces is known to be governed by hydrogen bonding and hydrophobic interactions, the former force being responsible for the interaction between the polymer and the oxide surface, while the latter one is necessary for the accumulation of the adsorbed polymer layer.²⁹ Hence, the adsorbed AIPE amount is supposed to be dependent on the balance between the hydrophilic PEG

chain length and the hydrophobic alkyl chain length, i.e. on the AIPE hydrophilic-lipophilic balance.

The higher adsorption amount on hydrophilic silica has been observed for the polymer D10 with longer hydrophobic fragments (2.2×10^{-7} mol/m²), as compared to the polymer S10 with shorter hydrophobic chains (0.8×10^{-7} mol/m², Figure 6.1A). A plausible explanation is that due to the energetically less favorable contact with water, the more hydrophobic AIPE D10 adsorbs onto the polar silica surface more readily compared to the more hydrophilic S10. Interestingly, a very slight change in the hydrophobic fragment length between D10 and S10 has resulted in a significantly different AIPE adsorption amount.

A much faster rate of increase of the amount of adsorbed polymer is recorded for the hydrophobized silica nanoparticles (Figure 6.1B) which is typical for the polymers that have high affinity to the substrate surface. Unlike the adsorption on polar silica when PEG fragments are responsible for the formation of physical bonding between AIPE and the substrate, the dominant driving force for the adsorption on the hydrophobized silica is the hydrophobic interaction between the dicarboxylic acid moieties and the substrate. Therefore, the higher AIPE adsorption amount for the more hydrophobic D10 can be explained by the higher surface activity of this AIPE that results in the adsorption of more compact micellar architectures as compared to the bulkier S10 micelles.

Hence, the ability of the AIPE macromolecules to adsorb on solid substrates strongly differing in surface polarity has been demonstrated. While AIPEs adsorb on the hydrophilic silica primarily due to the interaction between the polar substrate and AIPE PEG fragments, adsorption on the hydrophobized silica is predominantly controlled by the hydrophobic interactions of aliphatic $-(\text{CH}_2)_n-$ chains of the dicarboxylic acid moieties and the surface. After

establishing the mechanisms of AIPE adsorption onto surfaces with different polarity, further experiments on adsolubilization of sparingly soluble materials into adsorbed AIPE layer have been carried out.

6.4.2. Adsolubilization of 2-Naphthol Molecules into Adsorbed AIPEs

To demonstrate the ability of AIPEs to adsolubilize hydrophobic substances while being adsorbed onto substrates differing by polarity, a series of experiments on adsolubilization of sparingly water-soluble 2-naphthol have been carried out (Figure 6.2). After AIPE adsorption on silica nanoparticles, they have been dispersed in an aqueous solution of 2-naphthol, and the resulting suspension has been shaken for 24 h. After separation of the silica particles by centrifugation, the adsolubilized amount of 2-naphthol (Figure 6.3), as well as the amount of AIPE desorbed from the silica particles (Figure 6.4) have been estimated.

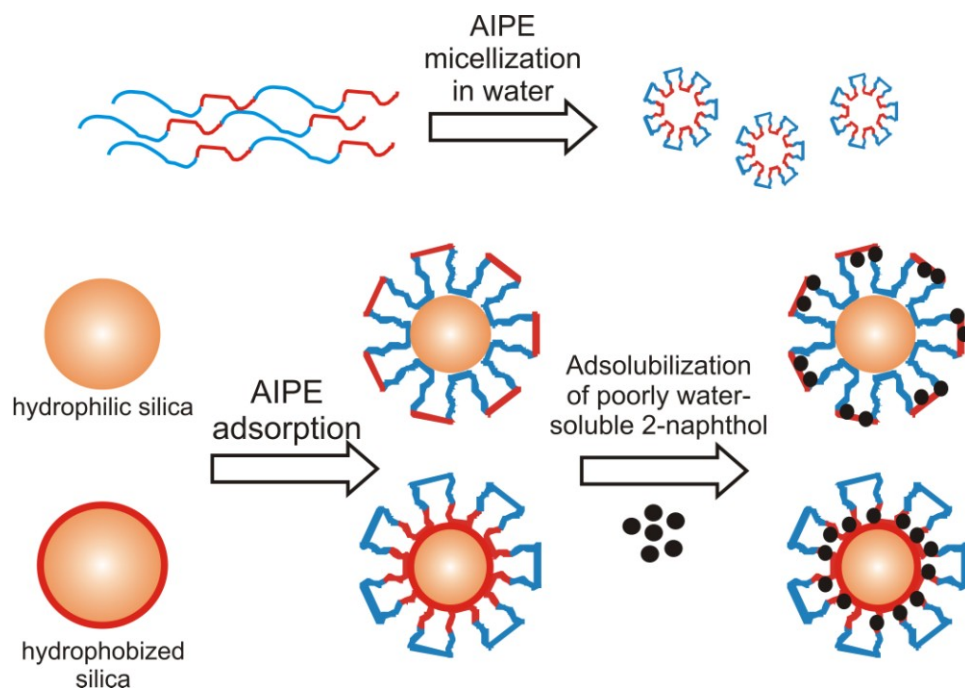


Figure 6.2. Adsolubilization of 2-naphthol by AIPE adsorbed on the surface of hydrophilic and hydrophobized silica nanoparticles.

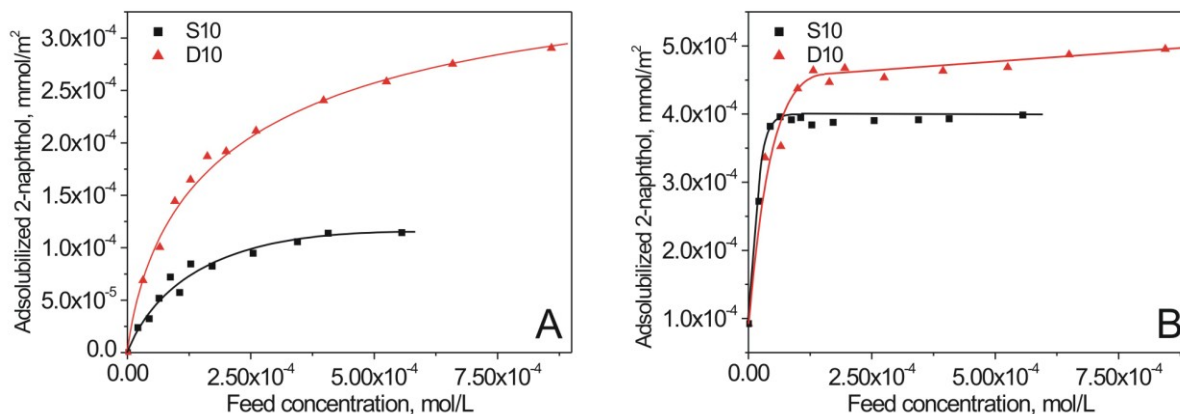


Figure 6.3. Amount of 2-naphthol adsolubilized into the adsorbed S10 and D10 layer on hydrophilic (A) and hydrophobized (B) silica.

Hydrophobic 2-naphthol does not adsorb onto hydrophilic silica nanoparticles,³⁰ while its adsorption amount on hydrophobized silica reaches 9.3×10^{-5} mmol/m². In the presence of the adsorbed AIPE, however, adsolubilization has been observed for both substrates. The amount of adsolubilized 2-naphthol increases with increasing AIPE concentration and reaches a plateau above a certain concentration value for S10 and D10 on both substrates (Figure 6.3). Similar trends have been shown for adsolubilization of 2-naphthol by Pluronic adsorbed on silica.^{9,30} For both hydrophilic and hydrophobized silica, the amount of 2-naphthol adsolubilized by the more hydrophobic polyester D10 is higher than that adsolubilized by S10. The data in Figure 6.3 demonstrate a substantial difference in adsolubilization behavior between the hydrophilic and hydrophobized silica substrate. On a polar substrate, a slow increase in adsolubilized 2-naphthol is observed with increasing feed polymer concentration for both AIPEs (Figure 6.3A). In contrast, the amount of adsolubilized 2-naphthol increases very rapidly and reaches a plateau at significantly lower polymer concentration on a hydrophobized silica (Figure 6.3B). Therefore,

for both silica substrates a good correlation between the shape of the AIPE adsorption curves and adsolubilization curves is observed.

Figure 6.4 shows data on desorption of D10 and S10 from both hydrophilic and hydrophobized silica during the adsolubilization. As expected, on a hydrophilic substrate the desorption was higher for the more hydrophilic S10 as compared to D10. On hydrophobized silica nanoparticles, the desorbed amount of the more hydrophobic polyester D10 remained almost unchanged, while desorption of S10 drastically decreased as compared to the hydrophilic silica. The results of desorption experiments provide additional evidence that the interaction of the AIPEs with hydrophilic and hydrophobic substrates during the adsorption is triggered by different fragments of the polyester macromolecule. Furthermore, the physical bonding between the polar silica and the polyester PEG fragments appears to be much weaker than the hydrophobic interactions between the AIPE nonpolar alkyl fragments and hydrophobized substrate.

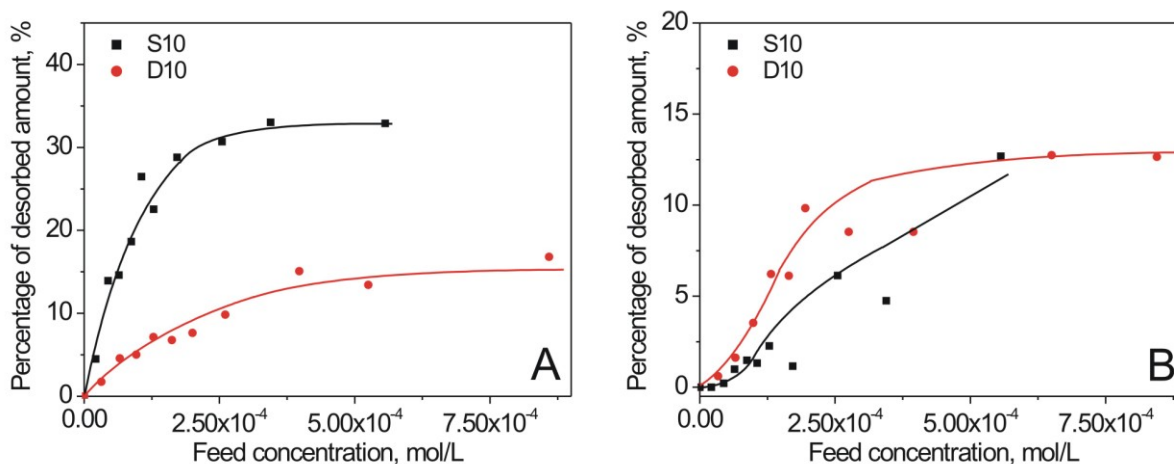


Figure 6.4. Desorption of S10 and D10 from hydrophilic (A) and hydrophobized (B) silica nanoparticles versus feed polymer concentration.

The amount of adsolubilized 2-naphthol in adsorbed polyesters plotted against the AIPE concentration for both AIPES adsorbed on both substrates is shown in Figure 6.5. Remarkably, the plots are linear for both S10 and D10, thus demonstrating that AIPE adsolubilization behavior is essentially independent on the nature of the substrate. The calculated correlation coefficients are about 0.94 for both polyesters, and the tangents of the slope angles are given as 2.42×10^3 for S10 and 1.69×10^3 for D10. The tangents indicate higher adsolubilization ability for S10, which has a longer macromolecular chain. In fact, the amount of adsolubilized 2-naphthol hydrophobic molecules by AIPES does not show any dependence on the polymer composition and depends only on the molecular weight of the amphiphilic copolymers.

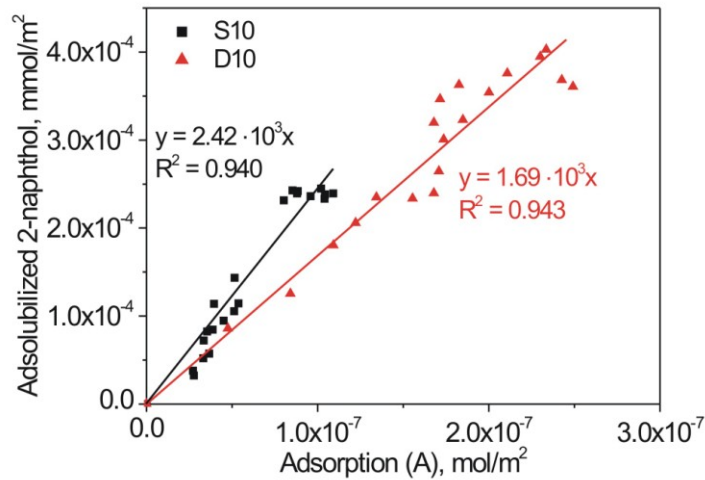


Figure 6.5. Adsolubilized amount of 2-naphthol versus AIPE adsorption.

Since both adsorption and adsolubilization stages are equilibrium processes, the data collected have been analyzed using the Langmuir equation to describe the experimental data recorded in the adsorption and adsolubilization stages, respectively:

$$\frac{c_e}{A} = \frac{k_d}{k_a} + \frac{1}{A_m c_e},$$

where A is the AIPE adsorption at the first (adsorption) stage (A_1) and at the second (adsolubilization) stage (A_2), k_a and k_d are the rate constants of polymer adsorption/desorption, A_m is the maximum polymer adsorption on the silica surface, and c_e is the equilibrium polymer concentration.

The c_e at the first stage (AIPE adsorption) can be calculated according to the following equation:

$$c_e = c_f - Ac_{s1},$$

where c_f is a feed polymer concentration, A is the AIPE adsorption at the first stage, and c_{s1} is the silica concentration in the mixture at the first stage.

The c_e at the second stage (adsolubilization of 2-naphthol) can be calculated according to the following equation:

$$c_e = (A_1 - A_2)c_{s2},$$

where c_{s2} is the silica concentration in the mixture at the second stage.

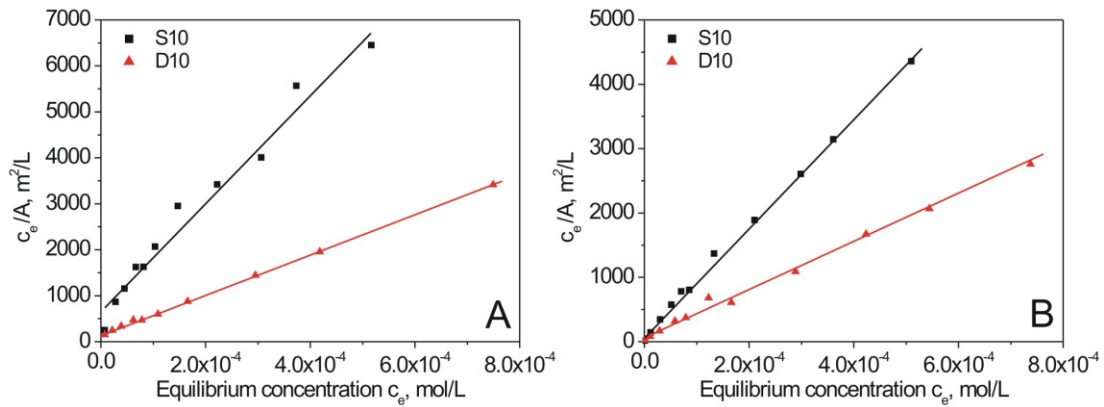


Figure 6.6. Polymer adsorption versus equilibrium polymer concentration at the first stage (adsorption of AIPEs on hydrophilic (A) and hydrophobic (B) silica substrate).

The linear Langmuir data fits for the first (polyester adsorption) and the second (2-naphthol adsolubilization) experiment stages are provided in Figures 6.6 and 6.7, respectively. The corresponding correlation coefficients, equilibrium constants, and values of maximum polymer adsorption are presented in Table 6.1.

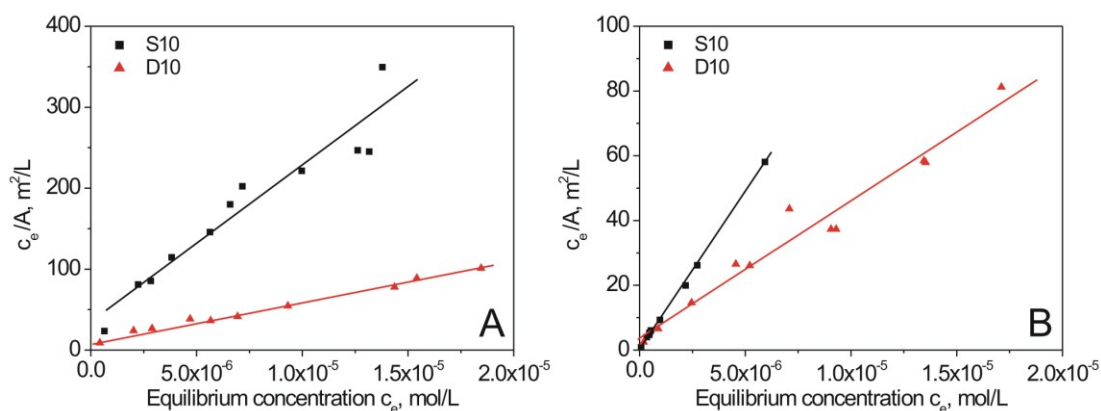


Figure 6.7. Polymer adsorption versus equilibrium polymer concentration at the second stage (adsolubilization of 2-naphthol on hydrophilic (A) and hydrophobic (B) silica substrate).

The data provided in Table 6.1 demonstrate that in case of D10 the area per molecule values are reasonably close for the hydrophilic and hydrophobic substrates, both after adsorption and adsolubilization, suggesting that no changes in D10 macromolecular conformation occur upon adsolubilization of 2-naphthol. In contrast, increase in the surface area per S10 molecule is observed after incorporation of 2-naphthol into the adsorbed polymer layer for both silica types. This behavior is most likely due to the conformational changes in S10 macromolecules and weaker bonding between the silica and the S10 fragments in comparison to D10. The increase in the surface area after adsolubilization is more pronounced for the S10 adsorbed on hydrophilic silica with the weaker physical bonding between the PEG fragments and the polar silica substrate.

Table 6.1. Correlation Coefficients, Equilibrium Constants, and A_m Values for AIPE Adsorption on Hydrophilic and Hydrophobized Silica

Polymer	Silica type	R^2	$k_d/k_a, \text{m}^2/\text{l}$	$A_m^{-1}, \text{m}^2/\text{mol}$	Area per molecule, nm^2
Polyester adsorption (first stage)					
S10	Hydrophilic	0.973	678	1.19×10^7	19.8
S10	Hydrophobic	0.998	112	8.41×10^6	14.0
D10	Hydrophilic	0.999	150	4.35×10^6	7.2
D10	Hydrophobic	0.995	73.9	3.66×10^6	6.1
Adsolubilization of 2-naphthol (second stage)					
S10	Hydrophilic	0.919	34.9	1.93×10^7	32.1
S10	Hydrophobic	0.999	0.3	9.64×10^6	16.0
D10	Hydrophilic	0.989	10.8	4.86×10^6	8.1
D10	Hydrophobic	0.963	3.7	4.24×10^6	7.0

The higher ratio of desorption : adsorption rate constants (k_d/k_a) for the polymer S10 adsorbed on hydrophilic silica nanoparticles indicates that S10 macromolecules are more mobile in the adsorption layer in comparison to D10. The adsolubilization of 2-naphthol into the AIPE fragments causes conformational changes of the AIPE macromolecules in the adsorption layer and apparently increases the bonding strength between the substrate and the polymer, thus decreasing the rate of polymer desorption and k_d/k_a ratio.

6.4.3. AIPes as Functional Additives in Precursors for Electrospinning Silicon-Containing Materials

Recently, a growing interest in developing novel functional materials for electronic devices has encouraged research in semiconductor chemistry and processing. Thus, the search

for alternate routes to create semiconductor materials has stimulated studies into liquid silicon precursors for potential low-cost, high-throughput deposition of metal silicide films and nanowires. Electronic semiconductor devices could be developed from liquid silicon precursors in a process similar to inkjet printing with precursors acting as ink material. In this regard, cyclohexasilane (Si_6H_{12}) is a strong prospect for being the next-generation, solution processed liquid precursor to silicon-based semiconductor devices due to its relatively simple and efficient synthesis and reduced processing costs in comparison to current methods of silane processing such as plasma-enhanced chemical vapor deposition. A unique synthetic pathway to cyclohexasilane has been previously discovered at NDSU based on the reaction of HSiCl_3 with pentaethyldiethylenetriamine yielding a corresponding ammonium salt with a $\text{Si}_6\text{Cl}_{14}^{2-}$ anion that is readily reduced to Si_6H_{12} .^{27,31} Readily purified by distillation, Si_6H_{12} is a promising alternative to silane (SiH_4) in chemical vapor deposition and may be enabling for direct-write fabrication of printed electronics. When heated or exposed to laser light, cyclohexasilane undergoes ring-opening polymerization to yield polydihydrosilane $(-\text{SiH}_2)_n-$ that could be transformed into first amorphous silicon and then crystalline silicon materials by thermolysis (Figure 6.8).³² Solution-based processing of the polydihydrosilane, however, is complicated by the insolubility of $(-\text{SiH}_2)_n-$ in typical solvents.

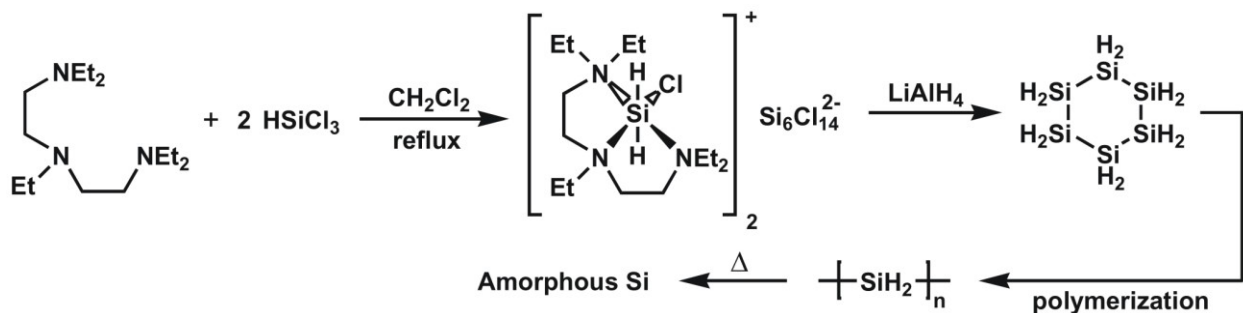


Figure 6.8. Development of silicon through the use of cyclohexasilane.

Recently, the “host-guest” interactions between cyclohexasilane and amphiphilic invertible polyester S6 based on poly(ethylene glycol) and sebacic acid have been studied in nonpolar benzene and polar acetonitrile.^{33,34} A systematic ¹H NMR study has demonstrated the ability of S6 to participate in “host-guest” interactions with the CHS in both micellar and nonmicellar state (Figure 6.9).

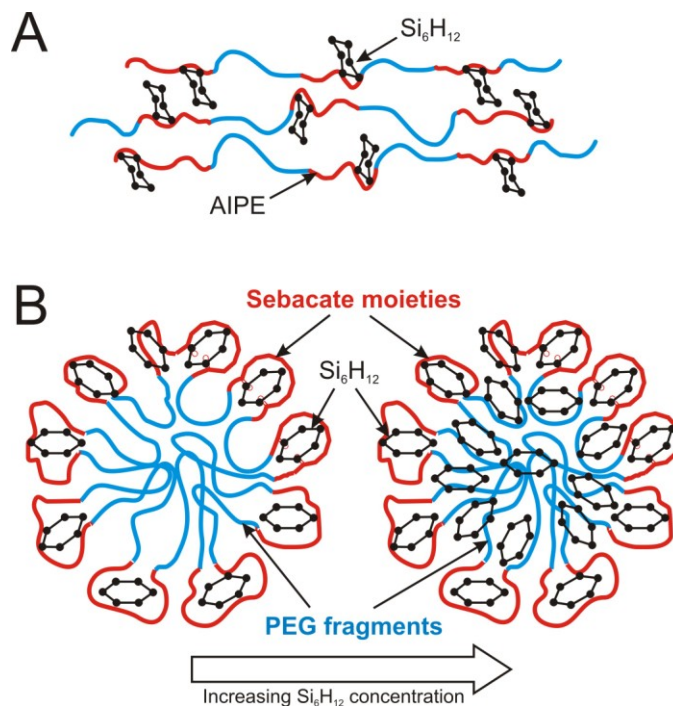


Figure 6.9. Interaction between CHS and S6 macromolecules in acetonitrile (A) and in benzene (B).

Polar acetonitrile neither dissolves CHS nor supports AIPE micellization and self-assembly, nevertheless the presence of hydrophilic and hydrophobic fragments in the AIPE macromolecules contributes to localizing CHS molecules by AIPE through the Lewis acid-base interactions between CHS and the AIPE carbonyl groups (Figure 6.9A).³³ In a nonpolar benzene S6 macromolecules self-assemble into micelles with a hydrophilic exterior composed of PEG fragments and a hydrophobic interior made from $-(CH_2)_n-$ chains that form micellar assemblies

with hydrophilic and hydrophobic domains at high polymer concentration (see Chapter 3 for more information). When CHS is added to a solution of S6 in benzene, CHS becomes localized in the micellar exterior due to a Lewis acid-base interaction between CHS molecules and the ester functional groups of the AIPE. At higher CHS concentrations, Si_6H_{12} starts interacting with the AIPE ether groups and becomes accommodated within the micellar interior (Figure 6.9B). At high S6 concentration, self-assembly of the amphiphilic invertible polyester gives rise to an additional interaction between cyclohexasilane and hydrophobic polymeric domains.³⁴ The ability of amphiphilic invertible polymers to participate in “host-guest” interactions with the CHS could be potentially useful in developing electronic functional materials on the basis of cyclohexasilane, as it expands the number of solvents thus facilitating processing of this silicon precursor.

Electrospinning is a continuous nanofabrication technique based on the principle of electrohydrodynamics that is capable of producing nanowires of synthetic and natural polymers, ceramics, carbon, and semiconductor materials with the diameter ranging from several nanometers to several micrometers. This technique is considered a viable option for utilizing cyclohexasilane in the development of electronic materials, as CHS is transformed directly into a useful form (i.e., a nanowire) before the formation of insoluble polydihydrosilane occurs. Recently, electrospinning technique has been used to fabricate silicon nanowires from a solution of Si_6H_{12} and poly(methyl methacrylate) in toluene for the purpose of using them as anode components in next-generation lithium ion batteries.³⁵ Depending on the processing conditions, Si_6H_{12} /PPMA wires with diameter ranging between 15–50 nm have been prepared. Thermal treatment at 350 °C resulted in their transformation into amorphous silicon nanowires. However, the quality of the nanowires fabricated by electrospinning has been greatly affected by formation

of globules reaching up to 20 μm in diameter. Therefore, exploiting CHS-AIPE interactions has been seen as a measure to improve the quality of the nanowires electrospun from both polar and nonpolar solvents. AIPE macromolecules have been expected to serve as functional additives to improve the distribution of the CHS in the nanowire composition. To this end, liquid CHS was substituted by hybrid composition where CHS molecules had been previously incorporated into the micelles developed from the polyester S6 (AIPE-1 based on PEG-600 and sebacic acid) prior to the electrospinning procedure.

Table 6.2. Post-Treatment of Silicon Containing Wires Electrospun from the AIPE/CHS/PMMA Composition

Sample	Treatment	
	UV	Thermal
I	no	no
II	yes	no
III	no	yes
IV	yes	yes

Two different electrospinning ink compositions have been prepared to study the effect of AIPE on the properties of silicon wires, the component ratios being S6 : CHS : PMMA as 0.5 : 5 : 10 (ink 1) and 1 : 5 : 10 (ink 2), respectively. The components have been dissolved in dichloromethane and toluene, two solvents differing by polarity, to consider solvent effect on the development of silicon wires. After electrospinning the two inks onto aluminum substrate, both deposits have been divided into four parts and subjected to different kinds of post-treatment (thermal and/or UV) to polymerize CHS, as summarized in Table 6.2. UV treatment (irradiation

of the sample by a UV lamp for five minutes using 1.10 W output power) is known to cause polymerization of the CHS into polydihydrosilane $-(\text{SiH}_2)_n-$, while thermal treatment (heating samples at 350 °C) is believed not only to cause CHS transformation to $-(\text{SiH}_2)_n-$, but also convert polysilane into amorphous silicon. Subsequently, the presence of silicon in the prepared wires has been evaluated by Raman imaging spectroscopy, while the wire morphology has been analyzed via SEM.

A typical Raman spectrum of the wires is given in Figure 6.10. The presence of amorphous silicon in the processed wires is revealed by a broad peak at ca. 480 cm^{-1} .³² Noteworthy, irradiation of the samples by Raman laser during measurement triggered conversion of polyhydrosilane into amorphous silicon in the samples I and II that had not undergone thermal treatment, as no peaks at ca. 460 cm^{-1} corresponding to Si–Si TO bonding mode in a polydihydrosilane are observed in their Raman spectra.

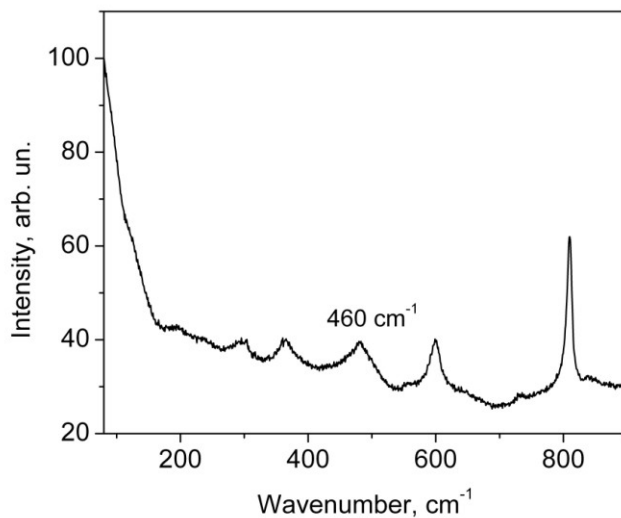


Figure 6.10. A representative Raman spectrum of electrospun CHS/S6/PMMA wires.

Preliminary SEM results obtained on the deposits from toluene-based compositions (both ink 1 and ink 2) have demonstrated that electrospinning has yielded droplets instead of

nanowires (micrographs not shown). A plausible explanation for the formation of droplets is that toluene is a thermodynamically poor solvent for PMMA, a matrix forming polymer. In the ink formulation PMMA molecules are contracted, therefore, they do not provide good matrix support for the CHS during electrospinning. Thus, further studies have been carried out using ink compositions dissolved in dichloromethane.

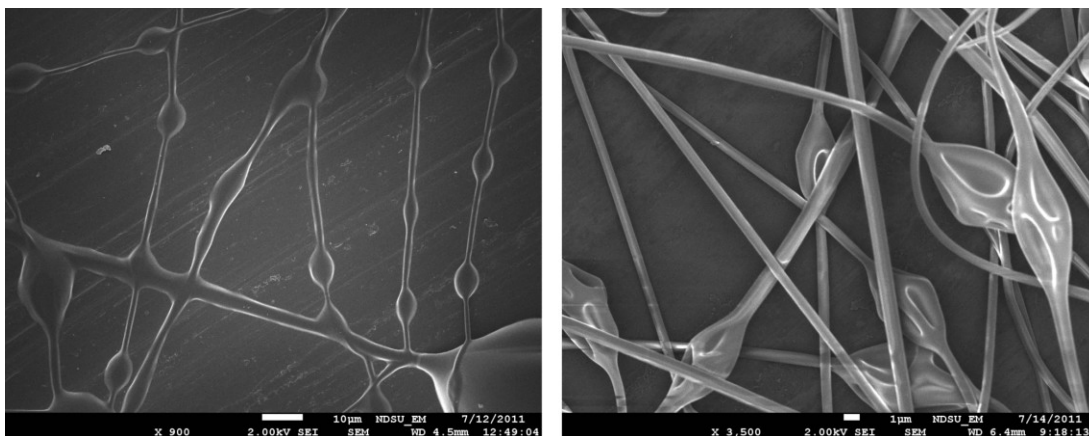


Figure 6.11. SEM micrograph of electrospun wires developed from the CHS/PMMA composition.

Figure 6.11 demonstrates SEM micrographs of the wires electrospun from CHS/PMMA composition that does not contain amphiphilic invertible polyester. The structure of electrospun wires is to a great extent affected by the presence of significant amount of globule-like structures leading to the substantial variation in wire diameter. The presence of globules is commonly attributed to the unrefined microfluidics of the composition.³² Similar globule-like or blob-like structures are observed in the SEM images of non-post-treated wires (sample I) developed from the AIPE containing ink formulation (Figures 6.12A, 6.12B and 6.13A). However, the globules disappear after post-treatment of the electrospun wires.

Depending on the type of post-treatment of wires, considerable differences in the nanowire appearance have been observed. Thus, UV treated wires (sample II) exhibited a fine

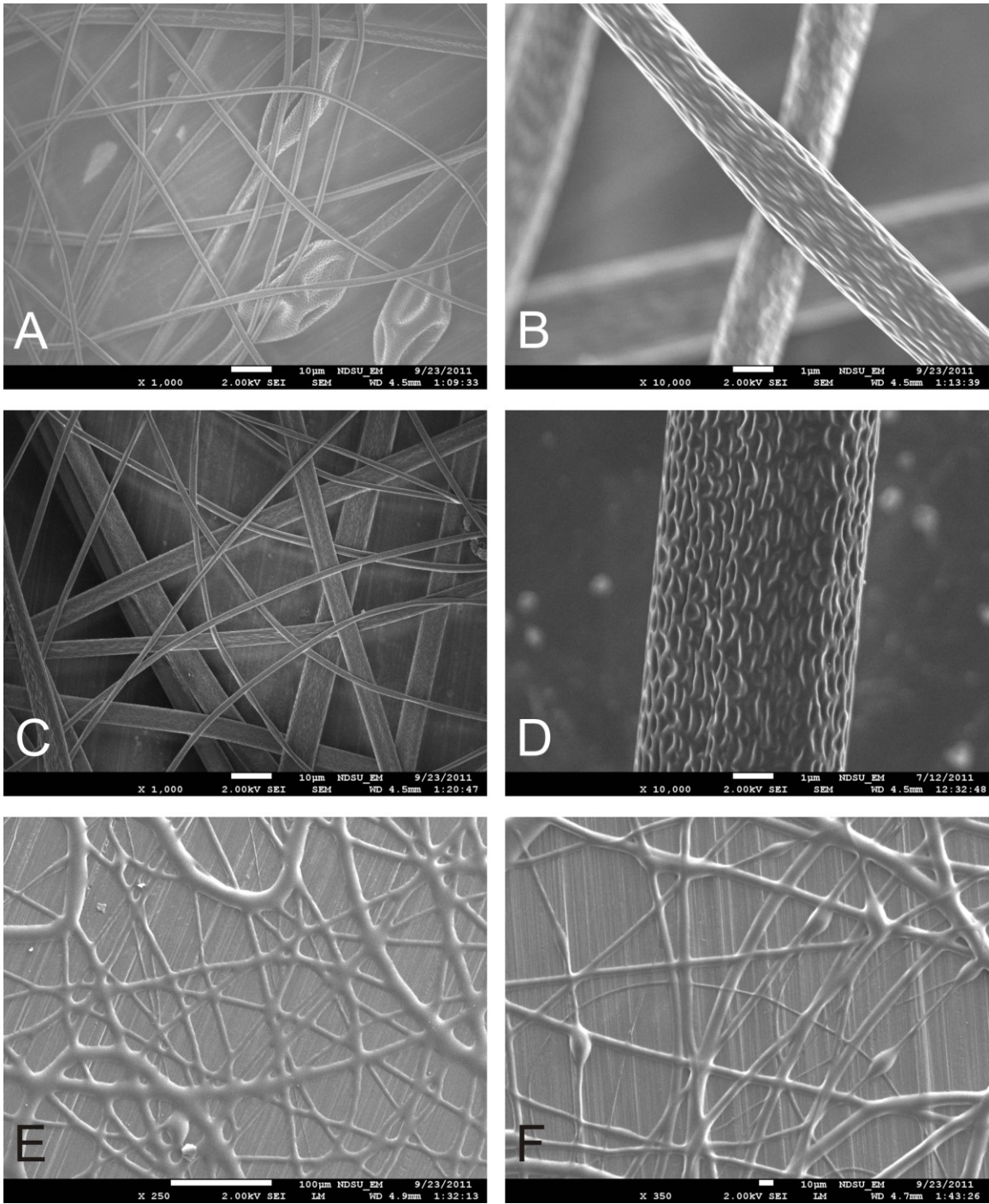


Figure 6.12. SEM micrographs of wires electrospun from ink 1 (S6:CHS:PMMA as 0.5:5:10) and subjected to different post-treatment types: Sample I (A, B), Sample II (C, D), Sample III (E), and Sample IV (F).

wire shape and a distinct dimpled (“strawberry-like”) morphology (Figures 6.12C, 6.12D, and 6.13B). Thermal treatment, however, destroyed the wire “strawberry-like” surface pattern, most likely due to the rearrangement of the polymer chains above their glass transition temperature (Figures 6.12E, 6.12F, 6.13C, and 6.13D). The wires nonetheless retained their inner grain-like morphology, obviously caused by phase separation, after a thermal treatment (Figure 6.13D).

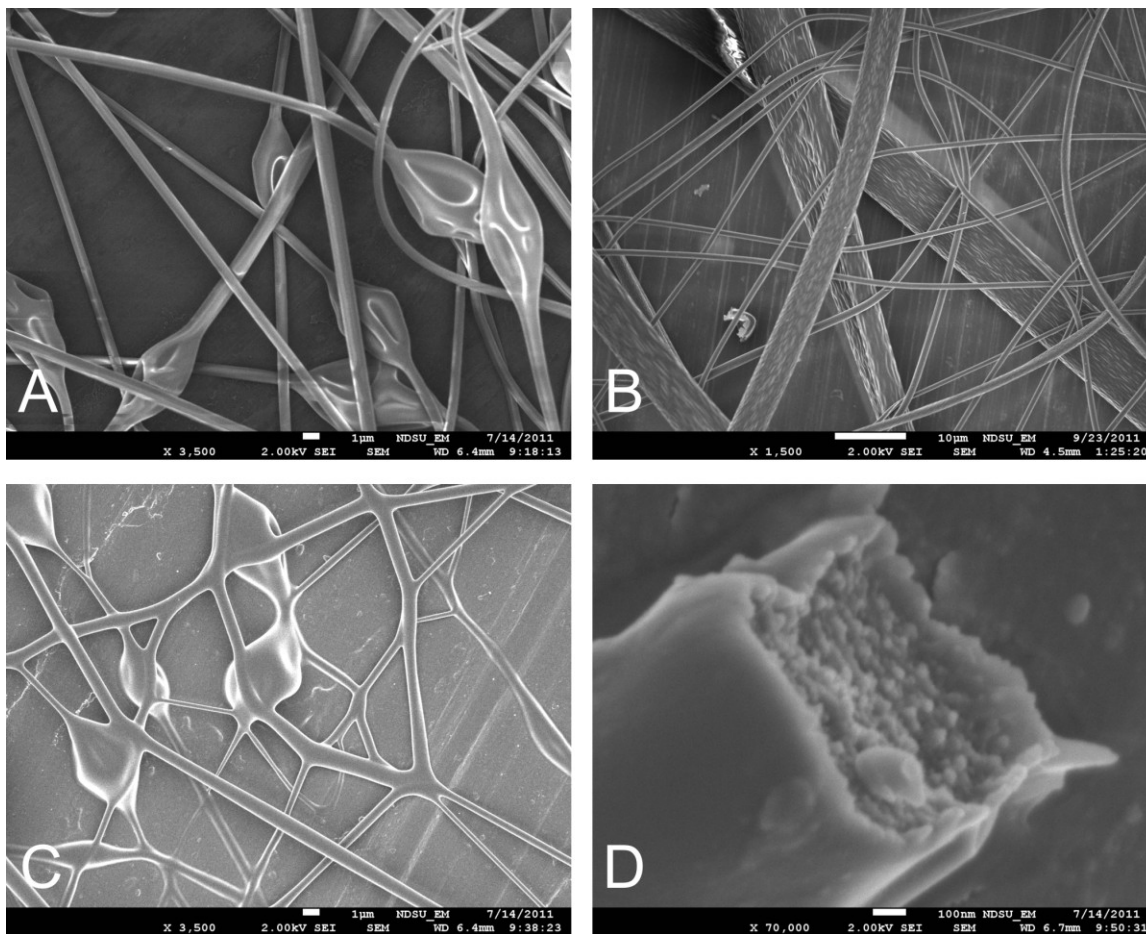


Figure 6.13. SEM micrographs of wires electrospun from ink 2 (S6:CHS:PMMA as 1:5:10) and subjected to different post-treatment types: Sample I (A), Sample II (B), and Sample IV (C, D).

Incorporation the AIPE S6 into electrospinning ink formulations has resulted in development of “strawberry-like” patterns on the surface of electrospun wires. Given the fact that no “strawberry-like” morphology has been detected in the wires developed from non-AIPE

containing inks, the appearance of this well-expressed surface pattern is most likely caused by phase separation in the AIPE during electrospinning. Due to the presence of hydrophilic and hydrophobic fragments in the macromolecule, amphiphilic invertible polymers are known to arrange themselves at the interfaces (see Chapter 3 for more information). During electrospinning, the air/wire interface is constantly renewed due to solvent evaporation, thus causing the constant rearrangements of the AIPE macromolecules. To this end, continuous rearrangements of the AIPE macromolecular conformation promote microphase separation that could obviously be considered as a driving force for the formation of “strawberry-like” morphology. The interaction of the AIPE macromolecules with highly hydrophobic CHS molecules in the ink might further facilitate microphase separation.

Noteworthy, electrospinning inks based on CHS, S6, and PMMA provide the wires where the active silicon agent forms after the liquid precursor is transformed into a nanosized material.³² The used approach enables tuning the chemical composition of silicon nanowires by adjusting precursor chemistry. Thus, any additives that do not interact with the CHS Si–Si or Si-H bonds, such as metal nanoparticles, solid electrolytes, quantum dots, etc. could be incorporated into the CHS-based electrospinning ink. As a result, a variety of electrospun composites with tunable properties (i.e. conductivity) could be developed.

6.5. Conclusions

Due to the presence of both hydrophilic and hydrophobic fragments in the backbone, amphiphilic invertible polyesters have been shown to adsorb onto the surface of both hydrophilic and hydrophobized silica nanoparticles. While AIPE adsorption on the hydrophilic silica primarily occurs due to the interaction between the polar substrate and polyester PEG fragments, adsorption of the amphiphilic invertible polyesters on the hydrophobized silica is predominantly

governed by the hydrophobic interactions between $-(CH_2)_n-$ chains of the dicarboxylic acid moieties and the surface. AIPE modified silica nanoparticles are able to adsorb and solubilize molecules of poorly water-soluble 2-naphthol into the nonpolar interior of the adsorbed polymer aggregates. The amount of adsorbed 2-naphthol increases with increasing amount of adsorbed AIPEs and does not depend on the nature of the silica and the length of the AIPE hydrophobic fragment.

Amphiphilic invertible polyester S6 has been used as a functional additive in fabrication of electrospun silicon nanowires on the basis of cyclohexasilane, a liquid silicon precursor. The use of AIPE in the electrospinning ink formulation has allowed to significantly reduce the number of globules formed during electrospinning thus improving wire appearance. Electrospinning AIPE-containing formulation with subsequent UV-induced conversion of CHS into polydihydrosilane has resulted in development of “strawberry-like” wire morphologies, unseen for the non-AIPE containing inks. The appearance of “strawberry-like” morphologies has been attributed to microphase separation in the AIPE on the air/wire interface. Electrospinning AIPE-containing inks based on the liquid cyclohexasilane precursor could find their application as a scalable method for fabricating silicon wires for electronic functional materials.

6.6. References

1. Sperling, R. A.; Parak, W. J. *Phil. Trans. R. Soc. A* **2010**, *368*, 1333–1383.
2. Freij-Larsson, C.; Jannasch, P.; Wesslén, B. *Biomaterials*. **2000**, *21*, 307–315.
3. Steinmetz, A.L.; Schall, N.; Dziwok, K.; Coutelle, H.; Simon, W.; Dick, S.; Krämer, I.; Schiessling, H. U.S. Patent 6,929,860, August 16, 2005.
4. Lau, A.K.T.; Lu, J.; Varadan, V.K.; Chang, F.K.; Tu, J.P.; Lam, P.M. *Adv. Mater. Res.* **2008**, *47–50*, 1311–1314.

5. Asvapathanagul, P.; Malakul, P.; O'Haver, J. *J. Colloid Interface Sci.* **2005**, *292*, 305–311.
6. Esumi, K.; Sakamoto, Y.; Nagahama, T.K. Meguro. *Bull. Chem. Soc. Jpn.* **1989**, *62*, 2502–2506.
7. Esumi, K.; Yamada, T. *Langmuir* **1993**, *9*, 622–624.
8. Sakhalkar, S.S.; Hirt, D.E. *Langmuir* **1995**, *11*, 3369–3373.
9. Tsurumi, D.; Sakai, K.; Yoshimura, T.; Esumi, K. *J. Colloid Interface Sci.* **2006**, *302*, 82–86.
10. Scamehorn, J.F.; Harwell, J.H.; In *Surfactants in Chemical/Process Engineering*; Wasan, D.T.; Ginn, M.E.; Shah, D.O., Eds.; Surfactant Science Series, Vol. 28; Dekker: New York, NY, 1988; pp 77–125.
11. Chorro, M.; Chorro, C.; Dolladille, O.; Partyka, S.; Zana, R. *J. Colloid Interface Sci.* **1999**, *210*, 134–143.
12. Velegol, S.B.; Fleming, B.D.; Biggs, S.; Wanless, E.J.; Tilton, R.D. *Langmuir* **2000**, *16*, 2548–2556.
13. Behrend, T.; Herrmann, R. *J. Colloid Surf.* **2000**, *162*, 15–23.
14. Jansen, J.; Treiner, C.; Vantion, C. *J. Colloid Interface Sci.* **1996**, *179*, 578–586.
15. Zhu, B.Y.; Xhao, X.; Gu, T. *J. Chem. Soc. Faraday Trans.* **1988**, *1 84*, 3951–3960.
16. Wu, J.; Harwell, J.H.; O'Rear, E.A. *J. Phys. Chem.* **1987**, *91*, 623–634.
17. Sakai, K.; Nakajima, E.; Takamatsu, Y.; Sharma, S.C.; Torigoe, K.; Yoshimura, T.; Esumi, K.; Sakai, H.; Abe, M.J. *J. Oleo Sci.* **2008**, *57*, 423–429.
18. Zhao, W.R.; Gu, J.L.; Zhang, L.X.; Chen, H.R.; Shi, J.L. *J. Am. Chem. Soc.* **2005**, *127*, 8916–8917.

19. Anastasiadis, S.H.; Gancarz, I.; Koberstein, J.T. *Macromolecules* **1989**, *22*, 1449–1453.
20. Xanthos, M.; Dagli, S.S. *Polym Eng Sci* **1991**, *31*, 929–936.
21. Browne, W.R.; Feringa, B.L. *Nature Nanotechnol.* **2006**, *1*, 25–35.
22. Avouris, P.; Chen, J. *Mater. Today* **2006**, *9*, 46–54.
23. Tian, B.; Zheng, X.; Kempa, T.J.; Fang, Y.; Yu, N.; Yu, G.; Huang, J.; Lieber, C.M. *Nature* **2007**, *449*, 885–889.
24. Björk, M.T.; Ohlsson, B. J.; Sass, T.; Persson, A. I.; Thelander, C.; Magnusson, M. H.; Deppert, K.; Wallenberg, L. R.; Samuelson, L. *Appl. Phys. Lett.* **2002**, *80*, 1058–1060.
25. Björk, M.T.; Ohlsson, B. J.; Sass, T.; Persson, A. I.; Thelander, C.; Magnusson, M. H.; Deppert, K.; Wallenberg, L. R.; Samuelson, L. *Nano Lett.* **2002**, *2*, 87–89.
26. Gudiksen, M.S.; Lauhon, L.J.; Wang, J.; Smith, D.C.; Lieber, C.M. *Nature* **2002**, *415*, 617–620.
27. Choi, S.-B.; Kim, B.-K.; Boudjouk, P.; Grier, D. G. *J. Am. Chem. Soc.* **2001**, *123*, 8117–8118.
28. Nuysink, J.; Koopal, L.K. *Talanta* **1982**, *29*, 495–501.
29. Esumi, K. *J. Jpn. Soc. Colour Mater.* **1997**, *70*, 675–685.
30. Tsurumi, D.; Yoshimura, T.; Esumi, K. *J. Colloid Interface Sci.* **2006**, *297*, 465–469.
31. Boudjouk, P.R.; Kim, B.K.; Remington, M.P.; Chauhan, B. U.S. Patent 5,942,637, August 24, 1999.
32. Han, S.; Dai, X.; Loy, P.; Lovaasen, J.; Huether, J.; Hoey, J.M.; Wagner, A.; Sandstrom, J.; Bunzow, D.; Swenson, O.F.; Akhatov, I.S.; Schulz, D.L. *J. Non-Cryst. Solids.* **2008**, *354*, 2623–2626.

33. Kohut, A.; Kudina, O.; Dai, X.; Schulz, D.L.; Voronov, A. *Langmuir* **2011**, *27*, 10356–10359.
34. Kohut, A.; Dai, X.; Pinnick, D.; Schulz, D. L.; Voronov, A. *Soft Matter*. **2011**, *7*, 3717–3720.
35. Schulz, D.L.; Hoey J.; Smith J.; Elangovan A.; Wu, X.; Akhatov I.; Payne S.; Moore J.; Boudjouk P.; Pederson L.; Jie X.; Zhang J.-G. *Electrochem. Solid State Lett.* **2010**, *13*, A143–A145.

CHAPTER 7. CONCLUSIONS

The focus of research in the field of polymeric materials has recently shifted towards development of polymers with responsive or “smart” behavior. Such polymers are able to adapt themselves to the surrounding environment by changing their chain conformation in a fast and reversible way. Nowadays, functional materials designed with this approach in mind are playing an increasingly important role in a variety of applications ranging from drug delivery, biosensors, tissue engineering and diagnostics to optical systems and adaptive coatings. However, until now little attention has been paid to studying self-assembly and environment-dependent rearrangement in responsive polymers triggered by the polarity of the medium.

The current work aims at the development of novel responsive functional polymeric materials by manipulating environment-dependent self-assembly of a new class of responsive macromolecules – amphiphilic invertible polymers (AIPs). Three AIP types have been developed: amphiphilic invertible polyesters based on PEG and aliphatic dicarboxylic acids (AIPes-1), amphiphilic invertible polyurethanes based on PEG and polytetrahydrofuran (AIPUs), and amphiphilic invertible polyesters based on PEG and PTHF (AIPes-2). Changing the AIP chemistry and the nature of the hydrophobic fragments in the invertible macromolecules has been used as a tool to tune the hydrophilic-lipophilic balance (HLB) of the AIPs in order to tailor their surface activity, self-assembly behavior, and invertible properties.

Environment-dependent self-assembly of amphiphilic invertible polymers has been demonstrated in solvents differing by polarity. In a polar aqueous medium, AIP micelles with a hydrophilic PEG corona and a hydrophobic interior are formed. Amphiphilic invertible macromolecules switch their conformation in nonpolar aromatic solvents forming micelles with a hydrophobic exterior and a hydrophilic inner part. Increasing AIP concentration in solution

leads to self-assembly and development of invertible micellar assemblies with hydrophilic and hydrophobic domains in both polar and nonpolar media. Depending on the AIP chemical composition and concentration, self-assembly of the amphiphilic invertible polymers gives rise to different micellar morphologies such as spheres, cylinders, and ellipsoids.

Environment-dependent behavior has been also shown for thin AIP films. Thus, such films change the surface energy of the substrate by increasing the hydrophilicity of the nonpolar substrates and making polar substrates more hydrophobic. AIP film responds to wetting liquids differing by polarity: if AIP film is in contact with water, the contact interface is enriched with hydrophilic PEG chains. Upon exposure to the nonpolar diiodomethane, AIP macromolecules invert their structure and hydrophobic fragments assemble at the surface.

Polarity-responsive properties of the AIPs make them promising functional materials for applications in polar and nonpolar media, as well as on the surfaces and interfaces. AIP micellar assemblies are capable of solubilizing poorly soluble substances by loading them in the micellar interior in polar and nonpolar solvents. Upon contact with the media of opposite polarity, loaded AIP micellar assemblies transfer their payload into this phase by inverting their macromolecular conformation in response to a polarity change. The unique ability of AIPs to invert the molecular conformation depending on the polarity of the environment has been used to establish the novel stimuli-responsive mechanism of solubilized drug release that is induced in response to a change of the environmental polarity. Thus, AIP micellar assemblies loaded with a poorly water-soluble curcumin, a phytochemical drug, have been shown to deliver this therapeutic agent to carcinoma cells. The release of curcumin from AIP micellar assemblies is primarily caused by macromolecular inversion due to changing local environmental polarity and can be controlled by adjusting the AIP chemical structure and concentration. AIP-based delivery vehicles have been

also shown to stabilize curcumin molecules against chemical decomposition and be nontoxic against human cells up to a concentration of 10 $\mu\text{g}/\text{ml}$, a concentration at which curcumin-loaded AIP vehicles demonstrate cytotoxicity against the breast carcinoma cells.

In a nonpolar medium, AIP micellar assemblies have been used as nanoreactors for developing silver nanoparticles by reduction of a polar $[\text{Ag}(\text{NH}_3)_2]\text{OH}$ precursor by the AIP PEG fragments. Depending on the AIP composition, chain configuration, and concentration, the size of nanoparticles has been varied between 6 and 14 nm. Owing to their invertible properties, AIP macromolecules provided effective stabilization of the developed silver nanoparticles in either polar or nonpolar media, where stable solutions of colloidal nanosilver have been formed. As one of the nanotechnological applications of developed nanosilver, the nanoparticles have been successfully used as seeds to aid anisotropic growth of cadmium selenide semiconductor particles using the modified solution-liquid-solid method. As a result, a population of monodisperse semiconductor particles with an average particles size of ca. 5 nm has been developed. Cadmium selenide nanoparticles developed in such a way have potential in a variety of applications ranging from physics to medicine.

Due to the presence of both hydrophilic and hydrophobic fragments in the backbone, AIPs have been shown to adsorb onto the surface of silica nanoparticles strongly differing in polarity. The adsorption of amphiphilic invertible polymers on polar and nonpolar substrate is governed by different types of interactions: polar substrate mainly interacts with the hydrophilic PEG fragments, while hydrophobized silica participates in the hydrophobic interactions with nonpolar AIP fragments. AIP modified silica nanoparticles are able to adsorb and solubilize molecules of poorly water-soluble 2-naphthol into the nonpolar interior of the adsorbed polymer aggregates. The amount of adsorbed 2-naphthol does not depend on the nature of the substrate silica and

the length of the AIP hydrophobic constituents but it increases with increasing amount of the adsorbed AIPs. Silica particles modified with amphiphilic invertible polymers could be the basis for development of enterosorbents for selective removal of toxins.

Amphiphilic invertible polymer has been used as a functional additive in fabrication of the electrospun silicon wires on the basis of cyclohexasilane, a liquid silicon precursor. The use of AIP in the electrospinning ink formulation has resulted in significant improvement of the wire appearance and development of “strawberry-like” wire morphologies. AIP-assisted fabrication of silicon wires from the liquid cyclohexasilane precursor could find application as a method for developing electronic functional materials.

7.1. Future Work

7.1.1. Evaluation of AIP Micellar Morphologies in the Nonpolar Media

Amphiphilic invertible polymers have been shown to build micelles and micellar assemblies in both polar and nonpolar media. While the shape and size of AIP micellar assemblies in a polar aqueous medium has been already established, the appearance of AIP nanoassemblies in nonpolar solvents such as benzene or toluene still remains a mystery. Therefore, a systematic study on AIP micellar morphologies using the data acquired by means of small angle neutron scattering, dynamic light scattering, and transmission electron microscopy will be carried out. While microscopy technique will be used to evaluate the micellar shape, scattering techniques will aid in determining the geometric parameters of the micellar assemblies.

7.1.2. Improvement of AIP Based Drug Delivery Vehicle Formulations

Positively charged drug carriers are known to undergo faster and more complete uptake by cancer cells. Hence, modification of AIP micelles with positively charged substances is seen

as one of the ways to improve their efficiency as anticancer drug delivery vehicles. In order to produce positively charged AIP micellar carriers, solubilization of a positively charged molecule, 3,4,5-tridodecyloxy aniline hydrochloride, will be carried out as a joint project with a Zhu group from the RWTH Aachen University (Aachen, Germany). Having a hydrophilic ammonium head and three hydrophobic long-chain aliphatic tails, 4,5-tridodecyloxy aniline hydrochloride developed by Dr. Zhu is effectively a surfactant, hence the charged heads of the solubilized molecules are assumed to be located in the AIP micellar exterior. The location of the positively charged head in the micellar exterior will facilitate interaction between the AIP micellar assemblies and the cancer cells thus promoting uptake of the drug delivery vehicle.

Another improvement of the anticancer efficiency of the AIP based formulation is substitution of curcumin with a more powerful anticancer drug such as paclitaxel. Paclitaxel is an established anticancer drug that is poorly soluble in water; therefore, incorporation of paclitaxel molecules in the AIP micellar interior is suggested to improve its solubility and bioavailability, which will obviously lead to increased anticancer efficiency of paclitaxel-loaded AIP vehicles.

Finally, the concept of theranostics which is envisioned as an integral part of the 21st century personalized medicine, requires the ability to provide simultaneous disease cure and monitoring of the treatment progress. This strategy could be implemented by using carrier vehicles to deliver both drugs and imaging agents to the target site. AIP micellar assemblies have been recently demonstrated to sequester small molecules in both micellar interior and exterior. This provides possibilities for incorporation of two cargo types in the AIP based delivery vehicles: hydrophobic drugs such as curcumin or paclitaxel could be loaded in the micellar interior, while polar contrast agents such as propidium iodide could be incorporated in the micellar PEG corona. After being introduced into the systemic blood flow, AIP micellar

assemblies loaded with two types of functional cargo molecules would migrate to the target tissue and release both drug and imaging agent into the cell via the stimuli-responsive release mechanism.